

UNIVERSITY OF SÃO PAULO  
SÃO CARLOS INSTITUTE OF PHYSICS

CAMILA DE SOUZA BARBOSA

Discovery of brussonol analogs as lead candidates for malaria

São Carlos  
2024



CAMILA DE SOUZA BARBOSA

Discovery of brussonol analogs as lead candidates for malaria

Thesis presented to the Graduate Program in Physics at the São Carlos Institute of Physics of the University of São Paulo to obtain the degree of Doctor of Science.

Concentration area: Applied Physics

Option: Biomolecular Physics

Advisor: Prof. Dr. Rafael V. C. Guido

Co-advisor: Prof<sup>ª</sup>. Dr<sup>ª</sup> Anna Caroline C. Aguiar

Corrected Version  
(original version available on the Program Unit)

São Carlos

2024

I AUTHORIZE THE REPRODUCTION AND DISSEMINATION OF TOTAL OR PARTIAL COPIES OF THIS DOCUMENT, BY CONVENTIONAL OR ELECTRONIC MEDIA FOR STUDY OR RESEARCH PURPOSE, SINCE IT IS REFERENCED.

Barbosa, Camila de Souza

Discovery of Brussonol analogs as lead candidate for malaria / Camila de Souza Barbosa; advisor Rafael Victório Carvalho Guido; co-advisor Anna Caroline Campos Aguiar - corrected version -- São Carlos 2024.

163 p.

Thesis (Doctorate - Graduate Program in Biomolecular Physics) -- Instituto de Física de São Carlos, Universidade de São Paulo - Brasil , 2024.

1. Brussonol. 2. Icetexane diterpenoids. 3. Antiplasmodial activity. 4. Calcium mobilization. I. Guido, Rafael Victório Carvalho, advisor. II. Aguiar, Anna Caroline Campos, co-advisor. III. Title.

## ACKNOWLEDGEMENTS

First, I would like to thank God for the opportunity to be here today. Even though I question sometimes what happened/happens to me, at the end I can see how everything was perfect, even when it seemed wrong. In fact, during my doctorate, I had the privilege to be started in Umbanda, and there I learned that “nothing is wrong, everything is just right”. Indeed, I became present in my own life because of this saying, and it helped me slow down and expect less from things. I also would give thanks to my Mentor, Orishas and Guardians, knowing that “I can be one person, but I am not alone” gives me strength to move forward, even when I am feeling hopeless.

Second, I would like to thank my parents, Gilda and Catuta; to my brother, Diego, he was sometimes more like a father to me; to my sister-in-law, Michele; and to my nephews, Gustavo, and Vitor. Even though you do not understand what I do, and its purpose, you were always by my side, celebrating each accomplishment and having my back when things were not good. I cannot forget to thank my cat Naruto. It is going to be seven years since I have made the best decision and adopted my baby. He is always guarding, supporting, and caring for me. It is good to know that, no matter where I go, I will have him with me.

Next, I would like to thank my supervisor, Rafael Guido, for the opportunity to be part of his group, and for the guidance throughout my doctorate. I also would like to thank Carol Aguiar, my co-supervisor. I came to IFSC through Carol’s indication, and she taught me how to be in love with *Plasmodium* parasites. Thank you for the tips, emotional support, for sharing your knowledge, everything I learned is already paving a great future ahead of me. Additionally, I had an opportunity to have Adele Lehane as my supervisor for six months at the Australian National University. I would like to thank her for all her guidance, for believing in me, even when I was doubting myself. Thank you, Adele, for sharing the hood and the bench with me. It was an amazing opportunity that had a huge impact on myself, not only as a PhD student and researcher, but also as a person. I miss our morning talks. During this time, I also had the privilege to spend time in Giel van Dooren’s lab. There, I saw *Toxoplasma* moving and learned many interesting facts about this intriguing parasite. Being around the Transporter Group opened a new area that I was not aware before, and it showed that there are many opportunities and things to learn from Apicomplexan parasites.

Finally, I would like to thank my friends, and lab colleagues. I am here today because, throughout all this time, I had my chosen family with me, and I am so grateful that it is getting bigger. Every place I went I had an opportunity to meet amazing and interesting people, that

hold me close when I needed, and my family was away. I will start with Gustavo Viana and Fernando Varotti. I was supervised by both researchers, and I learned a lot from them. I am fortunate to still maintain contact, even though it is not as frequent as usual. From my graduation and Master's time, I would like to thank Alessandra Gonçalves Neves, she was my first supervisor. I cannot forget Silmara, Felipe, Andressa, Simone, Matheus (China), Amanda, Karina, and Karen. I learned with each one of you, and I would like to thank you all for being part of my life. I feel grateful to realize that it does not matter how long it takes for us to meet, our friendship feels the same, like in the beginning. I could see you guys getting married, travelling abroad, growing your families, changing careers, and it feels good to share all of that with you.

From my doctorate in IFSC, I would like to thank Ketllyn and Nai, who were my saviours in the beginning and helped me through my adaptation. Camilinha, Juju, Victor and Gui, thank you for everything. We were able to share experiences, stories, learn from one another. I was glad to see you all grow in your careers and life. Igor, thank you for sharing with me a house, moments of happiness, cleaning, adopting Mulambo, moments of stress, thank you for being my brother in São Carlos. I learned every single day with and from you. Sarah, also known as Saricha, thank you for sharing the same birthday with me. It is so amazing how we are alike, and I feel that you guided me in so different ways. You inspire me. Giovana (Gi), thank you for being patient with me. I was difficult in the beginning, but, once I opened my heart, I saw a beautiful friendship grow. Thank you for supporting me. João Paulo (Jaú), Jorge, also known as Ricardo, and Letícia, thank you for being my friends, and listening all my complaints. I always felt safe with you all. Lívia, Flávia and Luana, we are so great together. You guys helped me through difficult times. Thank you for being there. I miss hugging and laughing with you guys. I also would like to thank Gabi Oliveira, Gabi Noske, Mari, Erick, Matías, and Nathy for sharing lab time with me, and all activities we had together during this time. Finally, I cannot forget Elaine, Jane, Li, Lhaís, and Nathan. Seeing you guys at the building, and talking, would always make me feel happier. I wish you guys all the best.

I cannot forget my beautiful Australian friends: Victor, Capella, Evie, Rachel, Deyun, Bridget, Sheehan, Farid, Elizabeth, Ansha, Heber, Jesús, Alejandra, Felipe, Weli, Tom, and Diego. Thank you for supporting me during my time in Canberra, I am glad that I still carry you guys with me. I miss talking to each one of you, and spending time together.

Like I said before, I am fortunate to always find great friends wherever I go. Because of my friends, I never felt alone. Thank you for all the support, talk, moments, for sharing life with me. All of you had, and still have, a huge impact on my life, and you helped me become the

person I am today. Thank you for being part of my adventure, and I want to have all of you in my future. I am excited for the future and would love to share everything with you all.

**THIS STUDY WAS FINANCED IN PART BY THE COORDENAÇÃO DE  
APERFEIÇOAMENTO DE PESSOAL DE NÍVEL SUPERIOR - BRASIL (CAPES) -  
FINANCE CODE 001.**



“Questions have got you this far, don’t stop asking now”

**From the podcast:** Supreme, the Battle for Roe

(2023)



## ABSTRACT

BARBOSA, C. S. **Discovery of brussonol analogs as lead candidates for malaria.** 2023. 163 p. Ph. D. Thesis (Doctor in Science) - Instituto de Física de São Carlos, Universidade de São Paulo, São Carlos, 2024.

Malaria is a disease caused by *Plasmodium* parasites affecting millions of people globally. Different strategies were applied throughout the years to decrease malaria burden, however the emergence of resistance parasites to antimalarials, especially related to artemisinin, threatens the progress achieved so far towards control, prevention, and elimination of the disease. In this sense, new antimalarials are critically needed, and natural products constitute an interesting source of new chemical scaffolds. A phenotypic screen identified brussonol (**1**) ( $IC_{50} = 16 \mu M$ ) as a promising antiplasmodial candidate. Structure optimization resulted in analogs 3-fold ( $IC_{50} \sim 5 \mu M$ ) more potent than brussonol. Further experiments determined that this chemical series shows a fast-acting inhibition, no cross-resistance with standard antimalarials, and potent inhibitory activity against *P. knowlesi* laboratory-based, *P. falciparum* and *P. vivax* clinical isolates. Moreover, brussonol displayed an additive profile when combined *in vitro* with artesunate. Molecular mode of action (MoA) studies indicated that brussonol derivatives disrupt  $Ca^{2+}$  homeostasis, but do not inhibit PfSERCA. Exposing isolated trophozoites to a brussonol derivative (compound **8**) resulted in hyperpolarization of the parasite's plasma membrane. In this sense, additional experiments are required to determine how compound **8** disrupts membrane potential. For example, applying genetic reverse methods in *Toxoplasma gondii* parasites, coupled to compound treatment, might help uncover this series MoA. Thus, *T. gondii* could be used as a model organism because the inhibitory effect of compound **8** ( $IC_{50} = 2.2 \pm 0.2 \mu M$ ) on this apicomplexan was demonstrated. In summary, the identification and characterization of brussonol as a new scaffold possessing promising antiplasmodial activity support the development of new derivatives with enhanced properties, aiming to discover new lead candidates for combating malaria.

Keywords: Brussonol. Icetexane diterpenoids. Antiplasmodial activity. Calcium mobilization.



## RESUMO

BARBOSA, C. S. **Descoberta de análogos de brussonol como candidatos líder para malária.** 2023. 163 p. Tese (Doutorado em Ciências) - Instituto de Física de São Carlos, Universidade de São Paulo, São Carlos, 2024.

A malária é uma doença causada por parasitas do gênero *Plasmodium* que afeta milhões de pessoas em todo o mundo. Diferentes estratégias foram aplicadas ao longo dos anos para diminuir o impacto da malária, no entanto, o surgimento de parasitas resistentes aos antimaláricos, especialmente relacionados com a artemisinina, ameaça o progresso alcançado no controle, prevenção e eliminação da doença. Neste sentido, novos antimaláricos são extremamente necessários e os produtos naturais constituem uma fonte interessante de novos esqueletos moleculares. Uma triagem fenotípica identificou o brussonol (**1**) ( $IC_{50} = 16 \mu M$ ) como um candidato promissor. A otimização da estrutura resultou em análogos 3 vezes ( $IC_{50} \sim 5 \mu M$ ) mais potentes que o brussonol. Estudos subsequentes determinaram que esta série química apresenta modo de inibição rápida, sem resistência cruzada com antimaláricos padrão e potente atividade inibitória contra cepa adaptada de *P. knowlesi* e isolados clínicos de *P. falciparum* e *P. vivax*. Além disso, o brussonol apresentou um perfil aditivo quando combinado *in vitro* com o artesunato. Estudos do modo de ação molecular (MoA) indicaram que os derivados do brussonol perturbam a homeostase do  $Ca^{2+}$ , mas não inibem o PfSERCA. A exposição de trofozoítos isolados a um derivado de brussonol (composto **8**) resultou na hiperpolarização da membrana plasmática do parasita. Neste sentido, são necessários experimentos adicionais para determinar como o composto **8** perturba o potencial da membrana. Por exemplo, a aplicação de métodos de genética reversa no parasita *Toxoplasma gondii*, poderia auxiliar na elucidação do MoA desta série. Assim, *T. gondii* poderia ser usado como organismo modelo pois foi demonstrado o efeito inibitório do composto **8** ( $IC = 2,2 \pm 0,2 \mu M$ ) neste organismo apicomplexo. Em resumo, a identificação e caracterização do brussonol como um novo esqueleto molecular com atividade antiplasmodial promissora indicam o potencial de desenvolvimento de novos derivados com propriedades melhoradas, com o objetivo de descobrir novos candidatos a compostos líderes para o combate da malária.

Palavras-chave: Brussonol. Ictexanos diterpenoides. Atividade antiplasmodial. Mobilização de cálcio.



## LIST OF FIGURES

<b>Figure 1</b> - <i>Plasmodium</i> life cycle.....	30
<b>Figure 2</b> - Malaria Prevention and Diagnosis strategies to avert malaria infections.....	35
<b>Figure 3</b> - Antimalarials chemical structures.....	36
<b>Figure 4</b> - Malaria treatment.. ..	39
<b>Figure 5</b> - Chemical structures of terpenes and diterpenoids. . ..	45
<b>Figure 6</b> – Chemical structures of icetexanes. (a) General structure for each subgroup of icetexanes.....	46
<b>Figure 7</b> – Design of brussonol analogs as new <i>P. falciparum</i> inhibitors.....	54
<b>Figure 8</b> - SAR summary around the icetexane diterpenoid scaffold.....	57
<b>Figure 9</b> - Analysis of resistance index (RI) of brussonol against a panel of resistant <i>P. falciparum</i> strains.. ..	59
<b>Figure 10</b> - <i>Ex vivo</i> susceptibility of <i>Plasmodium</i> spp. to brussonol.....	60
<b>Figure 11</b> - Speed-of-action assessment of brussonol. ....	62
<b>Figure 12</b> - Speed-of-action assessment of brussonol series. ....	64
<b>Figure 13</b> - Speed-of-action assessment of brussonol series with parasites starting at trophozoite stage. ....	66
<b>Figure 14</b> - Combination assessment between brussonol and artesunate.....	68
<b>Figure 15</b> – Isoprenoid biosynthesis in <i>Plasmodium</i> parasites.....	76
<b>Figure 16</b> - Ca <sup>2+</sup> -dependent signaling pathway in <i>Plasmodium</i> spp.....	79
<b>Figure 17</b> - Channels, carriers, and pumps. ....	80
<b>Figure 18</b> - Schematic representation of ion transports that occur in the malarial parasite. ....	82
<b>Figure 19</b> – Established normal glycolytic and tricarboxylic-acid (TCA) cycle compared with those specifically observed in <i>P. falciparum</i> . ....	83
<b>Figure 20</b> - Chemical “rescue” assay to evaluate the action of brussonol (1) in the metabolism of isoprenoids. ....	96
<b>Figure 21</b> - Effect of brussonol on the cytosolic Ca <sup>2+</sup> mobilization in <i>P. falciparum</i> loaded with Fluo-4 AM calcium indicator. ....	97
<b>Figure 22</b> - Effect of compounds 8 and 12 on the cytosolic Ca <sup>2+</sup> mobilization in <i>P. falciparum</i> loaded with Fluo-4 AM calcium indicator.....	98
<b>Figure 23</b> - Representative pH traces obtained from pH fingerprint assay, part 1.....	100
<b>Figure 24</b> – Representative pH traces obtained from pH fingerprin assay, part 2.....	101
<b>Figure 25</b> – Representative traces showing the effect of compound 12, or cip, on cytosolic [Na <sup>+</sup> ].....	102

<b>Figure 26</b> – Representative traces of bis-oxonol fluorescence.....	103
<b>Figure 27</b> – Morphological development of parasites cultured under pressure of compound 8. ....	105
<b>Figure 28</b> – Growth assays performed throughout in vitro studies. ....	107
<b>Figure 29</b> – Representative concentration-response curves of growth assays against <i>T. gondii</i> parasites. ....	109



## LIST OF TABLES

<b>Table 1</b> – <i>in vitro</i> antiplasmodial activity, cytotoxicity, and SI of brussonol and its derivatives.....	55
<b>Table 2</b> – Representative panel of MDR and sensitive <i>P. falciparum</i> strains. ....	58
<b>Table 3</b> - Brussonol's IC <sub>50</sub> values against a panel of sensitive (3D7) and MDR (K1, Dd2, TM90C6B) .....	59
<b>Table 4</b> - <i>Plasmodium</i> field isolates sensitivity to brussonol ( <b>1</b> ), divided by species. ....	60
<b>Table 5</b> - Concentration (mM) of components of solutions, salines and buffers used in the experiments described in this chapter. ....	88
<b>Table 6</b> - <i>In vitro</i> antiprotozoal activity of compound <b>8</b> against <i>P. falciparum</i> (3D7 and Dd2-Pol $\delta$ strains) and <i>T. gondii</i> (TatiAku80 strain). ....	108



## LIST OF ABBREVIATIONS AND ACRONYMS

AC	adenylyl-cyclase
ACTs	artemisinin-combination therapies
AL	artemether-lumefantrine
AQ	Amodiaquine
ART-R	artemisinin-partial resistance
ART	Artesunate
ASMQ	artesunate-mefloquine
ASPY	artesunate-pyronaridine
ATO	Atovaquone
BF <sub>3</sub> .Et <sub>2</sub> O	boron trifluoride diethyl etherate
Br <sub>2</sub>	Bromine
Ca <sup>2+</sup>	calcium ion
CaCl <sub>2</sub>	calcium chloride
CaM	Calmodulin
cAMP	cyclic-adenosine monophosphate
CC <sub>50</sub>	cytotoxic concentration needed to inhibit 50% of HepG2 growth
CDPK	calcium-dependent protein kinases
CDP-ME	4-diphosphocytidyl-2-C-methylerythritol
CDP-MEP	4-diphosphocytidyl-2-C-methylerythritol 2-phosphate
CEPEM	Research Center of Tropical Medicine
cGMP	cyclic-guanosine monophosphate
cip	Cipargamin
CO <sub>2</sub>	carbon dioxide
conA	concanamycin A
CPA	cyclopiazonic acid
CRISPR	clusters of regularly interspaced short palindromic repeats
cyt	Cytosolic
DAG	diacylglycerol
DCM	dichloromethane
DDT	dichlorodiphenyltrichloroethane
DHA	dihydroartemisinin
DHAP	dihydroartemisinin-piperaquine
DHFR	dihydrofolate reductase
DHPS	dihydropteroate synthase
DMAPP	dimethylallyl diphosphate
DMF	dimethylformamide
DMPU	<i>N,N'</i> -dimethylpropylene urea
DMSO	Dimethylsulfoxide
DNA	deoxyribonucleic acid
DV	digestive vacuole
DXP	1-deoxyxylulose 5-phosphate
DXR	deoxyxylulose-5-phosphate reductoisomerase
DXS	1-deoxy-D-xylulose 5-phosphate synthase

EDTA	ethylenediaminetetraacetic acid
EGTA	ethylene glycol-bis(2-aminoethylether)-N,N,N',N'-tetraacetic acid
EIPA	ethylisopropyl-amiloride
Epac	exchange protein directly activated by cAMP
ER	endoplasmic reticulum
Et <sub>3</sub> N	triethylamine
EtOH	Ethanol
EtSH	Ethanethiol
FBS	fetal bovine serum
FDA	Food and Drug Administration
F/GGPP	farnesyl/geranylgeranyl diphosphate synthase
FIC	fractional inhibitory concentration
FOS	fosmidomycin
Ftase	protein farnesyl transferase
GC	guanylyl-cyclase
GF	glucose-free saline
GMP	Global Malaria Programme
GMS	Greater Mekong Subregion
GPI	glycophosphatidylinositol
GPP	geranyl pyrophosphate
G6PD	glucose-6-phosphate dehydrogenase
H <sub>2</sub> O	Water
HCl	hydrochloric acid
HepG2	hepatocellular carcinoma cancer cell line
HMB-PP	( <i>E</i> ) 4-hydroxy-3-methyl-but-2-enyl pyrophosphate
IC <sub>50</sub>	half-maximum inhibitory concentration
IMC	inner membrane complex
IP <sub>3</sub>	inositol triphosphate
IP <sub>3</sub> R	inositol triphosphate receptor
IPP	isopentenyl pyrophosphate
IPTp	intermittent preventive treatment in pregnancy
IPTsc	intermittent preventive treatment in school-aged children
IQSC	Chemistry Institute of Sao Carlos
IRS	indoor residual spray
IspD	MEP cytidyltransferase
IspE	CDP-ME kinase
IspF	MEcPP synthase
IspG	HMB-PP synthase
IspH	HMB-PP reductase
ITNs	insecticide-treated nets
K <sup>+</sup>	potassium ion
K-13	Kelch propeller domain
propeller	
KCl	potassium chloride
K <sub>2</sub> CO <sub>3</sub>	potassium carbonate
KH <sub>2</sub> PO <sub>4</sub>	potassium dihydrogen phosphate

LAMP	loop-mediated isothermal amplification
LLINs	long-lasting insecticidal nets
LMICs	low- and middle-income countries
MDA	mass drug administration
MDR	multidrug-resistant
MeCN	acetonitrile
MeI	iodomethane
MeOH	methanol
MEP	methylerythritol phosphate pathway
MEcPP	2-C-methyl-D-erythritol 2,4-cyclopyrophosphate
MgSO <sub>4</sub>	magnesium sulfate
MoA	Mode of Action
MTT	3-(4,5-dimethylthiazol-2-yl)-2,5-diphenyltetrazolium bromide
“N”	category of natural product
N <sub>2</sub>	Nitrogen
NaCl	sodium chloride
NaH	sodium hydride
NaHCO <sub>3</sub>	sodium bicarbonate
NaH <sub>2</sub> PO <sub>4</sub>	monosodium phosphate
NaIO <sub>4</sub>	sodium periodate
“NB”	category of natural product “botanical”, it covers the “defined mixtures” recognized as drug entities
NBS	<i>N</i> -bromosuccinimide
<i>n</i> BuLi	<i>n</i> -butyllithium
ND	not determined
“ND”	category of natural product derivative, usually a semisynthetic modification
Ni	Nickel
NMO	4-methylmorpholine <i>N</i> -oxide
NPs	natural products
O <sub>2</sub>	Oxygen
OPPS	octaprenyl diphosphate synthase
OSO <sub>4</sub>	osmium tetroxide
PBO	pyrethroid-pyperonyl butoxide
PBS	phosphate buffer
PC	parasite clearance
PCR	polymerase chain reaction
Pd(dppf)Cl <sub>2</sub>	[1,1’-bis(diphenylphosphino)ferrocene]dichloropalladium(II)
PDMC	post-discharge malaria chemoprevention
PfCHA	Ca <sup>2+</sup> /H <sup>+</sup> antiporter PfCHA
PfCAX	Ca <sup>2+</sup> /H <sup>+</sup> exchanger
<i>pfhrp2</i>	<i>Plasmodium falciparum</i> histidine rich protein 2
<i>pfhrp3</i>	<i>Plasmodium falciparum</i> histidine rich protein 3
<i>pfmdr1</i>	<i>Plasmodium falciparum</i> multidrug resistant transporter 1
pH	potential of hydrogen

PIFA	[bis(trifluoroacetoxy)iodo]benzene
PIP <sub>2</sub>	phosphatidyl inositol biphosphate
PKA	protein kinase A
PKB	protein kinase B
PKG	protein kinase G
PLC	phospholipase C
PM	primary metabolite
PMC	perennial malaria chemoprevention
PPM	parasite plasma membrane
PSY	phytoene synthase
PV	parasitophorous vacuole
PYR	pyrimethamine
RBC	red blood cell
iRBC	infected red blood cell
pRBC	parasitized red blood cell
RDT	rapid diagnostic test
RI	resistance index
RSA	ring survival assay
RO	Rondônia
“S*”	NP inspired category, synthetic compound containing a NP pharmacophore
“S/NM”	NP inspired category, synthetic compound that mimic a NP, usually being a competitive inhibitor of a natural substrate
“S*/NM”	NP inspired category, synthetic compound containing a NP pharmacophore, and it is a competitive inhibitor of a natural substrate
SAR	structure-activity relationship
SD	standard deviation
SI	selectivity index
SM	secondary metabolite
SMA	schizont maturation assay
SMC	seasonal malaria chemoprevention
SP	sulfadoxine-pyrimethamine
SQS	squalene synthase
TGA	Therapeutic Goods Administration
THF	Tetrahydrofuran
TMEDA	<i>N,N,N',N'</i> -tetramethylethylenediamine
USP	University of Sao Paulo
VP1	vacuolar-H <sup>+</sup> -pyrophosphatase
V-ATPase	vacuolar-H <sup>+</sup> -ATPase
VC	Vector Control
WHO	World Health Organization

## LIST OF SYMBOLS

m/v	mass/volume
$x g$	multiples of the earth's gravitational field
v/v	volume/volume
$\mu\text{L}$	Microliters
$\mu\text{M}$	Micromolar
H	Hour
%	Percentage
Min	Minute
Nm	Nanometer
$\mu\text{g}$	Microgram
mL	Mililiter
Mg	Milligram
mM	Millimolar
$\lambda_{\text{ex}}$	excitation wavelength
$\lambda_{\text{em}}$	emission wavelength
F <sub>max</sub>	maximal fluorescence
F <sub>min</sub>	minimal fluorescence
F	fluorescence data collected
K <sub>d</sub>	dissociation constant
$\Delta\psi$	membrane potential





## CONTENTS

CHAPTER 1:	27
1 INTRODUCTION	29
1.1 Malaria Overview	29
1.2 Malaria prevention, diagnosis, and treatment	32
1.2.1 Malaria prevention	32
1.2.2 Diagnosis	34
1.2.3 Treatment	35
1.3 Antimalarial Drug Resistance	40
1.4 Development of new antimalarials	43
1.5 OBJECTIVES	47
1.5.1 General objectives	47
1.5.2 Specific objectives	47
1.6 MATERIALS AND METHODS	47
1.6.1 Maintenance of <i>P. falciparum</i> <i>in vitro</i> culture	47
1.6.2 <i>In vitro</i> evaluation of antiplasmodial activity against <i>P. falciparum</i> blood stage parasites	48
1.6.3 SYBR Green I assay	48
1.6.4 Cytotoxic tests using immortalized cells	49
1.6.5 Calculation of selectivity index (SI)	50
1.6.6 Resistance assessment and calculation of resistance index (RI)	50
1.6.7 Schizont maturation assay (SMA) with field isolates	51
1.6.8 Maintenance of <i>P. knowlesi</i> parasites and evaluation of inhibitory potency of compound 1	52
1.6.9 Speed of action assay	53
1.6.10 <i>In vitro</i> combination with artesunate	53
1.7 RESULTS	54
1.7.1 Brussonol and derivatives	54
1.7.2 Biological evaluation of brussonol and derivatives	55
1.7.3 Brussonol is active against a panel of <i>P. falciparum</i> resistant strains	58
1.7.4 Brussonol shows potent inhibition against <i>P. falciparum</i> and <i>P. vivax</i> field isolates	60
1.7.5 Brussonol inhibits <i>P. knowlesi</i> parasites	61
1.7.6 Compounds show fast-acting <i>P. falciparum</i> inhibition	61

1.7.7	<i>In vitro</i> combination of compound 1 with artesunate shows additive profile. ....	67
1.8	DISCUSSION .....	68
CHAPTER 2: .....		73
2	INTRODUCTION .....	75
2.1	Mode of Action (MoA) studies. ....	75
2.1.1	Isoprenoid biosynthesis. ....	75
2.1.2	Calcium signaling.....	77
2.1.3	Transport in malaria parasite plasma membrane (PPM).....	79
2.1.4	Na <sup>+</sup> -extruding transporter, <i>Plasmodium falciparum</i> P-type ATPase 4 (PfATP4). 81	
2.1.5	Lactate-extruding transporter, <i>Plasmodium falciparum</i> Formate-Nitrate Transporter (PfFNT). ....	82
2.1.6	V-type H <sup>+</sup> ATPase.....	83
2.1.7	Cl <sup>-</sup> transporter. ....	84
2.1.8	Membrane Potential. ....	85
2.1.9	<i>In vitro</i> evolution studies.....	86
2.1.10	Antiprotozoal activity against <i>Toxoplasma gondii</i> .....	87
2.2	OBJECTIVES .....	87
2.2.1	General objective.....	87
2.2.2	Specific objectives.....	88
2.2.3	Assessment of compound's 1 effect in isoprenoid biosynthesis.....	88
2.2.4	Determination of compounds 1, 8 and 12 interferences in cytosolic calcium levels. .....	88
2.2.5	Comparison of derivatives' pH fingerprint with known <i>Plasmodium</i> transporters inhibitors.....	88
2.2.6	Investigation of compound's 12 effect on cytosolic sodium levels.....	88
2.2.7	Evaluation of compound's 12 effect on parasite's membrane potential. ....	88
2.2.8	<i>In vitro</i> evolution studies with compound 8. ....	88
2.2.9	Evaluation of inhibitory activity of compound 8 against <i>Toxoplasma gondii</i> TatiΔku80 strain. ....	88
2.3	MATERIALS AND METHODS .....	88
2.3.1	Preparation of solutions and buffers. ....	88
2.3.2	Chemical rescue assay with IPP supplementation. ....	89
2.3.3	Fluorescent calcium cytosolic concentration measurements.....	89
2.3.4	pH fingerprint assay.....	89
2.3.5	Fluorescent cytosolic sodium measurements. ....	91
2.3.6	Membrane potential evaluation. ....	92

2.3.7	<i>In vitro</i> evolution studies. ....	93
2.3.8	Maintenance and inhibitory potency assessment of compound 8 activity against <i>Toxoplasma gondii</i> . ....	94
2.4	RESULTS .....	95
2.4.1	IPP supplementation does not reverse compound's 1 inhibition. ....	95
2.4.2	Compound 1 induced an increase in $[Ca^{2+}]_{cyt}$ in <i>P. falciparum</i> . ....	96
2.4.3	Compounds 8 and 12 do not target PfATP4, PfHT, PfFNT, and Cl <sup>-</sup> transporter. .	98
2.4.4	Compounds 12 did not disrupt parasite $[Na^{+}]_{cyt}$ . ....	101
2.4.5	Compound 12 may hyperpolarize the PPM. ....	102
2.4.6	<i>In vitro</i> evolution studies with Compound 8. ....	104
2.4.7	Compound 8 showed inhibition against <i>Toxoplasma gondii</i> . ....	108
2.5	DISCUSSION .....	109
3	GENERAL CONCLUSIONS AND PERSPECTIVES .....	113
	REFERENCES .....	115
	ANEXES .....	131



**CHAPTER 1:****INVESTIGATING THE PARASITOLOGICAL PROFILE OF  
BRUSSONOL AND DERIVATIVES AGAINST *PLASMODIUM SPP.*  
PARASITES**



## 1 INTRODUCTION

### 1.1 Malaria Overview

Malaria is a parasitic disease caused by protozoan parasites from the phylum Apicomplexa. Even though there are five *Plasmodium* species that naturally infect humans, *Plasmodium malariae*, *P. ovale*, *P. vivax*, *P. falciparum*, and *P. knowlesi*,<sup>1</sup> *P. vivax* and *P. falciparum* are the ones that pose a major threat. In one hand, *P. vivax* is the most widely distributed parasite,<sup>2-3</sup> being the dominant species across Central and South America, in the Horn of Africa, and in much of Asia-Pacific.<sup>3</sup> Additionally, the dormant liver-stage of vivax parasites, also known as hypnozoites, constitute a reservoir of infection, which contributes to extend the geographic range of vivax malaria.<sup>2</sup> On the other hand, *P. falciparum* is the deadliest malaria parasite, being prevalent in the African continent and accounting for more than 90% of malaria cases in the world.

The life cycle of *Plasmodium* spp. is complex and involves two hosts: one vertebrate, where the asexual phase happens; and one invertebrate, which serves as vector, and where the sexual reproduction occurs (**Figure 1**). The protozoan parasites are transmitted to humans during a blood meal of a malaria-infected female *Anopheles* mosquito, this is when the sporozoites are inoculated into the human's dermis.<sup>4-5</sup> Upon inoculation, the sporozoites traverse to the hepatic tissue, infiltrating hepatocyte cells wherein they engage in exoerythrocytic schizogony. This process entails an asexual division characterized by initial genomic duplication, giving rise to multinucleated cells. Subsequent cytokinesis ensues, culminating in the generation of numerous merozoites. Several days later, contingent upon the specific parasite species, a multitude of merozoites is liberated into the bloodstream, initiating the intra-erythrocytic phase by invading erythrocytes.<sup>6-8</sup> Furthermore, a small number of parasites, in case of *P. vivax* and *P. ovale* infections, may remain into the hepatocytes in hypnozoites form, which could lead to relapses months later without the occurrence of another infection.

The erythrocytic phase is characterized by a sequence of synchronous and periodic events. It begins with the contact between merozoite and red blood cell (RBC),<sup>9</sup> followed by its attachment to the erythrocyte's membrane,<sup>10</sup> which culminates with the merozoite entering the RBC. Once inside the erythrocyte, the parasite grows forming the ring stage, which enlarges to fill the cell forming the trophozoite stage. Next, the parasite undergoes erythrocytic schizogony becoming a schizont formed by merozoites. This cycle finishes upon release of the merozoites into the bloodstream, where other RBCs can be invaded restarting the cycle.<sup>7</sup> A small proportion

of the merozoites commit to sexual differentiation, producing male and female gametocytes, which are required for parasite transmission from the human host to the mosquito.<sup>8, 11</sup> The next phase begins when these gametocytes are ingested by a mosquito during a blood meal.

Inside the mosquito's midgut lumen, the gametocytes are exposed to specific conditions, such as lower temperature, increase in pH and exposure to xanthurenic acid,<sup>12</sup> required for them to mature and culminate with the formation of gametes. The following step is fusion between the gametes, forming the zygote, which develops into a motile form, the ookinete. This motile form penetrates the midgut epithelium, forming an oocyst in the basal side.<sup>13</sup> Subsequent to this stage, multiple rounds of mitosis occur, resulting in the generation of a profusion of sporozoites. These sporozoites are subsequently discharged following the rupture of the oocyst, facilitating their migration to the salivary glands of the mosquito. Upon an infectious bite, these sporozoites are transmitted to a vertebrate host.<sup>8, 11, 14</sup>

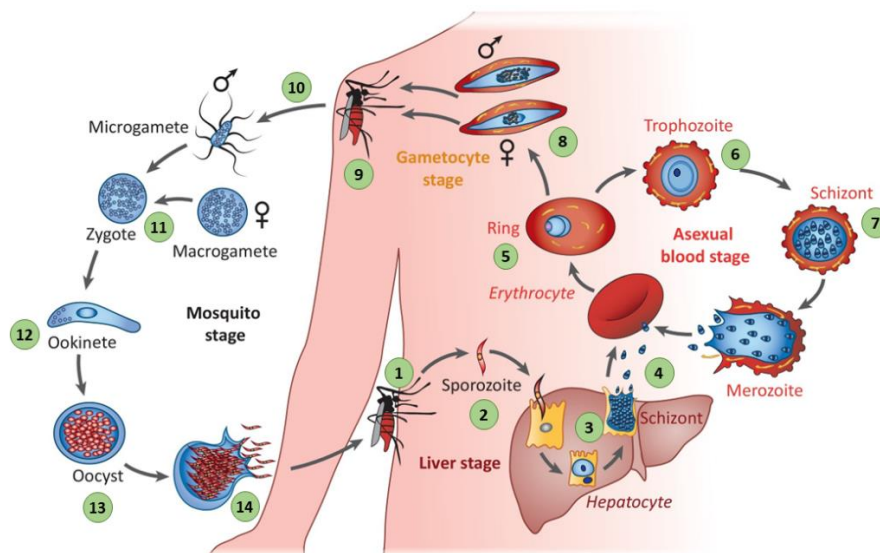


**Figure 1 - Plasmodium life cycle.** The two malarial hosts, vertebrate, and mosquito are depicted in this image. The parasite's life cycle starts with the inoculation of sporozoites (2) during a blood meal (1) of a female *Anopheles* mosquito. These sporozoites migrate to the liver, invading hepatocytes, where they undergo schizogony, leading to the production of merozoites (3). Later, merozoites are released into the bloodstream, where they invade RBCs (4). Once inside the erythrocyte, the parasite undergoes various developmental steps culminating with the formation of three different stages: rings (5), trophozoites (6) and schizonts (7), which contains merozoites. Following release of these merozoites, they can invade new RBCs (4), repeating this erythrocytic propagation cycle. Few merozoites are committed to sexual differentiation, it is when the male and female gametocytes are formed (8). Transmission from humans to mosquitoes occurs when a female anopheline mosquito ingest these gametocytes during a blood meal (9). Inside the mosquito gut, these gametocytes develop into gametes (10), which will form the zygote via fusion of the micro and the macrogamete (11). The zygote forms the ookinete (12), which encysts in the basal side of the midgut epithelium, forming the oocyst (13). Multiple mitosis cycles occur inside the oocyst, leading to the production of numerous sporozoites, that, once released, migrate to the salivary glands of the mosquito, awaiting to be delivered to another vertebrate host upon an infectious bite (14).

Source: Adapted from MAIER *et al.*<sup>15</sup>



Malaria is a tropical disease that affects low- and middle-income countries (LMICs), inflicting economic burdens in different aspects: public health spending, economic growth, foreign investment and tourism attraction, internal human movements, and cognitive development of affected children.<sup>16-17</sup> According to the World Health Organization (WHO),<sup>18</sup> the number of estimated malaria cases occurring in 85 endemic countries was 249 million, while 608 000 of estimated deaths in 2022. 93.6% of these cases and 95.4% of these deaths occurred in the WHO African Region, with more than 78% of these deaths being of children under the age of 5 years. In the WHO Region of the Americas, it was estimated the occurrence of 552 000 cases and 343 deaths, with 73% of all cases being accounted for in the Bolivarian Republic of Venezuela, Brazil, and Colombia.

Even though the percentage of malaria cases in the Americas (0,22%) is 451-fold lower than the number of cases in Africa (93.6%), this disease is still a serious public health issue in this region, especially due to biological characteristics of vivax malaria, which accounted for 72% of malaria cases in 2022. These biological traits pose challenges for control measures towards vivax infections, such as early gametocyte transmission to mosquitoes, low parasitemia hindering detection by light microscopy, hypnozoites ability to confer recurrences, and common asymptomatic infections favoring parasite repository.<sup>19</sup> Furthermore, more studies must be done to comprehend *P. vivax* biology and epidemiology, as well as the importance of bone marrow and spleen reservoirs for vivax infections and relapses.<sup>20-21</sup>

Malaria infections can be classified as asymptomatic, uncomplicated, and severe (or complicated). Normally, infections showing clinical symptoms are associated with patent parasitemia.<sup>16</sup> The onset of malaria symptoms start after the period of incubation is completed, and they appear because of the release of malaria parasites and toxins into the bloodstream following the schizont rupture.<sup>22</sup> The initial malaria symptoms are non-specific, and it can be difficult to diagnose. Some of them are headaches, fatigue, muscle aches, chills, sweating, and abdominal discomfort followed by irregular fever. For a portion of cases, these symptoms can escalate to severe life-threatening complications, namely severe anemia malaria, respiratory distress, cerebral malaria, acute renal failure, and so on.<sup>16, 22-23</sup>

Considering that malaria is an ancient disease, and yet still affects millions of people globally, causing the death of thousands, especially young children each year, efforts have been made throughout the years to control and eliminate this disease. A set of guidelines and recommendations was created by WHO to coordinate the international response to this disease. The Global Malaria Programme (GMP) has a vital role coordinating WHO's efforts in the fight

against malaria, as they support the Member States through their attempts to adapt, adopt, and implement WHO guidelines. WHO's strategy has three pillars<sup>24</sup>: (1) expand the access of malaria prevention, diagnosis, and treatment; (2) countries need to boost efforts to decrease transmission, especially in areas with low transmission. It is suggested implementation of case detections and investigations as part of the surveillance and response programmes; (3) use surveillance as a key intervention to accelerate progress. It requires a robust surveillance system where it would direct resources, identify gaps in coverage, detect outbreaks, and assess the impact of interventions to guide the national strategic plan.

## 1.2 Malaria prevention, diagnosis, and treatment

### 1.2.1 Malaria prevention

Malaria prevention is an attempt to avoid all the harm that this disease could cause to half the world's population at risk. *Plasmodium* spp. infections can be averted by three different strategies: vector control (VC), chemoprevention, and vaccines (**Figure 2**).

VC – since the discovery that arthropods have a role on transmitting diseases to humans, and while vaccines and treatment for these diseases were not always available, the idea of preventing transmission via VC was the convenient one. Some of the early VC strategies included screening of houses, use of mosquito nets, and drainage or filling of swamps used by mosquitoes as breeding sites. Nowadays, VC approaches focus on the use of insecticides to target both the larval and the adult stages of the mosquito. Control programs consider four points before determining which strategies are better suited to the region: (1) blood-feeding preferences of the mosquito (zoophily/anthropophily); (2) place where blood-feeding happens (endophagy/exophagy); (3) the interplay between biting peak and sleeping patterns of humans; and (4) the mosquito's choice of post-feeding place (endophily/exophily).<sup>25</sup> Currently, there are four options of insecticide-treated nets (ITNs) that WHO recommends for deployment: pyrethroid-only long-lasting insecticidal nets (LLINs), pyrethroid-piperonyl butoxide (PBO) nets, and, more recently, pyrethroid-chlorfenapyr nets and pyrethroid-pyriproxyfen nets. Additionally, indoor residual spray (IRS) with a product prequalified by the organization.<sup>26</sup> In South America, larval control is recommended in Colombia and Venezuela, and in Brazil the larval control is performed by cleaning selected breeding sites.<sup>27</sup> Consequently, the VC interventions not only has a direct benefit on health, but also can greatly contribute to human and economic development. Bhatt and colleagues<sup>28</sup> estimated that between 2000 and 2015,

these interventions prevented 663 million clinical cases in Africa, of which 68% were accounted for ITNs usage, and 10% for IRS.

Chemoprevention – consists of giving a treatment course of antimalarial drugs to a target population, even though they are not infected. WHO recommends six different chemoprevention strategies: (1) intermittent preventive treatment of malaria in pregnancy (IPTp): antimalarial treatment course is administered at predetermined intervals; (2) seasonal malaria chemoprevention (SMC): a curative dose is administered intermittently to a child during the malaria season, which is the period of high malaria danger; (3) perennial malaria chemoprevention (PMC) is used to avert illness in areas possessing moderate to high malaria transmission settings, and it comprises a full treatment course administration malaria medicines to young children, which poses greatest risk of severe malaria, at predefined intervals; (4) intermittent preventive treatment of malaria in school-aged children (IPTsc): consists in the application of full treatment courses at regular intervals to treat and prevent malaria in children old enough for attending school; (5) post-discharge malaria chemoprevention (PDMC) is the administration of a full malarial treatment to children admitted with severe anemia at regular intervals, preventing new infections in the period after hospital discharge; (6) mass drug administration (MDA) is the application of a full therapeutic antimalarial course at similar time, and often at repeated intervals, to all age groups of a population in a defined region. Finally, there is also an approach defined as chemoprotection, which describes the use of antimalarials, at prophylactic doses, to protect temporarily individuals entering a high endemic or recently malaria-free areas, to protect populations at risk from emergent epidemics.<sup>25</sup>

Vaccines – it is a safe approach that employs a biological product able to induce an immune response, conferring protection against an infection (or disease) upon later exposure to a pathogen.<sup>29</sup> There are numerous examples of how immunization has transformed public health and averted the deaths of countless people. For example, 23 million people had their lives saved upon measles immunization, between 2000 and 2018. In fact, through immunization, 20 life-threatening diseases can be prevented.<sup>25</sup> In regard to malaria, since late 1960s researchers were searching for a vaccine; it took more than 35 years for the vaccine RTS,S/AS01 to be developed and WHO approved its use to prevent malaria in children in 2021.<sup>25</sup> Nonetheless, this vaccine only provides 30 – 40% protection.<sup>29</sup> Even though efficacy of this vaccine is low, WHO reported that 2 million children from Ghana, Kenya and Malawi received RTS,S/AS01, which led to a 13% decrease in early childhood deaths from all causes and a significant decline in severe malaria cases.<sup>18</sup> In 2023, a new malaria vaccine, R21/Matrix-M, which exhibited

efficacy ranging from 67% to 75%<sup>30</sup>, was also recommended by WHO to be used as a prevention tool.<sup>31</sup> Both vaccines are indicated to prevent falciparum infections in endemic areas, focusing on areas with moderate and high transmission settings.<sup>18</sup> New malaria vaccines are in development with the desire to develop a vaccine with higher efficacy, targeting distinct stages of the parasite, or even avoiding mosquitoes' bite. These different vaccine approaches could have a significant impact on reducing malaria transmission.<sup>29</sup>

### 1.2.2 Diagnosis

An accurate and fast diagnosis (in less than 72 h) of *Plasmodium* spp. is not only essential to determine the correct treatment regimen, but also for malaria control measures that should be established in the region.<sup>32</sup> WHO recommends testing for all suspected malaria patients before treatment.<sup>33</sup> This assessment can be performed via light microscopy,<sup>34</sup> which allows the visualization of the parasite and its many stages on both blood thin and thick films of the same individual, or via a rapid diagnostic test (RDT),<sup>35</sup> which detects specific antigens (proteins) of the parasite in the individual's blood. WHO recommends the light microscopy method because it is inexpensive and it allows the differentiation between *Plasmodium* spp.; however, it could present low sensitivity when performed by poorly trained personnel, it is time consuming, and sequestered parasites cannot be detected<sup>36</sup> (**Figure 2**)

In the case of RDTs, they are easy and simple to use with little expertise required, and these tests are easily transported.<sup>36</sup> Nonetheless, occurrence of false positives, which could be caused by poor specificity and sensitivity, and by the persistence of the parasite's antigens even after their parasite clearance.<sup>37</sup> Additionally, another concern is the increasing reports of *P. falciparum* clinical isolates showing deletions for genes HRP2 (*pfhrp2*), which is the predominant target for the RDTs tests, and HRP3 (*pfhrp3*), which can also be detected using this method. Therefore, the expansion of *Pfhrp2/3*-deleted parasites could lead to an increase of false negative RDT results, and, unfortunately, alternative RDT options are limited, and there are no WHO-prequalified tests that detects other antigens available yet.<sup>26</sup> There are detecting methods (i.e. conventional, real-time or nested-PCR,<sup>38</sup> LAMP,<sup>38-39</sup> and CRISPR-based method<sup>40</sup>) with higher specificity and sensitivity available; however, those techniques are expensive, require heavy training, and they are not suited for field settings (**Figure 2**).

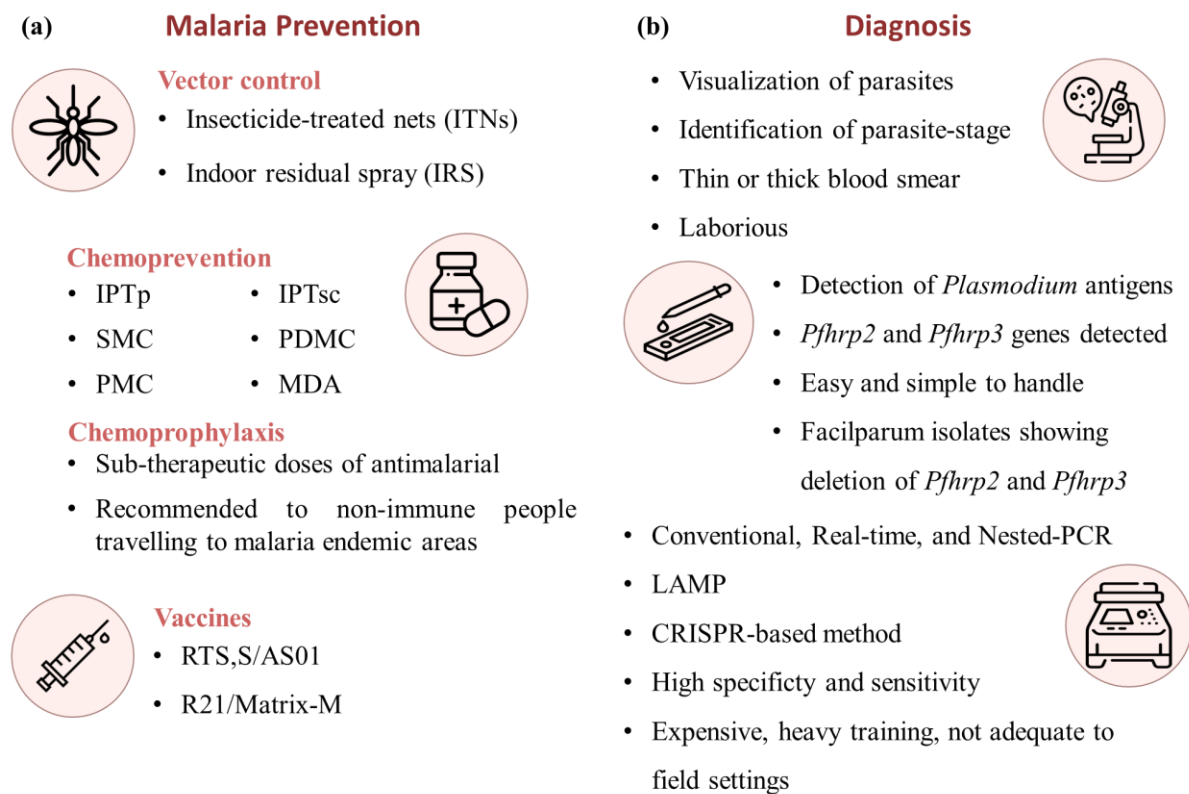


**Figure 2 - Malaria Prevention and Diagnosis strategies to avert malaria infections.** In this figure it is specified strategies used in malaria control programs. (a) Malaria Prevention comprises Vector Control, Chemoprevention, Chemoprophylaxis and Vaccines approaches, and (b) Diagnosis it is described the gold standard method, light microscope, to detect malaria infection. In this approach it is possible to visualize parasites from blood smears. Rapid Diagnostic Tests (RDTs) can detect plasmodium antigens in an easy and simple manner. Even though this approach made malaria detection faster, the emergence of parasites lacking *Pfhrp2* and *Pfhrp3* is a concern and could increase the number of false negatives. There are methods with higher specificity and sensitivity; however, they are expensive, require heavy training and are not adequate for field settings.

Source: By the author.

### 1.2.3 Treatment

The three main purposes for malaria treatment are avert death or long-term deficits from the disease, halt the morbidity of an acute infection, and clear the parasite, including hypnozoites, and halt transmission.<sup>41-42</sup> To do so, the malaria treatment course has changed over the years in response to declining drug efficacy. Before the introduction of synthetic antimalarials, treatment was commonly performed by using medicinal plants as a source of cure, such as the use of powdered bark of the Peruvian tree *Cinchona calisaya* since 1600s (discovery of quinine)<sup>43</sup> and the use of an herb obtained from *Artemisia annua* L. plant 2000 years back in China (discovery of artemisinin).<sup>44</sup> Currently, the antimalarials available for clinical use can be divided into five classes, which will be described in the following paragraphs. Structures of the described antimalarials are depicted in **Figure 3**.

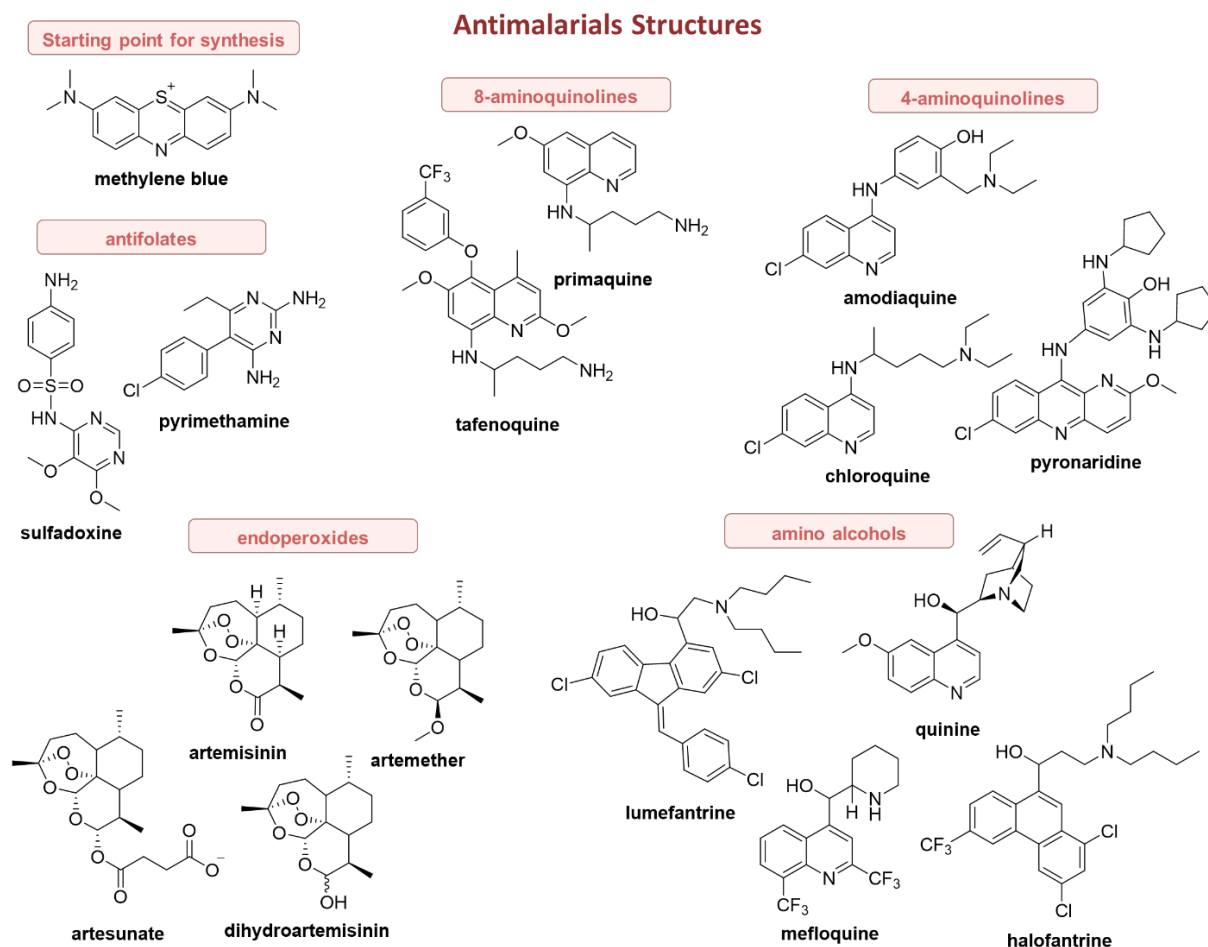


**Figure 3 - Antimalarials chemical structures.** In this figure it is depicted the chemical structure of the antimalarials used for treatment nowadays. These compounds are divided into 5 classes: 4-aminoquinolines, amino alcohols, 8-aminoquinolines, endoperoxides and antifolates. The structure of methylene blue is also depicted since this compound had a historical importance as a starting point for the synthesis of the compounds with antiplasmodial activity.

Source: By the author.

Following the identification of quinine as one of the bioactive compounds from the *Cinchona* tree's extract displaying antimalarial activity, chemist William Henry Perkins tried to synthesize this compound in 1856; however, his efforts resulted in the synthesis of methylene blue,<sup>45</sup> the first synthetic textile dye. Total synthesis of quinine was accomplished in 1944 by Woodward-Doering/Rabe-Kindler.<sup>46</sup> From the discovery that methylene blue could stain malaria parasites, and the use of this dye to cure two malaria patients in 1891, methylene blue was used as a starting point to synthesize compounds with antiplasmodial activity. In fact, structural modifications applied to this compound series yielded primaquine, an 8-aminoquinoline derivative, and chloroquine, a 4-aminoquinoline derivative. Another class of quinine derivatives is the amino alcohols, which are represented by halofantrine, mefloquine, lumefantrine and quinine itself.<sup>45</sup>

The 8-aminoquinolines show interesting antimalarial properties, especially displaying inhibitory activity against pre-erythrocytic forms of all *Plasmodium* spp. and being used for the radical cure of *P. vivax* and *P. ovale* due to their ability to kill hypnozoites.<sup>45</sup> Until recently, primaquine was the main representative of this class, requiring a 14-day treatment regimen (**Figure 4**); in 2018, tafenoquine was approved by two regulatory agencies, the United States Food and Drug Administration (FDA) and the Australian Therapeutic Goods Administration (TGA) to be used as a substitute of primaquine once it has the advantage of being a single-dose treatment. Indeed, the Brazilian Ministry of Health recently incorporated tafenoquine into the Unified Health System, known as SUS, to treat malaria.<sup>47</sup> One disadvantage of both compounds is the fact that they can cause hemolytic anemia in individuals with glucose-6-phosphate dehydrogenase (G6PD) deficiency.<sup>48</sup>

The 4-aminoquinoline series contains several antimalarials that are still recommended by WHO to be used for malaria treatment, some examples include amodiaquine, naphthoquine, piperazine, hydroxychloroquine, pyronaridine, and chloroquine (CQ), with the latter being the most effective antimalarial used so far. During the WHO Global Eradication Programme in 1950s and 1960s, CQ chemoprophylaxis in conjunction with DDT employment for vector control was an essential approach for eradications and control strategies in different parts of the world. With the advent of chloroquine resistance in 1960s, its use has declined.<sup>45,49-50</sup> Currently, chloroquine is used to treat non-falciparum uncomplicated malaria, namely *P. vivax*, *P. knowlesi*, *P. ovale* and *P. malariae*, where chloroquine resistance is not present, including Brazil (**Figure 4**).<sup>25</sup>

Antifolates are a class of antimalarials that interferes with the folate metabolism, which is crucial for the synthesis of thymine, purine nucleotides and amino acids, being an essential parasite pathway showing homologs in humans.<sup>49</sup> Compounds targeting two key enzymes of this pathway, dihydropteroate synthase (DHPS) and dihydrofolate reductase (DHFR), were developed in early 1930s, leading to the identification of sulfadoxine, a DHPS-inhibitor with long half-life and enhanced toxicological properties, and pyrimethamine, a DHFR inhibitor. Both compounds are still used as a combination, even though selection of resistant parasites has happened due to the widespread use of this formulation.

Since 2001, WHO recommended the use of artemisinin-combination therapies (ACTs) as first-line treatment due to the selection of resistant parasites to all antimalarials described. ACTs correspond to the combination of two drugs, one being artemisinin or its derivative, while the partner drug shows long half-life.<sup>50</sup> As mentioned previously, artemisinin is the bioactive

compound isolated from the *Artemisia annua* tree, and it belongs to the sesquiterpene lactone endoperoxides class. In addition, dihydroartemisinin, artesunate, and artemether are the most common derivatives. These compounds are considered the most active and fast-acting antimalarials because they can reduce parasite's biomass considerably in one asexual cycle.<sup>45</sup> The idea of using ACTs is based on the parasitological profiles of both compounds used in the combination: artemisinin (or its derivatives) show a rapid-acting inhibition and short half-life, while the partner drug, due to its long half-life, contributes by killing the parasites that averted artemisinin's inhibition.<sup>50</sup>

It is advised that malaria treatment starts after a definitive diagnosis, except when the patient shows high clinical suspicion for this disease or signs of severe malaria (**Figure 4**). Three factors must be considered before determining the appropriate therapeutic regimen: (1) the infecting *Plasmodium* spp., (2) the clinical status of the patient, and (3) the drug susceptibility of the infecting parasites.<sup>51</sup> In uncomplicated malaria, the recommended treatment is to use a highly efficient oral medicine with low adverse-effects profile. For falciparum malaria the recommendation is the following ACTs for 3 days: artemether-lumefantrine (AL), artesunate-amodiaquine (AS+AQ), artesunate-mefloquine (ASMQ), dihydroartemisinin-piperaquine (DHAP), artesunate + sulfadoxine-pyrimethamine (AS+SP), and artesunate-pyronaridine (ASPY). Three new ACTs combinations (arterolane-piperaquine, artemisinin + piperaquine base, and artemisinin + naphthoquine) are in the pre-registration phase. Even though WHO does not recommend these last three combinations, they are already being used in some countries. These medications can be administered to adults (including pregnant women in the second and third trimesters, and women breastfeeding), and children (including infants). In the case of pregnant women in the first trimester, WHO now recommends the use of artemether-lumefantrine.<sup>25</sup> In Brazil, AL and ASMQ are two ACT options recommended to treat *P. falciparum*, mixed infections, and *P. vivax* and *P. ovale* recurrences.<sup>42</sup>

For non-falciparum uncomplicated infections, WHO recommendations must also consider parasite's susceptibility to the medications. In chloroquine-susceptible infections' areas adults and children with infections caused by *P. malariae*, *P. ovale*, *P. vivax* and *P. knowlesi* should be treated with either ACTs or chloroquine. In the case of Brazil, the first choice of treatment is CQ associated, or not, with primaquine, depending on *Plasmodium* spp. infection.<sup>42</sup> On the contrary, areas with chloroquine-resistant infections the chosen treatment should be ACT. Additionally, adults and children (except pregnant women, women breastfeeding infants known to have G6PD deficiency, infants <6 months old, and people with



G6PD deficiency) must be administered primaquine to prevent relapses of *P. ovale* and *P. vivax* infections.<sup>25</sup>

In the case of severe malaria, caused by either *P. falciparum*, *P. vivax* or *P. knowlesi*, the situation is different. Since the rapid clearance of parasites from the blood is crucial, it is suggested the administration of full doses of effective parenteral (intravenous or intramuscular) antimalarial treatment, followed by a 3-day treatment of ACT.<sup>42</sup> The drug of choice for parenteral administration is artesunate. In the absence of this medicine, artemether should be considered prior to quinine because intravenous administration of it can be dangerous.<sup>25</sup>

## Malaria Treatment

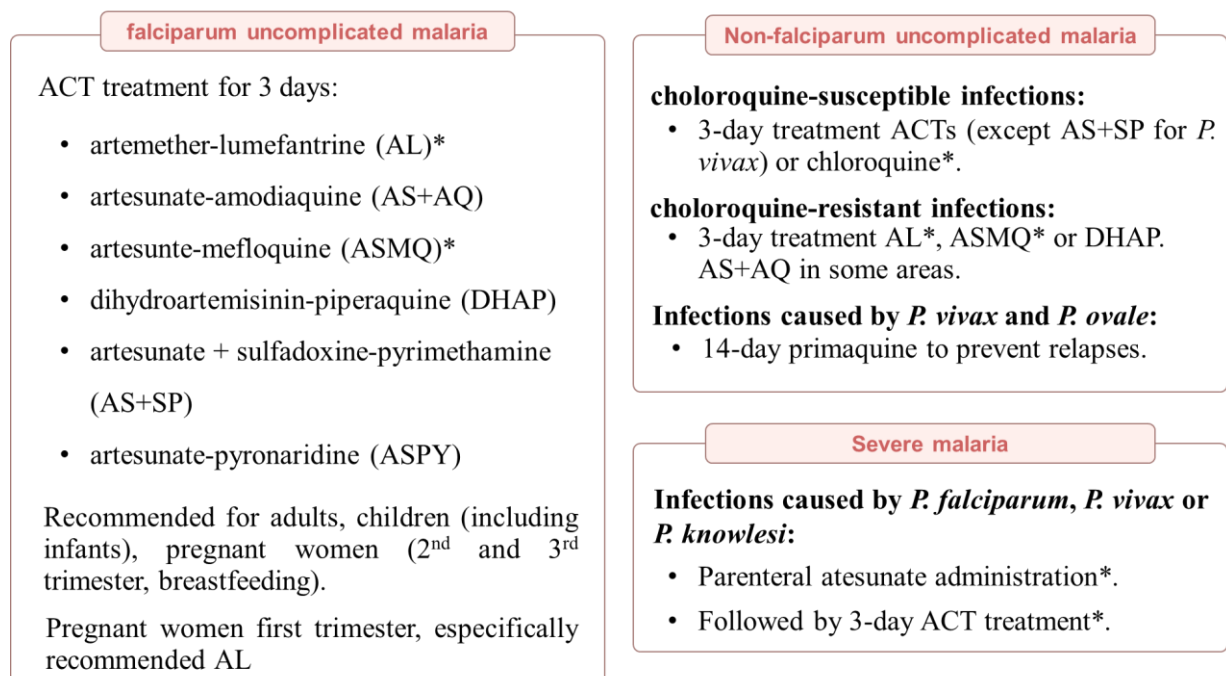


**Figure 4 - Malaria treatment.** It describes the recommended malaria treatment according to the type of infection the patient presents. It is important that the treatment starts after a proper diagnosis, so the best treatment course will be used, avoiding further complications and relapses. For falciparum uncomplicated malaria, it is recommended the use of ACTs for 3-day treatment. For non-falciparum uncomplicated malaria, it is recommended ACTs (except AS+SP for *P. vivax* infection) in chloroquine-sensitive infections; AL, ASMQ or DHAP, and in some areas AS+AQ, for chloroquine-resistant infections, followed by a 14-day course treatment of primaquine for infections caused by *P. vivax* and *P. ovale*. For severe malaria caused by *P. falciparum*, *P. vivax* or *P. knowlesi*, administration of parenteral artesunate for 24 h, or until the medication can swallow medicines, followed by 3-day course treatment of ACTs. Further information regarding malaria treatment can be found on WHO Guidelines for Malaria<sup>25</sup> and on Malaria Treatment Guidelines on Brazil<sup>42</sup>. \*Specifies the treatment for malaria recommended by the Ministry of Health in Brazil.

Source: By the author.

### 1.3 Antimalarial Drug Resistance

The spread of resistance to the currently available antimalarial therapy is a concern putting at risk all efforts that have been made towards reducing malaria burden.<sup>52</sup> According to the report on antimalarial drug efficacy from the GMP (2020), drug resistance is defined as “the ability of a parasite strain to survive or multiply despite the administration and absorption of a drug given in doses equal to or higher than those usually recommended, but within the tolerance of the subject”.<sup>53</sup> The common use of antimalarials in tropical regions, associated with significant need for malaria treatment and low patient compliance to treatment, increase the chances of selecting *Plasmodium* parasites with evolved resistance mechanisms.<sup>54</sup> Understanding these mechanisms is of utmost importance to design molecules less susceptible to select these resistant organisms. Genetic changes such as deletions, site mutations, and gene amplifications are often related to these mechanisms. Alternative strategies consist in the organism being able to decrease the drug’s therapeutic concentration or to eliminate the dependency on the drug’s target for survival.<sup>55</sup>

A surveillance system is needed to contain and monitor resistance’s spread, so that, in 1996, WHO developed a protocol to monitor antimalarial drug efficacy, and ever since, adjustments have been made according to local conditions and needs.<sup>56</sup> This protocol is important to policymakers collect information regarding drug efficacy, and once data is interpreted, they can decide whether maintaining malaria treatment policy or changing it to a more effective one. Treatment response is determined by observation of signs of clinical deterioration, presence of parasitemia and axillary temperature over a period of 28, or 42 days. Patients showing absence of parasitemia on day 28 (or 42), for *P. falciparum* or *P. vivax*, and who did not show signs of treatment failure, are considered a treatment success. For total treatment failure rates over 10%, WHO recommends a change in the first-line treatment for this disease.<sup>56-57</sup>

For some drugs, reduced drug sensitivity has been associated with specific genetic changes. It has been reported that resistance to quinolines is associated with gene mutations on the transmembrane protein of *P. falciparum* chloroquine resistance transporter (*pfcr*).<sup>58</sup> This is a transmembrane transporter localized in the digestive vacuole (DV) membrane, containing a negatively charged central cavity that is believed to accommodate positively charged drug/solutes that concentrate inside the DV, allowing its transport towards the cytosol, away from heme, the chloroquine’s target.<sup>52,54</sup> Another important player in resistance to heme-targeting antimalarials is *P. falciparum* multidrug resistance transporter 1 (*pfmdr1*), which

resembles a P-glycoprotein-type ABC transporter. It is also located in DV membrane, specifically on the cytosolic side. Mutations in this protein inhibit antimalarials transportation from the cytosol to the DV, thereby decreasing their concentration, limiting their access to their target.<sup>58</sup> On the other hand, there are situations where these mutations restrict transport of some antimalarials to DV, increasing sensitivity to these drugs because their target lies in the cytosol.<sup>58</sup>

Resistance to antifolates, pyrimethamine and sulfadoxine, is related to point mutations in DHFR and DHPS genes, respectively. Comparison in DHFR activity between sensitive (3D7) and resistant (HB3) strains suggested that resistance is likely due to structural modification in the protein's structure, due to changes in residue 108.<sup>59</sup> Additionally, identification of another residue (51) substitution in 7G8 strain, summing up to the fact that 7G8 is 50-fold more resistant than HB3 to pyrimethamine, suggests that this second mutation is required for high-level resistance.<sup>59</sup> In addition, analysis of both *dhps* genotype and IC<sub>50</sub> values against sulfadoxine were used to investigate if there is a correlation between genomic sequence and resistance levels. Wang and colleagues (1997)<sup>60</sup> reported that sulfadoxine susceptibility is affected by various identified mutations in the *dhps* gene. Change in residue A437G is enough to confer sulfadoxine resistance, and the level of resistance is increased (1-2 orders of magnitude) when this mutation is combined with further changes in the *dphs* structure. Finally, it has been suggested by Nzilla and colleagues (2000)<sup>61</sup> that pyrimethamine and sulfadoxine exert greater selective pressure on parasites than chlorproguanil/dapsone due to their longer half-lives.

Since 2000s, ACTs are the chosen first-line treatment of uncomplicated malaria in endemic areas. Signs of artemisinin partial resistance (ART-R) were first reported a decade ago in western Cambodia. A task force between WHO and the National Malaria Control Programmes of Cambodia and Thailand performed clinical trials to define treatment responses to artesunate (AS) in Pailin (Cambodia) and in Wang Pha (Thai-Burmese border).<sup>62</sup> Researchers reported that falciparum parasites had reduced *in vivo* susceptibility to ART in western Cambodia, especially because the overall median parasite clearance (PC) time in patients, after oral ART treatment, were 84 h in Pailin, while in Wang Pha it was 48 h.<sup>62</sup> It was highlighted that these differences in parasitologic responses were not explained by differences in patient's age, drug's pharmacokinetics, or molecular markers correlated with falciparum drug resistance. Furthermore, ART-R was not correlated to any molecular markers at this point.<sup>62</sup> This was the first time that drug resistance was associated with delayed PC instead of increasing levels of

drug to kill the parasite.<sup>54</sup> It is important to highlight that, as long as the partner drug stays effective, ART-R does not result in treatment failure.<sup>63</sup>

Currently, the phenotype associated with ART-R comprises delayed PC after treatment, which is defined as PC half-life > 5.5 h or detection of parasitemia 3 days after the beginning of treatment; and increased ring survival (> 1–2%) compared to control parasites upon 6 h exposure to 700 nM dihydroartemisinin to ring-stage parasites followed by 66 h of incubation.<sup>64–65</sup> The latter can be observed upon *in vitro* and *ex vivo* experiments, consisting of important surveillance approaches to identify parasites bearing artemisinin partial resistance where longer PC time is suspected.<sup>65</sup> Additionally, identification of reliable molecular markers to detect and monitor artemisinin resistance has proven difficult.

In 2014, Ariey and colleagues<sup>66</sup> associated mutations in the *PF3D7\_1343700* kelch propeller domain ('K13-propeller') as a potential artemisinin resistance molecular marker in Cambodia. In the beginning, they identified the M476I mutation in K13-propeller after a 5-year selection on the Tanzanian strain F32-ART5, and it was verified that this mutation correlated with increased RSA<sub>0-3h</sub> survival rates.<sup>66</sup> These findings were supported by clinical studies, which, upon analysis of 49 isolates from Cambodia, confirmed the significant association between polymorphisms in K13-propeller and RSA<sub>0-3h</sub> survival rates, with the mutant alleles having a 110-fold increase in survival rate.<sup>66</sup> Previous studies have shown a rapid dissemination of K13 C580Y mutation, which confers delayed PC *in vivo*, across Cambodia while there was a decline in frequencies of wild-type and non-C580Y mutants over time. Furthermore, in Southeast Asia, high rates of treatment failure as a consequence of ART-R in conjunction with ACT partner drug resistance.<sup>67-68</sup>

Now that high treatment failure rates have been associated with ART-R, when compounded with ACT partner drug resistance,<sup>67-68</sup> the likelihood of independent emergence of ART-R in sub-Saharan Africa is frightening, and its effects on malaria control and elimination might be devastating. Across the African continent, numerous studies have been conducted to examine the frequency of *Pfkl3* mutations. Throughout the years, different K13 mutations have established in different regions: R561H mutation showing prevalence of up to ~20% in Rwanda; C469F, C469Y, A675Y, R561H and P441I mutations show diverse frequencies with numbers as high as 40% in Uganda; and R662I mutation prevalence around 21% in 2019 in the Horn of Africa.<sup>64</sup> Additionally, despite P441I, the other five high prevalent mutations have been associated with both clinical and/or *in vitro* ART-R in Africa.<sup>64</sup> Regardless of the presented correlations above, not all K13 mutations confer ART-R.<sup>69</sup> A578S mutation

was observed at low frequency in Africa, and it did not confer ART-R *in vitro* in transfected Dd2 parasites.<sup>70</sup>

The emergence of antimalarial drug resistance has been a fact throughout the years, hence different strategies have been exploited to preserve the therapeutic lifespan of antimalarials. In the hope to minimize the threat and impact of antimalarial drug resistance, several interventions should be considered:

- Strengthen the surveillance of drug resistance, combining *in vivo* efficacy studies, *in vitro* assays and monitoring resistant molecular markers.<sup>71</sup>
- Optimize diagnostics before treatment, ensuring that drugs are administered only when parasites are detected.<sup>52</sup>
- Regulation of therapeutics use, preventing exposure of subtherapeutic drug levels and promoting equitable access to quality drugs.<sup>26</sup>
- Restricting drug use by focusing on malaria prevention strategies, such as ITNs and IRS.<sup>26, 52</sup>
- Recycling of antimalarials by complete withdrawal of the drug, until sensitive parasite reappears. This has been reported before.<sup>72-73</sup>
- Development of new treatments, triple ACTs (TACTs) for example.<sup>54</sup>
- Discovery and development of new antimalarials to limit malaria infection, transmission, and spread of resistance.<sup>26</sup>

#### 1.4 Development of new antimalarials

Numerous approaches, ranging from isolation and modification of natural products to screening of chemical libraries and designing inhibitors for known targets, have been applied to antimalarial drug discovery.<sup>74</sup> Phenotypic screens are whole-cell based assays of a specific parasite's lifecycle stage to determine compounds *in vitro* potency,<sup>75</sup> and it has some intrinsic advantages compared to the target-based screens.<sup>76</sup> This method allows compound assessment against all druggable targets within the cell,<sup>75</sup> so that identification of compounds having a cooperative effect or multiple targets are likely to occur.<sup>76</sup> Additionally, compounds showing poor physicochemical properties, such as membrane permeability, can be eliminated early on preclinical stages.<sup>75-76</sup> Finally, since prior knowledge on the compound's molecular target is not required to perform the assay, the probability of identifying molecules with new modes of action (MoA) is raised.<sup>76</sup> Nevertheless, compound optimization and safety evaluation might be

compromised due to the lack of information about molecular target, which could be a challenge to downstream development of the tested compounds.<sup>75,77-78</sup>

Since ancient times, humans have been using natural products (NPs), in the form of herbal formulations, as medicine to alleviate symptoms and treat diseases.<sup>79</sup> In fact, the therapeutic use of plants as medicine by humans might date back more than 60,000 years, according to fossil records.<sup>80</sup> NPs are substances holding attractive pharmacological effects, and which are produced by plants or animals, or found in nature.<sup>81</sup> These molecules are divided into three categories: primary metabolites (PM), secondary metabolites (SM), and high molecular weight polymeric molecules. The first and third categories consists of, respectively, intermediates of catabolic and anabolic pathways, which explains their requirement for survival, while polymeric components, which includes cellulose and proteins, are important for cell structure.<sup>81-82</sup> SMs, on the other hand, are smaller compounds possessing a wide variety of biological activities; they are important for the organism's interaction with its surroundings, and they are not needed for growth or development.<sup>81</sup>

Traditionally, NPs had a major role in drug discovery and development because of their structural diversity and biological activities.<sup>83</sup> Morphine (analgesic), quinine and artemisinin (antimalarials), tetracycline and penicillin (antibiotics), and lovastatin (lipid control agent) are some examples of naturally occurring compounds being marketed as drugs. In 1990, around 80% of marketed drugs were NPs or were based on NPs.<sup>83</sup> Since then, NP research has declined over the years, mainly in the pharmaceutical industry, for many reasons: the dominant model for drug discovery within the pharmaceutical industry, which prioritizes accurate and profitable hits.<sup>83</sup> Technical limitations, such as access to sufficient material to perform studies, variations in composition due to seasonal and environmental changes as well as extinction of organisms; the need to adapt assays based on NPs physicochemical properties;<sup>84</sup> regulations concerning intellectual property and benefit sharing with countries from where the biological material were obtained;<sup>85</sup> and so on. Moreover, to highlight the importance that NPs research still have on the drug discovery and development process, Newman and Cragg reported in 2020, upon revision of extensive data, that in almost 39 years, from 01/1981 until 09/2019, 36.3% (506) of the 1394 small molecules approved fell into the categories of natural product ("N"), natural product subdivisions ("NB", "ND"), or natural product-inspired categories ("S\*", "S\*/NM", and "S/NM"). Nonetheless, it is important to note that, for many diseases, synthetic compounds are the only category of the drugs approved.<sup>86</sup>

Plants constitute a major source of NPs. Because these organisms are sessile and face environmental challenges and stresses, they produce SMs as a mechanism of protection.<sup>87</sup> Plant

SMs are divided into phenols, terpenes, alkaloids, among others.<sup>87</sup> Certainly, terpenes constitute the largest and most diverse group of SMs, playing a major role in protecting plants from biotic and abiotic stresses.<sup>87-88</sup> Terpenes can be linear hydrocarbons or carbocyclic skeletons, and their classification is based on the number of isoprene units they contain (**Figure 5a**).<sup>88-89</sup> Oxygenation, hydrogenation and dehydrogenation are some reactions that terpenes might undergo to produce terpenoids.<sup>87</sup>

Due to the large number of compounds and structural diversity, a wide range of biological activities of human interest have been described for terpenes: applications in food, agricultural, cosmetic, and biotechnology industry; antitumor, antimicrobial, anti-inflammatory, and anti-insect activity; and inhibitory effects against microbes, fungi, herbivore pests, which explains their potential use to biopesticides production.<sup>87-88</sup> Two important examples of marketed terpene-based drugs are Taxol (anticancer drug, it is a diterpene that was isolated from *Taxus brevifolia* tree in 1964),<sup>90</sup> and artemisinin (antimalarial drug, it is a sesquiterpene lactone isolated from *Artemisia annua* in 1972). Finally, a recent literature review published by Tajuddeen and Heerden (2019)<sup>91</sup> presented 1524 NPs showing antiplasmodial activity reported from 2010 to 2017. Among all these compounds, 443 showed  $IC_{50} \leq 3.0 \mu M$  against at least one *P. falciparum* strain, and around 31% of these NPs were terpenoids, highlighting the potential that terpenes have as antiplasmodial agents.

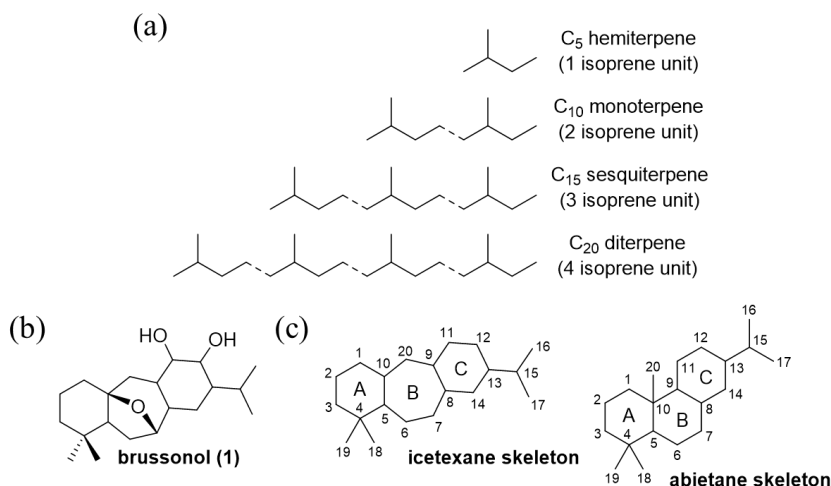


**Figure 5 - Chemical structures of terpenes and diterpenoids.** (a) isoprene units and some types of terpenes. (b) brussanol's (**1**) structure. (c) ictetexane and abietane skeletons.

Source: By the author.

A preliminary screening performed at the Sao Carlos Institute of Physics identified the NP brussonol (**1**) (**Figure 5b**) as a promising antiplasmodial agent. Brussonol showed an IC<sub>50</sub> value against *P. falciparum* 3D7 strain of 16 μM. Brussonol is an icetexane diterpenoid of the terpene class of SMs. There are numerous reports describing the isolation of icetexanes from different parts of terrestrial plants, including *Salvia*,<sup>92-101</sup> *Perovskia*<sup>102-106</sup> and *Dracocephalum*.<sup>107</sup> The icetexane skeleton stems from a rearrangement of the abietane skeleton (**Figure 5b**), giving rise to a key feature of these compounds the 6-7-6 tricyclic framework, also known as 9(10→20)-*abeo*-abietane.<sup>108</sup> The degree of oxidation in each ring of the icetexane skeleton may differ, which allow the classification of these compounds into five subgroups (classes 1, 2, 3, 4 and 5, **Figure 6a**). As can be seen in **Figure 6a**, brussonol (**1**) is part of class 2, showing an extra oxygen atom at position C11.<sup>108</sup> The structural diversity described for icetexanes reflects the numerous biological activities reported for this chemical series over the years, such as antibacterial,<sup>95,101</sup> antiprotozoal,<sup>92,96,107,109-110</sup> antiviral,<sup>105,111-112</sup> antifeedant,<sup>100</sup> anti-inflammatory,<sup>99,104,109</sup> antioxidant,<sup>95,99,113</sup> and cytotoxic activities<sup>93,97-99,103</sup> (**Figure 6b**).

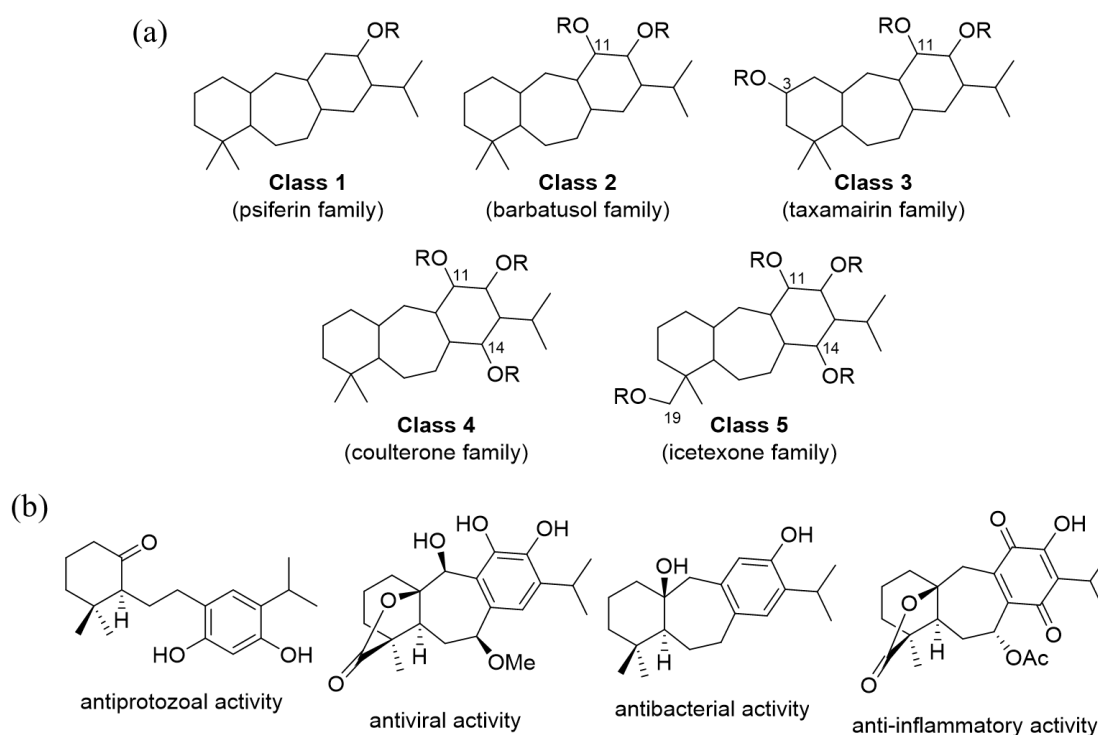


**Figure 6 – Chemical structures of icetexanes.** (a) General structure for each subgroup of icetexanes. Compounds are classified based on the presence or absence of oxygen atoms at positions C3, C11, C14 and C19.<sup>108</sup> (b) Examples of diterpenoids with antiprotozoal<sup>96</sup>, antiviral<sup>111</sup>, anti-inflammatory<sup>99</sup>, and bacterial<sup>101</sup> activities.

Source: By the author.



## 1.5 OBJECTIVES

### 1.5.1 General objectives

Evaluation of brussonol and derivatives as new lead candidates for malaria treatment.

### 1.5.2 Specific objectives

- Evaluation of the antiplasmodial activity of brussonol and derivatives (compounds **1** to **15**) against laboratory-based *P. falciparum* and *P. knowlesi* strains.
- Evaluation of the cytotoxic activity against a human cell line (HepG2).
- Evaluation of the antiplasmodial activity of brussonol (**1**) against a panel of *P. falciparum* resistant strains, and *P. falciparum* and *P. vivax* field isolates.
- Evaluation of the speed-of-action of brussonol (**1**) and derivatives (**8** and **12**)
- Determination of the *in vitro* association profile of brussonol (**1**) and artesunate.

## 1.6 MATERIALS AND METHODS

### 1.6.1 Maintenance of *P. falciparum* *in vitro* culture.

The *P. falciparum* strains were cultivated in human red blood cells (RBCs) O<sup>+</sup> (CAAE: 67462722.5.0000.5505) and in complete culture medium, containing RPMI-1640 (Sigma-Aldrich), supplemented with 0.2% NaHCO<sub>3</sub>, 25 mM HEPES (Sigma-Aldrich) (pH 7.4), 11 mM D-glucose (Sigma-Aldrich), 10 mg/L hypoxanthine (Sigma-Aldrich), 25 mg/L gentamicin (Sigma-Aldrich), and 0.5% (m/v) AlbuMAX<sup>TM</sup> II (Thermo Fisher Scientific). The cultures were maintained in T25 culture flasks, and the number of infected RBCs (iRBCs), also known as parasitemia, was counted using a light microscopy counting method to verify the parasite's propagation. The culture media was changed daily, and a gas mixture (90% N<sub>2</sub>, 5% CO<sub>2</sub>, 5% O<sub>2</sub>) was injected into the culture flask, which was later placed in an incubator at 37 °C to allow parasite's growth. This protocol was adapted from Trager and Jensen (1976).<sup>114</sup> The different *P. falciparum* strains were obtained through BEI Resources, NIAID, NIH: **K1**, MRA-159, contributed by Dennis E. Kyle; **Dd2**, MRA-156, contributed by Thomas E. Wellems; **TM90C6B**, MRA-205, contributed by Dennis E. Kyle; **3D7**, MRA-102, contributed by Daniel J. Carucci; **3D7'**\_MMV848, *in house* strain obtained via continuous growth of 3D7 strain exposed to the compound MMV692848.

### 1.6.2 *In vitro* evaluation of antiplasmodial activity against *P. falciparum* blood stage parasites.

The parasites were synchronized using 5% (m/v) sterile (D)-sorbitol treatment over 10 min at 37° C for the enrichment of ring-stage parasites, as described by Lambros and Vanderberg (1979).<sup>115</sup> The parasites were pelleted via centrifugation (600 x g, 5 min), and the parasitemia was determined by microscopic analysis of thin blood smears stained with Giemsa 10% (v/v) following fixation with methanol. Initially, the parasitemia is calculated for 1000 RBCs, subsequently the cultures were diluted to 0.5% parasitemia and 2% haematocrit by adding the appropriated volumes of blood and culture media. For the growth assay plate, a 2-fold serial dilution of 10-fold concentrated compounds (20 µL) is prepared, followed by the addition of 180 µL aliquots of parasites into the 96-well plates, totalizing 200 µL of final volume. Initially, the concentrations tested ranged from 10-1.53 µM, further adjustments in these concentrations were made if necessary. Negative and positive controls for parasite growth, which corresponded to non-parasitized erythrocytes and parasitized red blood cells (pRBCs) without treatment respectively, were set in parallel to determine the Z'-factor of the assay. Additionally, ART (0.1 µM or 0.3 µM, depending on how many wells were used for the inhibition curve) was used as a positive control for the growth assay. DMSO concentration was maintained below 0.05% (v/v) except for brussonol, which was 0.5%; this change was necessary to correctly determine the IC<sub>50</sub> value for this compound. The plates were incubated for 72 h, as described earlier (session 3.1). Each experiment was performed in duplicates, and the IC<sub>50</sub> values were determined based on the positive and negative control reads of parasite growth.

### 1.6.3 SYBR Green I assay.

The SYBR Green I assay is one of the many methods available to determine the IC<sub>50</sub> values of compounds, being described as faster, not labor-intensive, and less expensive than the other options. This fluorophore is an asymmetrical cyanine dye able to bind to double-stranded DNA, preferring G and C base pair, showing high fluorescence, when intercalating into DNA, and poor fluorescence, when it is not intercalated.<sup>116</sup> SYBR Green I intercalates DNA from dead or viable cells, leading to false positive results, which comprises one of the limitations of this method.

After the 72 h incubation of the growth plate, around 180 µL of the supernatant was removed from wells; it is important to avoid sudden movements with the plate, so that cell

resuspension will not occur. If resuspension ends up happening, you can always centrifuge the plate for 2 min at 150 x *g* to pellet RBCs again. Next, 100  $\mu$ L of PBS 1X (116 mM NaCl, 10 mM NaH<sub>2</sub>PO<sub>4</sub>, 3 mM KH<sub>2</sub>PO<sub>4</sub>) was added. RBCs were resuspended, followed by addition of 100  $\mu$ L of lysis buffer (20 mM Tris base, 5 mM EDTA, 0.0008% (v/v) Triton X-100, 0.008% (m/v) saponin, pH 8.0) containing 0.002% (v/v) SYBR Green I. Plates were incubated for 30 min at room temperature, and a SpectraMAX Gemini EM plate reader (Molecular Devices Corp., Sunnyvale, CA) was used to determine the fluorescence corresponding to parasitic density (excitation at 485 nm, emission at 535 nm).<sup>117</sup> The half maximal inhibitory concentration (IC<sub>50</sub><sup>Pf</sup>) was determined by non-linear regression analysis of the resulting concentration-response curve using the software GraphPad Prism version 8.0.1 for Windows (GraphPad Software, San Diego, California USA). This protocol is adapted from the method developed by Bennett and colleagues (2004).<sup>116</sup>

#### 1.6.4 Cytotoxic tests using immortalized cells.

Compounds exhibiting IC<sub>50</sub> against the malarial parasite had their cytotoxic effect evaluated against the human hepatocellular carcinoma cell line (HepG2). These cells are cultivated in RPMI media supplemented with 25  $\mu$ g/mL of gentamycin and 10% (v/v) fetal bovine serum (FBS). Additionally, T75 flasks are used to maintain cells, and they are incubated at 37 °C in a 5% CO<sub>2</sub> humidified incubator, and supplemented media is changed every 2 days.

For cytotoxicity evaluation, 1 mL of 0.05% trypsin-EDTA (1X) solution was added to the flask to detach HepG2 cells from the flask walls. Next, this cell suspension was transferred into a 15 mL centrifuge tube and centrifuged for 2 min at 150 x *g* to pellet these cells. After that, the supernatant was discarded and the cells were resuspended into 10 mL RPMI media to perform cell counting, which could be via a manual counting method employing the Neubauer chamber. Then, the appropriate dilutions were done to prepare cell plates with 30,000 cells per well (180  $\mu$ L). This cell plate was incubated for 24 h in a humidified incubator at 37 °C and 5% CO<sub>2</sub> to allow cell adhesion.

The drug plates were prepared the following day. 2-fold serial dilutions of 10-fold compound solution, and the concentrations tested ranged from 400 to 6.25  $\mu$ M. These concentrations were changed if needed in following experiments. HepG2 cells in the absence of compounds and wells containing only supplemented RPMI media were used as positive and negative growth controls, respectively. 20  $\mu$ L of this 2-fold serial dilution was added to the cell plates, which were further incubated for 72 h at the same conditions described earlier. After this

period, compound precipitation, corresponding to the presence of crystals or amorphous forms, was visually evaluated applying ZEISS Axio Vert.A1 microscope. This allowed us to determine which data points should be included in our analysis, or if it was necessary to perform further experiments changing the concentrations tested. After that, we performed a colorimetric assay to determine the cytotoxic concentration needed to inhibit 50% of HepG2 growth ( $CC_{50}$ ).

This colorimetric assay is based on the ability of viable cells' mitochondria to cleave the tetrazolium salt MTT (3-(4,5-dimethylthiazol-2-yl)-2,5-diphenyltetrazolium bromide) into dark blue formazan crystals.<sup>118</sup> In this sense, after incubation, 20  $\mu$ L of MTT solution (5 mg/mL in PBS buffer) were added to each well of the cell plate, and it was incubated for 3 – 4 h at 37 °C to allow the MTT cleavage in viable cells. Next, the supernatant was removed, followed by addition of 100  $\mu$ L of DMSO to solubilize formazan crystals, and later read absorbance, which is proportional to the number of viable cells. A SpectraMAX Plus 384 plate reader (Molecular Devices Corp., Sunnyvale, CA) was used to read absorbance of the solubilized purple crystal at  $\lambda=570$  nm, and GraphPad Prism version 8.0.1 for Windows (GraphPad Software, San Diego, California USA) was employed to determine the  $CC_{50}$  values.

#### 1.6.5 Calculation of selectivity index (SI).

Once the  $IC_{50}$  and  $CC_{50}$  values were determined against the parasite and the human cell line, respectively, the SI values were calculated using the formula:

$$SI = (CC_{50}^{HepG2} / IC_{50}^{Pf})$$

The SI shows the difference between the inhibitory potency against the parasite and the cytotoxic concentration for mammalian cells. For our reference, compounds with SI values higher than  $10^{119}$  are considered well tolerated by the cellular model used, and they are considered for further evaluation.

#### 1.6.6 Resistance assessment and calculation of resistance index (RI).

The antiplasmodial activity of brussonol (**1**) was assessed against a panel of *P. falciparum* strains: 3D7 (chloroquine-sensitive), K1 (resistant to chloroquine, mefloquine and sulfadoxine), Dd2 (resistant to chloroquine, mefloquine and pyrimethamine), TM90C6B (resistant to atovaquone), and 3D7<sup>r</sup>-MMV848 (*in house* strain resistant to MMV692848). The growth assay against these cell lines was carried out as described in sections **1.6.2** and **1.6.3**.

After determining the IC<sub>50</sub> value for each resistant strain, RI was calculated using the following equation:

$$RI = (IC_{50}^{Resistant\ Strain} / IC_{50}^{3D7})$$

RI is used to normalize the inhibitory potency against resistant strains by 3D7 our reference, allowing us to easily determine if there is a great difference in the compound's inhibitory effects regarding these strains. For our purposes, we consider RI values greater than 5 as indicative of cross-resistance, as described by Duffey and colleagues.<sup>120</sup>

#### 1.6.7 Schizont maturation assay (SMA) with field isolates.

These experiments were executed with the supervision of Amalia Ferreira and Dr. Carolina Bioni from the Malaria and Leishmaniasis Bioassay Platform – Oswaldo Cruz Foundation and the collaboration of Dr. Dhelio Batista from the Research Center of Tropical Medicine (CEPEM-SESAU), Porto Velho, RO. The SMA<sup>121</sup> was performed with parasites obtained directly from patients, who were approached and invited to participate in the study, approved by the Ethics Committee from the Research Center of Tropical Medicine (CEPEM-SESAU/RO) CAAE 58738416.1.0000.0011, infected with *P. falciparum* or *P. vivax*. Patients were included in this study according to the following criteria: patient should be at least 18 years of age, mono-infection of vivax or falciparum confirmed by light microscopy, patient should not show signs of severe malaria, and should not have received treatment 30 days prior to its inclusion in the study.

Samples (5 mL blood) were collected at CEPEM, and *Plasmodium* spp. was confirmed by thick blood smear stained with Giemsa. Only samples containing more than 50% of ring-stage parasites were included in the assay. Prior to the experiment, the host's white blood cells were removed by applying the CF11 cellulose method. *P. falciparum* and *P. vivax* parasites were maintained with RPMI and IMDM media, respectively, supplemented with 25 mM HEPES, 2 mM L-glutamine, 40 mg/mL gentamycin and 20% AB<sup>+</sup> plasma.<sup>122</sup> 2-fold serial dilutions of compound **1** with concentrations ranging from 50 to 0.0488 μM were prepared in a 96-well plate, followed by the addition of a solution with 2% hematocrit, and 0.5% parasitemia using the specific media for each *Plasmodium* spp. The plates were incubated at 37 °C, and from 24 – 42 h interval, thick blood smears of the non-treated control group were prepared to verify the maturation of schizonts. Upon 40% maturation, the parasite's sensitivity was evaluated by thick blood smears of the entire plate stained with Giemsa. Next, a differential

count of 200 asexual parasites on both the pre-incubated and the test slides were classified into ring, trophozoite and schizont stages. Parasites containing at least four well-defined chromatin dots were classified as schizont. The number of schizonts per 200 asexual parasites were determined for each drug concentration, and it was normalized to that of the control well. The IC<sub>50</sub> was determined by using a non-linear regression analysis using GraphPad Prism version 8.0.1 for Windows (GraphPad Software, San Diego, California USA)

#### 1.6.8 Maintenance of *P. knowlesi* parasites and evaluation of inhibitory potency of compound 1.

Assessment of the inhibitory potency of compound 1 against *P. knowlesi* parasites was performed in collaboration with Giovana A. H. Guerra and Prof. Dr. Roberto Barros from Escola Paulista de Medicina, UNIFESP, São Paulo. *P. knowlesi* strain H parasites were cultured in rhesus RBCs, RPMI-1640 media supplemented with 25 mM HEPES, 50 µg/mL hypoxanthine, 0.26% Na<sub>2</sub>CO<sub>3</sub>, 10 mg/mL gentamycin and 1% Albumax II. Cultures were maintained at 4% haematocrit and incubated at 37 °C under a mixture of gases (90% N<sub>2</sub>, 5% CO<sub>2</sub> and 5% O<sub>2</sub>) with daily media changing, as described previously.<sup>114</sup> The transgenic line *P. knowlesi* pvcen-pvhsp70-D-NanoLuc, expresses a bioluminescent protein, and its generation and use for assessment of antiplasmodial activity of compounds were published by Moraes and colleagues.<sup>123</sup>

2-fold serial dilution plates were prepared with compound 1. Dilution to 0.5% parasitemia and 2% haematocrit of blood-stage *P. knowlesi* cultures were done and added to the drug plates for growth assays in 96-well plates (200 µL/ well). Growth plates were incubated for 48 h at 37 °C in a humidified chamber containing the mixture of gases 5% CO<sub>2</sub>, 5% O<sub>2</sub>, and 90% N<sub>2</sub>. Parasite growth was determined by the Nanoluc Method,<sup>123</sup> which consisted in removing the growth plate from the incubator and addition of 100 µL of NanoGlo IC<sub>50</sub> solution (Promega NanoGlo reaction mixture 10-fold diluted in PBS, 20 µL of substrate) followed by pipette mixing. Next, the plate was incubated at room temperature for 3 min, prior to luminescence reading, using a luminometer (GloMax Explorer, Promega, Madison WI, EUA) with 0.3 s integration time. Luminescence readings were normalized with the highest and lowest growth readings of compound 1, IC<sub>50</sub> values were determined by fitting response curves with non-linear regression with variable slope, GraphPad Prism version 8.0.1 for Windows (GraphPad Software, San Diego, California USA). Data from two independent experiments were used to calculate the averaged IC<sub>50</sub> value against the *P. knowlesi* pvcen-pvhsp70-D-NanoLuc transgenic line.

### 1.6.9 Speed of action assay.

To determine whether compounds **1**, **8** and **12** were fast- or slow-acting inhibitors, a protocol adapted from Linares and colleagues (2015)<sup>124</sup> was used. In this method, three 96-well plates (A, B and C) were prepared by adding 180  $\mu$ L of the parasite's inoculum at the ring-stage with 0.5% parasitemia and 2% hematocrit. Equivalent experiments, with parasites starting at trophozoite-stage, were also performed. 2-fold serial dilutions of the compounds were added in each plate; the starting concentration were 6 x IC<sub>50</sub> for compound **1**, and 10 x IC<sub>50</sub> for ART, PYR (fast- and slow-acting controls, respectively), and compounds **8** and **12**. In addition, positive and negative controls, which corresponded to parasite cultures with no addition of inhibitor and non-parasitized erythrocytes respectively, were used for the parasite's control growth. Each plate had different drug incubation periods (A-24 h, B-48 h and C-72 h), and the plates A and B were washed twice with fresh media to remove the compound, followed by further incubation for 48 and 24 h, respectively. After the 72 h period, SYBR Green I assays were performed in all plates, as described in section **1.6.3**, to determine the IC<sub>50</sub> value for each incubation period. A statistical analysis using a one-way ANOVA test was done to compare each time point using GraphPad Prism version 8.0.1 for Windows (GraphPad Software, San Diego, California USA).

In parallel, the morphological development of the parasite under the compounds' pressure was assessed by adding the tested compounds at the highest concentration evaluated (6 x IC<sub>50</sub> or 10 X IC<sub>50</sub>). Blood smears of each well were made and stained at time points 0, 24, 48 and 72 h.

### 1.6.10 *In vitro* combination with artesunate.

This experiment was adapted from the work done by Fivelman and collaborators (2004)<sup>125</sup>, and a consideration of additivity ranges was included in the analysis, as described by Grabovsky and Tallarida (2004).<sup>126</sup> Brussonol (**1**) and artesunate were diluted and combined in a 96-well plate in seven fixed-ratio combinations (1:0, 6:1, 5:2, 4:3, 3:4, 2:5, 1:6, 0:1). Starting concentrations were 6 x IC<sub>50</sub> for both compounds. This experiment was performed with 0.5% parasitemia and 2% hematocrit, and growth controls were drug-free non-parasitized erythrocytes and parasitized erythrocytes. Serial dilutions of these combinations were prepared and incubated with the parasite, as described in section **3.2**. The SYBR Green I assay, section **3.3**, was applied to determine the IC<sub>50</sub> value for each combination, using the software GraphPad Prism version 8.0.1 for Windows (GraphPad Software, San Diego, California USA). The

absolute  $IC_{50}$ s of brussonol and artesunate (proportions 1:0 and 0:1), the partial  $IC_{50}$ s ( $IC_{50}^{\text{brussonol}}$  and  $IC_{50}^{\text{artesunate}}$ ) for each combination (6:1, 5:2, 4:3, 3:4, 2:5, 1:6), and the fractional inhibitory concentrations (FIC) for each combination were determined. FIC pairs were plotted as points in isobolograms, and if the majority of the  $FIC_{50}$  sum values were above or below the additive range, the combination showed antagonistic or synergic interaction, respectively.

## 1.7 RESULTS

### 1.7.1 Brussonol and derivatives.

Synthesis of brussonol (**1**) and analogs were performed by Dr. Anees Ahmad, a postdoctoral fellow of Prof. Dr. Antonio Burtoloso from the Chemistry Institute of São Carlos (IQSC-USP). A preliminary structure-activity relationship (SAR) evaluation was performed on the synthesized compounds (**Figure 7**). In this study, the main strategy involved modifications on A- and C- rings to determine the essential structural motifs for antiplasmodial activity. Detailed information on the synthetic routes and purification is found elsewhere.<sup>127-128</sup>

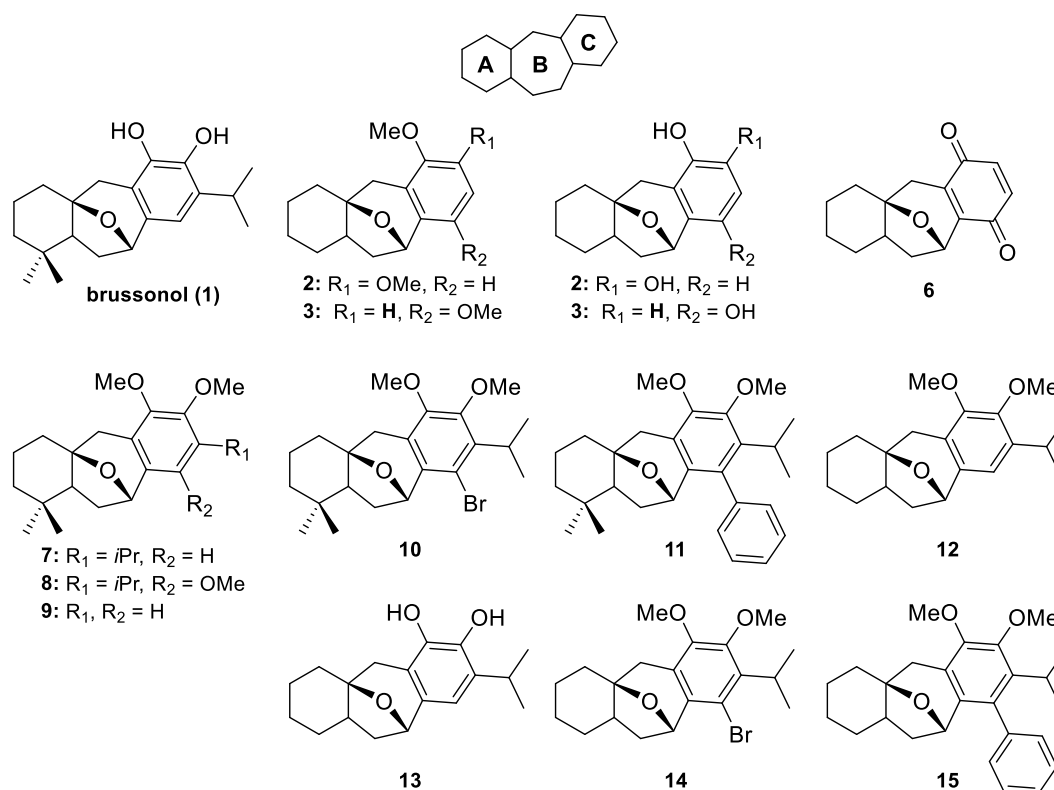


**Figure 7 – Design of brussonol analogs as new *P. falciparum* inhibitors.** At the top of the figure, there is an icetexane skeleton indicating A-, B- and C-rings.



### 1.7.2 Biological evaluation of brussonol and derivatives.

The first step was the assessment of the *in vitro* inhibitory activity of synthesized compounds against *P. falciparum* (3D7 strain), and the evaluation of the cytotoxic effect on the human cell line HepG2. The collection of these data allowed the determination of the SI (**Table 1**).

**Table 1** – *in vitro* antiplasmodial activity, cytotoxicity, and SI of brussonol and its derivatives.

Compd	R <sub>1</sub>	R <sub>2</sub>	R <sub>3</sub>	R <sub>4</sub>	R <sub>5</sub>	R <sub>6</sub>	IC <sub>50</sub> <sup>Pf</sup> (μM)	IC <sub>50</sub> <sup>HepG2</sup> (μM)	SI <sup>a</sup>
1	OH	OH	<i>i</i> Pr	H	Me	Me	16 ± 2	67 ± 4	4
2	OMe	OMe	H	H	H	H	>10	NT <sup>b</sup>	NT <sup>b</sup>
3	OMe	H	H	OMe	H	H	>10	NT <sup>b</sup>	NT <sup>b</sup>
4	OH	OH	H	H	H	H	>10	NT <sup>b</sup>	NT <sup>b</sup>
5	OH	OH	H	OH	H	H	>10	NT <sup>b</sup>	NT <sup>b</sup>
6							>10	NT <sup>b</sup>	NT <sup>b</sup>
7	OMe	OMe	<i>i</i> Pr	H	Me	Me	5.2 ± 0.4	>192	>37
8	OMe	OMe	<i>i</i> Pr	OMe	Me	Me	5 ± 2	170 ± 38	34
9	OMe	OMe	H	H	Me	Me	>10	NT <sup>b</sup>	NT <sup>b</sup>
10	OMe	OMe	<i>i</i> Pr	Br	Me	Me	5.6 ± 0.1	>400	>70
11	OMe	OMe	<i>i</i> Pr	Ph	Me	Me	5.8 ± 0.2	>12	>2
12	OMe	OMe	<i>i</i> Pr	H	H	H	5.6 ± 0.8	>400	>62
13	OH	OH	<i>i</i> Pr	H	H	H	>10	NT <sup>b</sup>	NT <sup>b</sup>
14	OMe	OMe	<i>i</i> Pr	Br	H	H	5.65 ± 0.05	>25	>4
15	OMe	OMe	<i>i</i> Pr	Ph	H	H	5.89 ± 0.02	>50	>8

<sup>a</sup>SI = IC<sub>50</sub><sup>HepG2</sup>/IC<sub>50</sub><sup>Pf</sup>, <sup>b</sup>NT – not tested.

The concentration required to inhibit 50% of parasite's growth ( $IC_{50}$ ) is a crucial parameter to determine the potency of a compound. In the phenotypic screening for antiplasmodial activity evaluation,  $IC_{50}$  values of 10  $\mu$ M are used as reference to select promising hit candidates.<sup>119</sup> In this sense, brussonol (**1**) showed an  $IC_{50}$  value of 16  $\mu$ M, which indicates that the natural product has promising antiplasmodial activity, encouraging this chemical series to proceed to optimization studies. Consequently, new analogs harboring modifications on A- and C- rings were designed to investigate the SAR underlying this series (**Figure 8** and **Table 1**).

First, we verified that analogs **4** and **13**, which contained phenolic groups ( $R_1$  and  $R_2$ ) and did not possess methyl groups ( $R_5$  and  $R_6$ ) and/or isopropyl group ( $R_3$ ), lost inhibitory activity ( $IC_{50} > 10 \mu$ M) compared to **1**. The replacement of the hydroxyl substituent with methoxy groups, derivatives **7** and **12**, determined an inhibitory activity enhancement of 3-fold compared to **1**, while analogs **2** and **9**, both lacking the isopropyl group ( $R_3$ ) and the latter having methyl groups ( $R_5$  and  $R_6$ ), lost potency. Next, assessment of analogs **3**, **5** and **6**, which did not show isopropyl groups, while having a different pattern of substitutions and C-ring oxidation lost inhibitory activity ( $IC_{50} > 10 \mu$ M). Based on this initial analysis, we identified some key features that are crucial for biological activity of brussonol's series (**Figure 8**). The isopropyl group in position  $R_3$  is essential for inhibitory activity of this chemical series, while substitution of hydroxyl by methoxy groups enhanced the inhibitory effect by 3-fold; comparable effects were reported by Tabefam and colleagues<sup>106</sup> Additionally, replacement of methyl groups with hydrogen atoms on positions  $R_5$  and  $R_6$  was tolerable as they retained the inhibitory activity.

In our subsequent investigation, we aimed to explore the chemical space surrounding the  $R_4$  position of the compound. The introduction of methoxy (**8**), bromine (**10** and **14**), and phenyl (**11** and **15**) substituents at  $R_4$  demonstrated negligible impact on the inhibitory potency within this chemical class, as evidenced by comparable  $IC_{50}$  values of approximately 5  $\mu$ M for all analogs. Consequently, these findings imply that the incorporation of bulky groups at  $R_4$  is well-tolerated (see **Figure 8**).

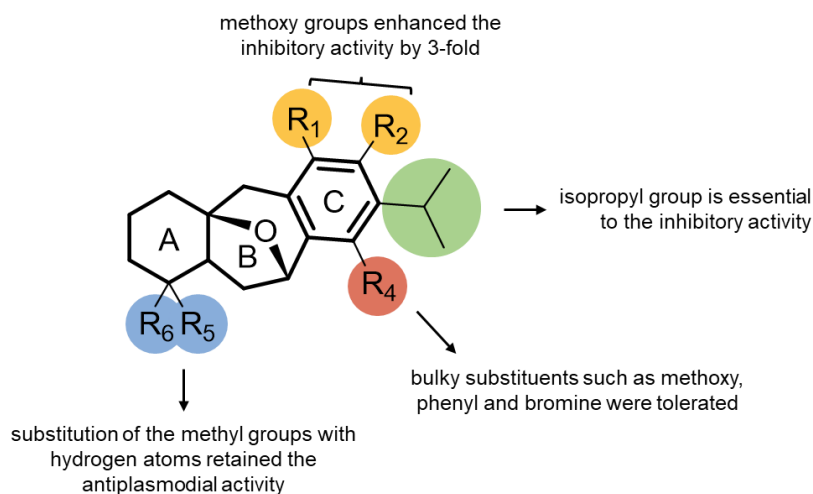


**Figure 8 - SAR summary around the icetexane diterpenoid scaffold.** Analysis data reported on Table 1 indicates that the isopropyl group is essential for inhibitory activity against *Plasmodium* parasites. In addition, substitution of hydroxyl groups by methoxy ones enhanced the inhibitory activity by 3-fold. The addition of bulky and hydrophobic substituents at position R<sub>4</sub> is tolerated. Finally, substitution of methyl groups by hydrogen atoms retained the antiplasmodial activity.

Source: Adapted from Barbosa, *et al.*<sup>128</sup>

The next step was to evaluate the cytotoxic effect of compounds ( $IC_{50}^{3D7} < 10 \mu M$ ) against a human hepatocellular cell line (HepG2). 8 out of 15 compounds had their  $CC_{50}$  values determined. The  $CC_{50}$  value is the concentration needed to reduce cell viability by 50%. These molecules showed varying  $CC_{50}$  values ranging from  $> 12$  to  $> 400 \mu M$  (**Table 1**). Substitution of hydroxyl by methoxy groups tended to decrease cytotoxicity against HepG2 cells by at least 3-fold. Similarly, Aoyagi *et al.*<sup>103</sup> reported that acetylation or methylation of phenolic groups present on C-ring (**Figure 8**) of demethylsalvicanol analogs showed decreased cytotoxicity against P388 murine leukemia cells. Furthermore, these phenolic groups on C-ring have been associated with the antioxidant capacity of diterpenes, as reported previously.<sup>104,113</sup>

Upon determination of  $IC_{50}$  and  $CC_{50}$  values, we determined the selectivity index (SI) value of compounds by calculating the ration between the  $CC_{50}^{HepG2}$  and  $IC_{50}^{3D7}$  values. This parameter is used as an indication of selectivity of compounds for parasite versus mammalian cells, and it is generally accepted that compounds showing  $SI > 10$  are promising for further development.<sup>119</sup> In this regard, brussonol's series shown low cytotoxic effects on human cells, (**Table 1**). In summary, the most promising compounds of the series considering the antiplasmodial inhibition and low cytotoxic effects were analogs **8**, **10** and **12**.

### 1.7.3 Brussonol is active against a panel of *P. falciparum* resistant strains.

Further experiments to investigate the parasitological profiling of this chemical series were performed with brussonol (**1**,  $IC_{50} = 16 \pm 2 \mu M$ ), unless explicitly stated otherwise. Our next approach was to evaluate the antiplasmodial activity of compound **1** against a representative panel of multidrug-resistant (MDR) and sensitive *P. falciparum* strains available in our laboratory (**Table 2**).

**Table 2** – Representative panel of MDR and sensitive *P. falciparum* strains.

Strain	Catalog No.	Resistance	Origin
<b>K1</b>	MRA-159	CQ, S, PYR, CYC	Isolated in Thailand.
<b>Dd2</b>	MRA-156	CQ, S, PYR, CYC, MQ	Clone selected after 2 events of continuous growth in the presence of mefloquine.
<b>TM90C6B</b>	MRA-205	CQ, PYR, ATO.	Isolated from a subject participating in an atovaquone clinical trial in Thailand.
<b>3D7<sup>r</sup>_MMV848</b>	-	MMV848	<i>In house</i> clone obtained from continuous growth in the presence of compound MMV848.
<b>3D7</b>	MRA-102	S	Cloned from limiting dilution of NF54 strain.

Abbreviations: ATO – atovaquone, CQ – chloroquine, CYC – cycloguanil, MQ – mefloquine, PYR – pyrimethamine, S – sulfadoxine.

Source: By the author.

Once growth assays were performed, the resistance index (RI) was determined by dividing the  $IC_{50}^{\text{resistant strain}}$  of each resistant strain for the  $IC_{50}^{3D7}$ , as described in section **1.6.6**. This parameter shows the  $IC_{50}$ -shift of the mutant parasites over our reference strain 3D7, and our threshold for cross-resistance to existing therapies is  $RI > 5$ . **Table 3** comprises  $IC_{50}$  values obtained for all *P. falciparum* strains, and calculated RIs.

**Table 3** - Brussonol's IC<sub>50</sub> values against a panel of sensitive (3D7) and MDR (K1, Dd2, TM90C6B 3D7<sup>r</sup>\_MMV848) *P. falciparum* strains.

Compound	<i>Pf</i> 3D7	<i>Pf</i> K1	<i>Pf</i> Dd2	<i>Pf</i> TM90C6B	<i>Pf</i> 3D7 <sup>r</sup> _MMV848
<b>1</b>	13 ± 2	6.6 ± 0.1 (0.5)*	7 ± 2 (0.5)*	7 ± 2 (0.5)*	12 ± 3 (1)*
<b>PYR</b>	0.06 ± 0.01	>10 (>166)*	>10 (>166)*	NT	NT
<b>ATO</b>	0.0007 ± 0.0003	NT	NT	3 ± 1 (4285)*	NT
<b>ART</b>	0.008 ± 0.004	0.007 ± 0.003 (1)*	0.011 ± 0.008 (1)*	0.006 ± 0.002 (1)*	0.013 ± 0.008 (2)*
<b>MMV848</b>	0.13 ± 0.02	NT	NT	NT	2.4 ± 0.4 (18)*

\* RI values. Data represents mean ± standard deviation of at least two independent experiments conducted in duplicate. RI = IC<sub>50</sub><sup>resistant strain</sup>/IC<sub>50</sub><sup>3D7</sup>; NT = not tested; PYR = pyrimethamine; ATO = atovaquone; ART = artesunate; MMV848 = *Pf*PI4K inhibitor.

Source: Adapted from BARBOSA *et al.*<sup>128</sup>

Brussonol shows equivalent inhibitory potencies against all resistant *P. falciparum* strains evaluated (**Table 3**) which is corroborated by the determined RI values lower than 5 (**Figure 9**). These data suggest that compound **1** does not show cross-resistance to the standard antimalarials.

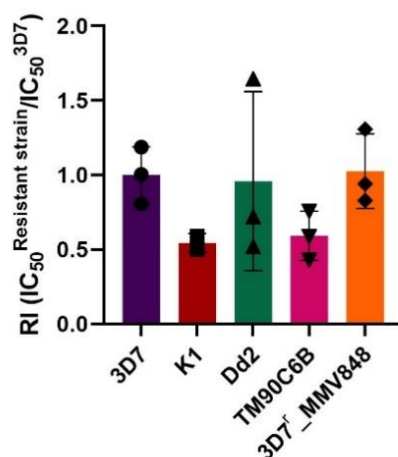


**Figure 9** - Analysis of resistance index (RI) of brussonol against a panel of resistant *P. falciparum* strains. RI values were determined based on the inhibitory activity of brussonol against *P. falciparum* resistant strains (K1, Dd2, TM90C6B and 3D7<sup>r</sup>\_MMV848) relative to the sensitive strain (3D7). Plot of the fold-change in the inhibitory potency of the tested compounds against the described *P. falciparum* strains. (n ≥ 2, mean IC<sub>50</sub> ± SD).

Source: Adapted from BARBOSA *et al.*<sup>128</sup>

#### 1.7.4 Brussonol shows potent inhibition against *P. falciparum* and *P. vivax* field isolates.

*In vitro* pre-clinical experiments are normally performed with *Plasmodium* strains that have been maintained for decades in the laboratory. Consequently, it is likely that these strains have accumulated spontaneous mutations in their genome so that it is unknown whether these strains are representative of circulating parasites, regarding drug susceptibility.<sup>129</sup> In this regard, it is advised to implement drug susceptibility assays against field isolates because it has been shown that *Plasmodium* parasites from endemic areas have different clones, and these clones might show different drug susceptibilities and genetic backgrounds.<sup>130</sup>

**Table 4** - *Plasmodium* field isolates sensitivity to brussonol (1), divided by species.

	<i>P. falciparum</i> (n = 5)	<i>P. vivax</i> (n = 6)
Compound	Median IC <sub>50</sub> (range) $\mu$ M	Median IC <sub>50</sub> (range) $\mu$ M
<b>Brussonol (1)</b>	7 (3 – 24)	16 (9 – 22)

*n* – number of field isolates.

Source: By the author.

In this sense, the inhibitory activity of compound **1** was evaluated against field isolates from Porto Velho (RO) (**Table 4**). Brussonol was evaluated against 5 *P. falciparum* field isolates, showing a median IC<sub>50</sub> value of 7  $\mu$ M, and against 6 *P. vivax* isolates, resulting in a median IC<sub>50</sub> value of 16  $\mu$ M. Hence, compound **1** showed comparable inhibitory potency against *P. falciparum* and *P. vivax* isolates (**Figure 10**).

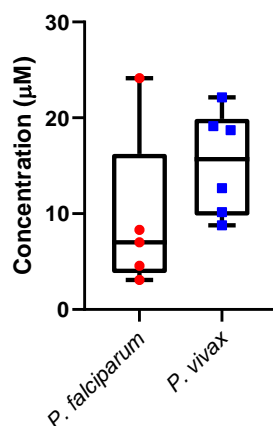


**Figure 10** - *Ex vivo* susceptibility of *Plasmodium* spp. to brussonol. Box and whisker plot of IC<sub>50</sub>s in  $\mu$ M for *P. falciparum* and *P. vivax*.

Source: By the author.

### 1.7.5 Brussonol inhibits *P. knowlesi* parasites.

Next, we evaluated if a representative compound of this chemical series would show inhibitory activity against a simian parasite, *P. knowlesi*, which causes zoonotic malaria in humans. This *Plasmodium* species is prevalent in Malaysia,<sup>131</sup> with 2505 zoonotic cases reported in 2022, despite 5 years without notification of human malaria in this area.<sup>18</sup> Compound **1** showed inhibitory activity against *P. knowlesi* ( $IC_{50} = 20 \pm 4 \mu\text{M}$ ) comparable to the potency observed against *P. falciparum* strains ( $IC_{50}$  values ranged from  $6.6 \pm 0.1 \mu\text{M}$  to  $16 \pm 2 \mu\text{M}$ ). This equipotency suggests that brussonol's series is an inhibitor of different *Plasmodium* species.

### 1.7.6 Compounds show fast-acting *P. falciparum* inhibition.

Our next step was to determine whether brussonol's series is a fast- or a slow-acting inhibitors. In this sense, we performed growth assays at different drug exposure times (24, 48 and 72 h) followed by compound removal and subsequent parasite incubation until 72 h was reached. After this period, we determined the  $IC_{50}$  values for each assessed time. Our controls for fast- and slow-acting antimalarials were artesunate (ART) and pyrimethamine (PYR), respectively. Moreover, we evaluated the morphological development of cultures in parallel to confirm the results obtained.

As depicted in **Figure 11a**, our growth controls, with parasites starting at ring stage, developed as expected over time. Upon ART exposure, a fast-acting antimalarial, within 24 h of drug exposure, it is possible to visualize pyknotic nuclei in the culture, which indicates cell stress and parasite death. On the other hand, PYR, a slow-acting antimalarial, allowed parasite development in the first 24 h, and, only after 48 h of drug exposure, it caused effective parasite death (**Figure 11a**). Brussonol, akin to ART, induced parasite death within 24 hours of drug exposure. The veracity of these observations is supported by the  $IC_{50}$  values recorded for each condition. Fast-acting compounds are anticipated to exhibit comparable  $IC_{50}$  values between the different exposure times, as seen with both artesunate and brussonol. In contrast, slow-acting inhibitors manifest a more pronounced inhibitory effect over extended time frame (**Figure 11b**). These results suggest that the brussonol derivatives are fast-acting inhibitors of *P. falciparum*.

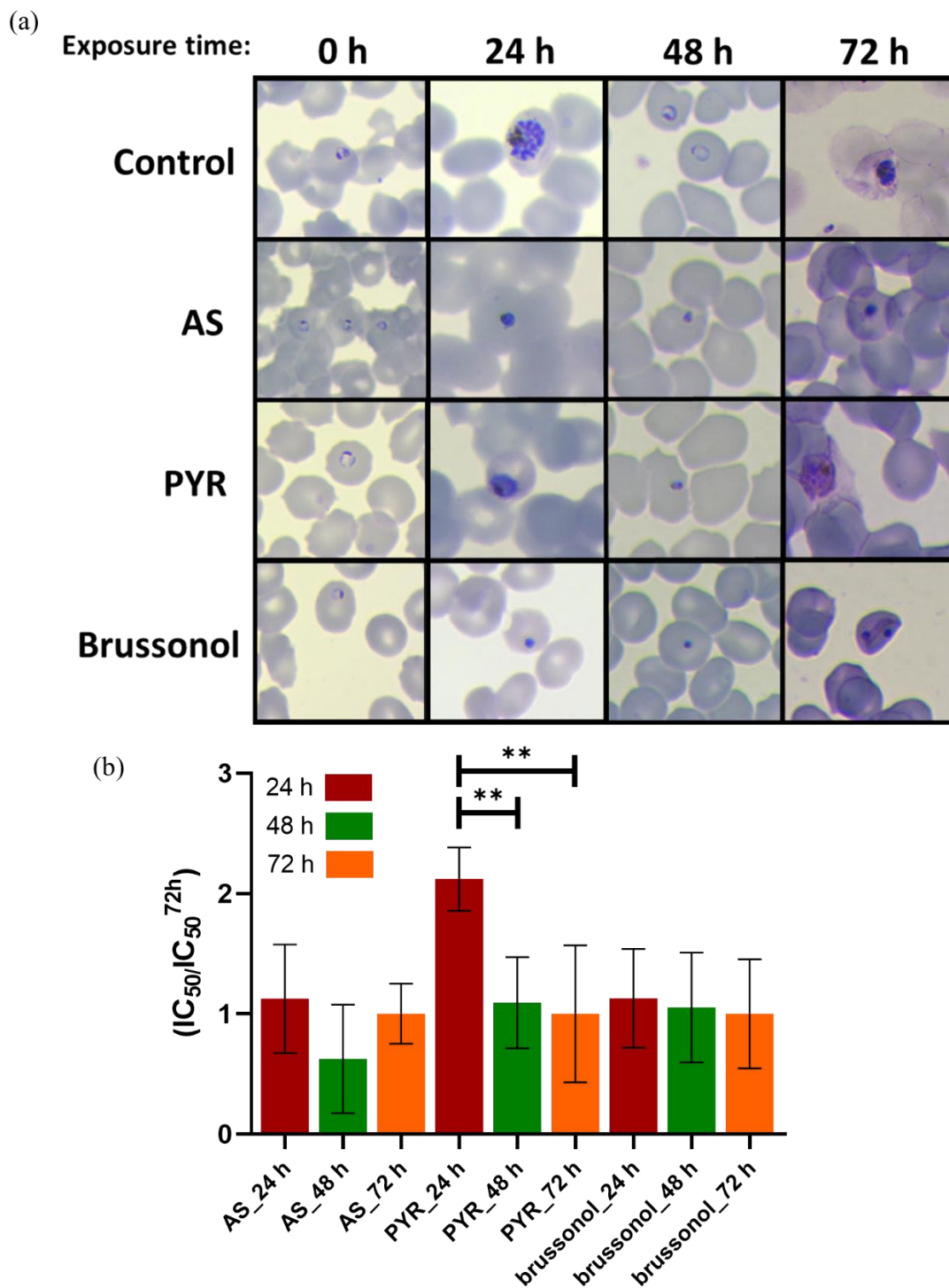


**Figure 11 - Speed-of-action assessment of brussonol.** (a) Morphological development evaluation of parasites over time in *P. falciparum* culture stained with Giemsa. (b)  $IC_{50}$  values were determined at 24, 48, and 72 h. Artesunate (ART) and pyrimethamine (PYR) were used as a positive control for fast- and slow-acting inhibition, respectively. The results were normalized with respect to the assessed  $IC_{50}$  value at 72 h. Statistical analysis was carried out by using ANOVA (\*\* $p < 0.01$ ; a  $p$ -value  $< 0.05$  indicates a significant difference within samples). These data correspond to three independent experiments, mean  $IC_{50} \pm SD$ .

Source: Adapted from BARBOSA *et al.*<sup>128</sup>



Similar results were obtained for compound **8** when assessing its speed-of-action (**Figure 12a**). Within 24 h of drug exposure, it was possible to visualize pyknotic nuclei in culture, and  $IC_{50}$  values for each assessed time were comparable (**Figure 12b**). Like brussanol, compound **8** seems to have a fast-acting inhibition. Surprisingly, the same does not happen with compound **12**. It appears that this compound allows parasites to develop within 24 h of drug pressure, similarly to PYR, and delayed morphological development is observed after this period (**Figure 12a**). These facts are corroborated by the discrepancies found in  $IC_{50}$  values obtained for the different exposure time points (**Figure 12b**). These data suggest that compound **12** is a slow-acting inhibitor.

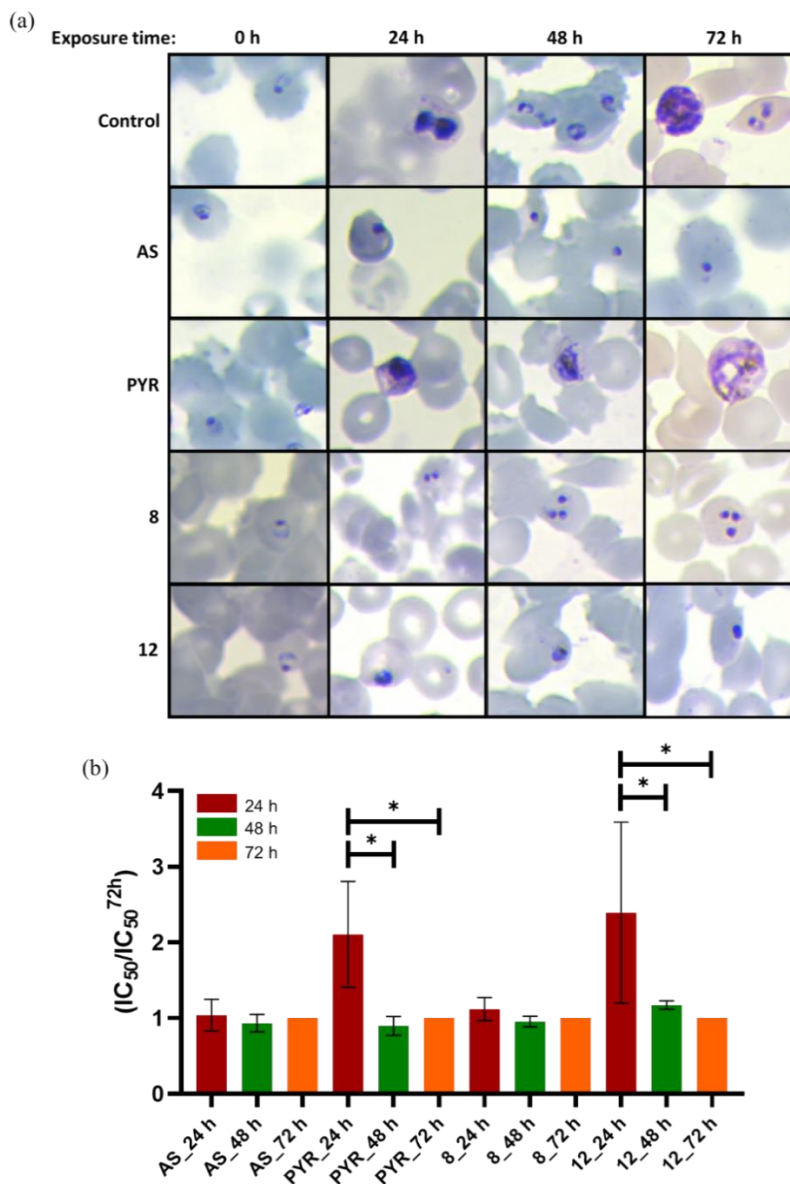


**Figure 12 - Speed-of-action assessment of brussnol series.** (a)  $IC_{50}$  values determined for plates with different drug exposure times (24, 48, and 72 h) of compounds 8 and 12, parasites started at ring stage. (b) Morphological development evaluation of parasites over time after exposure to compounds 8 and 12. Artesunate (AS) and pyrimethamine (PYR) were used as a positive control for fast- and slow-acting inhibition, respectively. The results were normalized with respect to the assessed  $IC_{50}$  value at 72 h. Statistical analysis was carried out by using ANOVA (\* $p < 0.05$ ; a p-value  $< 0.05$  indicates a significant difference within samples). These data correspond to three independent experiments, mean  $IC_{50} \pm SD$ .

Source: By the author

To better understand these controversial findings, we conducted the speed-of-action assay with parasites starting at trophozoite stage. The positive control wells for parasite growth developed as expected (**Figure 13a**). Again, ART and PYR were used as controls. We did not expect slow-acting effect for PYR on this condition. Both compounds, ART and PYR, displayed similar responses with parasite development stalled within 24 h of drug exposure

(**Figure 13a**), which culminated in parasite death, because  $IC_{50}$  values for different conditions were equipotent (**Figure 13b**). The same was observed for brussonol (**Figure 13a,b**). Notably, compounds **8** and **12** displayed different responses, with both compounds allowing parasite development in the first 24 h of drug exposure, especially compound **12** (**Figure 13a**). Discrepancies in  $IC_{50}$  values corroborated these findings (**Figure 13b**). Even though compounds **1**, **8** and **12** are analogs, they show different responses when assessing their speed of action. We hypothesize that this difference is not a consequence of divergent MoA, but a consequence of contrasting physicochemical properties.

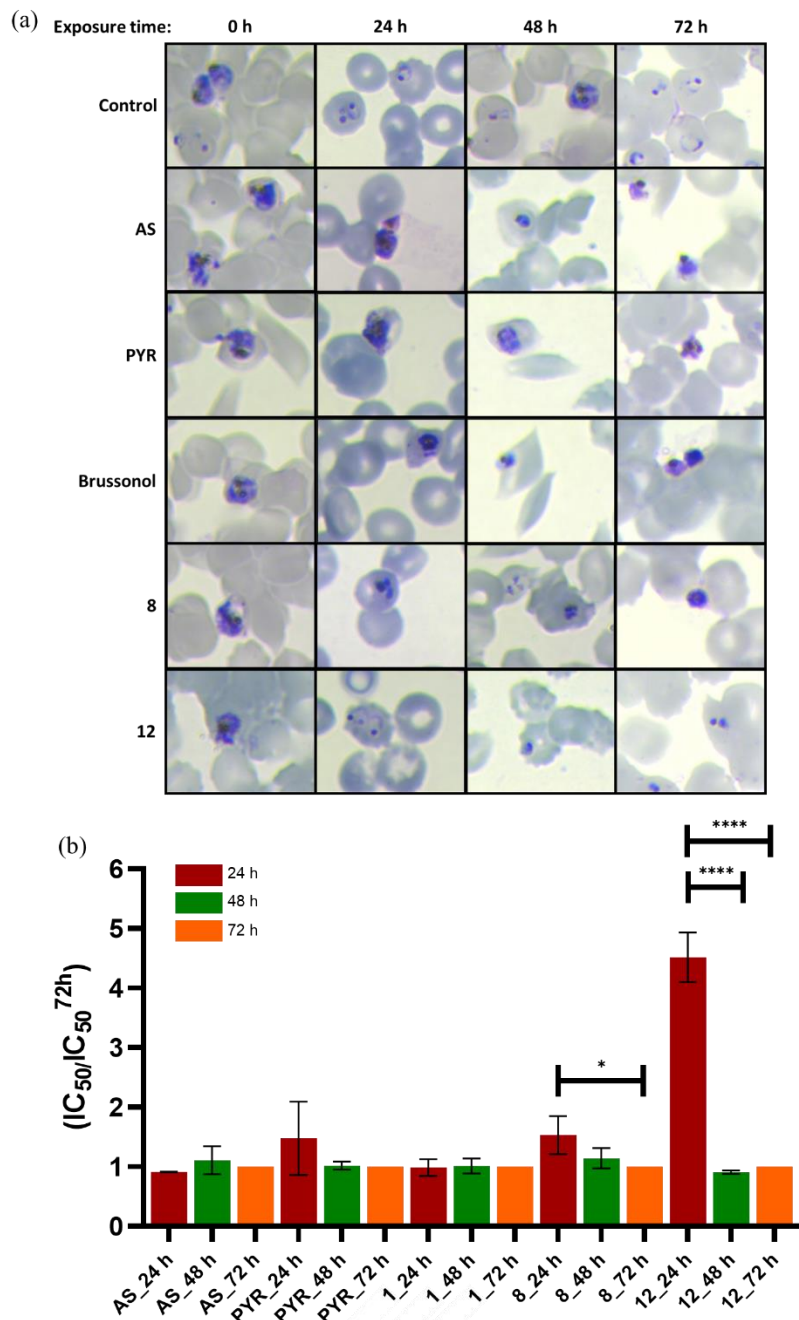


**Figure 13 - Speed-of-action assessment of brussonol series with parasites starting at trophozoite stage.** (a) IC<sub>50</sub> values determined for different plates after exposure to tested compounds (b) Morphological development evaluation of parasites over time after exposure to tested compounds. Artesunate (AS) and pyrimethamine (PYR) were used as a positive control for fast- and slow-acting inhibition, respectively. The results were normalized with respect to the assessed IC<sub>50</sub> value at 72 h. Statistical analysis was carried out by using ANOVA (\*p<0.05; \*\*\*\*p<0.0001; a p-value <0.05 indicates a significant difference within samples). These data correspond to three independent experiments, mean IC<sub>50</sub> ± SD.

Source: By the author.

### 1.7.7 *In vitro* combination of compound 1 with artesunate shows additive profile.

Administration of drug combination therapies for malaria treatment is a strategy to extend the lifespan of antimalarials by slowing down resistance selection pressure.<sup>132</sup> In this sense, we evaluated the combination profile of compound **1** when associated *in vitro* with ART. IC<sub>50</sub> values for compound **1** and ART alone, and for fixed ratio combinations of both compounds were calculated. Then, we determine the additive isobole, which determines the additive range. Next, fractional inhibitory concentrations (FIC<sub>50s</sub>) were determined for the fixed ratio combinations evaluated, and these experimental data were plotted at isobologram. If experimental data were within the additive range, the combination profile is additive; if data were above or below the additive range, the combination profile is antagonistic or synergistic, respectively.<sup>126</sup>

The examination of brissonol's isobologram alongside ART revealed that the experimental data did not significantly deviate from the additive range (**Figure 14**). Additionally, the total of fractional inhibitory concentrations at a 1:1 ratio (concerning each compound's IC<sub>50</sub> value) for the compound **1**-ART combination was  $1.1 \pm 0.1$ , whereas the additive region delineated by the additive isobole was  $1.0 \pm 0.2$ . Consequently, the lack of substantial disparity between these values (p-value = 0.4818) suggested an additive effect in inhibitory activity when compound **1** is associated with ART. These results imply that using compound **1** in conjunction with ART is advantageous for *in vitro* inhibitory activity.

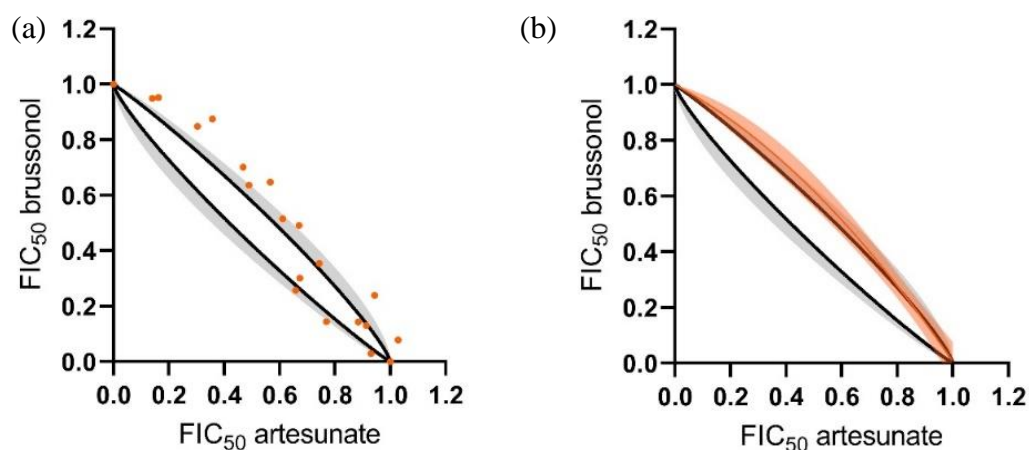


**Figure 14- Combination assessment between brussonol and artesunate.** Isobologram and additive isobole were calculated for the combination of brussonol with artesunate. Black lines correspond to the arithmetic average of the upper and lower limits of the additive area, and the gray area indicates the calculated standard deviations. (a) Experimentally determined  $FIC_{50}$  value pairs individually represented as orange dots. (b) Non-linear fit of experimental data, indicated by the fitted curve (dark orange) and the confidence interval of 95% (clear orange). Data analyzed are from three independent experiments.

Source: Adapted from BARBOSA *et al.*<sup>128</sup>

## 1.8 DISCUSSION

Despite efforts towards malaria elimination in the last decades, in 2022, it was estimated that there were 18 million more cases and 22,000 more deaths than in 2015.<sup>18</sup> This could be explained by different factors,<sup>75</sup> however, the emergence of parasites resistant to most available antimalarials, especially to artemisinin derivatives, is of great concern. Consequently, identification and development of new antimalarials to defeat this emerging drug resistance is paramount. NPs are an interesting source of new chemical scaffolds due to their chemical diversity and varied biological activities. Plants are a major source of NPs, with these organisms producing a wide range of secondary metabolites (SMs) for different purposes, including protection against biotic and abiotic stresses.<sup>87-88</sup> Terpenes constitutes the biggest group of SMs, possessing two important examples of medicines used in the clinic (Taxol and artemisinin).

Brussonol (**1**), an icetexane diterpenoid, was recognized as a promising candidate, showing an  $IC_{50}$  in low micromolar range ( $16 \pm 2 \mu M$ ). Brussonol's chemical series showed two properties important for their inhibitory activity: the isopropyl group (position  $R_3$ ) was essential for inhibition against the malarial parasite, and methoxylation of phenolic groups (C-ring) enhanced potency by 3-fold. The latter property was also reported elsewhere.<sup>106</sup> The most promising compounds, **8**, **10** and **12**, exhibited  $IC_{50}^{3D7} \sim 5 \mu M$ , low cytotoxicity ( $CC_{50}^{HepG2} >$

170  $\mu\text{M}$ ), and, consequently, high SIs ( $>30$ ). Finally, since biological activity was assessed with compounds as racemates, it is possible that the  $\text{IC}_{50}$ s obtained are underestimated because it is likely that only one of the enantiomers show the desired effect, although this is not always true.<sup>133</sup>

Assessing the risks of resistance evolution as early as possible in the preclinical studies is essential for selecting next generation antimalarials, decision-making through the drug development process, and enhanced clinical predictions.<sup>120</sup> One strategy consists of three assessments: (1) the potential of a compound to select resistant parasites *in vitro*, (2) cross-resistance of a compound with known antimalarials using a panel of MDR parasites, it also allows evaluation of common mechanisms of resistance, and (3) inhibitory activity against contemporary field isolates from endemic areas.<sup>120</sup> In this work, assessments 2 and 3 were performed with compound **1**. The panel of MDR parasites contained *P. falciparum* strains K1, Dd2, TM90C6B, and 3D7<sup>r</sup>\_MMV848. Compound **1** showed comparable  $\text{IC}_{50}$  values between sensitive ( $\text{IC}_{50}^{3\text{D}7} = 13 \pm 2 \mu\text{M}$ ) and resistant parasites ( $\text{IC}_{50}$ s ranged from  $6.6 \pm 0.1 \mu\text{M}$  to  $12 \pm 3 \mu\text{M}$ ); and, consequently, low RIs ( $\text{RI} < 5$ ). From these data we deduced that compound **1** did not show cross-resistance with the known antimalarials used as reference, as well as it is likely that this chemical series may have a different MoA and mechanism of resistance from our references.

Moreover, compound **1** was evaluated against 5 *P. falciparum* and 6 *P. vivax* clinical isolates from Porto Velho, RO. Brussonol (**1**) showed similar inhibitory potency between both species (Median  $\text{IC}_{50}^{\text{Pf}} = 7.0 \mu\text{M}$  and Median  $\text{IC}_{50}^{\text{Pv}} = 15.7 \mu\text{M}$ ). To evaluate whether a compound has species-specific activity, we consider that the  $\text{IC}_{50}$  values must be at least 5-fold different. In addition, compound **1** was evaluated against *P. knowlesi* ( $\text{IC}_{50} = 20 \pm 4 \mu\text{M}$ ) parasites, showing comparable inhibitory effect against 5 *P. falciparum* strains ( $\text{IC}_{50}$ s values ranged from  $6.6 \pm 0.1 \mu\text{M}$  to  $13 \pm 2 \mu\text{M}$ ). This equipotency against laboratory-based strains and clinical isolates indicates that brussonol (**1**) is a promising antiplasmodial agent against different *Plasmodium* species, and it could potentially be applied in areas where MDR strains, showing similar resistance to our MDR panel, are prevalent.

Our next strategy was to evaluate the speed-of-action of this chemical series to further characterize the parasitological profile of these compounds. In an attempt to find molecules less prone to select resistant parasites, fast-acting compounds are the most preferable choice due to their capacity to rapidly kill the malarial parasites, consequently decreasing the number of

organisms in the blood, minimizing the chances of recrudescence parasites to emerge and rapidly alleviating the symptoms.<sup>134, 135</sup> For our experiment, ART and PYR were used as fast- and slow-acting controls, respectively. Starting from synchronized ring-stage, compounds **1** and **8** were able to kill the parasites within 24 h of exposure, just like ART. Growth assays supported this finding, with fast-acting compounds having similar IC<sub>50</sub> values at each time assessed. By contrast, compound **12** exhibited a pattern similar to PYR, requiring 48 h to achieve its maximal effect.

Analogous effects were visualized when our speed-of-action experiment started at synchronous trophozoite-stage, with compounds **1** and **8** displaying maximal effect within 24 h while compound **12** needed 48 h to completely kill the parasite. This difference in time needed to fully exert their effect may be explained by differences in the polar surface area (PSA) for these compounds (molecular weight, clogP, hydrogen bond donors and acceptors are similar between these compounds). PSA corresponds to the sum of polar atomic atoms' surfaces in a molecule. Ertl and colleagues<sup>136</sup> described a method to calculate the topological PSA (TPSA), and, once TPSA of compounds **1**, **8** and **12** were calculated, we verified that compound **12** have the lowest value (27.69 Å<sup>2</sup>), followed compound **8** and **1** (36.92 Å<sup>2</sup>, 49.69 Å<sup>2</sup>, respectively). Since polar interactions require polar atoms, we hypothesize that lower PSA indicates less possibility of polar interactions, which may result in lower affinity of the molecule with its target. Consequently, this could explain why compound **12** needed more time to completely kill the parasite.

Another strategy to reduce the possibility of emerging resistance is applying combination therapies, the same manner as ACTs have been applied worldwide since 2000. Finally, our next step for this work was to evaluate the combination profile of compound **1** when associated with ART *in vitro*.<sup>137</sup> Various scientific methodologies exist for evaluating such combinations *in vitro*.<sup>138</sup> In this investigation, we employed isobologram analysis along with fractional inhibitory concentrations (FICs) to discern the nature of interaction (e.g., additive, synergistic, or antagonistic) between compound **1** and the gold-standard antimalarial.<sup>139</sup> The adoption of ACTs as the primary treatment for malaria has been pivotal in mitigating the emergence and spread of artemisinin resistance.<sup>140</sup> Within this framework, the concurrent utilization of multiple agents for malaria treatment is recommended, potentially enhancing the efficacy and longevity of antimalarial agents.<sup>139</sup> Analysis of the isobologram from our combination study indicated an additive relationship between compound **1** and ART,



suggesting a favorable *in vitro* inhibitory activity. This observation aligns with previous findings demonstrating the promise of hits and lead compounds as viable candidates for ACTs.



## **CHAPTER 2:**

# **MODE OF ACTION STUDIES OF BRUSSONOL'S CHEMICAL SERIES**



## 2 INTRODUCTION

### 2.1 Mode of Action (MoA) studies.

A broad understanding of the molecular target and/or elucidation of the mechanism of action (MoA) of the evaluated compounds can significantly expedite downstream development processes. This understanding facilitates a rational chemical design approach, leading to the discovery of molecules with enhanced potency, an improved selectivity index, and favorable pharmacological properties.<sup>75-76</sup> The elucidation of the target through forward screens can be achieved through a single or a combination of various methodologies. These methodologies include phenotyping, involving physiological, analytical, and cytological studies that aim to unravel the compound-induced phenotype, thereby forming a basis for target hypothesis.<sup>141</sup> Genetic interaction methods constitute another strategy, where hypotheses regarding the target are derived from genetic interactions induced by the tested compounds.<sup>141-142</sup> Biochemical screening entails the direct detection of binding interactions, and computational inference methods leverage pattern recognition to compare the effects induced by small-molecule compounds to known references.<sup>141-142</sup> These diverse approaches collectively contribute to the effective deconvolution of the target, expediting the development of promising compounds.<sup>142</sup>

#### 2.1.1 Isoprenoid biosynthesis.

Apicomplexa phylum contains several obligate parasites, with some being the etiologic agent of diseases in vertebrates. *Plasmodium* spp., *Toxoplasma gondii* and *Cryptosporidium* spp. are a few examples.<sup>143</sup> Most apicomplexan parasites possess a peculiar cellular organelle called apicoplast, a plastid-like organelle unable to perform photosynthesis and essential for intraerythrocytic<sup>144</sup> and intrahepatic<sup>145</sup> parasite development.<sup>143,146-147</sup> This organelle harbors a small genome, which mainly encodes genes required for its maintenance,<sup>143</sup> while most proteins that function in this organelle are nuclear-encoded.<sup>146</sup>

Isoprenoid biosynthesis is a key apicoplast metabolic pathway, and a source of diverse compounds. Isoprenoids, also known as terpenoids, are required for the synthesis of molecules essential for the *Plasmodium* parasite's cellular functions, such as carotenoids, which have unknown function in those organisms, but researchers speculate that they may be involved in the cellular response to oxidative stress, as in other organisms<sup>148</sup>; ubiquinone, which acts as an electron acceptor for dihydroorotate dehydrogenase, an enzyme necessary for pyrimidine biosynthesis<sup>149</sup>; dolichols, which are required for protein glycosylation<sup>150</sup>; and so on.<sup>147, 151</sup>

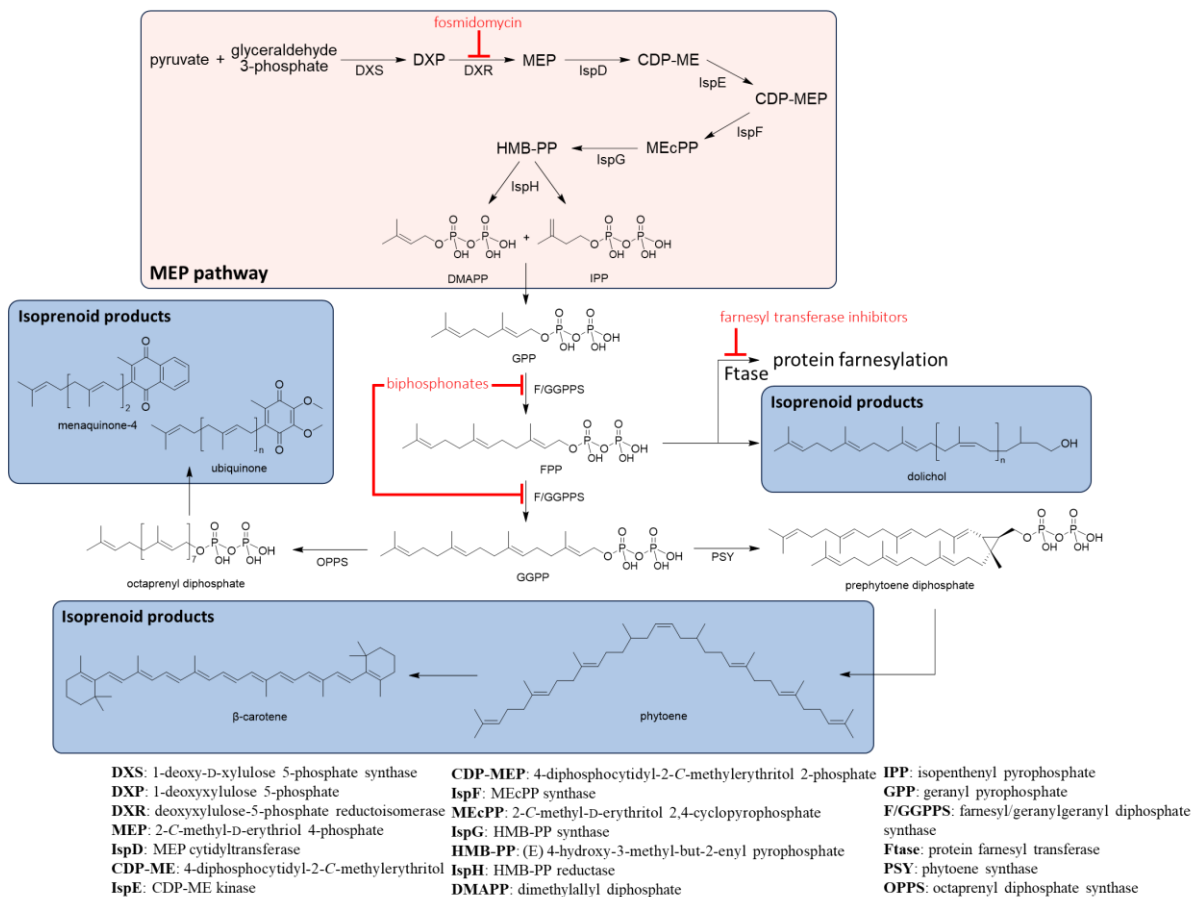


**Figure 15 - Isoprenoid biosynthesis in *Plasmodium* parasites.** IPP and DMAPP are building blocks for the synthesis of several isoprenoids with diverse functions. Both compounds are obtained via MEP pathway (pink area), an alternative route to the mevalonate pathway, which occurs in humans. A bifunctional farnesyl/geranyl diphosphate synthase (F/GGPPS) is responsible for synthesizing geranyl (GPP), farnesyl (FPP) and geranyl geranyl diphosphate (GGPP), intermediates utilized in further reactions that yield diverse isoprenoids.

Source: Adapted from GUGGISBERG;<sup>108</sup> RICCI *et al.*<sup>109</sup>

The isoprenoid pathway involves synthesis of several compounds, with diverse functions, which are made by the condensation of two isomers: isopentenyl pyrophosphate (IPP) and dimethylallyl diphosphate (DMAPP) (**Figure 15**).<sup>147,152</sup> Both building blocks are obtained via the mevalonate pathway in humans, while in *Plasmodium* parasites, these compounds are biosynthesized via an alternative route, the methylerythritol phosphate (MEP) pathway, highlighted in the pink area (**Figure 15**).<sup>147,152</sup> Through sequential condensation reactions between IPP and DMAPP by a bifunctional farnesyl/geranyl diphosphate synthase (F/GGPPS) geranyl (C<sub>10</sub>), farnesyl (C<sub>15</sub>) and geranyl geranyl diphosphate (C<sub>20</sub>) are synthesized, with the latter two being utilized in a variety of reactions, of which protein prenylation, quinone, dolichol and carotenoid biosyntheses are some examples (**Figure 15**).<sup>152</sup>

Since the MEP pathway does not show counterparts in the human host, this metabolic route is an attractive antimalarial therapeutic target.<sup>146,153-154</sup> Yeh and collaborators (2011)<sup>154</sup> developed a strategy, equivalent to genetic deletion/complementation method, based on drug inhibition/chemical rescue to facilitate studies related to apicoplast, its sufficiency and essentiality. This chemical rescue assay consists of observing whether IPP supplementation (200  $\mu\text{M}$ ) can reverse growth inhibition caused by the tested compounds. For example, Yeh and collaborators reported that growth inhibition by fosmidomycin (FOS) in blood-stage *P. falciparum* W2 strain ( $\text{IC}_{50} = 0.98 \mu\text{M}$ ) was reversed by supplementing IPP in growth media, even when FOS concentration was up to 100  $\mu\text{M}$ .<sup>154</sup> Following this article's publication, the use of this chemical rescue method as a strategy to identify inhibitors for isoprenoid biosynthesis has been reported in the literature.<sup>151,153, 155-157</sup>

### 2.1.2 Calcium signaling.

Several biological processes in prokaryotes and eukaryotes have calcium ( $\text{Ca}^{2+}$ ) ion as a second messenger, and it can be obtained from both intracellular and extracellular sources.<sup>158</sup> In *Plasmodium* parasites,  $\text{Ca}^{2+}$  signaling plays an important role in motility, cell differentiation, fertilization, invasion to and egress from RBCs.<sup>158-159</sup> Moreover, tight regulation of the parasite's life cycle involves fluctuations in cellular calcium levels, and  $\text{Ca}^{2+}$  deficiency leads to a decreased invasion rate and parasite growth.<sup>158</sup>

Normally, eukaryotic cells require extracellular calcium levels close to 1 mM to maintain intracellular calcium storages for calcium signaling.<sup>160</sup> Once malaria parasites invade RBCs, they encounter an environment with low  $[\text{Ca}^{2+}]$ , approximately 100 nM, which constitutes the first parasite survival challenge.<sup>161</sup> Gazarini and collaborators (2003)<sup>161</sup> have shown that *Plasmodium* parasites solve this problem by increasing calcium levels inside the parasitophorous vacuole (PV), around 40  $\mu\text{M}$ , which is sufficient to ensure maintenance of intracellular calcium stores and use of  $\text{Ca}^{2+}$ -based signaling mechanisms.

Another challenge encountered is that  $\text{Ca}^{2+}$  ion must cross many barriers, including RBC and PV membranes, to reach the parasite.<sup>158</sup> One strategy to overcome this is facilitating RBC membrane permeability by increasing  $\text{Ca}^{2+}$  influx and decreasing  $\text{Ca}^{2+}$  efflux.<sup>162</sup> One proposed mechanism for  $\text{Ca}^{2+}$  permeability is a nonselective cation conductance at the RBC membrane, which could potentially involve a channel sensitive to ethylisopropyl-amiloride (EIPA).<sup>158</sup> In relation to the PV membrane, a 140-pS channel permeable to nutrients,  $\text{Ca}^{2+}$ , and other ions was identified and proposed to be involved in this membrane's transport activity.<sup>163</sup>

Additionally, reduced membrane permeability to calcium upon conditional knockdown of a translocon responsible for exporting parasite proteins into the host cell, PTEX, reported by Kushwaha and colleagues,<sup>164</sup> may indicate that calcium entry is associated with hosts' altered protein (s) or protein encoded by the parasite and transported to the host cell.<sup>164</sup> Indeed, mechanisms involving calcium transport and signaling in the malaria parasite are still not fully understood.<sup>158</sup>

Oliveira and colleagues reviewed (2021)<sup>158</sup> some calcium-dependent signaling pathways in the malaria parasite that have been described (**Figure 16**). For example, activation of the complex calmodulin (CaM)/protein kinase B (PKB) in *P. falciparum*, as a response of intracellular Ca<sup>2+</sup> increase, results in phosphorylation of PfGAP5, a protein member of the inner membrane complex (IMC), an upstream event of parasite invasion. Furthermore, PfsR25, a serpentine GPCR-like protein, was shown to modulate Ca<sup>2+</sup> homeostasis, depending on potassium (K<sup>+</sup>) availability, mediated via inositol triphosphate (IP<sub>3</sub>) signaling (**Figure 16**). In addition, melatonin is also described as a trigger for IP<sub>3</sub>-dependent pathways, which involves cleavage of phosphatidyl inositol biphosphate (PIP<sub>2</sub>) by phospholipase C (PLC)<sup>165</sup>, releasing diacylglycerol (DAG) and IP<sub>3</sub>. Upon binding of IP<sub>3</sub> to its receptor present in the membrane of the endoplasmic reticulum (ER), Ca<sup>2+</sup> is released to the cytosol (**Figure 16**).<sup>166</sup> Pharmacological evidence<sup>167</sup> suggest that Apicomplexa parasites possess an IP<sub>3</sub> receptor (IP<sub>3</sub>R) even though it has not been identified yet. The ER serves as the primary calcium reservoir, where its uptake is likely dependent on SERCA-type Ca<sup>2+</sup>-ATPases.

Both vacuolar-H<sup>+</sup>-pyrophosphatase (VP1) and vacuolar-H<sup>+</sup>-ATPase (V-ATPase) present on the acidocalcisome<sup>168</sup> and food vacuole (FV)<sup>169</sup>, respectively, provide acidification of these organelles through inward proton pumping (**Figure 16**). Additionally, acidocalcisomes may possess an IP<sub>3</sub>R facilitating calcium release.<sup>158</sup> Moreover, calcium influx into mitochondria is facilitated by the Ca<sup>2+</sup>/H<sup>+</sup> antiporter PfCHA (or Ca<sup>2+</sup>/H<sup>+</sup> exchanger, PfCAX)<sup>170</sup>; activation of protein kinase A (PKA) via cyclic-adenosine monophosphate (cAMP), and activation of protein kinase G (PKG) via cyclic-guanosine monophosphate (cGMP), generated respectively by adenylyl-cyclase (AC)<sup>171</sup> and guanylyl-cyclase (GC), could contribute to Ca<sup>2+</sup> homeostasis, although the membrane receptors stimulating these pathways are yet to be identified (**Figure 16**). Furthermore, upon HCO<sub>3</sub><sup>-</sup> activation, AC can stimulate activation of Epac (exchange protein directly activated by cAMP) via cAMP<sup>171</sup> production, thereby triggering IP<sub>3</sub> signaling through PLC activation. Moreover, merozoite egress mediated by proteolytic cascade events is proposed to occur via crosstalk among kinases (**Figure 16**).





antimalarial resistance, as well as candidate drug targets.<sup>173-174</sup> Channels allow a rapid passage of molecules or ions of specific size and charge through an aqueous pathway (**Figure 17a**). Consequently, this type of transporter can transport up to  $10^8$  molecules per second down its electrochemical gradient.

Carriers and pumps, however, transport their substrates in a slower manner,  $10^2 - 10^4$  molecules per second, because both transporters undergo conformational changes during the substrate's translocation. Carriers bind to their substrate to perform translocation, and depending on their process, they can be classified as 'uniporters', in which transport occurs down the substrate's electrochemical gradient; they can also be classified as 'symporters' and as 'antiporters', in which both transporters couple the electrochemical energy stored in one or more solutes (commonly  $\text{Na}^+$  or  $\text{H}^+$ ) to the translocation of a substrate against its electrochemical gradient (**Figure 17b**). While symporters transport substrates in the same direction, antiporters translocate substrates in opposite directions. Last, pumps drive transportation of substrates down their electrochemical gradient by applying energy from a primary source, such as hydrolysis of ATP (**Figure 17c**).<sup>173</sup>

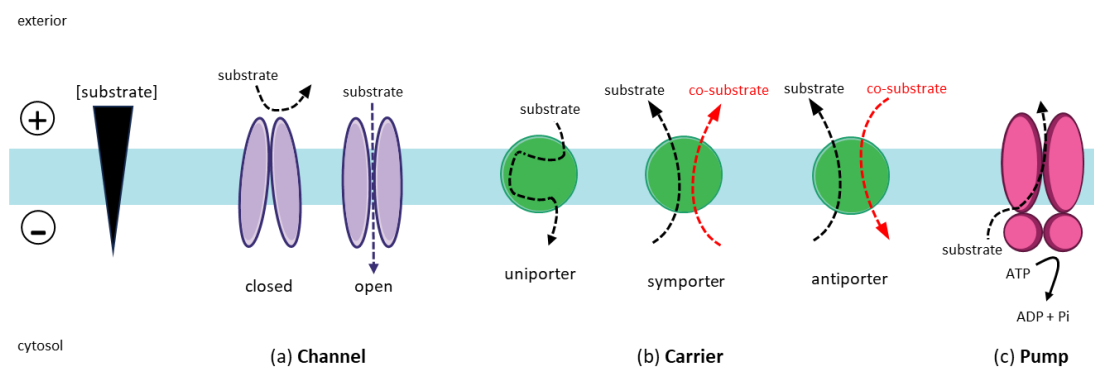


**Figure 17 - Channels, carriers, and pumps.** In this diagram, it is reported a membrane (light blue) which there is a membrane potential across (symbols plus and minus) and an inwardly electrochemical gradient (black triangle). A channel (purple) allows the rapid passage of substrate down its electrochemical gradient when it is on an open state. Channels normally rest in a closed state, and they are opened by changes in the membrane potential, ligand binding, for example. Carriers (green) bind the substrate, which then will undergo conformational changes to translocate the substrate to the other side of the membrane. Carriers can be classified as uniporter, mediate the substrate translocation down its electrochemical gradient; symporters and antiporter use the energy stored in the electrochemical gradient of a co-substrate (red), which is often  $\text{Na}^+$  or  $\text{H}^+$ , to drive the substrate's transportation against its electrochemical gradient. Pumps (pink) apply the energy of a primary source, such as ATP hydrolysis, to translocate the substrate against its electrochemical gradient.

Source: Adapted from MARTIN.<sup>173</sup>

#### 2.1.4 Na<sup>+</sup>-extruding transporter, *Plasmodium falciparum* P-type ATPase 4 (PfATP4).

Upon establishment of malaria infection, the growing parasite modifies the RBC's plasma membrane to increase permeability to low-molecular-mass solutes required for their survival, such as nucleosides, monosaccharides, peptides, polyols, amino acids, and various organic and inorganic ions, via parasite-induced new permeability pathways (NPPs).<sup>174</sup> NPPs are an additional route for Na<sup>+</sup> leaking into and K<sup>+</sup> out of the cell, consequently increasing [Na<sup>+</sup>] and decreasing [K<sup>+</sup>] in the RBC's cytosol (**Figure 18a**). Even though the intraerythrocytic parasite is surrounded by high levels of [Na<sup>+</sup>], it maintains low levels of cytosolic Na<sup>+175</sup>, and, until recently, it was via unknown mechanisms.<sup>176</sup>

The search for new antiplasmodial inhibitors via high-throughput whole-cell screenings led to the identification of the spiroindolone NITD609, also known as cipargamin, which is potent against *in vitro* and *ex vivo* blood-stage falciparum and vivax parasites<sup>177</sup>, and clinical trials in humans confirmed it rapidly clears parasites in adults infected with uncomplicated falciparum and vivax malaria<sup>178</sup>. Rottmann and colleagues<sup>177</sup> performed *in vitro* evolution studies in an attempt to identify NITD609's mechanism of action, and they discovered mutations in PfATP4, a P-type ATPase, that conferred resistance to this compound. Originally, this protein has been annotated as a Ca<sup>2+</sup> pump<sup>179</sup>, however, Spillman and colleagues<sup>176</sup> indicated similarities between PfATP4 and ENA P-type Na<sup>+</sup>-ATPase, a Na<sup>+</sup> extruding protein used by lower eukaryotes, including some protozoa.<sup>180-181</sup>

Spillman and colleagues<sup>176</sup> postulated that Na<sup>+</sup> efflux in plasmodium parasites, which counters Na<sup>+</sup> leaks, is performed by PfATP4, maintaining low cytosolic Na<sup>+</sup> levels. This extrusion is accompanied by an influx of H<sup>+</sup> ions, which was confirmed by an increase in cytosolic pH of parasites suspended on the presence of extracellular Na<sup>+</sup>, upon addition of spiroindoles from NITD609 class and orthovanadate (a phosphate analogue that inhibits P-type ATPases<sup>182</sup>) (**Figure 18b**). H<sup>+</sup> influx via PfATP4 constitutes a significant acid load on the parasite, which is countered by the H<sup>+</sup>-extruding V-type H<sup>+</sup>-ATPase.<sup>183</sup>

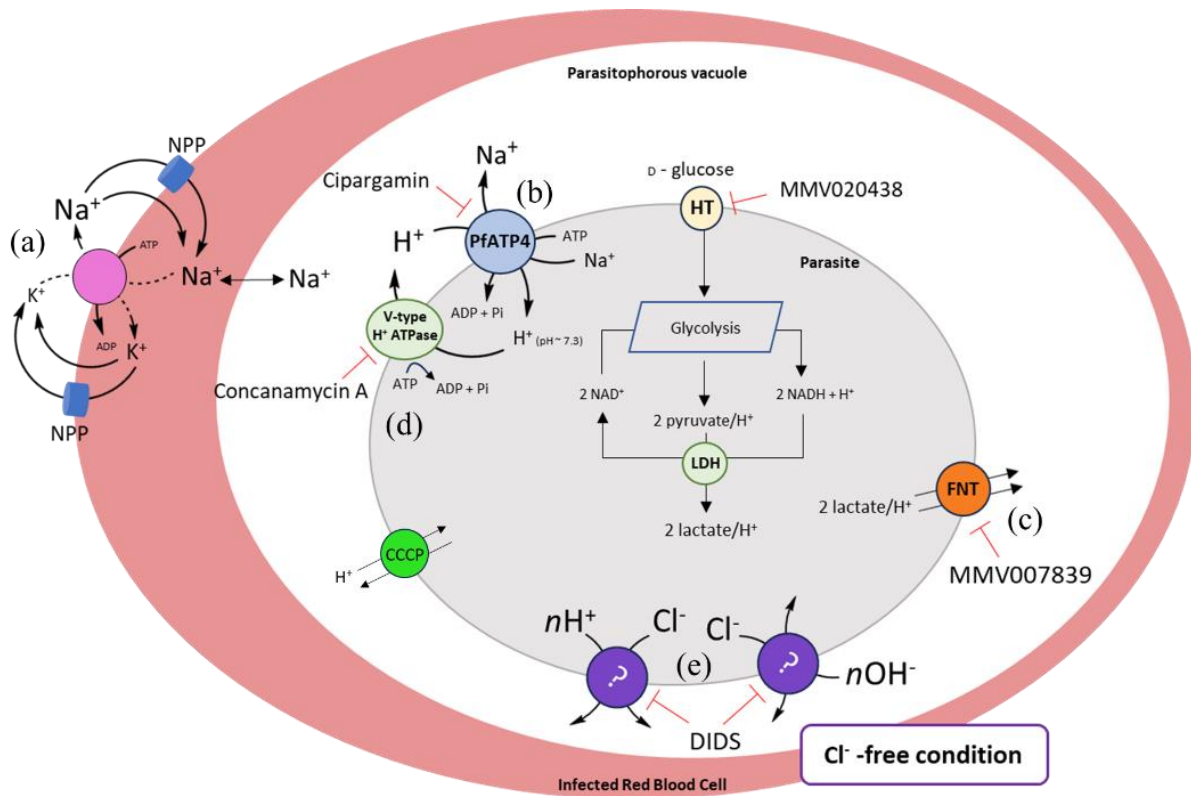


**Figure 18 - Schematic representation of ion transports that occur in the malarial parasite.** (a) NPPs are parasite-induced permeability pathways to increase permeability molecules required for survival, including leaking of  $\text{Na}^+$  into the RBC, and  $\text{K}^+$  out of the RBC. (b) PfATP4 mechanism of extruding  $\text{Na}^+$  coupled to  $\text{H}^+$  influx, maintaining low cytosolic levels of  $[\text{Na}^+]$ . (c) PfFNT exports lactate and  $\text{H}^+$  that are highly produced during ATP production. (d) V-type  $\text{H}^+$ -ATPase has been reported to extrude  $\text{H}^+$  from the parasite's cytosol, being responsible for maintaining  $\text{pH}_i$  around 7.3. (e) Studies confirmed  $\text{Cl}^-$  transportation throughout the PPM even though its transporter is not known yet. Additionally, pH-fingerprint assay is able to identify compounds able to inhibit enzymes involved in glycolysis, as well as showing protonophoric activity.

Source: By the author.

### 2.1.5 Lactate-extruding transporter, *Plasmodium falciparum* Formate-Nitrate Transporter (PfFNT).

The main energy source of *Plasmodium* parasites is glucose.<sup>184</sup> Normally, in eukaryotic cells, ATP production starts by the cell taking up glucose, which it is then broken down into two pyruvate molecules, that will further move into the mitochondria, leading to the production of acetyl-CoA and  $\text{CO}_2$  (Figure 19).<sup>185</sup> However, malaria parasites are not able to convert pyruvate into acetyl-CoA into their mitochondrion. Instead, production of energy occurs via glycolysis in the parasite's cytoplasm, and pyruvate is converted into lactate, yielding two ATP molecules.

Since the parasite's fast growth and virulence requires a high glycolytic flow rate, high levels of glucose are consumed. In fact, it has been shown that glucose consumption by

erythrocytes infected with *Plasmodium* spp. is 100 times faster than uninfected erythrocytes.<sup>184</sup> Consequently, this high glucose influx results in high rates of lactate and proton efflux as well.<sup>186</sup> This waste product (lactic acid) subsequently needs to be removed from the parasite, and it has been reported that lactate removal occurs via a H<sup>+</sup>/lactate symporter<sup>187</sup> (**Figure 18c**), which were later uncovered to be the *P. falciparum* Formate-Nitrite Transporter (PfFNT).<sup>186</sup> Additionally, because this protein shows sufficient disparities with its human counterpart, it is considered a potential drug target.<sup>188</sup>

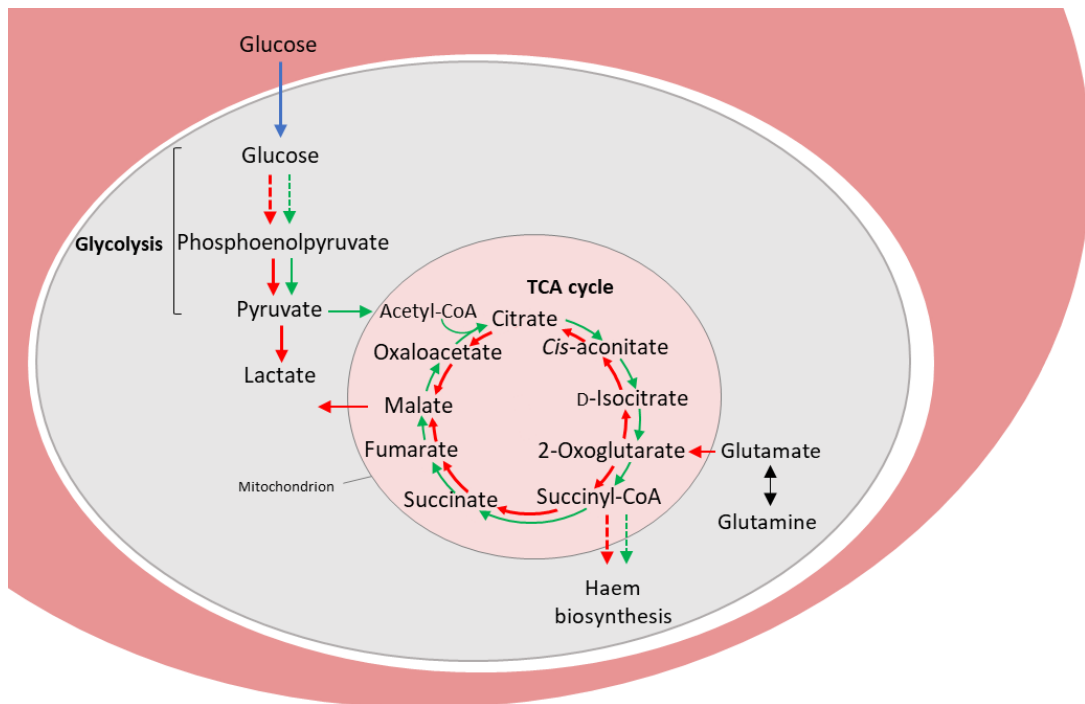


**Figure 19** – Established normal glycolytic and tricarboxylic-acid (TCA) cycle compared with those specifically observed in *P. falciparum*. An infected erythrocyte is depicted showing normal glycolysis and the TCA cycle (green arrows) and the similar reactions that occur in the malarial parasite (red arrows). Reactions containing multiple steps are represented by dashed arrows.

Source: Adapted from GINSBURG.<sup>185</sup>

### 2.1.6 V-type H<sup>+</sup> ATPase.

Upon entering erythrocytes, the human malaria parasite *P. falciparum* goes through a somewhat quiescent stage (ring stage), followed by a period of rapid growth, where biosynthetic and metabolically activities are intense (trophozoite stage), subsequently undergoing division (schizont stage), generating 16-32 merozoites (Figure 1). A significant acid load is imposed on the parasite due to its intensive metabolically activity. Therefore, these parasites need to have a H<sup>+</sup> extrusion mechanism to protect their intracellular pH (pH<sub>i</sub>), which is approximately 7.3, from intracellular and extracellular perturbations.<sup>189</sup>

Many studies<sup>190-191</sup> were performed to identify how H<sup>+</sup> extrusion occurred in the malaria parasite. There are diverse mechanisms by which eukaryotic cells extrude H<sup>+</sup>. Different organisms (plants, fungi, protozoa), as well as many vertebrate and invertebrate cell types possess in their plasma membrane H<sup>+</sup>-ATPases responsible to transport H<sup>+</sup> from the cytosol upon hydrolysis of ATP.<sup>189</sup> This transporter can be classified either as a P-type ATPase, which forms a phosphorylated intermediate during its cycle, hence the ‘P’ designation; or as V-type ATPase, which were earlier defined to be associated with membrane bound organelles. They have the ‘V’ designation because they were first discovered in vacuoles.<sup>192</sup> Another possible mechanism for H<sup>+</sup> extrusion is by using the inward Na<sup>+</sup> gradient to energize this transport, and Na<sup>+</sup>/H<sup>+</sup> exchangers (NHE) are the most well understood.<sup>193</sup>

Saliba and Kirk,<sup>189</sup> reported that H<sup>+</sup> extrusion in *P. falciparum* parasites saponin-permeabilized is Na<sup>+</sup>-independent. Additionally, pH<sub>i</sub> recovery upon intracellular acidification was not inhibited by replacing Na<sup>+</sup> with either choline or *N*-methyl-D-glucamine (NMDG), suggesting that H<sup>+</sup> extrusion does not occur via NHE. It was hypothesized that this process occurs via a V-type H<sup>+</sup>-ATPase (**Figure 18d**) because this translocation requires ATP hydrolysis, and bafilomycin A<sub>1</sub> inhibited both H<sup>+</sup> extrusion into the extracellular medium and from the cytosol, as well as the intracellular pH recovery upon intracellular acidification.

### 2.1.7 Cl<sup>-</sup> transporter.

Cells tightly regulate their intracellular pH because these changes can interfere in biological processes, and this is no different with *Plasmodium* parasites. Two mechanisms are available to regulate pH<sub>cyt</sub>: when cytosolic pH goes up, which means that [H<sup>+</sup>]<sub>cyt</sub> decreased, transporters known as “acid-loaders” will move H<sup>+</sup> into the cell and/or move bases OH<sup>-</sup>, or HCO<sub>3</sub><sup>-</sup>, out of the cell, so that pH<sub>cyt</sub> will increase. On the other hand, when pH<sub>i</sub> goes down, meaning that [H<sup>+</sup>]<sub>i</sub> increased, transporters also known as “acid-extruders” will move H<sup>+</sup> out of the cell and/or move bases OH<sup>-</sup>, or HCO<sub>3</sub><sup>-</sup>, inside the cell, decreasing intracellular pH.<sup>194</sup>

In malaria parasites, two known “acid-extruders” mechanisms are H<sup>+</sup> extrusion performed by V-type ATPase, and the one performed by PffNT, which is a H<sup>+</sup>/lactate symporter, both mechanisms were described previously in this chapter. Little is known about “acid-loading” transporters in this organism; what is familiar is that “acid-loading” mechanisms involves “H<sup>+</sup>-equivalents” uptake being often exchanged by Cl<sup>-</sup> ions. Additionally, it is estimated that intracellular [Cl<sup>-</sup>] ([Cl<sup>-</sup>]<sub>cyt</sub>) in the malaria parasite is around 40 mM.<sup>195</sup>

Comparisons of Cl<sup>-</sup> content between uninfected and infected erythrocytes showed that parasitized cells have a slightly lower [Cl<sup>-</sup>], estimated to be 12% lower, conferring a [Cl<sup>-</sup>]

ranging from 65-85 mM at the parasite's extracellular surface. If  $\text{Cl}^-$  ions were able to passively cross the PPM, by applying the Nernst equation, the predicted  $[\text{Cl}^-]_i$  would be below 3 mM. The fact that the actual  $[\text{Cl}^-]_i$  is way bigger than expected corroborates with  $\text{Cl}^-$  being taken up into the cell, and this process maintains chloride concentration away from its electrochemical equilibrium.<sup>195</sup> Nonetheless,  $\text{Cl}^-$  transporter is not known yet.

Henry and colleagues<sup>195</sup> investigated the  $\text{Cl}^-$ -dependent acid-loading mechanism occurring in the PPM, to determine the physiological characteristics behind it (**Figure 18e**). This group reported that, upon removal of extracellular  $\text{Cl}^-$ , a marked cytosolic alkalinization was observed in the malaria parasite. It supports the presence of a  $\text{Cl}^-$ -dependent pathway in the PPM, which, upon imposition of an outward  $\text{Cl}^-$  gradient,  $\text{H}^+$ -equivalents are exported to the external environment. On the contrary, extracellular  $\text{Cl}^-$  restoration led to recovery of  $\text{pHi}$  close to its initial value. Moreover, it is suggested that alkalinization and re-acidification have the same  $\text{Cl}^-$ -dependent pathway involved, since both processes were blocked by DIDS, an anion transport blocker.

### 2.1.8 Membrane Potential.

Cellular processes require a tight control of ion regulation. Through their plasma membrane, cells can maintain different concentrations of charged ions amidst the intracellular and the extracellular environment, through the action of protein transporters.<sup>196</sup> Consequently, a membrane potential ( $\Delta\psi$ ) arises across the plasma membrane. Additionally,  $\Delta\psi$  is defined as the intracellular voltage in relation to the extracellular one.

All cells have an inward negative  $\Delta\psi$ , and different mechanisms may be involved in its generation. A “diffusion potential” of ions, especially  $\text{K}^+$ , through membrane transporters, down their concentration gradients, is a primary mechanism of generating  $\Delta\psi$  in animal cells; while, in non-animal cells, a proton extrusion mechanism (usually  $\text{H}^+$ ) that utilizes a process based on energy-consumption, involving mainly ATP hydrolysis, is responsible for  $\Delta\psi$  formation.

In fact, Mikkelsen *et al.*<sup>190</sup> while studying isolated *P. chabaudi* murine parasites, verified that  $\Delta\psi$  is around  $-93$  mV, in these parasites; Allen & Kirk reported a similar value for the  $\Delta\psi$  of isolated falciparum trophozoites,  $-95 \pm 2$  mV. In both studies, it was hypothesized that  $\Delta\psi$  in the malaria parasites arose mainly from the activity of the V-type  $\text{H}^+$  ATPase because dicyclohexylcarbodiimide (DCCD), carbonylcyanide m-chlorophenyl hydrazone (CCCP) (both electrogenic protonophores) and orthovanadate (a  $\text{H}^+$ -ATPase inhibitor) collapsed the parasite's

$\Delta\psi$ .<sup>190</sup> Additionally, upon valinomycin treatment followed by bafilomycin A<sub>1</sub>, resulted in hyperpolarization, even though influx of K<sup>+</sup> was reduced.<sup>197</sup> Finally, both studies showed that  $\Delta\psi$  can be interfered upon increasing or decreasing the influx of ions across the parasite's plasma membrane.

#### 2.1.9 *In vitro* evolution studies.

*In vitro* evolution is a compound-dependent method<sup>75</sup> that has been successfully applied to the identification of *Plasmodium* drug targets (for example, ATP4<sup>177</sup>, PI4K<sup>198</sup>, AcAS<sup>199</sup>, eEF2<sup>200</sup>). It is a culture-based method in which parasites are exposed to an appropriate compound concentration able to kill all the drug-sensitive organisms.<sup>120, 201</sup> Whole-genome analysis of recrudescence parasites is performed to identify the gene (or genes) that confer the resistance phenotype. This approach is laborious, time-consuming (there is one study that reported the time to resistance onset ranging from 15 - 300 days<sup>202</sup>) and, despite efforts, it may not be able to identify a molecular target, or a mechanism of action, for the tested compounds. For those compounds which this approach was unsuccessful, they have been termed 'irresistible'. Even though it does not necessarily mean that resistance may never occur in the field, the low propensity for resistance is an attractive attribute.<sup>203</sup>

Because of what this approach may uncover, K mpornsin and colleagues<sup>203</sup> reported the generation of a mutant *P. falciparum* Dd2 parasite possessing a DNA polymerase  $\delta$  catalytic subunit deficient in proof-reading activity, this approach was inspired by previous report.<sup>204</sup> An impaired proof-reading activity of DNA polymerase  $\delta$  reduced fidelity in DNA replication, increasing the level of basal spontaneous mutations, therefore, increasing genetic diversity. Additionally, they showed that a shorter time and lower inoculum size are required to select parasites resistant to cipargamin, a compound known to inhibit PfATP4, when using this engineered *P. falciparum* strain.



### 2.1.10 Antiprotozoal activity against *Toxoplasma gondii*

*Toxoplasma gondii* is a zoonotic protozoan parasite and, like *Plasmodium* spp, is part of the phylum Apicomplexa. It is estimated that this parasite infects approximately one-third of humanity, as well as being an important pathogen of warm-blooded animals, including livestock and marine mammals, which could affect the food production industry.<sup>205</sup> As a consequence, this infection can cause an economic impact in this sector, with millions (maybe billions) being lost due to a decrease in food production or animal death, and due to treatment and prevention costs to protect the livestock. Additionally, human contamination via consumption of infected food, could also inflict an economic burden.<sup>206</sup> Even though toxoplasmosis is a common infection, most patients seem to have an asymptomatic disease; however, this disease can be fatal, especially to immunocompromised people and developing foetus.

*T. gondii* is considered a model organism to study apicomplexan parasites for different reasons: (1) culture and maintenance of pathogenic stages of this organism in the laboratory is easy; (2) classic and reverse genetic methods are well established. Because genetic manipulation of apicomplexan parasites, especially *Plasmodium* spp., is difficult, *T. gondii* has been used as an expression system for these parasites; and (3) mouse animal model is well-established. Therefore, similarities between apicomplexan parasites allowed the use of *T. gondii* as an experimental model to study the biology of these organisms. However, researchers should keep in mind that biological differences do occur between apicomplexan, which requires careful application of this model.<sup>207</sup>

## 2.2 OBJECTIVES

### 2.2.1 General objective

Investigation of brussanol's chemical series mode of action (MoA).

### 2.2.2 Specific objectives

- Assessment of compound's **1** effect in isoprenoid biosynthesis.
- Determination of compounds **1**, **8** and **12** interferences in cytosolic calcium levels.
- Comparison of derivatives' pH fingerprint with known *Plasmodium* transporters inhibitors.
- Investigation of compound's **12** effect on cytosolic sodium levels.
- Evaluation of compound's **12** effect on parasite's membrane potential.
- *In vitro* evolution studies with compound **8**.
- Evaluation of inhibitory activity of compound **8** against *Toxoplasma gondii* Tati $\Delta$ ku80 strain.

## 2.3 MATERIALS AND METHODS

### 2.3.1 Preparation of solutions and buffers.

The solutions, salines and buffers used in the experiments were prepared with water purified by MilliQ<sup>®</sup>, and pH-calibrations were performed prior to sterilization using a pH meter (Mettler Toledo Seven Compact<sup>TM</sup>). Unless otherwise stated, HCl or KOH/NaOH solutions were used to calibrate the solutions. Compositions of solutions, salines and buffers are described in **Table 5** below.

**Table 5** - Concentration (mM) of components of solutions, salines and buffers used in the experiments described in this chapter.

	Malaria Saline (MS)	Cl <sup>-</sup> free saline	Glucose-free saline (GF)	Bicarbonate-free RPMI-1640 (BCF)	130 mM Na <sup>+</sup> calibration saline	0 mM Na <sup>+</sup> calibration saline	MOPS buffer	Calibration saline pH-fingerprint
NaCl	125		135		50		116	
KCl	5		5			50	5.4	130
CaCl <sub>2</sub>							2	
MgCl <sub>2</sub>	1		1		1	1		1
MgSO <sub>4</sub>		1					0.8	
Na <sup>+</sup> -gluconate		135			80			
K <sup>+</sup> -gluconate		5				80		
hypoxanthine				200 $\mu$ M				
glucose	20			11	20	20	5.5	20
MOPS							50	
HEPES	25	25	25	25	25	25		25
pH	7.1	7.1	7.1	7.1	7.1	7.1	7.2	6.8, 7.1, 7.4, 7.8

Source: By the author.

### 2.3.2 Chemical rescue assay with IPP supplementation.

The chemical rescue assay was carried out as described by Yeh and DeRisi (2011).<sup>154</sup> This experiment consisted in determining the IC<sub>50</sub> values of compound **1** with and without 200 μM IPP supplementation. Briefly, 3D7 strain ring stages were cultured in 96-well plates, with 0.5% parasitemia and 2% hematocrit. Non-parasitized erythrocytes and parasitized erythrocytes without drugs were used as growth controls, fosmidomycin (FOS) was used as a positive control for chemical rescue. 2-fold serial dilutions of compound **1** and FOS were prepared in duplicates. Plates were incubated as described in section 1.6.2, and SYBR Green I assay was performed as described in section 1.6.3.

### 2.3.3 Fluorescent calcium cytosolic concentration measurements.

Isolated trophozoite parasites were incubated for 1 h at 37 °C with 5 μM of Fluo-4 AM in 1 mL MOPS buffer (**Table 5**), with 1 mM probenecid, which is used to minimize compartmentalization and extrusion of the probe. The parasites were washed three times with the same buffer and transferred to a quartz cuvette. Intracellular calcium was measured continuously using a Hitachi F-7000 spectrofluorimeter (parameters: 700 mV, emission slit: 10, excitation slit: 10, 1000 s reading) (Tokyo, Japan) by measurement of the fluorescence ( $\lambda_{\text{ex}} = 488 \text{ nm}$  and  $\lambda_{\text{em}} = 530 \text{ nm}$ ) at 37 °C, under agitation. 10 μM of cyclopiazonic acid (CPA) or 10 μM of brussanol (**1**) were added to the cuvette, when indicated. Controls of maximal fluorescence (F<sub>max</sub>) and minimal fluorescence (F<sub>min</sub>) were determined after cell lysis with digitonin 0.15% (m/v), and upon addition of 25 mM EGTA in 3 M Tris, pH 8.8, until no further decrease in fluorescence was observed, respectively. The cytosolic calcium concentration ( $[\text{Ca}^{2+}]_{\text{cyt}}$ ) was calculated from the fluorescence data (F) using a K<sub>d</sub> value of 345 nM through the formula:

$$[\text{Ca}^{2+}]_{\text{cyt}} = 345 * [(F - F_{\text{min}})/(F_{\text{max}} - F_{\text{min}})]$$

The results (n=2) were analyzed through One-Way ANOVA with Tukey post-test. This experiment was performed as described by Budu and colleagues (2016).<sup>208</sup>

### 2.3.4 pH fingerprint assay.

The following experiments were performed during my internship at the Australian National University (ANU, Canberra/Australia), under the supervision of Dr. Deyun Qiu and

Prof. Dr. Adele Lehane. A manuscript under review describing this method will soon be published by Lindbom, Zhang and Lehane. The cytosolic pH change of the parasite, after drug exposure, was assessed under three conditions (composition of salines are described in **Table 5**): parasites in malaria saline (MS); parasites in MS and concanamycin A (conA) (100 nM), and parasites in Cl<sup>-</sup>-free saline, by applying the most widely used fluorescent indicator for pH<sub>i</sub>, BCECF (2',7'-bis-(2-carboxyethyl)-5-(and-6)-carboxyfluorescein). First, the drug plate was prepared with compounds at 1000-X the desired final concentration. Since each compound is tested in the three conditions described, 5 µL of the compound into 180 µL of the respective saline. Next, trophozoites were isolated from the RBCs upon a brief exposure to 0.05% saponin solution (2.5 mL 1% w/v saponin combined with 47.5 mL cell culture), followed by 5 min centrifugation at 1000 x g. Then, the saponin-isolated parasites were washed (3x, 12,000 x g, 30 s) with bicarbonate-free RPMI-1640 (BCF; content described in **Table 5**). The next step was to load the isolated parasites resuspended in BCF with BCECF (5 µM) and incubate for 10 min at 37°C in the dark. After this period, the parasites were washed (3x) with glucose-free (GF) saline (**Table 5**) and incubated for further 20 min at 37°C to allow de-esterification of the dye and depletion of glucose. In the meantime, the pH calibration salines (**Table 5**) were prepared by adding 1 µL of nigericin (5 mM) into 1 mL of each pH calibration saline. Once incubation time was completed, 4 aliquots of 15 µL of cell suspension were pelleted and resuspended in each pH calibration saline, followed by their fluorescence measured in the Tecan fluorescence plate-reader (excitation wavelengths 440 and 495 nm; emission wavelength 520 nm). At the Tecan, the gain was determined for the calibration saline of pH 7.8, followed by measuring the fluorescence for all calibration salines for 3 min. After that, 15 µL of the resuspended parasites in GF saline were added to each well, and the fluorescence was monitored straight away for 40 min at 37°C, with the excitation and emission wavelengths described earlier.

The analysis of the collected data was performed using GraphPad Prism version 8.0.1 for Windows, and Microsoft Excel. First, the ratio of emission intensities, both detected at 520 nm, is calculated when the dye is excited at 490 nm, and when it is excited at its isosbestic point of 440 nm. With the average of each pH calibration saline collected data, it is possible to determine the equation that fits this calibration curve:

$$y = ax + b$$

where  $y$  corresponds to the fluorescence ratio,  $x$  corresponds to the unknown pH, and  $a$  and  $b$  are constants obtained by fitting the linear equation. This equation can be arranged in the following way:

$$\text{pH}_{\text{cyt}} = ((490 \text{ nm}/440 \text{ nm}) + b)/a$$

Once the equation is defined, the next step was to calculate the ratio for each collected data point, followed by determination of pH for each data point. After this process, graph plots are constructed for each well (time versus  $\text{pH}_{\text{cyt}}$ ), at each condition. The main objective of this assay is to compare the pH fingerprint of the tested compounds against all the controls used in this assay. Final concentration tested for each control: MMV007839 (2  $\mu\text{M}$ ), cipargamin (cip) (50 nM), conA (100 nM), CCCP (100 nM), DIDS (100  $\mu\text{M}$ ), MMV020438 (5  $\mu\text{M}$ ), compounds **8** and **12** (20  $\mu\text{M}$ ), DMSO (0.1%).

### 2.3.5 Fluorescent cytosolic sodium measurements.

The parasite cytosolic  $\text{Na}^+$  concentration was measured by applying the  $\text{Na}^+$ -sensitive fluorescent dye, sodium-binding benzofuran isophthalate (SBFI).<sup>176</sup> First, calibration salines containing varying  $[\text{Na}^+]$  (0 mM, 10 mM, 20 mM, 50 mM, and 130 mM) were prepared. Preparation of these salines were done by mixing up different proportions of two solutions: 0 mM  $[\text{Na}^+]$  and 30 mM  $[\text{Na}^+]$ , the content of both solutions is described in **Table 5**. Then, 1  $\mu\text{L}$  of gramicidin (10 mM) ( $\text{Na}^+$  ionophore) were added to 2 mL of each calibration saline, and all solutions were maintained warm (37 °C). Next, two different conditions were assessed in this assay: one, where compounds were diluted in MS, and the other, where compounds were in cipargamin saline (MS containing 100 nM cip). Then, these solutions were used to prepare 500  $\mu\text{L}$  of the compounds (at 1000-X the desired concentration) in both conditions. Finally, the plates were set up by adding 100  $\mu\text{L}$  of each solution in a 96-well plate, which should be maintained warm.

The second part consisted of preparing the parasites. Trophozoites were isolated by briefly exposing 47.5 mL of parasite culture to 2.5 mL of (1% w/v) saponin solution, followed by centrifugation at 1000 x g for 5 min. Then, the parasites were washed (3x, 12,000 x g, 30 s) and resuspended in BCF. Subsequently, equal volumes (1.25  $\mu\text{L}$  of each per 2 mL of cell suspension) of SBFI-AM (5 mM, in DMSO) and Pluronic F-127 (0.1% w/v, in DMSO) were previously mixed, and then added to resuspended parasites. Pluronic F-127 is used to aid SBFI-AM solubilization in the medium. To minimize light exposure, the tubes containing the SBFI-loaded parasites were wrapped in foil, and incubated at 37 °C for 20 min. Then, parasites were washed (3x, 12,000 x g, 30 s) in BCF; resuspended in BCF and incubated 37 °C for around 20 min to allow de-esterification of the dye.

Five aliquots (100  $\mu\text{L}$ ) of cell suspension were centrifuged (12,000  $\times g$ , 30 s) and resuspended in each calibration saline. The gain was determined for 0 mM  $[\text{Na}^+]$  calibration saline, and the calibration wells were read for 5 min. Readings were performed on a Tecan fluorescence spectrometer plate-reader. SBFI-loaded parasites were excited at 340 nm and 380 nm wavelengths, and emission was recorded at 515 nm. To determine the parasite's  $[\text{Na}^+]_{\text{cyt}}$ , a ratio of fluorescence intensities recorded, measured at both excitation wavelengths, (340 nm/380 nm), was used. In addition, calibrations were performed for every batch of SBFI-loaded parasites.

While the calibration wells were reading, the rest of the suspension cells were divided in half, centrifuged, and resuspended, an appropriate volume, of each saline. Finally, 100  $\mu\text{L}$  of these resuspended parasites were added to each non-calibration well, and readings were recorded for 90 min, as described above. Compound **12** was tested at 30  $\mu\text{M}$ , while DMSO was tested at 0.1%.

Once calibration readings were finished, the fluorescence ratios were determined for each calibration saline, and these data were plotted, and analysis was done by fitting a three-parameter hyperbolic equation, described below, to the data. This calibration approach was established by Diarra and colleagues.<sup>209</sup>

$$R = R_{\text{min}} \times (\alpha \times [\text{Na}^+]_{\text{cyt}}) / (b + [\text{Na}^+]_{\text{cyt}})$$

where  $R$  is the emission fluorescence for the unknown  $[\text{Na}^+]_{\text{cyt}}$ , and  $R_{\text{min}}$  is the emission for the calibration saline at 0 mM  $\text{Na}^+$ .  $\alpha$  and  $b$  are fitted constants, and the software used to analyze the data provides them. This equation can be rearranged in the following way:

$$[\text{Na}^+]_{\text{cyt}} = b \times (R - R_{\text{min}}) / (R_{\text{min}} + \alpha + R)$$

Consequently, this equation can be used to directly determine  $[\text{Na}^+]_{\text{cyt}}$  from the calculated emission fluorescence ratio.

### 2.3.6 Membrane potential evaluation.

This experiment was performed, according to Allen and Kirk<sup>197</sup>, to measure membrane potential by applying bisoxonol (bis-1,3-dibutylbarbituric acid)trimethine oxonol), an anionic fluorescent dye. *P. falciparum* trophozoite parasites were isolated with saponin (0.05%) treatment, followed by centrifugation (1000  $\times g$ , 5 min), and cell resuspension in BCF (**Table 5**) (maintained at 37  $^{\circ}\text{C}$ ). At the time of measurement, an aliquot of cell suspension (containing

~  $2\text{-}3 \times 10^7$  cell/mL) was centrifuged (3x, 12,000 x g, 30 s) to pellet the parasites. The supernatant was removed and the cells resuspended in 2 mL MS (**Table 5**), and transferred to a 2 mL square bottomed cuvette with a magnetic bar. Then, 2  $\mu$ L of bisoxonol (0.2 mM dissolved in EtOH) was added to 2 mL cell suspension. At the fluorometer, the parameters used were excitation wavelength 492 nm, and emission wavelength 515 nm, slit widths: 15 nm for excitation and 5 nm for emission, 1 s for sampling time and stirring was kept at slow speed. Once we started reading, we waited for approximately 15 min until the fluorescence was stable, and, if the fluorescence range was not in the 200 – 400 range, we would resuspend new cells or isolate more trophozoites. Once the fluorescence stabilized, compound **12** (30  $\mu$ M) or conA (100 nM) were added and readings were done until fluorescence stabilized.

### 2.3.7 *In vitro* evolution studies.

Compound **8** was used for *in vitro* selection of resistant parasites, using an engineered *P. falciparum* strain, Dd2-Pol $\delta$ <sup>203</sup>, kindly provided by Dr. Marcus Lee from the University of Dundee, Scotland/UK. Two independent experiments were performed. Only the second attempt was described in this study. Two flasks of ring-stage cultures of Dd2-Pol $\delta$  were tested with an inoculum of  $3 \times 10^8$  parasites. In ‘Flask 1’ parasites were cultured with DMSO (3.35  $\mu$ L), while parasites in ‘Flask 2’ were cultured with 16.8  $\mu$ M of compound **8** for 3 days, with media and compound changed daily. On day 4, compounds were washed out, and parasites were allowed to grow for 1 day. Then, ‘Flask 2’ was divided into 4 flasks with different concentrations of compound **8**: ‘Flask 3’ with no drug added, ‘Flask 4’ with 5.6  $\mu$ M (IC<sub>90</sub>); ‘Flask 5’ with 8.4  $\mu$ M (1.5 x IC<sub>90</sub>) and ‘Flask 6’ with 16.8  $\mu$ M (3 x IC<sub>90</sub>). Parasites were cultured in these flasks under pressure for 2 days. Once viable parasites were not visualized in culture (day 7), compounds were washed out and cultures were maintained, media changed every 2 days, until visualization of viable parasites occurred, and drug susceptibility assays were performed (day 19), following the same method described in sections **1.6.2** and **1.6.3**. After that, parasites were cultured again under pressure for 11 days, media changed every 2 days, when compound **8** was washed out. At this third round, parasites on ‘Flask 5’ and ‘Flask 6’ were growing even under pressure; consequently, concentration of compound **8** was increased by 20% every 2 days, until concentration reached 8.06  $\mu$ M and 12.24  $\mu$ M, respectively. After 7 days, viable parasites were visualized in ‘Flask 5’, and after 16 days viable parasites were observed in ‘Flask 6’. After this period, it was decided to perform microdilution to obtain clones from these cultures. Two plates with 0.5 parasites/well and 0.1 parasites/well were prepared by diluting the cultures at 2.5

parasites/mL and 0.5 parasites/mL, respectively, at 2% hematocrit. Cell suspensions were dispensed in 96-well plates and cultured at 37°C in a humidified incubator, with media being changed twice a week, and blood replacement once a week, until parasites were visualized and further expanded in T25 flasks.

### 2.3.8 Maintenance and inhibitory potency assessment of compound 8 activity against *Toxoplasma gondii*.

Evaluation of inhibitory activity of compound 8 activity against *T. gondii* TATi  $\Delta$ ku80 were performed during my internship in the ANU (Canberra/Australia), under the supervision of Fadza (Victor) Makota and Prof. Dr. Giel van Dooren. Human foreskin fibroblasts (HFF) were used to propagate tachyzoites. These cells were maintained in Dulbecco's Modified Eagle's Medium (DMEM) supplemented with 10% (v/v) bovine calf serum, 50 units/mL penicillin, 50  $\mu$ g/mL streptomycin, 10  $\mu$ g/mL gentamycin, 0.25  $\mu$ g/mL amphotericin B and 0.2 mM L-glutamine. Flasks were incubated at 37 °C gassed to 5% CO<sub>2</sub>. *T. gondii* TATi  $\Delta$ ku80 parasites expressing tdTomato red fluorescent protein were cultured in T25 flasks containing confluent HFFs and maintained with DMEM medium supplemented with 1% fetal calf serum, 50 units/mL penicillin, and 50  $\mu$ g/mL streptomycin, 10  $\mu$ g/mL gentamycin, 0.25  $\mu$ g/mL amphotericin B and 0.2 mM L-glutamine.

Fluorescence growth assays were performed as described previously.<sup>210, 211</sup> Prior to growth experiments, optical bottom 96-well plates were prepared with confluent HFF cells. To perform the assay, 2-fold serial dilutions of compound 8 (ranging 50 – 0.19  $\mu$ M) and ATO (ranging 400 – 1.56 nM) were prepared in sterile 96-well plates. Parasites were mechanically released from HFF cells by passing those cells through 26-gauge needles, which were then filtered by a 3- $\mu$ m polycarbonate filter and transferred to a 15 mL centrifuge tube. Parasites were manually counted using a Neubauer chamber, and cell suspension was diluted to a final concentration of 11764 tachyzoites/mL. Aliquots of 170  $\mu$ L of cell suspension were added in the appropriate wells, totaling 2000 parasites/well with a final volume of 200  $\mu$ L. tdTomato fluorescence was measured daily using a BMG Fluostar fluorescent plate reader (Offenburger, Germany) for 5 – 8 days, until growth of 'no drug parasitized cells' wells reached a plateau of fluorescence reading. Readings were taken from the bottom of the plate with excitation wavelength 544 nm and emission wavelength 590 nm. IC<sub>50</sub> values were determined using fluorescence data when parasites cultured in the absence of the drug were in log phase of growth, and averaged fluorescence were expressed as percentage positivity (PP), with 0% PP corresponding to background level, and 100% PP representing the maximal fluorescence signal



obtained during the experiment on the ‘no drug parasitized cells’ well. GraphPad Prism version 8.0.1 for Windows (GraphPad Software, San Diego, California USA) and Microsoft Excel software were used to calculate  $IC_{50}$  values and analyze the growth curves, respectively.

## 2.4 RESULTS

### 2.4.1 IPP supplementation does not reverse compound 1’s inhibition.

Given that we had no information regarding brussonol’s MoA, our first attempt in the second part of the project was to conduct a similarity search in the SciFinder database aiming at discovering similar molecules with known MoA. In this search, we identified carnosol as the best hit, showing structural similarity greater than 80% with brussonol. The similarity index between brussonol (**1**) and carnosol was also calculated by the Tanimoto coefficient, via the online service ChemMine Tools<sup>212</sup> (**Figure 20a**).

Macías-Alonso *et al.*<sup>213</sup> reported, while studying NPs extracted from *Salvia canariensis* L for hyperlipidemia treatment, that carnosol was the most potent NP able to inhibit squalene synthase (SQS) enzyme from rat liver. SQS is part of the steroid’s biosynthesis<sup>213</sup>, being the first enzyme entirely committed to cholesterol synthesis.<sup>214</sup> Since the malarial parasite does not synthesize cholesterol, which is supported by the non-success in identifying a SQS in the *Plasmodium* genome through homology search,<sup>147</sup> we decided to evaluate compound’s **1** effect on the steroid’s biosynthesis of the parasite.

Isoprenoids are a large and diverse group of compounds synthesized through sequential additions of 5-carbon subunits, IPP and DMAPP. These molecules show varied biological activities, and they have been reported to be essential for parasite’s survival.<sup>147</sup> To assess if compound **1** disrupts isoprenoid biosynthesis, we performed a chemical rescue assay. 154-157 In this assay, compounds able to interfere in isoprenoid biosynthesis have their growth inhibition reversed by IPP supplementation, as reported by Yeh and DeRisi (2011).<sup>154</sup>

Growth assays were performed in the presence and absence of IPP (200  $\mu$ M) for compound **1** and FOS, our positive control for the chemical “rescue” experiment. As expected, upon IPP supplementation, FOS had its inhibitory effect reversed, which is supported by the  $IC_{50}$  shift (~16-fold) when IPP was supplemented (**Figure 20b**). Compound **1**, differently from FOS, displayed comparable inhibitory potencies in both conditions (IPP supplementation:  $IC_{50} = 13.9 \pm 0.2 \mu$ M, and IPP absence:  $IC_{50} = 18 \pm 1 \mu$ M) (**Figure 20c**), suggesting that brussonol does not interfere in isoprenoids biosynthesis.

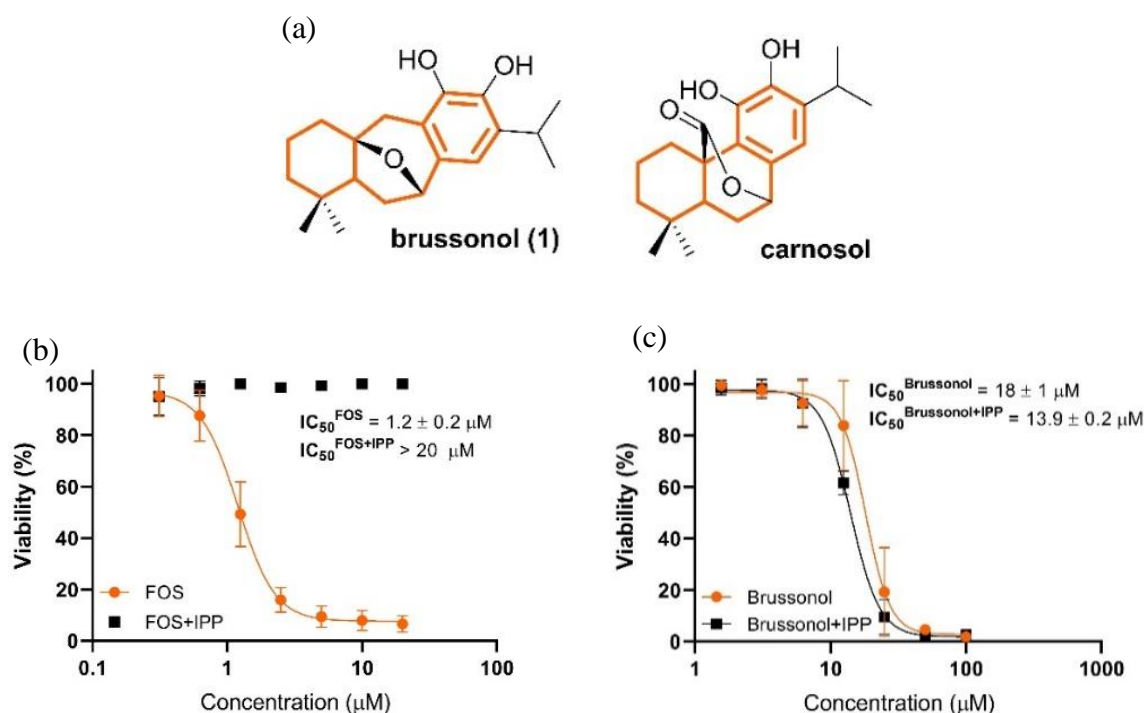


**Figure 20 - Chemical “rescue” assay to evaluate the action of brussonol (1) in the metabolism of isoprenoids.** (a) Molecular structures of carnosol and brussonol. (b) Concentration-response curves for FOS (positive control) against *P. falciparum* 3D7 strain with and without the supplementation of IPP. (c) Concentration-response curves for brussonol against *P. falciparum* 3D7 strain with and without supplementation of IPP ( $n \geq 2$ , mean  $\text{IC}_{50} \pm \text{SD}$ ). Orange and black plots correspond to the growth assay with and without IPP supplementation, respectively.

Source: Adapted from BARBOSA *et al.*<sup>128</sup>

#### 2.4.2 Compound 1 induced an increase in $[\text{Ca}^{2+}]_{\text{cyt}}$ in *P. falciparum*.

Another hit identified was cyclopiazonic acid (CPA) (**Figure 21a**), which is a potent inhibitor of *P. falciparum* sarco/endoplasmic reticulum  $\text{Ca}^{2+}$ -ATPase (PfSERCA) pump.<sup>159, 179, 215</sup> Upon release of  $\text{Ca}^{2+}$  from the ER required as a second messenger for metabolic pathways, PfSERCA regulates  $\text{Ca}^{2+}$  uptake from the cytosol once this signal is not needed anymore.<sup>159</sup> In this sense, we evaluated compound 1 effect on cytosolic calcium levels, by loading trophozoite saponin-isolated parasites with Fluo-4 AM, a calcium indicator. Exposure of Fluo-4 AM-loaded parasites, suspended in  $\text{Ca}^{2+}$  MOPS buffer, to 10  $\mu\text{M}$  CPA led to a transient cytosolic calcium increase ( $23 \pm 2 \text{ nM}$ ) (**Figure 21b**) relative to the basal level, similar to previous reports. When exposing trophozoite-loaded parasites to 10  $\mu\text{M}$  of compound 1, a sustained  $[\text{Ca}^{2+}]_{\text{cyt}}$  increase was observed ( $19 \pm 4 \text{ nM}$ ) (**Figure 21c**) relative to the basal level, which were comparable to the increase caused by the CPA control.

In order to determine if compound **1** also modulates PfSERCA activity, and within the scope of our experiment, we assessed cytosolic calcium increase of compound **1** on parasites pre-treated with CPA (both compounds at 10  $\mu\text{M}$ ), and vice-versa. Again, CPA led to an increase in  $[\text{Ca}^{2+}]_{\text{cyt}}$  ( $23 \pm 2$  nM), and, once fluorescence reached a plateau, 10  $\mu\text{M}$  of brussonol was added, incrementing cytosolic  $[\text{Ca}^{2+}]$  ( $19 \pm 8$  nM) to comparable level to compound **1** alone ( $19 \pm 4$  nM) (**Figure 21d**). Additionally, an increase in  $[\text{Ca}^{2+}]_{\text{cyt}}$  was also observed when 10  $\mu\text{M}$  of CPA was added to parasites pre-treated with compound **1** (**Figure 21d**). These data suggest that compound **1** disrupts calcium homeostasis in the malarial parasite, and it is likely that it mobilizes calcium through a different mechanism than CPA.

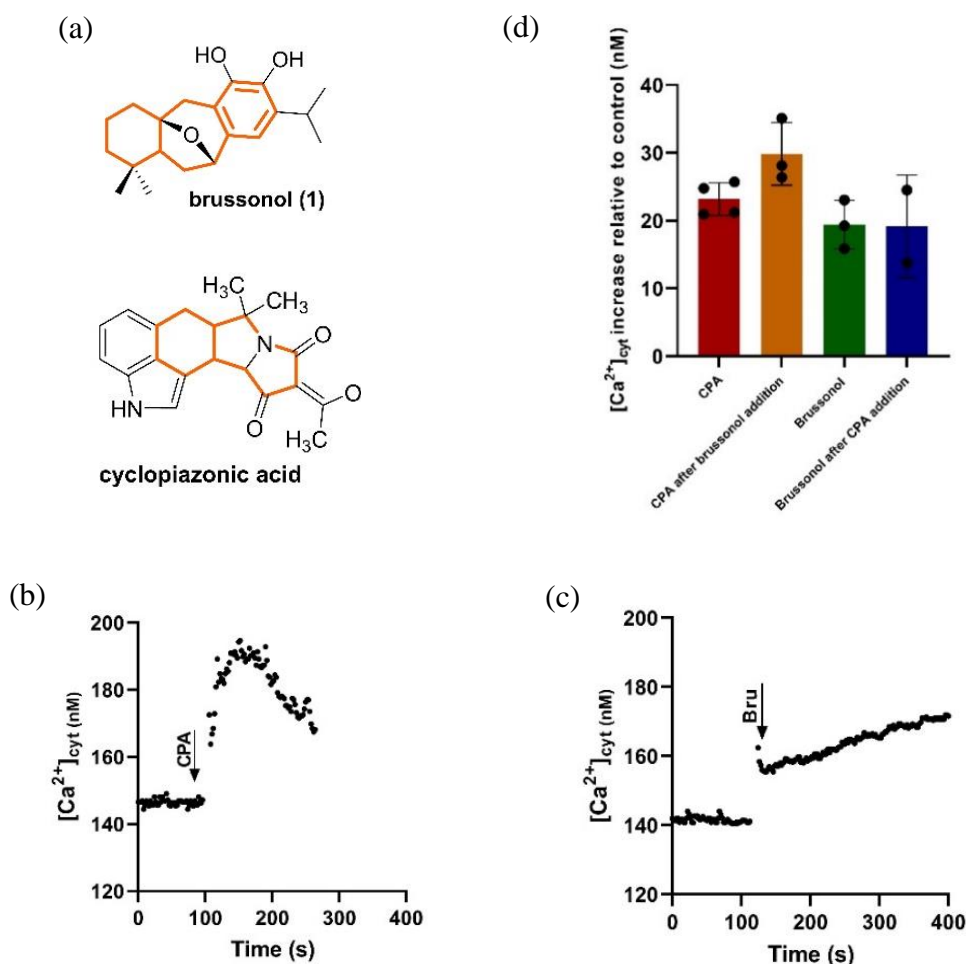


**Figure 21 - Effect of brussonol on the cytosolic  $\text{Ca}^{2+}$  mobilization in *P. falciparum* loaded with Fluo-4 AM calcium indicator.** (a) Chemical structure of brussonol and CPA. The fused rings are highlighted for comparison purposes. (b) Representative traces of  $[\text{Ca}^{2+}]_{\text{cyt}}$  rise induced by 10  $\mu\text{M}$  CPA and (c) 10  $\mu\text{M}$  brussonol in MOPS buffer containing  $\text{Ca}^{2+}$ . (d) Histograms of the increase in the cytosolic  $\text{Ca}^{2+}$  levels upon addition sequential addition of brussonol and CPA, and vice-versa (10  $\mu\text{M}$  of each). \*Indicates the significant statistical difference between the conditions ( $p < 0.05$ , One-Way ANOVA with Turkey post hoc analysis). The data analyzed was collected from two independent experiments.

Finally, the effect of compounds **8** and **12** on calcium homeostasis were also assessed. In at least one experiment, exposing parasites loaded with Fluo-4 AM to compounds **8** and **12** (10  $\mu$ M) displayed a sustained cytosolic calcium increment (**Figure 22a, b**), comparable to compound **1**. Further experiments are needed to confirm and quantify these increments, but both derivatives may exhibit similar effects to compound **1** on calcium homeostasis of the parasite.

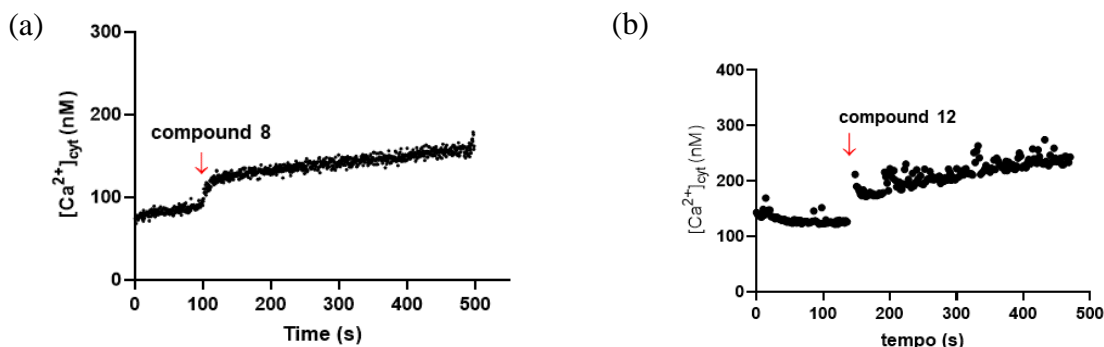


**Figure 22 - Effect of compounds 8 and 12 on the cytosolic  $Ca^{2+}$  mobilization in *P. falciparum* loaded with Fluo-4 AM calcium indicator.** (a) Representative traces of  $[Ca^{2+}]_{cyt}$  rise induced by 10  $\mu$ M compound 8 and (b) 10  $\mu$ M compound 12 in MOPS buffer containing  $Ca^{2+}$ . The data analyzed was collected from one experiment. Arrows indicate when compounds were added into the cuvette.

Source: By the author.

#### 2.4.3 Compounds 8 and 12 do not target PfATP4, V-type $H^+$ -ATPase PfHT, PfFNT, or the $Cl^-$ transporter.

Taking into account that activities of ion transporters are interrelated<sup>216</sup>, and previous results suggested that brissonol interfered in  $Ca^{2+}$  homeostasis, added to the fact that many chemically diverse compounds have been found to inhibit PfATP4<sup>177, 217- 218</sup>, we used an assay that would simultaneously detect inhibitors of PfATP4 as well as various other transporters on the plasma membrane. The pH fingerprint assay has the purpose of associating the biochemical signature, in this case being how parasite's cytosolic pH behaves over time upon drug exposure, of compounds inhibiting transporters and their MoA. It is suggested by Lindbom, Zhang and Lehane (personal communication), the possibility to identify inhibitors for the following transporters via this assay: PfATP4, V-type  $H^+$  ATPase, PfFNT and  $Cl^-$  transporter. Moreover, it is also possible to identify compounds showing protonophore activity (compounds rendering membranes more permeable to  $H^+$ ; and compounds that inhibit proteins required for glycolysis - *i.e.*, glucose transporter, PfHT).

In this experiment, compound inhibition was assessed in three conditions: parasites were resuspended in MS; or MS containing conA (100 nM), a known inhibitor of the V-type H<sup>+</sup>-ATPase<sup>169</sup>; or in a solution containing low [Cl<sup>-</sup>], content of these solutions was described in **Table 5**. Prior to the experiment, the isolated parasites are suspended in a GF buffer to deplete their ATP content. Consequently, at the beginning of fluorescence readings, the parasite's pH<sub>cyt</sub> will be the same as the buffers, pH = 7.1. Upon glucose restoration, parasites undergo cytosolic alkalization reaching pH close to physiological conditions, pH = 7.4 (**Figure 23a.1-4**, and **Figure 24a.5-7**).

Our control compounds (cipargamin, conA, MMV007839, DIDS, CCCP and MMV020438) showed the expected results. Inhibition of PfATP4 by cipargamin caused an immediate increase in pH<sub>cyt</sub>, which was faster than DMSO control in conditions MS and MS+conA (**Figure 23, a.1 and b.1**), while no changes were visualized for 'low Cl<sup>-</sup>' condition (**Figure 23c.3**). V-type H<sup>+</sup> ATPase inhibition by conA resulted in cytosolic acidification, with pH levels being lower than the DMSO control in MS (**Figure 23a.2**). Additionally, there was no change in pH<sub>cyt</sub> in MS+conA (**Figure 23b.2**), since conA is already in this solution, and no changes were expected in 'low Cl<sup>-</sup>' condition (**Figure 23c.2**). Inhibition of PfFNT by compound MMV007839 leads to cytosolic acidification, and this effect can be seen in all three assessed conditions, where the final pH is lower than the DMSO control (**Figure 23a.3, b.3 and c.3**).

When isolated parasites are exposed to low [Cl<sup>-</sup>] media, an outward Cl<sup>-</sup> gradient is created and, consequently, H<sup>+</sup> extrusion occurs resulting in cytosolic alkalization. Under this condition, inhibition of the Cl<sup>-</sup> transporter by DIDS constrained the increase in pH<sub>cyt</sub>, (**Figure 23c.4**), which was also seen in MS and MS+conA (**Figure 23a.4 and b.4**). Upon exposure to compound MMV020438, a PfHT inhibitor, there was a reduction in the rate at which the cytosol alkalizes compared to the DMSO control, as a consequence of ATP depletion (**Figure 24a.5**), and no changes from DMSO were visualized in MS+conA and 'low Cl<sup>-</sup>' condition (**Figures 24b.5 and c.5**). Finally, upon exposure to CCCP, a protonophore that increases membrane permeability to protons, there was cytosolic acidification in MS, compared to control (**Figure 24a.6**); and no significant difference from control in MS+conA (**Figure 24b.6**) while an increased rate of cytosolic alkalization in 'low Cl<sup>-</sup>' condition was seen (**Figure 24c.6**).

Once the isolated parasites were exposed to compounds **8** and **12** (30 μM), no significant differences from the DMSO control were visualized in all conditions assessed (**Figure 24a7, b7 and c.7**). These data indicated that both compounds did not show a pH fingerprint

comparable to the controls used, suggesting that the compounds do not target PfATP4, V-type H<sup>+</sup>-ATPase, PfFNT, PfHT or the Cl<sup>-</sup> transporter.

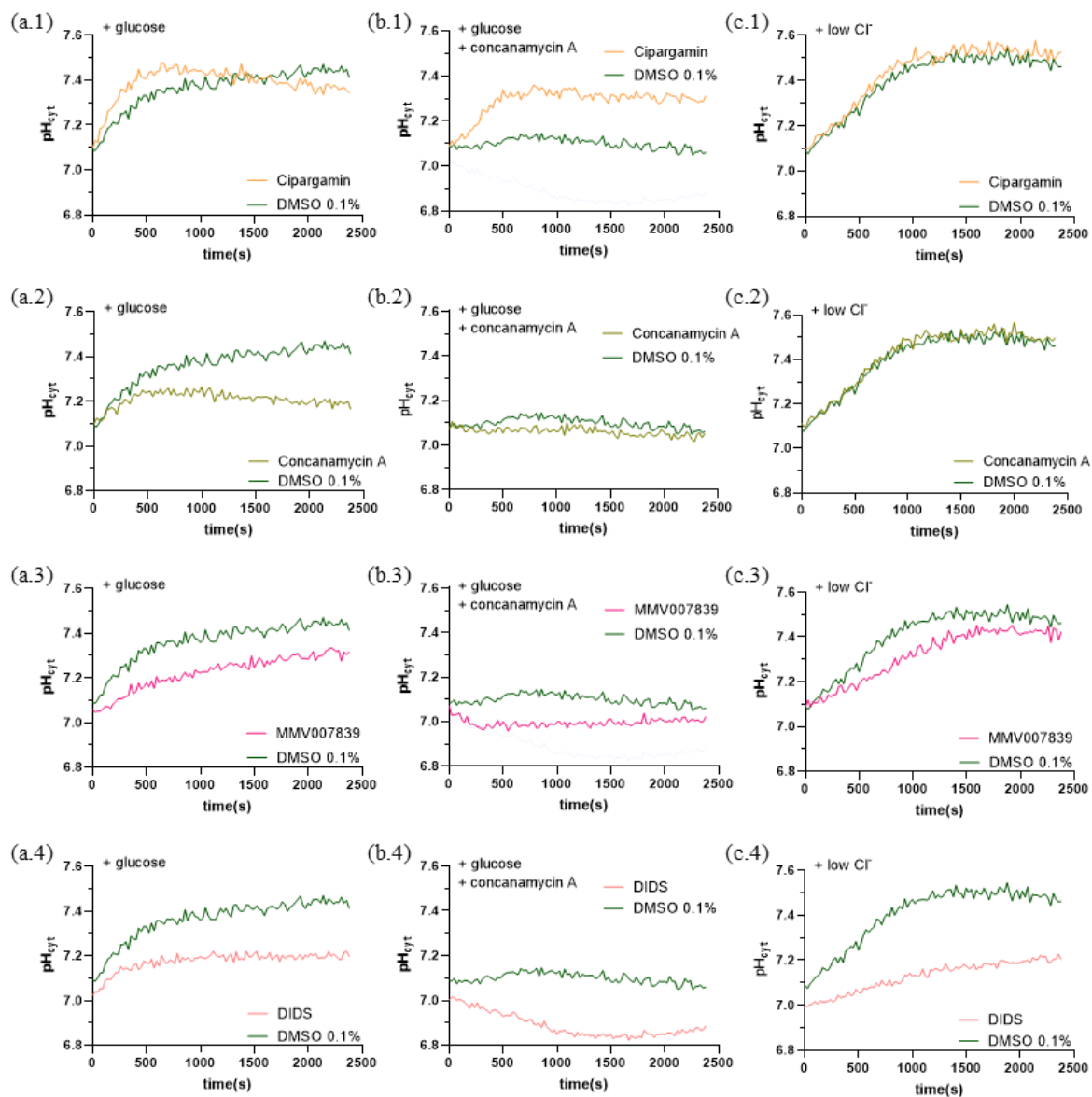


**Figure 23 - Representative pH traces obtained from pH fingerprint assay, part 1.** Each plot was defined with a 2-digit code, a letter followed by a number (1.n). The letters correspond to the condition evaluated (MS, MS+conA, or low Cl<sup>-</sup>), while the numbers correspond to the compound assessed. cip (PfATP4 inhibitor) (a.1, b.1, c.1); conA (V-type H<sup>+</sup> ATPase inhibitor) (a.2, b.2, c.2); MMV007839 (PfFNT inhibitor) (a.3, b.3, c.3); DIDS (a non-specific anion transporter inhibitor) (a.4, b.4, c.4). Graphs are representative traces of three independent experiments.

Source: By the author.

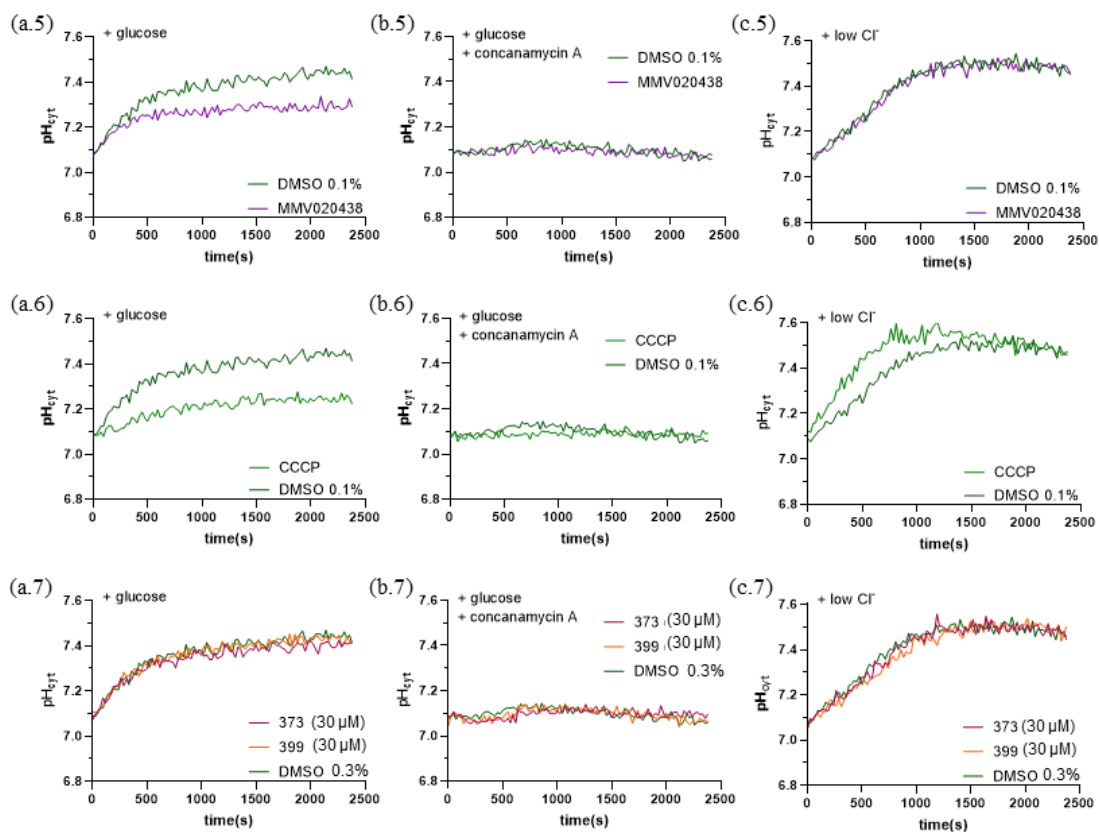


**Figure 24 – Representative pH traces obtained from pH fingerprint assay, part 2.** Each plot was defined with a 2-digit code, a letter followed by a number (l.n). The letters correspond to the condition evaluated (MS, MS+conA, or low Cl<sup>-</sup>), while the numbers correspond to the compound assessed. MMV020438 (PfHT inhibitor) (a.5, b.5, c.5); CCCP (protonophore) (a.6, b.6, c.6); compounds **8** and **12** (a.7, b.7, c.7). Graphs are representative traces of three independent experiments.

Source: By the author.

#### 2.4.4 Compounds **12** did not disrupt parasite [Na<sup>+</sup>]<sub>cyt</sub>.

Another method to identify PfATP4 inhibitors is through Na<sup>+</sup> cytosolic monitoring with SBFI, a Na<sup>+</sup>-sensitive fluorescent dye. Compound **12** was assessed with and without cipargamin (50 nM), a known PfATP4 inhibitor. Saponin-isolated SBFI-loaded trophozoites were resuspended in MS or MS+cip, followed by exposure to compound **12** (30 μM) or DMSO (0.15%).

Under MS conditions, as expected, no increase in [Na<sup>+</sup>]<sub>cyt</sub> was observed upon addition (or not) of DMSO (0.1% v/v) (**Figure 25a**). On the contrary, a marked cytosolic [Na<sup>+</sup>] were visualized when SBFI-loaded parasites were resuspended in MS+cip, with or without addition of DMSO (0.15% v/v) (**Figure 25a**). When parasites were exposed to compound **12** (**Figure 25b**), no increment in cytosolic Na<sup>+</sup> concentration was visualized in MS, while the marked

[Na<sup>+</sup>] increase in condition MS+cip is likely due to the presence of cip in the solution. These results suggest that compound **12** does not disrupt sodium homeostasis in the malarial parasites, excluding the potential of PfATP4 inhibition, which is supported by the results obtained in the pH fingerprint assay.

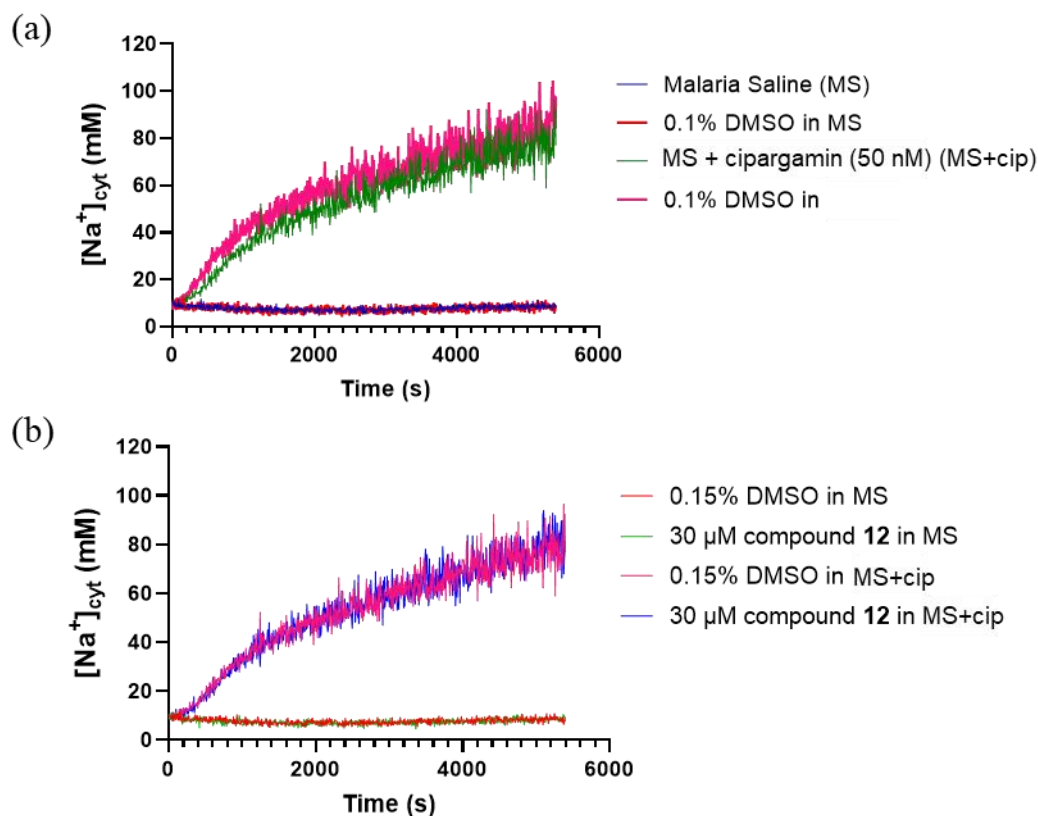


**Figure 25 – Representative traces showing the effect of compound **12**, or cip, on cytosolic [Na<sup>+</sup>].** Trophozoite-isolated parasites were resuspended in MS or MS+cip (a) and exposed to compound **12** or DMSO (b). These graphs are representative of two independent experiments.

Source: By the author.

#### 2.4.5 Compound **12** may hyperpolarize the PPM.

Since changes in ion concentration inside the cell can interfere in its membrane potential ( $\Delta\psi$ ), and because compound **1** elicited an increase in cytosolic [Ca<sup>2+</sup>], we investigated if compound **12** would disrupt  $\Delta\psi$  of *P. falciparum* parasites using bis-oxonol, a fluorescent indicator for  $\Delta\psi$ . Bis-oxonol is an anionic probe that, upon membrane depolarization, enters the cell increasing fluorescence, as opposed to membrane hyperpolarization, when the probe is excluded from the cell, decreasing fluorescence. Moreover, conA was used as positive control for membrane depolarization (marked by fluorescence increase). Inhibition of V-type H<sup>+</sup> ATPase by conA induces cytosolic acidification, as showed in the pH fingerprint assay (**Figure**



**23a.2**), leading to increased uptake of the anionic dye by the cells, culminating in an increase in bis-oxonol fluorescence.

As expected, addition of DMSO (0.1% v/v) to cell suspension did not interfere in membrane potential (**Figure 26a**). Upon addition of conA (100 nM), an increase in bis-oxonol fluorescence was observed, corresponding depolarization of PPM (**Figure 26a**). Interestingly, compound **12** (30  $\mu$ M) had an opposite effect, a reduction in bis-oxonol fluorescence was visualized once this compound was added to the cell suspension, indicating membrane hyperpolarization (**Figure 26b**). Moreover, addition of conA to parasites pre-treated with compound **12** showed similar effect to conA treatment alone (**Figure 26**). These results raise the possibility that compound **12** hyperpolarize PPM, but further experiments are required to confirm this finding.

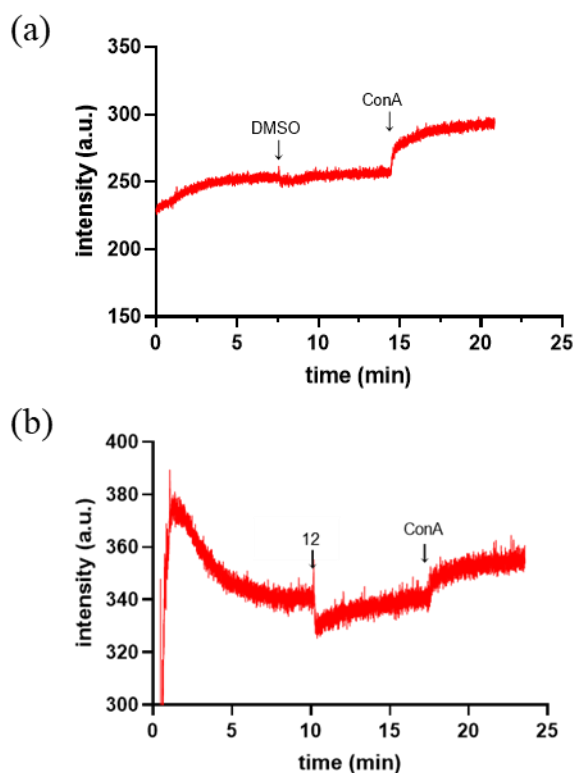


**Figure 26 – Representative traces of bis-oxonol fluorescence.** Trophozoite-isolated parasites were exposed to DMSO and conA (a) and compound **12** and conA (b). Both plots are representative of two independent experiments.

Source: By the author.

#### 2.4.6 *In vitro* evolution studies with Compound 8.

Another strategy used to identify brussanol's MoA was by selecting recrudescence parasites upon continuous culture under compound's **8** pressure. Synchronous ring-stage parasites were used to prepare two T25 flasks with an inoculum size of  $3 \times 10^8$  parasites; in 'Flask 1' DMSO was added (0.03% v/v) while a concentration of  $3 \times IC_{90}$  (16.8  $\mu$ M) of compound **8** was added in 'Flask 2'. Parasites were cultured for three days, with medium changed daily maintaining DMSO and compound **8** concentrations. Vacuolized parasites were observed within two days of drug exposure (arrows) and delay in parasite development, compared to flask 1, and pyknotic nuclei started to appear on cell culture from day 3 (**Figure 27a**).

Subsequently, compound **8** was washed out, and parasites were allowed to grow without the drug for one day. Additionally, four culture flasks containing different concentrations of compound **8** were created from 'Flask 2': 'Flask 3', no drug was added; 'Flask 4', concentration equivalent to compound's  $IC_{90}$  (5.6  $\mu$ M); 'Flask 5', 8.4  $\mu$ M ( $1.5 \times IC_{90}$ ) of compound was added; and 'Flask 6', 16.8  $\mu$ M ( $3 \times IC_{90}$ ) of compound was added. Since all culture flasks exhibited similar results, 'Flask 5' was picked as representative of this method.

Prior to performing growth assays, parasites in 'Flask 5' were exposed to 8.4  $\mu$ M of compound **8** for two more days, then, parasites were allowed to grow without drug pressure. At this point, treated parasites started to display slower growth rates, which can be seen by stained blood smears depicted in **Figure 27b**. Despite that, no significant  $IC_{50}$  shift, as a result of compound **8** pressure, was detected on growth assay performed (**Figure 28a,b**), cipargamin was used as a positive control for inhibition. Consequently, we decided to perform another round of drug pressure.

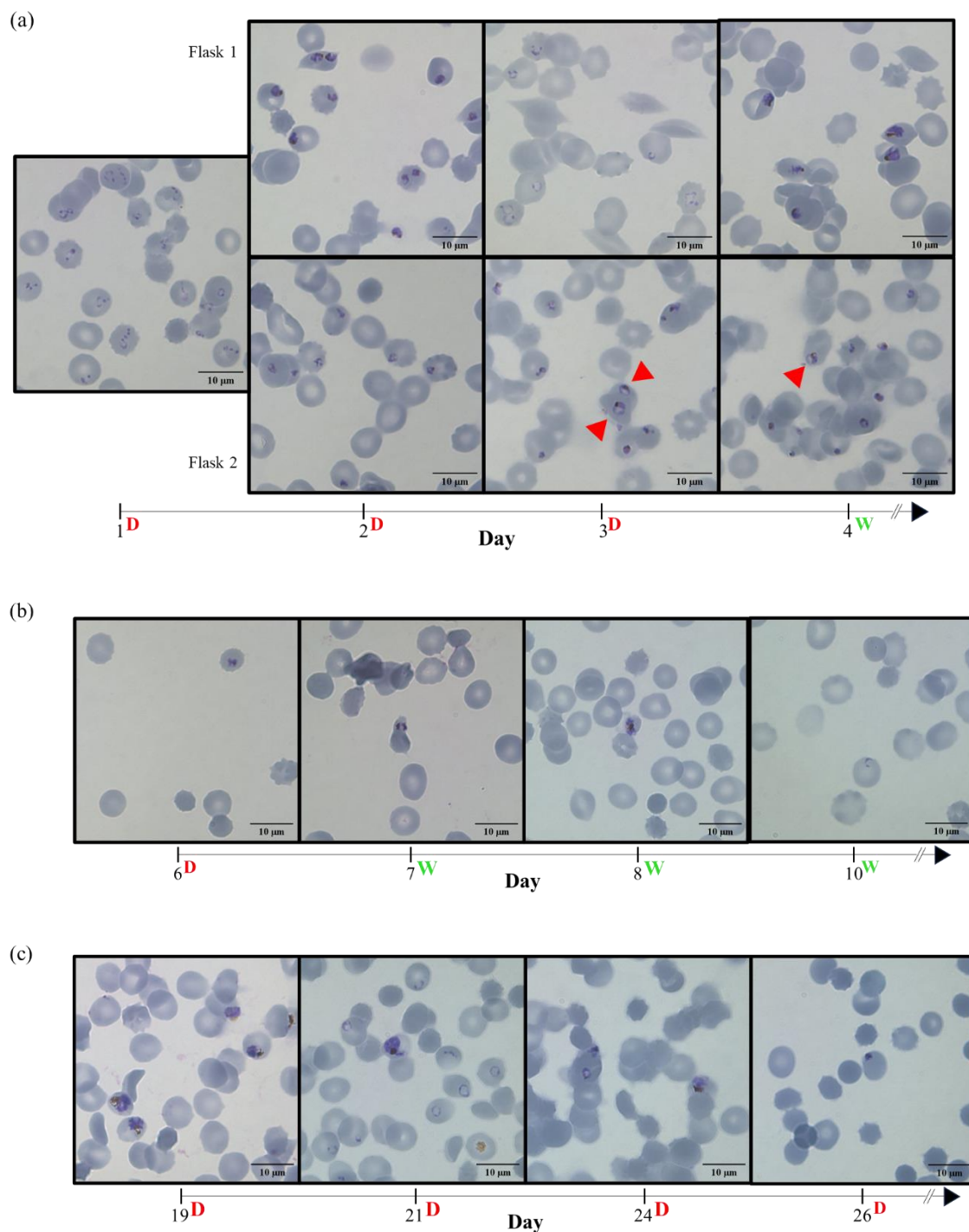


**Figure 27 – Morphological development of parasites cultured under pressure of compound 8.** Stained thin blood smears were prepared to be visualized by light microscopy and monitor the morphological development of the cultures. (a) Blood smears prepared daily from day 1 of the experiment to determine when parasites were dead. (b) Daily blood smears prepared after ‘Flask 2’ was divided into 4 flasks and determine when cultures were dead. (c) Blood smears prepared every 2 days after third pulse of drug pressure started. Red arrows indicate vacuolized parasites. ‘D’ means ‘under drug pressure’ and ‘W’ means ‘the drug was washed’.

Source: By the author.

Next, parasites were cultured under pressure for 11 days. During this period, it was observed that parasites were growing despite the presence of compound **8**, so it was decided to increase compound's concentration by 20% every two days, until the final [compound **8**] reached 12.24  $\mu\text{M}$  in 'Flask 5'. At this point, indication of culture death was observed, i.e. pyknotic nuclei (**Figure 27c**). Then, another round of growth assays was performed and treated parasites were showing the same susceptibility to compounds **8** and **12**. However, different from the first round of growth assays, parasites were still detected (around 5% compared to full growth wells) from concentrations 50 to 3.1  $\mu\text{M}$  of compound **8**, which could indicate the presence of recrudescence parasites less susceptible to compound **8** (**Figure 28c**), but not to compound **12** (**Figure 28e**) or cipargamin (**Figure 28d**). Due to the possibility of a mixed culture of sensitive and resistant parasites in 'Flask 5', microdilution of parasites was performed to isolate clones possessing low susceptibility to compound **8**.

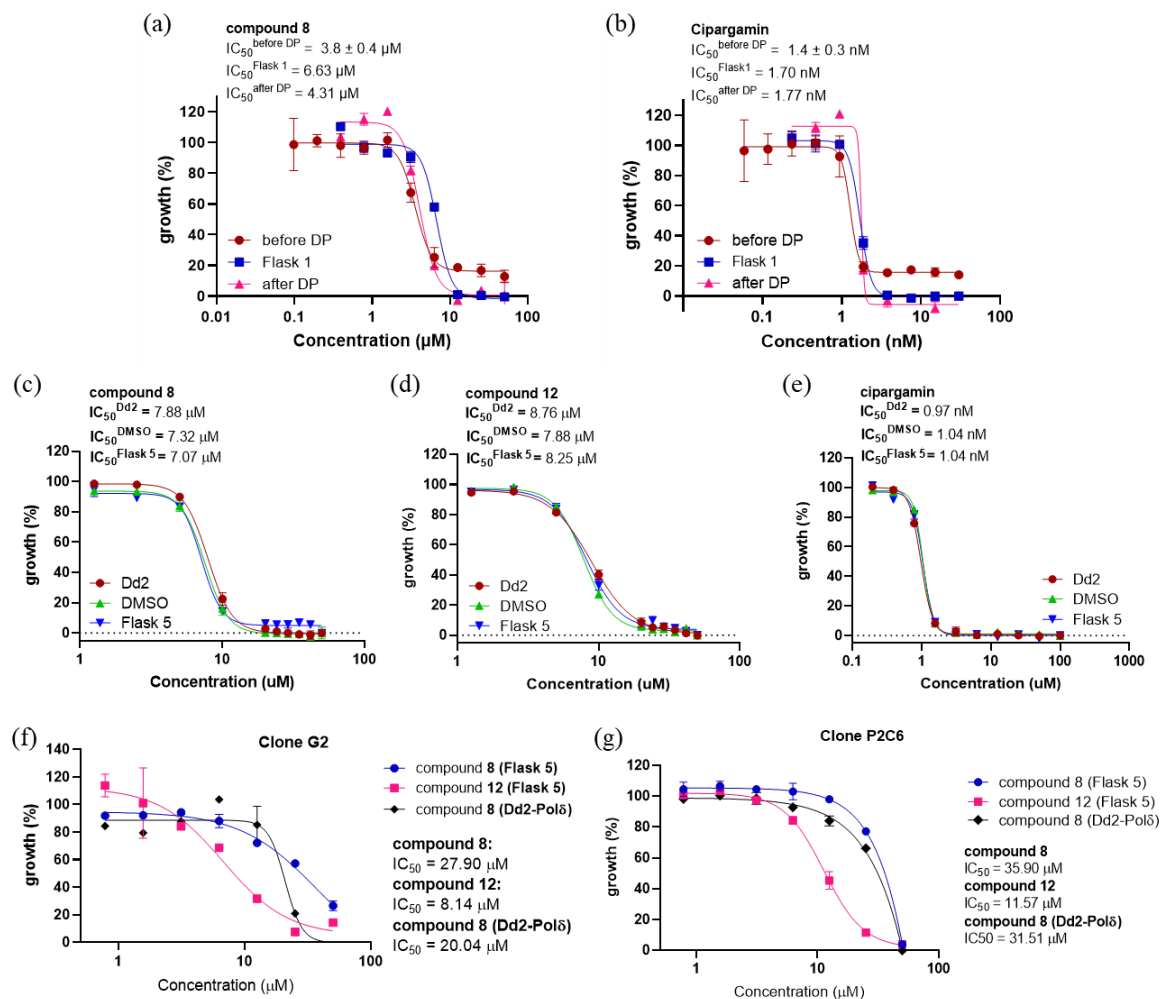


**Figure 28 – Growth assays performed throughout in vitro studies.** Changes in parasite susceptibility as a consequence of continuous growth under pressure of the interested compound is detected via growth assays. (a,b) first round of growth assays performed to comparing  $IC_{50}$  values of parental line, ‘Flask 1’ and ‘Flask 2’ cultures. Cipargamin was used as a positive control for growth inhibition. (c,d,e) second round of growth assays performed with parasite culture from ‘Flask 5’,  $IC_{50}$  values from parental line, ‘Flask 1’ and ‘Flask 5’ were compared. (f,g) growth assays performed with clones obtained via microdilution. Each experiment was performed once.

Source: By the author.

After proceeding with microdilution, seven clones were obtained from ‘Flask 5’, which had not all their growth assays performed due to lack of time. To exemplify some results obtained, growth assays performed for two clones, G2 obtained from ‘Flask 5’ (**Figure 28f**) and P2C6 obtained from ‘Flask 6’ (**Figure 28g**). Both parasite cultures were more susceptible to compound 12 than to compound 8, around 3-fold change; however, no change in  $IC_{50}$  values were observed for clones or parental line. These studies were performed over 30 days, and yet

no resistant parasites were isolated, which may suggest it is difficult selecting for resistance to these compounds. Nonetheless, further experiments are required to confirm the data obtained.

#### 2.4.7 Compound 8 showed inhibition against *Toxoplasma gondii*.

*T. gondii* is an apicomplexan parasite, like *Plasmodium* spp., which has been known as a model organism to study the biology of these obligate intracellular parasites.<sup>207</sup> Advances in CRISPR/Cas9 technologies facilitated genetic manipulation of organisms and cells, especially *T. gondii*, allowing genome-wide screenings to identify gain- and loss-of-function studies.<sup>219</sup> Recently, association of genetic perturbations with drug treatment is a powerful tool able to provide further information related to the compound's MoA, or even its molecular target.

Prior to using *T. gondii* as a tool for MoA and/or drug target identification, first it is necessary to determine if the compound in question has the ability to kill the parasite. In this sense, a fluorescence growth assay was performed with the engineered *T. gondii* Tati  $\Delta ku80$ <sup>220</sup> strain to determine the inhibitory potency of compound 8. Fluorescence was measured daily until reading from the 'full growth' wells reached a plateau, allowing selection of data when parasites were on exponential growth phase. The next step was to determine the IC<sub>50</sub> values for ATO and compound 8. As expected, ATO displayed inhibitory potency at low nanomolar range (IC<sub>50</sub> = 10 ± 3 nM), while compound 8 inhibited parasite growth at low micromolar range (IC<sub>50</sub> = 2.2 ± 0.2 μM). It is important to highlight that this compound showed comparable inhibitory effect against different *P. falciparum* strains and *T. gondii* (Figure 29 and Table 6).

**Table 6** - *In vitro* antiprotozoal activity of compound 8 against *P. falciparum* (3D7 and Dd2-Polδ strains) and *T. gondii* (Tati $\Delta ku80$  strain).

Compound	<i>P. falciparum</i> (3D7)	<i>P. falciparum</i> (Dd2-Polδ)	<i>T. gondii</i> (Tati $\Delta ku80$ )
8	5.8 ± 0.8 μM	3.8 ± 0.4 μM	2.2 ± 0.2 μM
atovaquone	ND <sup>a</sup>	ND <sup>a</sup>	10 ± 3 nM

<sup>a</sup>ND – not determined.

Source: By the author.

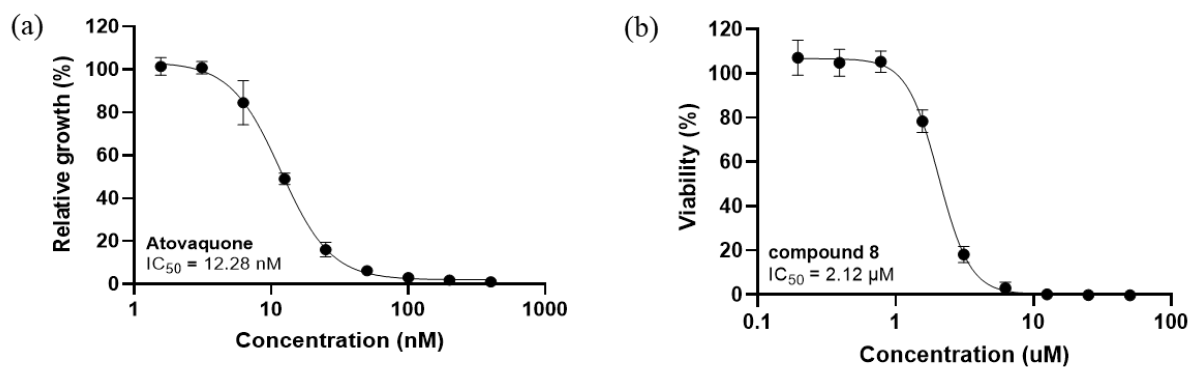


**Figure 29** – Representative concentration-response curves of growth assays against *T. gondii* parasites. Inhibitory potency of ATO (a) and compound **8** (b) were assessed in three independent experiments.

Source: By the author.

These results suggest the use of *T. gondii* to identify the MoA and/or molecular target of this chemical series may be possible. Furthermore, this chemical scaffold is promising since it showed comparable inhibitory effects against two different apicomplexan parasites, suggesting it could be developed as a pan-apicomplexan inhibitor.

## 2.5 DISCUSSION

Knowledge of the molecular MoA and/or molecular target is desirable during the drug discovery process. This information might speed-up compound safety assessment and lead optimization, potentially anticipating the occurrence of resistance mechanisms.<sup>77</sup> In this sense, target deconvolution and MoA studies is a complex and laborious task that may require plenty of time, money, and intense research activities.<sup>221</sup>

Molecular MoA studies of brussanol's chemical series started with a similarity search of chemical databases using SciFinder. This search identified two attractive hits: carnosol and CPA. Carnosol is a terpenoid described to inhibit *in vitro* squalene synthase (SQS) enzyme<sup>213</sup>, the first enzyme solely committed to cholesterol biosynthesis in humans.<sup>214</sup> The lack of this enzyme in the malarial parasite prompted an investigation of brussanol's chemical series effect on the *P. falciparum* isoprenoid biosynthesis, especially because a pathway-specific screen was developed.<sup>154</sup> Compound **1**, however, did not have its growth inhibition reversed by IPP supplementation, indicating that this chemical series does not modulate isoprenoid biosynthesis in *P. falciparum*.

The next step was to investigate if compound **1** would show an effect comparable to CPA, a known inhibitor of PfSERCA. Similarly to previous reports,<sup>159, 179, 215</sup> *P. falciparum* isolated trophozoites exposed to 10  $\mu\text{M}$  CPA exhibited transient increase in cytosolic  $[\text{Ca}^{2+}]$ , which is a consequence of PfSERCA inhibition. Upon compound **1** (10  $\mu\text{M}$ ) exposure, an increase in  $\text{Ca}^{2+}$  cytosolic levels was observed; however, differently from CPA, this effect was sustained over time. Moreover, exposing parasites pre-treated with compound **1** (or CPA) to CPA (or compound **1**) displayed increase in  $[\text{Ca}^{2+}]_{\text{cyt}}$  at equivalent levels when parasites were treated with compounds separately. It is known that  $[\text{Ca}^{2+}]$  within the ER decreases upon SERCA inhibition.<sup>222, 223</sup> In fact, no cytosolic  $[\text{Ca}^{2+}]$  increments were expected upon addition of a second SERCA inhibitor, since the ER would be depleted. In this sense, given that cytosolic  $\text{Ca}^{2+}$  increase was observed after addition of compound **1** (or CPA) in pre-treated parasite, it is likely that compound **1** modulates  $\text{Ca}^{2+}$  homeostasis via a different mechanism, which could be from the intracellular environment (e.g., mitochondrion or acidic organelles) or from the extracellular media mediated by calcium channels at the PPM.<sup>158</sup>

The malarial parasites exert tight control over its internal ionic concentrations through the action of ion transporters, and it is known that these processes are interrelated, which could interfere, or be interfered by, the parasite's  $\text{pH}_{\text{cyt}}$  and  $\Delta\psi$ .<sup>216</sup> In this regard, an assessment of the effect of compound **8** and **12** on the parasite cytosolic pH were conducted by employing a pH fingerprint assay (manuscript reporting this method is under review). This assay compares the pH profile of ATP-depleted trophozoites exposed to compounds **8** or **12** to the pH profile of parasites exposed to known inhibitors of PfATP4, PfFNT, V-type  $\text{H}^+$ -ATPase, and  $\text{Cl}^-$  transporter, as well as PfHT and compounds displaying protonophoric activity. Usually, ATP-depleted parasites exhibit an acidified cytosol, which is recovered to physiological conditions when glucose levels are restored. In this sense, the pH dynamics of ATP-depleted trophozoites exposed to these compounds (reference and tested) were monitored and compared to identify the molecular targets of brussonol's derivatives. Differently from the positive controls for inhibition, compounds **8** and **12** exhibited a pH fingerprint comparable to DMSO control (negative control for inhibition), ruling out these transporters as molecular targets of this chemical series. Furthermore, PfATP4 inhibition can be confirmed by analysis of  $\text{Na}^+$  dynamics after drug exposure, since it is postulated that this ion transporter promotes  $\text{Na}^+$  extrusion coupled to  $\text{H}^+$  influx, as observed after cipargamin exposure.<sup>217,224</sup> Treatment of isolated parasites with compound **12** did not disrupt  $\text{Na}^+$  homeostasis, confirming the results obtained in the pH fingerprint assay.



The next strategy was to determine whether compound **12** disrupted the parasites's  $\Delta\psi$  based on the fluorescent anionic dye, bis-oxonol.<sup>197,225</sup> Inhibition of V-type H<sup>+</sup>-ATPase by conA results in cytosolic acidification, followed by influx of bis-oxonol visualized as increase in fluorescence, which characterizes depolarization of the PPM. Differently from conA, reduction of bis-oxonol fluorescence followed parasite exposure with compound **12**, corresponding to PPM hyperpolarization. The possibility of other parasite organelles (i.e. mitochondrion or digestive vacuole) interfering in these  $\Delta\psi$  measurements were discussed by Allen & Kirk (2004).<sup>197</sup> In their study, they used a cationic probe (<sup>3</sup>H]TPP<sup>+</sup>), which could accumulate in organelles possessing an inwardly negative potential. In the conditions studied, these researchers reported no significant effect of other organelles on the PPM  $\Delta\psi$ .

Our results suggest that compound **12** disrupts the PPM membrane potential, however, further experiments are required to quantify this effect and confirm whether this compound disrupts the membrane potential of other organelles. So far, it is unknown how brussanol's chemical series interferes in the parasite's  $\Delta\psi$ ; however, it is possible that both processes, membrane hyperpolarization and increase in [Ca<sup>2+</sup>]<sub>cyt</sub>, could be related. In fact, it is known that Ca<sup>2+</sup> influx, specifically in skeletal muscle cells, causes membrane hyperpolarization by activating Ca<sup>2+</sup>-activating K<sup>+</sup> channels, leading to K<sup>+</sup> being exported from the cell, hence causing hyperpolarization.<sup>196</sup> It is not confirmed if the same process occurs in the malaria parasite, so investigating if this chemical series interferes in intracellular [K<sup>+</sup>] could potentially provide more insights into its MoA.

*In vitro* evolution followed by whole-genome analysis is a successful reverse-genetic method to identify chemically validated targets. We performed *in vitro* evolution studies exposing *P. falciparum* parasites Dd2-Pol $\delta$  strain, which is an engineered strain possessing deficient proofing-reading activity.<sup>203</sup> Consequently, the level of basal spontaneous mutations in this strain is higher than other *P. falciparum* strains. After two attempts of *in vitro* evolution by continuous growth under compound **8** pressure, we were unable to provide evidence of selecting parasites less susceptible to this compound. Nonetheless, during the first round of drug exposure, vacuolized parasites were visualized microscopically within 2 days of inhibitor pressure. Vacuolization in parasites can be related to stress in culture, or it could be related to the compound's MoA. For example, vacuolization may be related to alterations in metabolism and/or ionic equilibrium.<sup>92</sup> Additionally, after 2 and 3 rounds of inhibitor pressure, we observed that parasite growth was slower, compared to parasite's growth prior to the experiment. At the last round of inhibitor pressure, parasites from 3 Flasks ('Flask 5', 'Flasks 6' and 'Flask 2'

(3xIC<sub>90</sub>) from first attempt) showed normal growth rate under pressure. Even though no experiments were performed to determine growth rates for these treated cultures, these observations indicated that parasites' fitness under inhibitor pressure was impacted, but further evaluation is required. In this experiment, 21 clones were obtained from two independent experiments that will have their genome analysed.

*T. gondii* is considered a model organism to study apicomplexan parasites, as well as host-parasite interactions.<sup>207</sup> Development and advances in target deconvolution, such as chemical proteomics, gene expression profiling, genetic screenings, and resistance generation, broaden the strategies available for MoA studies.<sup>226</sup> Before using *T. gondii* as a model to study the effect of the compound of interest on apicomplexans, by applying for example CRISPR/Cas9 methods in this organism to construct a library of conditional targeted genetic modifications associated with compound treatment, it is required to determine whether this compound kills the protozoan parasite. If no inhibition is detected, it is not possible to use this strategy to identify mutants less susceptible to the tested compound. After assessing the inhibitory activity of compound **8** against *T. gondii* parasites, the brussonol derivative exhibited comparable inhibitory potency to *Plasmodium* spp. Thus, it is likely that compound **8** shares similar MoAs and/or molecular target in both parasites. If this is the case, it is probable that this compound series likely targets other apicomplexans, potentially providing new compound candidates to treat humans and livestock affected by these organisms. Nonetheless, further experiments are required to confirm this result. In summary, application of the forward genetic screens described with *T. gondii* is an attractive approach and could be used to unravel the MoAs of the brussonol series.

### 3 GENERAL CONCLUSIONS AND PERSPECTIVES

Brussonol (**1**) is an icetexane diterpenoid that exhibited promising antiplasmodial activity. In the course of this Ph.D. thesis investigation, we provided evidence that this chemical series is attractive to follow-up studies aiming at developing new lead candidates for malaria. In this sense, no cross-resistance, or similar resistance mechanisms, were detected against the panel of resistant *P. falciparum* parasites used. In addition, our results suggest that this chemical series needed 24 h of exposure to kill the malarial parasite, despite some discrepancies detected for compound **12**. Moreover, compound **1** exhibited comparable inhibitory potencies against different species of *Plasmodium* parasites, namely *P. knowlesi*, *P. falciparum*, and *P. vivax* clinical isolates, while compound **8** displayed equipotent IC<sub>50</sub> values against *T. gondii* parasites. Finally, compound **1** showed an additive profile when combined with ART, corroborating the potential use of these compounds in the clinic.

To shed light on the molecular MoA underlying the antiplasmodial activity of the brussonol derivatives, we verified that compound **1** modulated Ca<sup>2+</sup> homeostasis in the parasite, causing an increase in [Ca<sup>2+</sup>]<sub>cyt</sub> after exposing trophozoites to this compound. It is likely that compound **1** disrupts cytosolic Ca<sup>2+</sup> differently from CPA, which could be released from another intracellular organelle or through a transporter in the PPM. We demonstrated that exposing isolated trophozoites to compound **12** hyperpolarized the PPM.

In summary, our investigations have revealed that brussonol and its analogs represent novel molecular scaffolds with compelling antiplasmodial activities. This underscores the rationale for devising new derivatives with enhanced properties, aiming to generate the next generation of lead candidates for malaria.



## REFERENCES

- 1 WHITE, N. J. *Plasmodium knowlesi*: the fifth human malaria parasite. **Clinical Infectious Diseases**, v. 46, n. 2, p 172-173, 2008. DOI: 10.1086;524889.
- 2 HOWES, R. E. *et al.* Global epidemiology of *Plasmodium vivax*. **American Journal of Tropical Medicine and Hygiene**, v. 95, n. 6, p 15-34, 2016. DOI: 10.4269/ajtmh.16-0141.
- 3 ANGRISANO, F.; ROBINSON, L. J. *Plasmodium vivax* – how hidden reservoirs hinder global malaria elimination. **Parasitology International**, v. 87, p 102526, 2022. DOI: 10.1016/j.parint.2021.102526.
- 4 BEIER, J. C. Malaria parasite development in mosquitoes. **Annual Review Entomology**, v. 43, p 519-562, 1998. DOI: 10.1146/annurev.ento.43.1.519.
- 5 AMINO, R. *et al.* Quantitative imaging of *Plasmodium* transmission from mosquito to mammal. **Nature Medicine**, v. 12, n. 2, p. 220–224, 2006. DOI: 10.1038/nm1350.
- 6 ARNOT, D. E.; RONANDER, E.; BENGTSSON, D. C. The progression of the intra-erythrocytic cell cycle of *Plasmodium falciparum* and the role of the centriolar plaques in asynchronous mitotic division during schizogony. **International Journal for Parasitology**, v. 41, n. 1, p 71–80, 2011. DOI: 10.1016/j.ijpara.2010.07.012.
- 7 DESPOMMIER D. D.; GWADZ R. W.; HOTEZ P. J. Malaria: *Plasmodium falciparum* (Welch 1898), *Plasmodium vivax* (Grassi and Filetti 1889), *Plasmodium ovale* (Stephens 1922), *Plasmodium malariae* (Laveran 1881). In: DESPOMMIER D. D.; GWADZ R. W.; HOTEZ P. J. (ed.) **Parasitic diseases**. New York: Springer, 2011, p 174–189. DOI: 10.1007/978-1-4612-2476-1.
- 8 SATO, S. *Plasmodium*—a brief introduction to the parasites causing human malaria and their basic biology. **Journal of Physiological Anthropology**, v. 40, n. 1, 2021. DOI: 10.1186/s40101-020-00251-9.
- 9 DVORAK, J. A. *et al.* Invasion of erythrocytes by malaria merozoites. **Science**, v. 187, n. 4178, p 748–750, 1975.
- 10 LADDA, R.; AIKAWA, M.; SPRINZ, H. Penetration of erythrocytes by merozoites of mammalian and avian malarial parasites. **Journal of Parasitology**, v. 87, n. 3, p 470–478, 2001. DOI: 10.164/0022-3395(2001)087[0470:poebmo]2.0.co;2.
- 11 JOSLING, G. A.; LLINÁS, M. Sexual development in *Plasmodium* parasites: knowing when it's time to commit. **Nature Reviews Microbiology**, v. 13, n. 9, p 573-587, 2015. DOI: 10.1038/nrmicro3519.
- 12 BILLKER, O. *et al.* Identification of xanthurenic acid as the putative inducer of malaria development in the mosquito. **Letters to Nature**, v. 392, p 289-292, 1998. DOI: 10.1038/32667.
- 13 SICILIANO, G. *et al.* Critical steps of *Plasmodium falciparum* ookinete maturation. **Frontiers in Microbiology**, v. 11, 2020. DOI: 10.3389/fmicb.2020.00269.
- 14 VAUGHAN, J. A. Population dynamics of *Plasmodium* sporogony. **Trends in Parasitology**, v. 23, n. 2, p 63-70, 2007. DOI: 10.1016/j.pt.2006.12.009.

- 15 MAIER, A. G. *et al.* *Plasmodium falciparum*. **Trends in Parasitology**, v. 35, n. 6, p 481-482, 2019. DOI: 10.1016/j.pt.2018.11.010.
- 16 WHITE, N. J. *et al.* Malaria. **Lancet**, v. 383, n. 9918, p 723-735, 2014. DOI: 10.1016/S0140-6736(13)60024-0.
- 17 GALLUP, J. L.; SACHS, J. D. The economic burden of malaria. **American Journal of Tropical Medicine and Hygiene**, v. 64, n. 1- 2, p 85–96, 2001.
- 18 WORLD HEALTH ORGANIZATION. **World Malaria Report 2023**. Available at: <https://www.who.int/teams/global-malaria-programme/reports/world-malaria-report-2023>. Accessible at: 23 Jan. 2023.
- 19 CARLOS, B. C. *et al.* A comprehensive analysis of malaria transmission in Brazil. **Pathogens and Global Health**, v. 113, n. 1, p 1-13, 2019. DOI: 10.1080/20477724.2019.15811463.
- 20 KHO, S. *et al.* Hidden biomass of intact malaria parasites in the human spleen. **New England Journal of Medicine**, v. 384, n. 21, p 2067–2069, 2021. DOI: 10.1056/nejmc2023884.
- 21 OBALDIA, N. *et al.* Bone marrow is a major parasite reservoir in plasmodium vivax infection. **American Society of Microbiology**, v. 9, n. 3, e00625-18, 2018. DOI: 10.1128/mBio.00625-18.
- 22 MAWSON, A. R. The pathogenesis of malaria: a new perspective. **Pathogens and Global Health**, v. 107, n. 3, p 122–129, 2013. DOI: 10.1179/2047773213Y.0000000084.
- 23 BARTOLONI, A.; ZAMMARCHI, L. Clinical aspects of uncomplicated and severe malaria. **Mediterranean Journal of Hematology and Infectious Diseases**, v. 4, n. 1, 2012. DOI: 10.4084/MJHID.2012.026.
- 24 WORLD HEALTH ORGANIZATION. **Global technical strategy for malaria 2016–2030** - update. Available at: <https://iris.who.int/bitstream/handle/10665/342995/9789240031357-eng.pdf?sequence=1>. Accessible at: 23 Jan. 2023.
- 25 WORLD HEALTH ORGANIZATION. **Guidelines for malaria**. Available at: <https://iris.who.int/handle/10665/373339>. Accessible at: 30 Oct. 2023.
- 26 WORLD HEALTH ORGANIZATION. **World malaria report 2022**. Available at: <https://www.who.int/teams/global-malaria-programme>. Accessible at: 30 Oct. 2023.
- 27 RECHT, J. *et al.* Malaria in Brazil, Colombia, Peru and Venezuela: current challenges in malaria control and elimination. **Malaria Journal**, v. 16, n. 1, 2017. DOI: 10.1186/s12936-017-1925-6.
- 28 BHATT, S. *et al.* The effect of malaria control on *Plasmodium falciparum* in Africa between 2000 and 2015. **Nature**, v. 526, n. 7572, p 207–211, 2015. DOI: 10.1038/nature15535.
- 29 POLLARD, A. J.; BIJKER, E. M. A guide to vaccinology: from basic principles to new developments. **Nature Reviews Immunology**, v. 21, n. 2, p 83-100, 2021. DOI: 10.1038/s41577-020-00479-7.
- 30 DATOO, M. S. *et al.* Safety and efficacy of malaria vaccine candidate R21/Matrix-M in African children: a multicentre, double-blind, randomised, phase 3 trial. **Lancet**, v. 403, p 533-544, 2024. DOI: 10.1016/S0140-6736(23)02511-4.

- 31 WORLD HEALTH ORGANIZATION. **WHO recommends R21/Matrix-M vaccine for malaria prevention in updated advice on immunization.** Available at: <https://www.who.int/news/item/02-10-2023-who-recommends-r21-matrix-m-vaccine-for-malaria-prevention-in-updated-advice-on-immunization>. Accessible at: 01 Feb. 2024.
- 32 BERZOSA, P. *et al.* Comparison of three diagnostic methods (microscopy, RDT, and PCR) for the detection of malaria parasites in representative samples from Equatorial Guinea. **Malaria Journal**, v. 17, n. 1, 2018. DOI: 10.1186/s12936-018-2481-4.
- 33 WORLD HEALTH ORGANIZATION. **Diagnostic testing.** Available at: <https://www.who.int/teams/global-malaria-programme/case-management/diagnosis>. Accessible at: 23 Oct. 2023.
- 34 WORLD HEALTH ORGANIZATION. **Microscopy.** Available at: <https://www.who.int/teams/global-malaria-programme/case-management/diagnosis/microscopy>. Accessible at: 23 Oct. 2023.
- 35 WORLD HEALTH ORGANIZATION. **Rapid diagnostic tests.** Available at: <https://www.who.int/teams/global-malaria-programme/case-management/diagnosis/rapid-diagnostic-tests>. Accessible at: 23 Oct. 2023.
- 36 MOUATCHO, J. C.; DEAN GOLDRING, J. P. Malaria rapid diagnostic tests: challenges and prospects. **Journal of Medical Microbiology**, v. 62, p 1491-1505, 2013. DOI: 10.1099/jmm.0.052506-0.
- 37 HOUZÉ, S. *et al.* PfHRP2 and PfLDH antigen detection for monitoring the efficacy of artemisinin-based combination therapy (ACT) in the treatment of uncomplicated falciparum malaria. **Malaria Journal**, v. 8, n. 1, 2009. DOI: 10.1186/1475-2875-8-211.
- 38 ROTH, J. M. *et al.* Molecular malaria diagnostics: a systematic review and meta-analysis. **Critical Reviews in Clinical Laboratory Sciences**, v. 53, n. 2, p 87-105, 2016. DOI: 10.3109/10408363.2015.1084991.
- 39 PICOT, S.; CUCHERAT, M.; BIENVENU, A. L. Systematic review and meta-analysis of diagnostic accuracy of loop-mediated isothermal amplification (LAMP) methods compared with microscopy, polymerase chain reaction and rapid diagnostic tests for malaria diagnosis. **International Journal of Infectious Diseases**, v. 98, p 408-419, 2020. DOI: 10.1016/j.ijid.2020.07.009.
- 40 LEE, R. A. *et al.* Ultrasensitive CRISPR-based diagnostic for field-applicable detection of *Plasmodium* species in symptomatic and asymptomatic malaria. **Proceedings of the National Academy of Sciences USA**, v. 117, n. 47, p 25722-25731, 2020. DOI: 10.1073/pnas.2010196117.
- 41 ARROW, K. J.; PANOSIAN, C.; GELBAND, H. *et al.* Saving lives, buying time: economics of malaria drugs in an age of resistance. Washington: National Academies Press, 2004. DOI: 10.17226/11017.
- 42 MINISTÉRIO DA SAÚDE. **Guia de tratamento da malária no Brasil.** Available at: <https://www.gov.br/saude/pt-br/assuntos/saude-de-a-a-z/m/malaria/arquivos/guia-tratamento-malaria-2ed-el-27ago20-isbn.pdf>. Accessible at: 25 Mar. 2024.
- 43 EYAL, S. The fever tree: From malaria to neurological diseases. **Toxins**, v. 10, n. 12, 2018. DOI: 10.3390/toxins10120491.

44 MA, N. *et al.* The birth of artemisinin. **Pharmacology and Therapeutics**, v. 216, 2020. DOI: 10.1016/j.pharmthera.2020.107658.

45 SCHLITZER, M. Malaria chemotherapeutics part I: History of antimalarial drug development, currently used therapeutics, and drugs in clinical development. **ChemMedChem**, v. 2, n. 7, p 944-986, 2007. DOI: 10.1002/cmdc.200600240.

46 SEEMAN, J. I. The woodward-doering/rabe-kindler total synthesis of quinine: Setting the record straight. **Angewandte Chemie: international edition**, v. 46, n. 9, p 1378-1413, 2007. DOI: 10.1002/anie.200601551.

47 GOTLIB, J.; MINISTÉRIO DA SAÚDE. **Ministério da Saúde incorpora medicamento inovador para malária ao SUS**. Available at: <https://www.gov.br/saude/pt-br/assuntos/noticias/2023/junho/ministerio-da-saude-incorpora-medicamento-inovador-para-malaria-ao-sus>. Accessible at: 20 Feb. 2024.

48 WATERS, N. C.; EDSTEIN, M. D. 8-Aminoquinolines: Primaquine and tafenoquine. *In*: STAINES, H. M.; KRISHNA, S. (ed.) **Treatment and prevention of malaria: antimalarial drug chemistry, action and use**. New York: Springer, 2012. p 69–94. (Milestones in drug therapy). DOI: 10.1007/978-3-0346-0480-2\_4.

49 ROSENTHAL, P. J. Antimalarial Chemotherapy. *In*: ROSENTHAL, P. J. (ed.) **Infectious disease**. Totowa: Humana Press, 2001. p 409. (New directions in drug discovery).

50 GRIMBERG, B. T.; MEHLOTRA, R. K. Expanding the antimalarial drug arsenal-now, but how? **Pharmaceuticals**, v. 4, n. 5, p 681–712, 2011. DOI: 10.3390/ph4050681.

51 HILL, S. R.; THAKUR, R. K.; SHARMA, G. K. Antimalarial medications. *In*: ABOUBAKR, S. *et al.* (ed.) **StatPearls, treasure island**. 2023. Available at: [https://www-ncbi-nlm-nih.ez67.periodicos.capes.gov.br/books/NBK470158/](https://www.ncbi-nlm-nih.ez67.periodicos.capes.gov.br/books/NBK470158/). Accessible at: 30 Oct. 2023.

52 EGWU, C. O. *et al.* Impact of drug pressure versus limited access to drug in malaria control: the dilemma. **Medicines**, v. 9, n. 1, p. 2, 2022. DOI: 10.3390/medicines9010002.

53 WORLD HEALTH ORGANIZATION. **Report on antimalarial drug efficacy, resistance and response: 10 years of surveillance (2010–2019)**. Available at: <https://www.who.int/publications/i/item/9789240012813>. Accessible at: 30 Oct. 2023.

54 WICHT, K. J.; MOK, S.; FIDOCK, D. A. Molecular mechanisms of drug resistance in plasmodium falciparum malaria. **Annual Review of Microbiology**, v. 74, p 431-454, 2020. DOI: 10.1146/annurev-micro-020518-115546.

55 KURT YILMAZ, N.; SCHIFFER, C. A. Introduction: drug resistance. **Chemical Reviews**, v. 121, n. 6, p 3235-3237, 2021. DOI: 10.1021/acs.chemrev.1c00118.

56 WORLD HEALTH ORGANIZATION. **Methods for surveillance of antimalarial drug efficacy**. Available at: <https://www.who.int/publications/i/item/9789241597531>. Accessible at: 30 Apr. 2023.

57 YEUNG, S. Malaria - update on antimalarial resistance and treatment approaches. **Pediatric Infectious Disease Journal**, v. 37, n. 4, p 367–369, 2018. DOI: 10.1097/INF.0000000000001887.

58 FIDOCK, D. A. *et al.* Mutations in the *P. falciparum* digestive vacuole transmembrane protein pfert and evidence for their role in chloroquine resistance. **Molecular Cell**, v. 6, p 861–871, 2000.



- 59 COWMAN, A. F. *et al.* Amino acid changes linked to pyrimethamine resistance in the dihydrofolate reductase-thymidylate synthase gene of *Plasmodium falciparum*. **Proceedings of the National Academy of Sciences USA**, v. 85, p 9109-9113, 1988.
- 60 WANG, P. *et al.* Sulfadoxine resistance in the human malaria parasite *Plasmodium falciparum* is determined by mutations in dihydropteroate synthetase and an additional factor associated with folate utilization. **Molecular Microbiology**, v. 23, n. 5, p 979–986, 1997. DOI: 10.1046/j.1365-2958.1997.2821646.x.
- 61 NZILA, A. M. *et al.* Molecular evidence of greater selective pressure for drug resistance exerted by the long-acting antifolate pyrimethamine/sulfadoxine compared with the shorter-acting chlorproguanil/dapsone on kenyan *Plasmodium falciparum*. **Journal of Infectious Diseases**, v. 181, p 2023-2028, 2000. DOI: 10.1086/315520.
- 62 DONDORP, A. M. *et al.* Artemisinin resistance in *Plasmodium falciparum* malaria. **New England Journal of Medicine**, v. 361, n. 5, p 455–467, 2009. DOI: 10.1056/nejmoa0808859.
- 63 STOKES, B. H. *et al.* *Plasmodium falciparum* k13 mutations in Africa and Asia impact artemisinin resistance and parasite fitness. **eLife**, v. 10, e66277, 2021. DOI: 10.7554/eLife.66277.
- 64 ROSENTHAL, P. J.; ASUA, V.; CONRAD, M. D. Emergence, transmission dynamics and mechanisms of artemisinin partial resistance in malaria parasites in Africa. **Nature Reviews Microbiology**, 2024. DOI: 10.1038/s41579-024-01008-2.
- 65 WITKOWSKI, B. *et al.* Novel phenotypic assays for the detection of artemisinin-resistant *Plasmodium falciparum* malaria in Cambodia: *in-vitro* and *ex-vivo* drug-response studies. **Lancet Infectious Diseases**, v. 13, n. 12, p 1043–1049, 2013. DOI: 10.1016/S1473-3099(13)70252-4.
- 66 ARIEY, F. *et al.* A molecular marker of artemisinin-resistant *Plasmodium falciparum* malaria. **Nature**, v. 505, n. 7481, p 50–55, 2014. DOI: 10.1038/nature12876.
- 67 VAN DER PLUIJM, R. W. *et al.* Determinants of dihydroartemisinin-piperazine treatment failure in *Plasmodium falciparum* malaria in Cambodia, Thailand, and Vietnam: a prospective clinical, pharmacological, and genetic study. **Lancet Infectious Diseases**, v. 19, n. 9, p 952–961, 2019. DOI: 10.1016/S1473-3099(19)30391-3.
- 68 PHYO, A. P. *et al.* Declining efficacy of artemisinin combination therapy against *P. Falciparum* malaria on the Thai-Myanmar Border (2003-2013): the role of parasite genetic factors. **Clinical Infectious Diseases**, v. 63, n. 6, p 784–791, 2016. DOI: 10.1093/cid/ciw388.
- 69 MUKHERJEE, A. *et al.* Artemisinin resistance without pfcy5p mutations in *Plasmodium falciparum* isolates from Cambodia. **Malaria Journal**, v. 16, n. 1, 2017. DOI: 10.1186/s12936-017-1845-5.
- 70 MÉNARD, D. *et al.* A worldwide map of *Plasmodium falciparum* K13-propeller polymorphisms. **New England Journal of Medicine**, v. 374, n. 25, p 2453–2464, 2016. DOI: 10.1056/NEJMoa1513137.
- 71 SIDDIQUI, F. A.; LIANG, X.; CUI, L. *Plasmodium falciparum* resistance to ACTs: emergence, mechanisms, and outlook. **International Journal for Parasitology: drugs and drug resistance**, v. 16, p. 102–118, 2021. DOI: 10.1016/j.ijpddr.2021.05.007.

- 72 KUBLIN, J. G. *et al.* Reemergence of chloroquine-sensitive *Plasmodium falciparum* malaria after cessation of chloroquine use in Malawi. **Journal of Infectious Diseases**, v. 187, n. 12, p 1870–1875, 2003. DOI: 10.1086/375419.
- 73 LAUFER, M. K. *et al.* Return of chloroquine antimalarial efficacy in Malawi. **New England Journal of Medicine**, v. 355, n. 19, p 1959–1966, 2006. DOI: 10.1056/NEJMoa062032.
- 74 TSE, E. G.; KORSIK, M.; TODD, M. H. The past, present and future of anti-malarial medicines. **Malaria Journal**, v. 18, 2019. DOI: 10.1186/s12936-019-2724-z.
- 75 SIQUEIRA-NETO, J. L. *et al.* Antimalarial drug discovery: progress and approaches. **Nature Reviews Drug Discovery**, v. 22, n. 10, p 807-826, 2023. DOI: 10.1038/s41573-023-00772-9.
- 76 HOVLID, M. L.; WINZELER, E. A. Phenotypic screens in antimalarial drug discovery. **Trends in Parasitology**, v. 32, n. 9, p 697-707, 2016. DOI: 10.1016/j.pt.2016.04.014.
- 77 YANG, T. *et al.* MalDA, accelerating malaria drug discovery. **Trends in Parasitology**, v. 37, n. 6, p 493-507, 2021. DOI: 10.1016-j.pt.2021.01.009.
- 78 FORTE, B. *et al.* Prioritization of molecular targets for antimalarial drug discovery. **ACS Infectious Diseases**, v. 7, n. 10, p 2764-2776, 2021. DOI: 10.1021/acsinfecdis.1c00322.
- 79 YUAN, H. *et al.* The traditional medicine and modern medicine from natural products. **Molecules**, v. 21, n. 5, 2016. DOI: 10.3390/molecules21050559.
- 80 SOLECKI, R. S. Shanidar IV, a neanderthal flower burial in northern Iraq. **Science**, v. 190, n. 4217, p 880–881, 1975. DOI: 10.1126/science.190.4217.880.
- 81 UMARU, I. J. Introduction to natural product. *In*: BHAWANI, S. A.; KHAN, A.; AHMAD, F. B. (ed.) **Extraction of natural products from agro-industrial wastes: a green and sustainable approach**. Elsevier, 2023. p 19-34.
- 82 SALTAN ÇİTOĞLU, G.; BAHADIR ACIKARA, Ö. Column Chromatography for Terpenoids and Flavonoids. *In*: DHANARASU, S. (ed.) **Chromatography and its Applications**. IntechOpen. 2012. p 224.
- 83 W-H LI, J.; VEDERAS, J. C. Drug discovery and natural products: end of an era or an endless frontier? **Science**, v. 325, n. 5937, p 161–165, 2009. DOI: 10.1126/science.1168243.
- 84 HENRICH, C. J.; BEUTLER, J. A. Matching the power of high throughput screening to the chemical diversity of natural products. **Natural Product Reports**, v. 30, n. 10, p 1284–1298, 2013. DOI: 10.1039/c3np70052f.
- 85 ATANASOV, A. G. *et al.* Natural products in drug discovery: advances and opportunities. **Nature Reviews Drug Discovery**, v. 20, 2021. DOI: 10.1038/s41573-020-00114-z.
- 86 NEWMAN, D. J.; CRAGG, G. M. Natural products as sources of new drugs over the Nearly Four Decades from 01/1981 to 09/2019. **Journal of Natural Products**, v. 83, n. 3, p 770-803, 2020. DOI: 10.1021/acs.jnatprod.9b01285.
- 87 NINKUU, V. *et al.* Biochemistry of terpenes and recent advances in plant protection. **International Journal of Molecular Sciences**, v. 22, n. 11, 2021. DOI: 10.3390/ijms22115710.

- 88 COX-GEORGIAN, D. *et al.* Therapeutic and medicinal uses of terpenes. *In*: JOSHEE, N.; DHEKNEY, S. A.; PARAJULI, P. (ed.) **Medicinal Plants**. Cham: Springer, 2019. p 333–359. DOI: 10.1007/978-3-030-31269-5\_15.
- 89 PERVEEN, S. Introductory chapter: terpenes and terpenoids. *In*: PERVEEN, S.; AL-TAWEEL (ed.) **Terpenes and terpenoids**. IntechOpen, 2018. DOI: 10.5772/intechopen.79683.
- 90 WANI, M. C.; HORWITZ, S. B. Nature as a remarkable chemist: a personal story of the discovery and development of Taxol. **Anticancer Drugs**, v. 25, n. 5, p 482–487, 2014. DOI: 10.1097/CAD.0000000000000063.
- 91 TAJUDEEN, N.; VAN HEERDEN, F. R. Antiplasmodial natural products: an update. **Malaria Journal**, v. 18, p 404, 2019. DOI: 10.1186/s12936-019-3026-1.
- 92 SANCHEZ, A. M. *et al.* A novel icetexane diterpene, 5-epi-icetexone from *Salvia gilliessi* is active against *Trypanosoma cruzi*. **Acta Tropica**, v. 98, n. 2, p 118–124, 2006. DOI: 10.1016/j.actatropica.2005.12.007.
- 93 AKABERI, M.; MEHRI, S.; IRANSHAHI, M. Multiple pro-apoptotic targets of abietane diterpenoids from *Salvia* species. **Fitoterapia**, v. 100, p 118–132, 2015. DOI: 10.1016/j.fitote.2014.11.008.
- 94 LUIS, J. G.; ANDRÉS, L. S. An eremophyllane-type sesquiterpene and diterpenes from roots of *Salvia mellifera*. **Natural Product Letters**, v. 14, n. 1, p 25–30, 1999. DOI: 10.1080/10575639908045430.
- 95 BUSTOS-BRITO, C. *et al.* Structure and absolute configuration of abietane diterpenoids from *Salvia clinopodioides*: antioxidant, antiprotozoal, and antipropulsive activities. **Journal of Natural Products**, v. 82, n. 5, p 1207–1216, 2019. DOI: 10.1021/acs.jnatprod.8b00952.
- 96 FARIMANI, M. M. *et al.* Phytochemical study of *Salvia leriifolia* roots: rearranged abietane diterpenoids with antiprotozoal activity. **Journal of Natural Products**, v. 81, n. 6, p 1384–1390, 2018. DOI: 10.1021/acs.jnatprod.7b01019.
- 97 WU, C. Y. *et al.* Cytotoxic diterpenoids from *Salvia yunnanensis*. **Phytochemistry**, v. 106, p 171–177, 2014. DOI: 10.1016/j.phytochem.2014.07.001.
- 98 ESQUIVEL, B. *et al.* Abietane diterpenoids from the roots of some Mexican *Salvia* species (Labiatae): chemical diversity, phytogeographical significance, and cytotoxic activity. **Chemistry and Biodiversity**, v. 2, n. 6, p 738–747, 2005. DOI: 10.1002/cbdv.200590051.
- 99 ESQUIVEL, B. Structure, absolute configuration, and antiproliferative activity of abietane & icetexane diterpenoids from *Salvia ballotiflora*. **Molecules**, v. 22, n. 10, 2017. DOI: 10.3390/molecules22101690.
- 100 FRAGA, B. M. *et al.* Diterpenes from *Salvia broussonetii* transformed roots and their insecticidal activity. **Journal of Agricultural and Food Chemistry**, v. 53, n. 13, p 5200–5206, 2005. DOI: 10.1021/jf058045c.
- 101 EL-LAKANY, A. M. *et al.* Lanigerol: a new antimicrobial icetexane diterpene from *Salvia lanigera*. **Planta Medica**, v. 61, n. 6, p 559–560, 1995. DOI: 10.1055/s-2006-959372.
- 102 KHALIQ, S.; VOLK, F.-J.; FRAHM A W. Phytochemical investigation of *Perovskia abrotanoides*. **Planta Medica**, v. 73, p 77–83, 2007. DOI: 10.1055/s-2006-951766.

- 103 AOYAGI, Y. *et al.* Semisynthesis of icetexane diterpenoid analogues and their cytotoxic activity. **Chemical and Pharmaceutical Bulletin**, v. 54, n. 11, p 1602–1604, 2006. DOI: 10.1248/cpb.54.1602.
- 104 AHMAD, I. *et al.* Anti-inflammatory constituents from *Perovskia atriplicifolia*. **Pharmaceutical Biology**, v. 53, n. 11, p 1628–1631, 2015. DOI: 10.3109/13880209.2014.997250.
- 105 JIANG, Z. Y. *et al.* Icetexane diterpenoids from *Perovskia atriplicifolia*. **Planta Medica**, v. 81, n. 3, p 241–246, 2015. DOI: 10.1055/s-0034-1396151.
- 106 TABEFAM, M. *et al.* Antiprotozoal diterpenes from *Perovskia abrotanoides*. **Planta Medica**, v. 84, n. 12–13, p 913–919, 2018. DOI: 10.1055/a-0608-4946.
- 107 UCHIYAMA, N. *et al.* New icetexane and 20-norabietane diterpenes with trypanocidal activity from *Dracocephalum komarovi*. **Journal of Natural Products**, v. 66, n. 1, p 128–131, 2003. DOI: 10.1021/np020308z.
- 108 SIMMONS, E. M.; SARPONG, R. Structure, biosynthetic relationships and chemical synthesis of the icetexane diterpenoids. **Natural Product Reports**, v. 26, n. 9, p 1195–1217, 2009. DOI: 10.1039/b908984e.
- 109 CEZAROTTO, C. S. *et al.* Leishmanicidal and antichemotactic activities of icetexanes from *Salvia uliginosa* Benth. **Phytomedicine**, v. 58, n. October 2018, p 152748, 2019. DOI: 10.1016/j.phymed.2018.11.009.
- 110 UCHIYAMA, N. *et al.* Antichagasic activity of komaroviquinone is due to generation of reactive oxygen species catalyzed by *Trypanosoma cruzi* old yellow enzyme. **Antimicrobial Agents and Chemotherapy**, v. 49, n. 12, p 5123–5126, 2005. DOI: 10.1128/AAC.49.12.5123-5126.2005.
- 111 DENG, R. *et al.* Bioactive icetexane and abietane diterpenes from *Isodon phyllopodus*. **Natural Product Research**, v. 37, n. 1, p 68–76, 2023. DOI: 10.1080/14786419.2021.1950716.
- 112 ZHOU, B. *et al.* Diverse types of diterpenoids with an aromatized c ring from the twigs of *Podocarpus imbricatus*. **Journal of Natural Products**, v. 83, n. 8, p 2416–2424, 2020. DOI: 10.1021/acs.jnatprod.0c00291.
- 113 ESCUDER, B. *et al.* Antioxidant capacity of abietanes from *Sphacele salviae*. **Natural Product Letters**, v. 16, n. 4, p 277–281, 2002. DOI: 10.1080/10575630290020631.
- 114 TRAGER, W.; JENSEN, J. B. Human malaria parasites in continuous culture. **Science**, v. 193, n. 4254, p 673–5, 1976. DOI: 10.1645/0022-3395(2005)091[0484:HMPICC]2.0.CO;2.
- 115 LAMBROS, C.; VANDERBERG, J. P. Synchronization of *Plasmodium falciparum* erythrocytic stages in culture. **Journal of Parasitology**, v. 65, n. 3, p 418–420, 1979.
- 116 BENNETT, T. N. *et al.* Novel, rapid, and inexpensive cell-based quantification of antimalarial drug efficacy. **Antimicrobial Agents and Chemotherapy**, v. 48, n. 5, p 1807–1810, 2004. DOI: 10.1128/AAC.48.5.1807-1810.2004.
- 117 VOSSEN, M. G. *et al.* The SYBR green I malaria drug sensitivity assay: performance in low parasitemia samples. **American Journal of Tropical Medicine and Hygiene**, v. 82, n. 3, p 398–401, 2010. DOI: 10.4269/ajtmh.2010.09.0417.

118 MOSMANN, T. Rapid colorimetric assay for cellular growth and survival: application to proliferation and cytotoxicity assays. **Journal of Immunological Methods**, v. 65, n. 1–2, p 55–63, 1983. DOI: 10.1016/0022-1759(83)90303-4.

119 KATSUNO, K. *et al.* Hit and lead criteria in drug discovery for infectious diseases of the developing world. **Nature Reviews Drug Discovery**, v. 14, n. 11, p 751–8, 2015. DOI: 10.1038/nrd4683.

120 DUFFEY, M. *et al.* Assessing risks of *Plasmodium falciparum* resistance to select next-generation antimalarials. **Trends in Parasitology**, v. 37, n. 8, 2021. DOI: 10.1016/j.pt.2021.04.006.

121 MEDEIROS, D. S. S. *et al.* Epidemiological characterization and sensitivity to traditional antimalarials of *Plasmodium* spp. isolates from Porto Velho, western Amazon, Brazil. **Revista Eletrônica Acervo Saúde**, v. 15, n. 9, p e10745, 2022. DOI: 10.25248/reas.e10745.2022.

122 MARFURT, J. *et al.* *Ex vivo* activity of histone deacetylase inhibitors against multidrug-resistant clinical isolates of *Plasmodium falciparum* and *P. vivax*. **Antimicrobial Agents and Chemotherapy**, v. 55, n. 3, p 961–966, 2011. DOI: 10.1128/AAC.01220-10.

123 MORAES BARROS, R. R. *et al.* Activity of *Plasmodium vivax* promoter elements in *Plasmodium knowlesi*, and a centromere-containing plasmid that expresses NanoLuc throughout the parasite life cycle. **Malaria Journal**, v. 20, n. 1, 2021. DOI: 10.1186/s12936-021-03773-4.

124 LINARES, M. *et al.* Identifying rapidly parasitocidal anti-malarial drugs using a simple and reliable *in vitro* parasite viability fast assay. **Malaria Journal**, v. 14, n. 1, 2015. DOI: 10.1186/s12936-015-0962-2.

125 FIVELMAN, Q. L.; ADAGU, I. S.; WARHURST, D. C. Modified fixed-ratio isobologram method for studying *in vitro* interactions between atovaquone and proguanil or dihydroartemisinin against drug-resistant strains of *Plasmodium falciparum*. **Antimicrobial Agents and Chemotherapy**, v. 48, n. 11, p 4097–4102, 2004. DOI: 10.1128/AAC.48.11.4097-4102.2004.

126 GRABOVSKY, Y.; TALLARIDA, R. J. Isobolographic analysis for combinations of a full and partial agonist: curved isoboles. **Journal of Pharmacology and Experimental Therapeutics**, v. 310, n. 3, p 981–986, 2004. DOI: 10.1124/jpet.105.095091.

127 AHMAD, A.; BURTOLOSO, A. C. B. Total Synthesis of (±)-brussonol and (±)-komaroviquinone via a regioselective cross-electrophile coupling of aryl bromides and epoxides. **Organic Letters**, v. 21, n. 15, p 6079–6083, 2019. DOI: 10.1021/acs.orglett.9b02221.

128 BARBOSA, C. S. *et al.* synthesis, structure–activity relationships, and parasitological profiling of brussonol derivatives as new *Plasmodium falciparum* inhibitors. **Pharmaceuticals**, v. 15, n. 7, 2022. DOI: 10.3390/ph15070814.

129 HEFNAWY, A. *et al.* Importance of secondary screening with clinical isolates for anti-leishmania drug discovery. **Scientific Reports**, v. 8, n. 1, 2018. DOI: 10.1038/s41598-018-30040-5.

130 CHIRAWURAH, J. D. *et al.* Antimalarial activity of Malaria Box compounds against *Plasmodium falciparum* clinical isolates. **International Journal for Parasitology: drugs and drug resistance**, v. 7, n. 3, p 399–406, 2017. DOI: 10.1016/j.ijpddr.2017.10.005.

131 YUSOF, R. et al. High proportion of knowlesi malaria in recent malaria cases in Malaysia. **Malaria Journal**, v. 13, n. 1, 2014. DOI: 10.1186/1475-2875-13-168.

132 KREMSNER, P. G.; KRISHNA, S. Antimalarial combinations. **Lancet**, v. 364, n. 9430, p 285–94, 2004. DOI: 10.1016/S0140-6736(04)16680-4.

133 CASADO, N. *et al.* Enantiomeric Determination of Drugs in Pharmaceutical Formulations and Biological Samples by Electrokinetic Chromatography. **Critical Reviews in Analytical Chemistry**, 2020. DOI: 10.1080/10408347.2019.1670043.

134 BURROWS, J. N. et al. Challenges in antimalarial drug discovery. **Future Medicinal Chemistry**, v. 3, n. 11, p 1401–1412, 2011. DOI: 10.4155/fmc.11.91.

135 LE MANACH, C. *et al.* Medicinal chemistry optimization of antiplasmodial imidazopyridazine hits from high throughput screening of a softfocus kinase library: Part 2. **Journal of Medicinal Chemistry**, v. 57, n. 21, p 8839–8848, 2014. DOI: 10.1021/jm500887k.

136 ERTL, P.; ROHDE, B.; SELZER, P. Fast calculation of molecular polar surface area as a sum of fragment-based contributions and its application to the prediction of drug transport properties. **Journal of Medicinal Chemistry**, v. 43, n. 20, p 3714–3717, 2000. DOI: 10.1021/jm000942e.

137 CO, E. M. A. *et al.* Assessment of malaria in vitro drug combination screening and mixed-strain infections using the malaria SYBR green I-based fluorescence assay. **Antimicrobial Agents and Chemotherapy**, v. 53, n. 6, p 2557–2563, 2009. DOI: 10.1128/AAC.01370-08.

138 FOUCQUIER, J.; GUEDJ, M. Analysis of drug combinations: current methodological landscape. **Pharmacology Research and Perspectives**, v. 3, n. 3, 2015. DOI: 10.1002/prp2.149.

139 VAN DER PLUIJM, R. W. *et al.* Triple artemisinin-based combination therapies for malaria – a new paradigm? **Trends in Parasitology**, v. 37, n. 1, p 15-24, 2021. DOI: 10.1016/j.pt.2020.09.011.

140 DING, X. C.; UBBEN, D.; WELLS, T. N. A framework for assessing the risk of resistance for antimalarials in development. **Malaria Journal**, v. 11, 2012. DOI: 10.1186/1475-2875-11-292.

141 TRESCH, S. Strategies and future trends to identify the mode of action of phytotoxic compounds. **Plant Science**, v. 212, p 60-71, 2013. DOI: 10.1016/j.plantsci.2013.08.005.

142 SCHENONE, M. *et al.* Target identification and mechanism of action in chemical biology and drug discovery. **Nature Chemical Biology**, v. 9, n. 4, p 232-240, 2013. DOI: 10.1038/nchembio.1199.

143 ARISUE, N.; HASHIMOTO, T. Phylogeny and evolution of apicoplasts and apicomplexan parasites. **Parasitology International**, v. 64, n. 3, p 254–259, 2015. DOI: 10.1016/j.parint.2014.10.005.

144 DAHL, E. L. *et al.* Tetracyclines specifically target the apicoplast of the malaria parasite *Plasmodium falciparum*. **Antimicrobial Agents and Chemotherapy**, v. 50, n. 9, p 3124–3131, 2006. DOI: 10.1128/AAC.00394-06.

145 STANWAY, R. R. *et al.* GFP-targeting allows visualization of the apicoplast throughout the life cycle of live malaria parasites. **Biology of the Cell**, v. 101, n. 7, p 415–435, 2009. DOI: 10.1042/bc20080202.

- 146 BOTTÉ, C. Y. *et al.* *Plasmodium falciparum* apicoplast drugs: targets or off-targets? **Chemical Reviews**, v. 112, n. 3, p 1269-1283, 2012. DOI: 10.1021/cr200258w.
- 147 GUGGISBERG, A. M.; AMTHOR, R. E.; ODOM, A. R. Isoprenoid biosynthesis in *Plasmodium falciparum*. **Eukaryotic Cell**, v. 13, n. 11, p 1348–1359, 2014. DOI: 10.1128/EC.00160-14.
- 148 TONHOSOLO, R. *et al.* Carotenoid biosynthesis in intraerythrocytic stages of *Plasmodium falciparum*. **Journal of Biological Chemistry**, v. 284, n. 15, p 9974–9985, 2009. DOI: 10.1074/jbc.M807464200.
- 149 PAINTER, H. J. *et al.* Specific role of mitochondrial electron transport in blood-stage *Plasmodium falciparum*. **Nature**, v. 446, n. 7131, p 88–91, 2007. DOI: 10.1038/nature05572.
- 150 D'ALEXANDRI, F. L. *et al.* Protein dolichylation in *Plasmodium falciparum*. **FEBS Letters**, v. 580, n. 27, p 6343–6348, 2006. DOI: 10.1016/j.febslet.2006.10.042.
- 151 OKADA, M.; SIGALA, P. A. The interdependence of isoprenoid synthesis and apicoplast biogenesis in malaria parasites. **PLoS Pathogens**, v. 19, n. 10, e1011713, 2023. DOI: 10.1371/journal.ppat.1011713.
- 152 RICCI, C. G. *et al.* Dynamic structure and inhibition of a malaria drug target: geranylgeranyl diphosphate synthase. **Biochemistry**, v. 55, n. 36, p 5180–5190, 2016. DOI: 10.1021/acs.biochem.6b00398.
- 153 EDWARDS, R. L. *et al.* MEPicides: Potent antimalarial prodrugs targeting isoprenoid biosynthesis. **Scientific Reports**, v. 7, n. 1, p 1–11, 2017. DOI: 10.1038/s41598-017-07159-y.
- 154 YEH, E.; DERISI, J. L. Chemical rescue of malaria parasites lacking an apicoplast defines organelle function in blood-stage *Plasmodium falciparum*. **PLoS Biology**, v. 9, n. 8, 2011. DOI: 10.1371/journal.pbio.1001138.
- 155 WU, W. *et al.* A chemical rescue screen identifies a plasmodium falciparum apicoplast inhibitor targeting MEP isoprenoid precursor biosynthesis. **Antimicrobial Agents and Chemotherapy**, v. 59, n. 1, p 356–364, 2015. DOI: 10.1128/AAC.03342-14.
- 156 BOWMAN, J. D. *et al.* Antiapicoplast and gametocytocidal screening to identify the mechanisms of action of compounds within the malaria box. **Antimicrobial Agents and Chemotherapy**, v. 58, n. 2, p 811–819, 2014. DOI: 10.1128/AAC.01500-13.
- 157 GISSELBERG, J. E. *et al.* Specific inhibition of the bifunctional farnesyl/geranylgeranyl diphosphate synthase in malaria parasites via a new small-molecule binding site. **Cell Chemical Biology**, v. 25, n. 2, p. 185- 193.e5, 2018. DOI: 10.1016/j.chembiol.2017.11.010.
- 158 OLIVEIRA, L. S. *et al.* Calcium in the Backstage of malaria parasite biology. **Frontiers in Cellular and Infection Microbiology**, v. 11, 2021. DOI: 10.3389/fcimb.2021.708834.
- 159 PANDEY, K. *et al.* Ca<sup>2+</sup> monitoring in *Plasmodium falciparum* using the yellowameleon-Nano biosensor. **Scientific Reports**, v. 6, 2016. DOI: 10.1038/srep23454.
- 160 CAMACHO, P. Malaria parasites solve the problem of a low calcium environment. **Journal of Cell Biology**, v. 161, n. 1, p. 17–9, 2003. DOI: 10.1083/jcb.200303116.

- 161 GAZARINI, M. L. *et al.* Calcium signaling in a low calcium environment: How the intracellular malaria parasite solves the problem. **Journal of Cell Biology**, v. 161, n. 1, p 103–110, 2003. DOI: 10.1083/jcb.200212130.
- 162 TANABE, K.; MIKKELSEN, R. B.; WALLACH, D. F. H. Calcium Transport of *Plasmodium chabaudi*-infected Erythrocytes. **Journal of Cell Biology**, v. 93, n. 3, p 680-684, 1982. DOI: 10.1083/jcb.93.3.680.
- 163 DESAI, S. A.; KROGSTAD, D. J.; MCCIESKEYT, E. W. A nutrient-permeable channel on the intraerythrocytic malaria parasite. **Nature**, v. 362, n. 6421, p 643-646, 1993. DOI: 10.1038/36263a0.
- 164 KUSHWAHA, A. K. *et al.* Increased Ca ++ uptake by erythrocytes infected with malaria parasites: Evidence for exported proteins and novel inhibitors. **Cellular Microbiology**, v. 20, n. 9, e12853, 2018. DOI: 10.1111/cmi.12853.
- 165 BERRIDGE, M. J. Inositol trisphosphate and calcium signalling. **Nature**, v. 361, n. 6410, p. 315-325, 1993.
- 166 ROSS, C. A. *et al.* Inositol 1,4,5-trisphosphate receptor localized to endoplasmic reticulum in cerebellar Purkinje neurons. **Nature**, v. 339, n. 6224, p. 468-470, 1989.
- 167 LOVETT, J. L. *et al.* *Toxoplasma gondii* microneme secretion involves intracellular Ca<sup>2+</sup> release from inositol 1,4,5-trisphosphate (IP<sub>3</sub>)/ryanodine-sensitive stores. **Journal of Biological Chemistry**, v. 277, n. 29, p 25870–25876, 2002. DOI: 10.1074/jbc.M202553200.
- 168 DOCAMPO, R. *et al.* Acidocalcisomes - conserved from bacteria to man. **Nature Reviews Microbiology**, v. 3, 2005. DOI: 10.1038/nrmicro1097.
- 169 SALIBA, K. J. *et al.* Acidification of the malaria parasite's digestive vacuole by a H<sup>+</sup>-ATPase and a H<sup>+</sup>-pyrophosphatase. **Journal of Biological Chemistry**, v. 278, n. 8, p 5605–5612, 2003. DOI: 10.1074/jbc.M208648200.
- 170 ROTMANN, A. *et al.* PfCHA is a mitochondrial divalent cation/H<sup>+</sup> antiporter in *Plasmodium falciparum*. **Molecular Microbiology**, v. 76, n. 6, p 1591–1606, 2010. DOI: 10.1111/j.1365-2958.2010.07187.x.
- 171 DAWN, A. *et al.* The central role of cAMP in regulating *Plasmodium falciparum* merozoite invasion of human erythrocytes. **PLoS Pathogens**, v. 10, n. 12, e1004520, 2014. DOI: 10.1371/journal.ppat.1004520.
- 172 KIRK, K. Membrane transport in the malaria-infected erythrocyte. **Physiological Reviews**, v. 81, n. 2, 2001.
- 173 MARTIN, R. E. The transportome of the malaria parasite. **Biological Reviews of the Cambridge Philosophical Society**, v. 95, n. 2, p 305–332, 2020. DOI: 10.1111/brv.12565.
- 174 KIRK, K.; LEHANE, A. M. Membrane transport in the malaria parasite and its host erythrocyte. **Biochemical Journal**, v. 457, p 1-18, 2014. DOI: 10.1042/BJ20131007.
- 175 MAURITZ, J. M. A. *et al.* X-ray microanalysis investigation of the changes in Na, K, and hemoglobin concentration in *Plasmodium falciparum*-infected red blood cells. **Biophysical Journal**, v. 100, n. 6, p 1438–1445, 2011.



- 176 SPILLMAN, N. J. *et al.* Na<sup>+</sup> regulation in the malaria parasite *Plasmodium falciparum* involves the cation ATPase PfATP4 and is a target of the spiroindolone antimalarials. **Cell Host and Microbe**, v. 13, n. 2, p 227–237, 2013. DOI: 10.1016/j.chom.2012.12.006.
- 177 ROTTMANN, M. *et al.* Spiroindolones, a potent compound class for the treatment of malaria. **Science**, v. 329, n. 5996, p 1175–1180, 2010. DOI: 10.1126/science.1193225.
- 178 WHITE, N. J. *et al.* Spiroindolone KAE609 for falciparum and vivax malaria. **New England Journal of Medicine**, v. 371, n. 5, p 403–410, 2014. DOI: 10.1056/NEJMoa1315860.
- 179 KRISHNA, S. *et al.* Expression and functional characterization of a *Plasmodium falciparum* Ca<sup>2+</sup>-ATPase (PfATP4) belonging to a subclass unique to apicomplexan organisms. **Journal of Biological Chemistry**, v. 276, n. 14, p 10782–10787, 2001. DOI: 10.1074/jbc.M010554200.
- 180 MA, Q. *et al.* An ENA ATPase, MaENA1, of *Metarhizium acridum* influences the Na<sup>+</sup>-, thermo- and UV-tolerances of conidia and is involved in multiple mechanisms of stress tolerance. **Fungal Genetics and Biology**, v. 83, p 68–77, 2015. DOI: 10.1016/j.fgb.2015.08.011.
- 181 IIZUMI, K. *et al.* Molecular cloning and characterization of ouabain-insensitive Na<sup>+</sup>-ATPase in the parasitic protist, *Trypanosoma cruzi*. **Biochimica et Biophysica Acta**, v. 1758, n. 6, p 738–746, 2006. DOI: 10.1016/j.bbamem.2006.04.025.
- 182 CANTLEY, L. C.; CANTLEY, L. G.; JOSEPHSON, L. A characterization of vanadate interactions with the (Na,K)-ATPase. **Journal of Biological Chemistry**, v. 253, n. 20, p 7361–7368, 1978.
- 183 SPILLMAN, N. J.; ALLEN, R. J. W.; KIRK, K. Na<sup>+</sup> extrusion imposes an acid load on the intraerythrocytic malaria parasite. **Molecular and Biochemical Parasitology**, v. 189, n. 1–2, p 1–4, 2013. DOI: 10.1016/j.molbiopara.2013.04.004.
- 184 MCKEE, R. W. *et al.* Studies on malarial parasites: VI. the chemistry and metabolism of normal and parasitized (*P. knowlesi*) monkey blood. **Journal of Experimental Medicine**, v. 84, n. 6, p 569–582, 1946.
- 185 GINSBURG, H. Malaria parasite stands out. **Nature**, v. 466, 2010. DOI: 10.1038/466702a.
- 186 WU, B. *et al.* Identity of a *Plasmodium* lactate/H<sup>+</sup> symporter structurally unrelated to human transporters. **Nature Communications**, v. 6, p 6284, 2015. DOI: 10.1038/ncomms7284.
- 187 ELLIOTT, J. L.; SALIBA, K. J.; KIRK, K. Transport of lactate and pyruvate in the intraerythrocytic malaria parasite, *Plasmodium falciparum*. **Biochemical Journal**, v. 355, p 733–739, 2001.
- 188 MARCHETTI, R. V. *et al.* A lactate and formate transporter in the intraerythrocytic malaria parasite, *Plasmodium falciparum*. **Nature Communications**, v. 6, p 6721, 2015. DOI: 10.1038/ncomms7721.
- 189 SALIBA, K. J.; KIRKI, K. pH regulation in the intracellular malaria parasite, *Plasmodium falciparum*. H<sup>+</sup> extrusion via a V-type H<sup>+</sup>-ATPase. **Journal of Biological Chemistry**, v. 274, n. 47, p. 33213–33219, 1999.

- 190 MIKKELSEN, R. B. *et al.* Membrane potential of erythrocytic stages of *Plasmodium chabaudi* free of the host cell membrane. **Molecular and Biochemical Parasitology**, v. 21, p 83-92, 1986.
- 191 BOSIA, A. *et al.* Kinetic characterization of Na<sup>+</sup>/H<sup>+</sup> antiport of *Plasmodium falciparum* membrane. **Journal of Cellular Physiology**, v. 154, n. 3, p 527–534, 1993.
- 192 PEDERSEN, P. L.; CARAFOLI, E. Ion motive ATPases. I. Ubiquity, properties, and significance to cell function. **Trends in Biochemical Sciences**, v. 12, p 146-150, 1987. DOI: 10.1016/0968-0004(87)90071-5.
- 193 WAKABAYASHI, S.; SHIGEKAWA, M.; POUYSSEGUR, J. Molecular Physiology of Vertebrate Na<sup>+</sup>/H<sup>+</sup> Exchangers. **Physiological Reviews**, v. 77, n. 1, 1997.
- 194 BORON, W. F. REFRESHER COURSE Cellular Homeostasis Regulation of intracellular pH. **Advances in Physiology Education**, v. 28, p 160–179, 2004. DOI: 10.1152/advan.00045.2004.
- 195 HENRY, R. I. *et al.* An acid-loading chloride transport pathway in the intraerythrocytic malaria parasite, *Plasmodium falciparum*. **Journal of Biological Chemistry**, v. 285, n. 24, p. 18615–18626, 2010. DOI: 10.1074/jbc.M110.120980.
- 196 CARDOZO, D. An intuitive approach to understanding the resting membrane potential. **Advances in Physiology Education**, v. 40, n. 4, p 543–547, 2016. DOI: 10.1152/advan.00049.2016.
- 197 ALLEN, R. J. W.; KIRK, K. The membrane potential of the intraerythrocytic malaria parasite *Plasmodium falciparum*. **Journal of Biological Chemistry**, v. 279, n. 12, p 11264–11272, 2004. DOI: 10.1074/jbc.M311110200.
- 198 PAQUET, T. *et al.* Antimalarial efficacy of MMV390048, an inhibitor of *Plasmodium* phosphatidylinositol 4-kinase. **Science Translational Medicine**, v. 9, n. 387, 2017. DOI: 10.1126/scitranslmed.aad9735.
- 199 SUMMERS, R. L. *et al.* Chemogenomics identifies acetyl-coenzyme A synthetase as a target for malaria treatment and prevention. **Cell Chemical Biology**, v. 29, n. 2, p 191- 201.e8, 2022. DOI: 10.1016/j.chembiol.2021.07.010.
- 200 BARAGAÑA, B. *et al.* A novel multiple-stage antimalarial agent that inhibits protein synthesis. **Nature**, v. 522, n. 7556, p 315–320, 2015. DOI: 10.1038/nature14451.
- 201 NZILA, A.; MWAI, L. *In vitro* selection of *Plasmodium falciparum* drug-resistant parasite lines. **Journal of Antimicrobial Chemotherapy**, v. 65, p 390-398, 2009. DOI: 10.1093/jac/dkp449.
- 202 COREY, V. C. *et al.* A broad analysis of resistance development in the malaria parasite. **Nature Communications**, v. 7, p 11901, 2016. DOI: 10.1038/ncomms11901.
- 203 KÜMPORNSIN, K. *et al.* Generation of a mutator parasite to drive resistome discovery in *Plasmodium falciparum*. **Nature Communications**, v. 14, n. 1, p 3059, 2023. DOI: 10.1038/s41467.023-38774-1.
- 204 HONMA, H. *et al.* Generation of rodent malaria parasites with a high mutation rate by destructing proofreading activity of DNA polymerase  $\delta$ . **DNA Research**, v. 21, n. 4, p 439–446, 2014. DOI: 10.1093/dnares/dsu009.

- 205 RODRIGUEZ, J. B.; SZAJNMAN, S. H. An updated review of chemical compounds with anti-*Toxoplasma gondii* activity. **European Journal of Medicinal Chemistry**, v. 262, p 115885, 2023. DOI: 10.1016/j.ej.mech.2023.115885.
- 206 STELZER, S. *et al.* *Toxoplasma gondii* infection and toxoplasmosis in farm animals: Risk factors and economic impact. **Food and Waterborne Parasitology**, v. 12, e00037, 2019. DOI: 10.1016/j.fawpar.2019.e00037.
- 207 KIM, K.; WEISS, L. M. *Toxoplasma gondii*: The model apicomplexan. **International Journal for Parasitology**, v. 34, n. 3, p. 423, 2004.
- 208 BUDU, A. *et al.* Calmidazolium evokes high calcium fluctuations in *Plasmodium falciparum*. **Cellular Signalling**, v. 28, n. 3, p 125–135, 2016. DOI: 10.1016/j.cellsig.2015.12.003.
- 209 DIARRA, A.; SHELDON, C.; CHURCH, J. *In situ* calibration and [H<sup>+</sup>] sensitivity of the fluorescent Na<sup>+</sup> indicator SBFI. **American Journal of Physiology-Cell Physiology**, v. 280, n. 6, 2001. DOI: 10.1152/ajpcell.2001.280.6.C1623.
- 210 VAN DOOREN, G. G. *et al.* *Toxoplasma gondii* Tic20 is essential for apicoplast protein import. **PNAS**, v. 105, n. 36, 2008. DOI: 10.1073/pnas.0803862105.
- 211 GUBBELS, M. J.; LI, C.; STRIEPEN, B. High-throughput growth assay for *Toxoplasma gondii* using yellow fluorescent protein. **Antimicrobial Agents and Chemotherapy**, v. 47, n. 1, p 309–316, 2003. DOI: 10.1128/AAC.47.1.309-316.2003.
- 212 BACKMAN, T. W. H.; CAO, Y.; GIRKE, T. ChemMine tools: an online service for analyzing and clustering small molecules. **Nucleic Acids Research**, v. 39, w486-w491, 2011. DOI: 10.1093/nar/gkr320.
- 213 MACÍAS-ALONSO, M. *et al.* Inhibition of squalene synthase of rat liver by abietane diterpenes derivatives. **Natural Product Research**, p 1–5, 2019. DOI: 10.1080/14786419.2019.1678614.
- 214 CERQUEIRA, N. M. F. S. A. *et al.* Cholesterol biosynthesis: a mechanistic overview. **Biochemistry**, v. 55, n. 39, p 5483–5506, 2016. DOI: 10.1021/acs.biochem.6b00342.
- 215 DIMARINO, D. *et al.* Characterization of the differences in the cyclopiazonic acid binding mode to mammalian and *P. Falciparum* Ca<sup>2+</sup> pumps: a computational study. **Proteins**, v. 83, n. 3, p 564–574, 2015.
- 216 KIRK, K. Ion Regulation in the Malaria Parasite. **Annual Review of Microbiology**, v. 69, p 341-359, 2015. DOI: 10.1146/annurev-micro-091014-104506.
- 217 LEHANE, A. M. *et al.* Diverse chemotypes disrupt ion homeostasis in the malaria parasite. **Molecular Microbiology**, v. 94, n. 2, p 327–339, 2014. DOI: 10.1111/mmi.12765.
- 218 JIMÉNEZ-DÍAZ, M. B. *et al.* (+)-SJ733, a clinical candidate for malaria that acts through ATP4 to induce rapid host-mediated clearance of Plasmodium. **Proceedings of the National Academy of Sciences of the United States of America**, v. 111, n. 50, p E5455–E5462, 2014. DOI: 10.1073/pnas.1414221111.
- 219 VINCENT, F. *et al.* Phenotypic drug discovery: recent successes, lessons learned and new directions. **Nature Reviews Drug Discovery**, v. 21, 2022. DOI: 10.1038/s41573-022-00472-w.

220 SHEINER, L. *et al.* A systematic screen to discover and analyze apicoplast proteins identifies a conserved and essential protein import factor. **PLoS Pathogens**, v. 7, n. 12, e1002392, 2011. DOI: 10.1371/journal.ppat.1002392.

221 NEGGERS, J. E. *et al.* Target identification of small molecules using large-scale CRISPR-Cas mutagenesis scanning of essential genes. **Nature Communications**, v. 9, n. 1, 2018.

222 CARRERAS-SUREDA, A.; PIHÁN, P.; HETZ, C. Calcium signaling at the endoplasmic reticulum: fine-tuning stress responses. **Cell Calcium**, v. 70, p 24-31, 2018. DOI: 10.1016/j.ceca.2017.08.004.

223 LA FUENTE, S. *et al.* Ca<sup>2+</sup> homeostasis in the endoplasmic reticulum measured with a new low-Ca<sup>2+</sup>-affinity targeted aequorin. **Cell Calcium**, v. 54, n. 1, p 37–45, 2013. DOI: 10.1016/j.ceca.2013.04.001.

224 DENNIS, A. S. M. **PfATP4 and the biochemical signature of PfATP4-associated compounds**. Thesis. Canberra: Australian National University, 2018.

225 KITAYAMA, S. *et al.* Bis-oxonol experiment on plasma membrane potentials of bovine adrenal chromaffin cells: depolarizing stimuli and their possible interaction. **Neuroscience Letters**, v. 116, p 275-279, 1990.

226 Wilkinson, I. V. L.; Terstappen, G. C.; Russell, A. J. Combining experimental strategies for successful target deconvolution. **Drug Discovery Today**, v. 25, n. 11, p 1998–2005, 2020. DOI: 10.1016/j.drudis.2020.09.016.

## ANEXES



Article

## Synthesis, Structure–Activity Relationships, and Parasitological Profiling of Brussonol Derivatives as New *Plasmodium falciparum* Inhibitors

Camila S. Barbosa <sup>1,†</sup>, Anees Ahmad <sup>2,†</sup>, Sarah El Chamy Maluf <sup>1</sup>, Igor M. R. Moura <sup>1</sup>, Guilherme E. Souza <sup>1</sup>, Giovanna A. H. Guerra <sup>3</sup>, Roberto R. Moraes Barros <sup>3</sup>, Marcos L. Gazarini <sup>4</sup>, Anna C. C. Aguiar <sup>1,4,\*</sup>, Antonio C. B. Burloloso <sup>2,\*</sup> and Rafael V. C. Guido <sup>1,\*</sup>

- <sup>1</sup> São Carlos Institute of Physics, University of São Paulo, Av. João Dagnone, 1100, Santa Angelina, São Carlos 13563-120, Brazil; camilasbarbosa@ifsc.usp.br (C.S.B.); sarahmaluf@usp.br (S.E.C.M.); igormmoura@usp.br (I.M.R.M.); guilherme.eduardosouza@usp.br (G.E.S.)
- <sup>2</sup> São Carlos Institute of Chemistry, University of São Paulo, Av. João Dagnone, 1100, Santa Angelina, São Carlos 13563-120, Brazil; anees\_chemist@yahoo.com
- <sup>3</sup> Department of Microbiology, Immunology and Parasitology, Escola Paulista de Medicina, Federal University of São Paulo, São Paulo 04023-062, Brazil; giovanna.abreu31@gmail.com (G.A.H.G.); moraes.barros@unifesp.br (R.R.M.B.)
- <sup>4</sup> Department of Biosciences, Federal University of São Paulo, Rua Silva Jardim, 136, Santos 11015-020, Brazil; marcos.gazarini@unifesp.br
- \* Correspondence: caroline.aguiar@unifesp.br (A.C.C.A.); antonio@iqsc.usp.br (A.C.B.B.); rvcguido@usp.br (R.V.C.G.)
- † These authors contributed equally to the work.



Citation: Barbosa, C.S.; Ahmad, A.; Maluf, S.E.C.; Moura, I.M.R.; Souza, G.E.; Guerra, G.A.H.; Barros, R.R.M.; Gazarini, M.L.; Aguiar, A.C.C.; Burloloso, A.C.B.; et al. Synthesis, Structure–Activity Relationships, and Parasitological Profiling of Brussonol Derivatives as New *Plasmodium falciparum* Inhibitors. *Pharmaceuticals* 2022, 15, 814. <https://doi.org/10.3390/ph15070814>

Academic Editors: Jean Leandro dos Santos and Chung Man Chin

Received: 2 June 2022

Accepted: 26 June 2022

Published: 30 June 2022

**Publisher's Note:** MDPI stays neutral with regard to jurisdictional claims in published maps and institutional affiliations.



Copyright © 2022 by the authors. Licensee MDPI, Basel, Switzerland. This article is an open access article distributed under the terms and conditions of the Creative Commons Attribution (CC BY) license (<https://creativecommons.org/licenses/by/4.0/>).

**Abstract:** Malaria is a parasitic disease caused by protozoan parasites from the genus *Plasmodium*. *Plasmodium falciparum* is the most prevalent species worldwide and the causative agent of severe malaria. The spread of resistance to the currently available antimalarial therapy is a major concern. Therefore, it is imperative to discover and develop new antimalarial drugs, which not only treat the disease but also control the emerging resistance. Brussonol is an icetexane derivative and a member of a family of diterpenoids that have been isolated from several terrestrial plants. Here, the synthesis and antiplasmodial profiling of a series of brussonol derivatives are reported. The compounds showed inhibitory activities in the low micromolar range against a panel of sensitive and resistant *P. falciparum* strains (IC<sub>50</sub>s = 5–16 μM). Moreover, brussonol showed fast-acting *in vitro* inhibition and an additive inhibitory behavior when combined with the antimalarial artesunate (FIC<sub>index</sub> ~1). The mode of action investigation indicated that brussonol increased the cytosolic calcium levels within the parasite. Hence, the discovery of brussonol as a new scaffold endowed with antiplasmodial activity will enable us to design derivatives with improved properties to deliver new lead candidates for malaria.

**Keywords:** malaria; icetexane diterpenoids; antimalarials; resistance; *Plasmodium falciparum*

### 1. Introduction

Malaria is a parasitic disease caused by protozoan parasites from the genus *Plasmodium* spp. *Plasmodium falciparum* is the most prevalent species worldwide [1] and the causative agent of severe malaria. Despite the reduction in malaria incidence and mortality over the last 20 years, the disease affects millions of people annually. In 2020, the World Health Organization (WHO) estimated the occurrence of 241 million cases and over 600 thousand deaths globally. Children aged under 5 years were the most vulnerable group affected by the disease. In 2020, they accounted for 77% of all malaria deaths worldwide [1]. The spread of resistance to the currently available antimalarial therapy is a major concern, especially the recent evidence of the independent emergence of artemisinin partial resistance in the

WHO African Region (World Health Organization, 2020). A WHO protocol to monitor antimalarial drug efficacy, as well as surveillance for resistance markers, are common routines used in endemic countries to readapt the protocol for the management and control of malaria cases [2]. All progress achieved over the past two decades in controlling, managing, and preventing malaria cases can be lost if the spread of artemisinin resistance outruns the speed of new antimalarials delivery [2]. Therefore, it is imperative to discover and develop new antimalarial drugs, which would not only treat symptoms, but also control the emerging resistance, and contribute toward the elimination and eradication of the disease.

A valuable source for the discovery of new potential drug candidates relies on the synthesis of active compounds inspired by natural products. Plant extracts have been used by humans to treat diseases since ancient times, and their chemical complexity and diversity are attractive features to medicinal chemists [3]. The icetexanes are a family of diterpenoids that have been isolated from different parts of terrestrial plants. They are found in several genera, such as *Salvia*, *Perovskia*, and *Dracocephalum* [4–6]. These compounds have a 6-7-6 tricyclic framework, which is a key feature of the icetexane skeleton (Figure 1). Antibacterial [4,7], antiprotozoal [6,8–10], and antiproliferative activities [11] have been reported for some diterpenes. In this work, we investigated brussonol and synthetic derivatives as *P. falciparum* inhibitors (Figure 1). In this sense, we conducted extensive synthetic and biological profiling efforts to assess the antiplasmodial properties of the brussonol series. Our findings indicated that the natural compound derivatives are new antiplasmodial hit candidates.

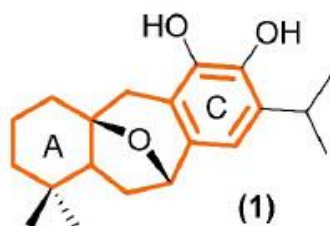


**Figure 1.** Molecular structure of brussonol (1). The structure in orange indicates the 6-7-6 tricyclic framework characteristic of icetexanes diterpenes.

## 2. Results

### 2.1. Synthesis of Brussonol and Derivatives

In our initial structure–activity relationship (SAR) campaign, the design and synthesis of natural product brussonol (1) and 14 analogs were executed (Figure 2). The design strategy involved modifications to the aromatic and six-membered cyclic ring of the brussonol (1) skeleton to determine the necessary motifs required for antiplasmodial activity.

Three synthetic routes were explored to obtain desired brussonol analogs 1–15 as new antimalarial agents (Schemes 1–3). Target compounds 2 with 1,2-disubstitution on the aromatic ring were synthesized according to the protocol reported previously by our group [12]. Thus, following the same synthetic route, the synthesis of 1,4-disubstituted analog 3 was accomplished (Scheme 1). After preparing epoxide 16, it was subjected to a regioselective epoxide ring-opening reaction mediated by the *ortho*-lithiated nucleophile 17, derived from 1,4-dimethoxybenzene. In the next step, oxidative cleavage of the terminal olefin into aldehydes was employed using Lemieux–Johnson oxidation conditions. Marsden-type Friedel–Crafts acylation of aldehyde 18 using  $\text{BF}_3 \cdot \text{Et}_2\text{O}$  as the Lewis acid afforded the synthesis of tricyclic moiety 3 in 80% yield. Finally, the hydroquinone type brussonol analogs 4 and 5 were prepared from respective tricyclic moieties 2 and 3 via demethylation protocol using  $\text{EtSH}$ ,  $\text{NaH}$ , and  $\text{DMF}$  as solvents in good yields [13]. Similarly, *p*-quinone 6, a komaroviquinone-type derivative, was synthesized from 3 via oxidative demethylation of phenol ethers using a hypervalent iodine (III) reagent (PIFA) in 62% yield [14].

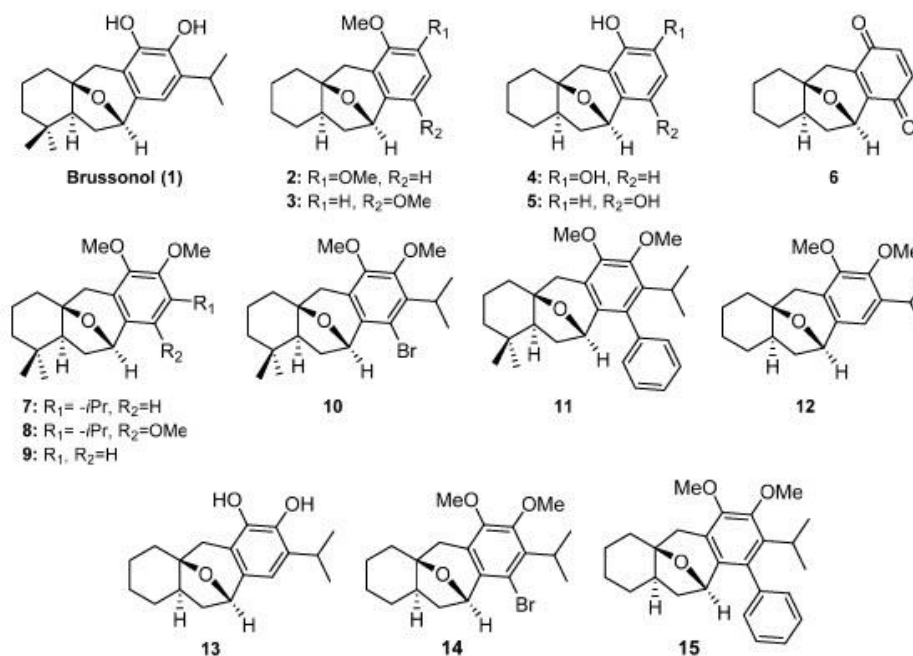
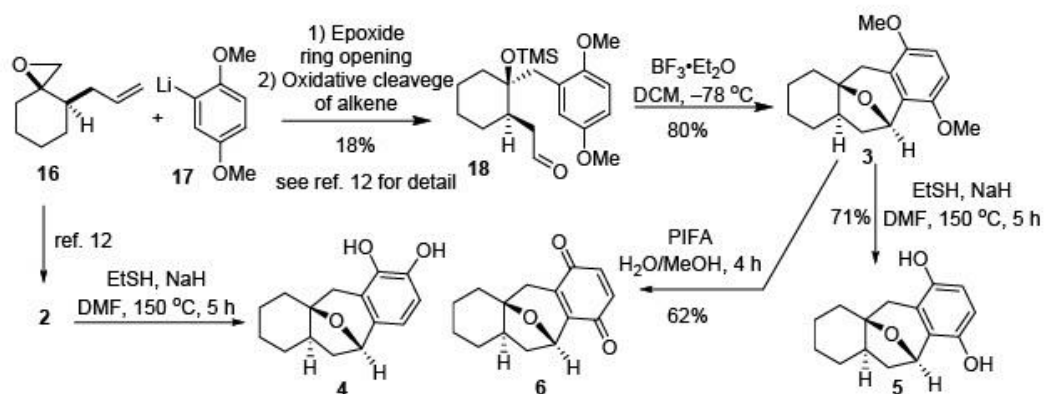
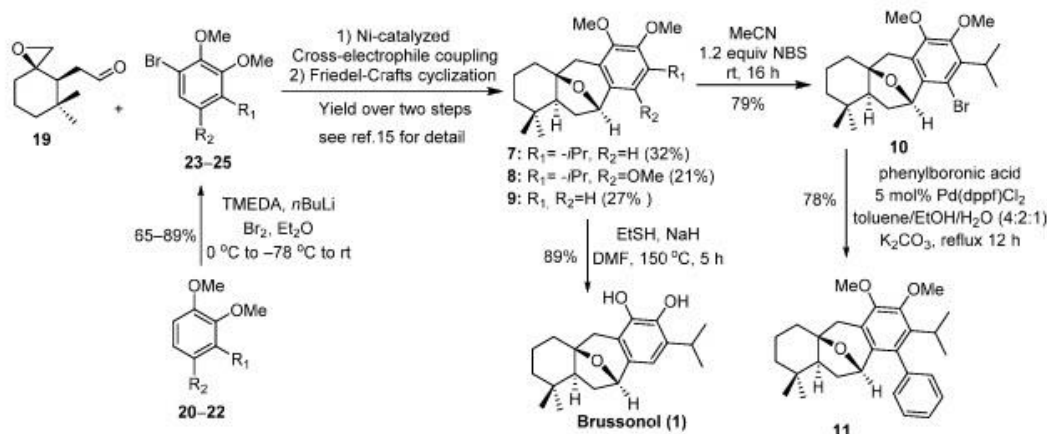


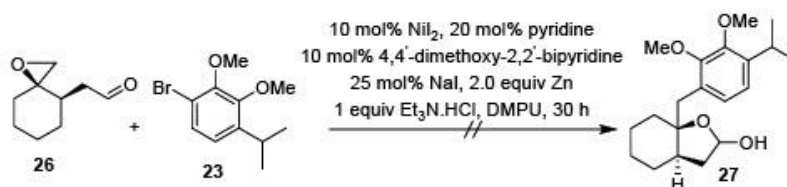
Figure 2. Design of brussonol analogs as new *Plasmodium falciparum* inhibitors.



Scheme 1. Synthetic route for the synthesis of brussonol analogs



Scheme 2. Synthesis of brussonol (1) and analogs.



Scheme 3. Cross-electrophile coupling between aryl bromide and epoxy-aldehyde.

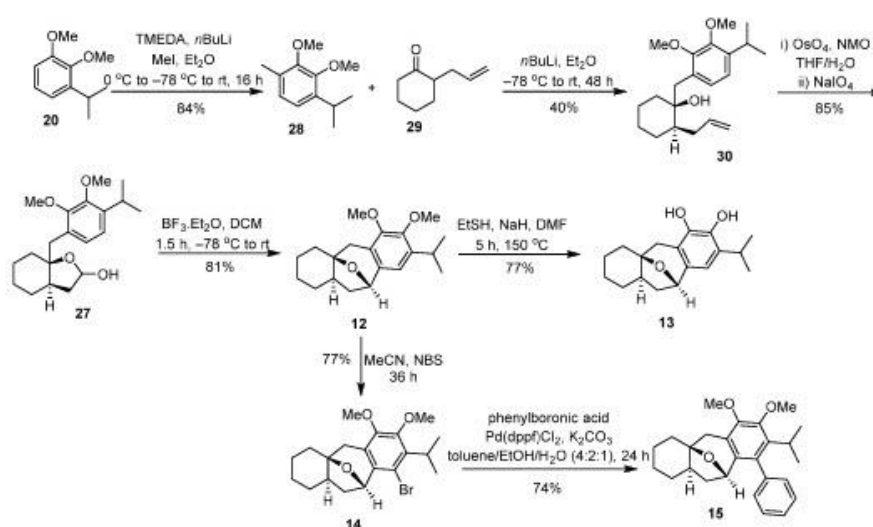
Recently, we reported a short and stereoselective synthesis of (±)-brussonol and (±)-komaroviquinone, via a Ni-catalyzed epoxide ring-opening approach in the presence of aryl halides [15]. Using the same protocol, we successfully prepared brussonol (1) and several other analogs (7–9, 10, and 11) in good quantities (Scheme 2). The coupling fragments, such as epoxide 19 and aryl bromides (23–25), were prepared as previously described in the literature [15–18]. The hemiacetal intermediates obtained via a regioselective cross-electrophile coupling of aryl bromides 23–25 and epoxy-aldehyde 19 were readily subjected to Friedel–Crafts cyclization reaction to afford the formation of the tricyclic compounds (icetexane diterpenes skeleton) 7–9 in 21–32% yields. The subsequent demethylation of compound 7 furnished brussonol (1) in an 89% yield. After optimization studies, we obtained the bromine-substituted analog 10 from compound 7 in the presence N-Bromosuccinimide (NBS) in acetonitrile as the solvent in 79% yield [19]. At this stage, we were set for the Suzuki cross-coupling reaction as we had the bromine-substituted analog 10 in hand. The Suzuki cross-coupling reaction between substrate 10 and phenylboronic acid catalyzed by Pd(dppf)Cl<sub>2</sub>, in the presence of K<sub>2</sub>CO<sub>3</sub> as the base, provided our desired coupled product 11 in 79% yield when the reaction was allowed to run for 24 h [20].

Similarly, we also planned the synthesis of isopropyl containing dimethoxy analog, but this time without the geminal dimethyl on the cyclohexane ring. Unfortunately, we were not able to isolate the desired acetal product 27 in pure form when aryl bromide 23 and epoxy-aldehyde 26 were subjected to the nickel/iodide catalyzed cross-electrophile coupling reaction (Scheme 3).

To overcome the difficulties and failures associated with the preparation of our desired acetal intermediate 27, we switched to an alternative synthetic plan reported in the literature [21]. Following the reported protocol, ortho-directed metalation in the presence of nBuLi and TMEDA in diethyl ether as a solvent, with subsequent electrophilic quench



with iodomethane, provided the methylated aryl moiety **28** in 84% yield (Scheme 4). Deprotonation of the methyl group in **28**, followed by the addition of ketone **29**, gave the desired tertiary alcohol **30** in 40% yield. Oxidative cleavage of the allyl group in tertiary alcohol **30**, followed by hemiacetalization, provided acetal **27** in good yield. After successful synthesis of hemiacetal **27**, it was readily subjected to Marson-type Friedel–Crafts cyclization, which resulted in tricyclic structure **12** in 81% yield. The demethylation of compound **12** afforded **13** in 77% yield. We also successfully obtained brominated analog **14** in the presence of NBS and phenylboronic acid furnished the anticipated analog **15** in 74% yield [20]. Similarly, the Suzuki cross-coupling reaction between substrate **14** and phenylboronic acid furnished the anticipated analog **15** in 74% yield [20]. With the above-given strategy, we prepared four additional synthetic analogs (**12–15**) in good quantities for biological activity assessment. All compounds were synthesized as a racemic mixture.

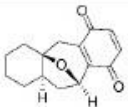


Scheme 4. Synthesis of brussanol analogs.

## 2.2. Brussanol and Derivatives Showed Antiplasmodial Activity and Low Cytotoxic Activity

The *in vitro* inhibitory activity against *P. falciparum* (3D7 strain), cytotoxic effect on HepG2 cells, and selectivity index (SI) of brussanol and derivatives were assessed (Table 1). The assessed  $IC_{50}$  value of brussanol was 16  $\mu$ M, indicating that the icetexane diterpenoid scaffold is endowed with promising antiplasmodial activity. Because of that, we designed new analogs to investigate the SAR underlying the central molecular scaffold (Schemes 1–4 and Table 1). The SAR investigation indicated that some key structural features are crucial for antiplasmodial activity (Figure 3). For example, the removal of the isopropyl group at  $R^3$  in derivatives 2–6 and 9 abrogated the antiplasmodial activity, suggesting that the bulky substituent at  $R^3$  is favorable for the inhibitory activity. By contrast, the substitution of the hydroxyl substituent at  $R^1$  and  $R^2$  with methoxy groups enhanced by 3-fold the inhibitory activity (e.g., **1** vs. **7**; **12** vs. **13**). The substitution with bulkier and hydrophobic substituents, such as methoxy (**8**), bromine (**10**), and phenyl (**11**), at  $R^4$  was tolerated. Finally, the substitution of the methyl groups at positions  $R^5$  and  $R^6$  with hydrogen atoms retained the antiplasmodial activity (e.g., **7** vs. **12**; **10** vs. **14**; **11** vs. **15**). In sum, brussanol and derivatives showed  $IC_{50}$  values that ranged from 5 to  $>10$   $\mu$ M, and 7 out of 14 derivatives showed  $IC_{50}$  values  $< 10$   $\mu$ M, thereby suggesting that structural modifications around the icetexane diterpenoid scaffold modulate the inhibitory activity of this series.

Table 1. In vitro antiplasmodial activity, cytotoxicity, and SI of brussonol and its derivatives.

Code	R <sup>1</sup>	R <sup>2</sup>	R <sup>3</sup>	R <sup>4</sup>	R <sup>5</sup>	R <sup>6</sup>	IC <sub>50</sub> <sup>Pf</sup> (μM)	IC <sub>50</sub> <sup>HepG2</sup> (μM)	SI <sup>1</sup>
1	OH	OH	<i>iPr</i>	H	Me	Me	16 ± 2	67 ± 4	4
2	OMe	OMe	H	H	H	H	>10	ND <sup>2</sup>	ND <sup>2</sup>
3	OMe	H	H	OMe	H	H	>10	ND <sup>2</sup>	ND <sup>2</sup>
4	OH	OH	H	H	H	H	>10	ND <sup>2</sup>	ND <sup>2</sup>
5	OH	H	H	OH	H	H	>10	ND <sup>2</sup>	ND <sup>2</sup>
6							>10	ND <sup>2</sup>	ND <sup>2</sup>
7	OMe	OMe	<i>iPr</i>	H	Me	Me	5.2 ± 0.4	>192	>37
8	OMe	OMe	<i>iPr</i>	OMe	Me	Me	5 ± 2	170 ± 38	34
9	OMe	OMe	H	H	Me	Me	>10	ND <sup>2</sup>	ND <sup>2</sup>
10	OMe	OMe	<i>iPr</i>	Br	Me	Me	5.6 ± 0.1	>400	>70
11	OMe	OMe	<i>iPr</i>	Ph	Me	Me	5.8 ± 0.2	>12	>2
12	OMe	OMe	<i>iPr</i>	H	H	H	5.6 ± 0.8	>400	>62
13	OH	OH	<i>iPr</i>	H	H	H	>10	ND <sup>2</sup>	ND <sup>2</sup>
14	OMe	OMe	<i>iPr</i>	Br	H	H	5.65 ± 0.05	>25	>4
15	OMe	OMe	<i>iPr</i>	Ph	H	H	5.89 ± 0.02	>50	>8

<sup>1</sup> SI = IC<sub>50</sub><sup>HepG2</sup> / IC<sub>50</sub><sup>Pf</sup>; <sup>2</sup> ND = not determined.

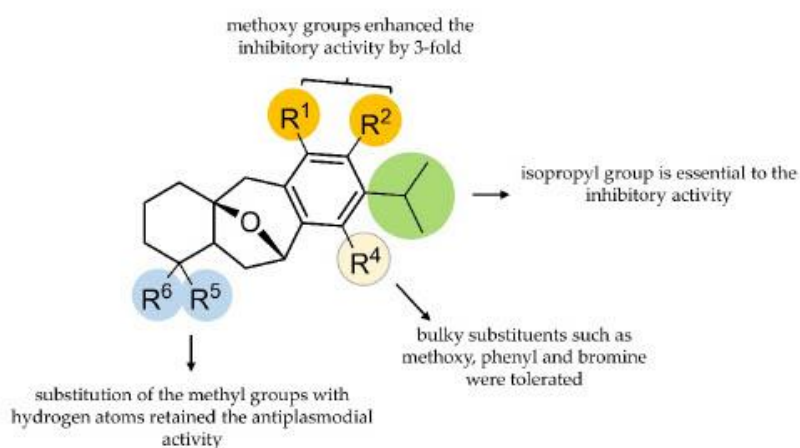


Figure 3. SAR summary around the icetexane diterpenoid scaffold.

Compounds with IC<sub>50</sub> values < 10 μM had their cytotoxic effect assessed against a human hepatocellular carcinoma (HepG2) cell line. Brussonol and derivatives showed

#### 2.4. Brussonol Is a Potent *P. knowlesi* Inhibitor

To evaluate whether this series of brussonol derivatives show inhibitory activity against other Plasmodium species, we assessed the antiplasmodial activity of brussonol (1) against *P. knowlesi*, a simian parasite that causes zoonotic malaria in humans. This parasite is prevalent in Malaysia [24], and more than 2600 zoonotic cases were reported in 2020, after 3 years without notification of human malaria in this region [1]. Compound 1 showed inhibitory activity against *P. knowlesi* parasites in the low micromolar range ( $IC_{50} = 20 \pm 4 \mu M$ ), which corresponds to a similar inhibitory activity observed against *P. falciparum* ( $IC_{50} = 16 \pm 2 \mu M$ ). This finding suggests that brussonol is an inhibitor of different Plasmodium species.

#### 2.5. Brussonol Is a Fast-Acting *P. falciparum* Inhibitor

The speed-of-action assay assesses the inhibitory activity of the tested compounds after 24, 48, and 72 h of drug exposure. The  $IC_{50}$  values for each time were defined and then compared to each other to determine whether the compound is a fast- or slow-acting inhibitor. Fast-acting inhibitors show similar  $IC_{50}$  values for each assessed time, whereas slow-acting inhibitors show pronounced inhibitory activity over the later hours. Moreover, to confirm the speed-of-action, the morphological development of the parasite in parallel with the  $IC_{50}$  assessment was verified. The parasites in the negative control wells developed according to the expected timeline (Figure 5a). Artesunate, a fast-acting inhibitor, caused parasite death within the first 24 h, as verified by the appearance of pyknotic nuclei (Figure 5a). By contrast, pyrimethamine, a slow-acting inhibitor, allowed the parasite to develop until 24 h, delaying the development past this point (Figure 5a). Effective parasite death was observed for pyrimethamine at the 48 and 72 h time points, indicating its slow-acting inhibitory activity. Brussonol caused parasite death within the first 24 h of incubation as observed for artesunate (Figure 5a). At this time point, we verified the appearance of several pyknotic nuclei, suggesting cellular death caused by a toxic effect on the parasite. Furthermore, the  $IC_{50}$  values for artesunate and brussonol at 24, 48, and 72 h were in good agreement, whereas the  $IC_{50}$  values for pyrimethamine were statistically different between 24 h and 48 h, and 24 h and 72 h (Figure 5b). These findings indicated that brussonol showed inhibitory activity comparable with artesunate, thereby suggesting a fast-acting inhibition.

#### 2.6. Brussonol Shows an Additive Combination Profile with Artesunate

A drug combination investigation is important to assess whether the combination of the tested compound with a known antimalarial drug is advantageous or not [25]. In this assay, a fixed molar ratio was used to assess the combination profile of brussonol and artesunate. The range of concentrations tested was based on the assessed  $IC_{50}$  values of both the compounds previously determined. In this method, we first determined the additive isobole, which defined the range of  $IC_{50}$  values pairs to be attributed to an additive (neutral) character of combination. Next, the combination pairs were plotted. Data points distributed below or above the additive isobole indicate a synergic or antagonistic profile, respectively [26]. The analysis of the isobologram of brussonol in combination with artesunate indicated the experimental combination data do not diverge significantly from the additivity region (Figure 6a,b). Moreover, the sum of fractional inhibitory concentrations in the proportion of 1:1 (relative to each compound's  $IC_{50}$  value) for the brussonol-artesunate pair was  $1.1 \pm 0.1$ , while the additive region defined by the additive isobole was  $1.0 \pm 0.2$ . Therefore, the absence of a significant difference between these values ( $p = 0.4818$ ) indicated an additive effect in the inhibitory activity when brussonol is used in combination with artesunate. These findings suggest that the combination of brussonol with artesunate was favorable for the in vitro inhibitory activity.

varying cytotoxic effects on HepG2 cells. For instance, brussonol showed an  $IC_{50}$  value of  $67 \mu\text{M}$  against the mammalian cells (Table 1). The  $IC_{50}$ s of this set of derivatives ranged from  $>12$  to  $>400 \mu\text{M}$ , therefore, the compounds were not generally cytotoxic, as demonstrated by the assessed SI values greater than 10 against the liver cells [22].

### 2.3. Brussonol Is a Potent Inhibitor of Resistant *P. falciparum* Strains

We selected brussonol ( $1$ ,  $IC_{50} = 16 \mu\text{M}$ ) as a representative of the series for parasitological profiling because the molecule was our first identified hit. Thus, we first assessed the inhibitory activity of brussonol against a small panel of representative-resistant strains of *P. falciparum* (Table 2). The panel included K1 (resistant to chloroquine, sulfadoxine, pyrimethamine, and cycloguanil), Dd2 (resistant to chloroquine, sulfadoxine, pyrimethamine, mefloquine, and cycloguanil), TM90C6B (resistant to chloroquine, pyrimethamine, and atovaquone), and 3D7<sup>r</sup>-MMV848 (resistant to MMV692848) strains. As the  $IC_{50}$  values were determined for the resistant parasite strains, we determined the resistance index (RI), which corresponds to the ratio between the  $IC_{50}$  values against each resistant strain and the 3D7 strain (Figure 4). In this context, a molecule shows cross-resistance if the RI value is greater than five [23]. Brussonol showed comparable inhibitory activities between the resistant and the sensitive strains ( $RI < 5$ ), thereby indicating no cross-resistance with the standard antimalarials used as inhibition control.

**Table 2.**  $IC_{50}$  values of compound brussonol against a panel of sensitive and resistant *P. falciparum* strains.

<i>Pf</i> Strain	$IC_{50}$ brussonol ( $\mu\text{M}$ )	RI	$IC_{50}^{P\text{YR}}$ ( $\mu\text{M}$ )	RI	$IC_{50}^{A\text{T}\text{V}}$ ( $\mu\text{M}$ )	RI	$IC_{50}^{A\text{R}\text{T}}$ ( $\mu\text{M}$ )	RI	$IC_{50}^{\text{MMV848}}$ ( $\mu\text{M}$ )	RI
3D7	$13 \pm 2$	1	$0.06 \pm 0.01$	1	$0.0007 \pm 0.0003$	1	$0.008 \pm 0.004$	1	$0.13 \pm 0.02$	1
K1	$6.6 \pm 0.1$	0.5	$>10$	$>166$	NT	NT	$0.007 \pm 0.003$	1	NT	NT
Dd2	$7 \pm 2$	0.5	$>10$	$>166$	NT	NT	$0.011 \pm 0.008$	1	NT	NT
TM90C6B	$7 \pm 2$	0.5	NT	NT	$3 \pm 1$	4285	$0.006 \pm 0.002$	1	NT	NT
3D7 <sup>r</sup> -MMV848	$12 \pm 3$	1	NT	NT	NT	NT	$0.013 \pm 0.008$	2	$2.4 \pm 0.4$	18

Data represent mean  $\pm$  standard deviation of at least two independent experiments conducted in triplicate; RI =  $IC_{50}^{\text{resistant strain}} / IC_{50}^{3\text{D}7}$ ; NT = not tested; PYR = pyrimethamine; ATV = atovaquone; ART = artesunate; MMV848 = *Pf*PI4K inhibitor.

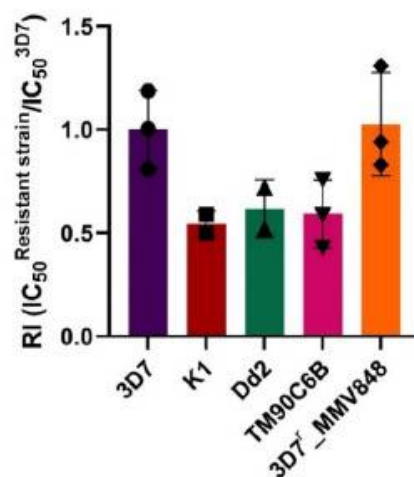
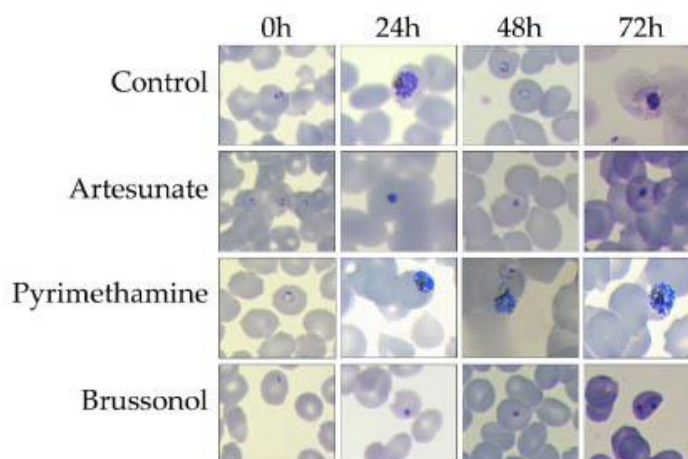
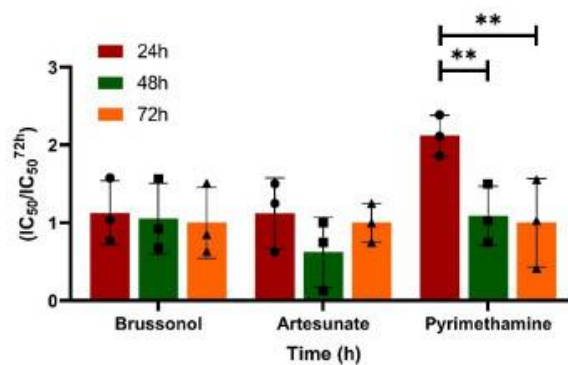


**Figure 4.** Analysis of resistance index (RI) of brussonol against a panel of sensitive and resistant *P. falciparum* strains (K1, Dd2, TM90C6B, and 3D7<sup>r</sup>-MMV848) relative to the sensitive strain (3D7). Plot of the fold-change in the antiparasitodal potency of brussonol against a panel of resistant strains relative to the sensitive strain. ( $n \geq 2$ , mean  $IC_{50} \pm SD$ ).



(a)



(b)

**Figure 5.** Speed-of-action assessment of brussonol. (a) Morphological development evaluation of parasites over time in *P. falciparum* culture stained with giemsa. (b)  $IC_{50}$  values were determined at 24, 48, and 72 h. Artesunate and pyrimethamine were used as a positive control for fast- and slow-acting inhibition, respectively. The results were normalized with respect to the assessed  $IC_{50}$  value at 72 h. Statistical analysis was carried out by using ANOVA (\*\*  $p < 0.01$ ; a  $p$ -value  $< 0.05$  indicates a significant difference within samples). These data correspond to three independent experiments, mean  $IC_{50} \pm SD$ .

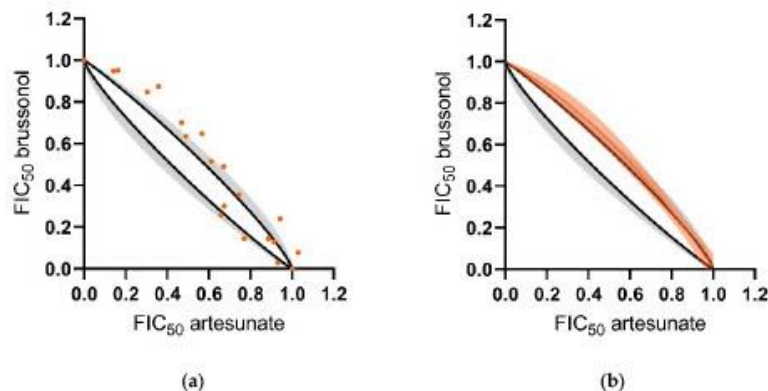


**Figure 6.** Isobologram and additive isobole were calculated for the combination of brussonol with artesunate. Black lines correspond to the arithmetic average of the upper and lower limits of the additive area, and the gray area indicates the calculated standard deviations. (a) Experimentally determined FIC<sub>50</sub> value pairs are individually represented as orange dots. (b) Non-linear fit of experimental data, indicated by the fitted curve (dark orange) and the confidence interval of 95% (clear orange). Data analyzed are from three independent experiments.

### 2.7. *Brussonol Does Not Interfere with Isoprenoid Biosynthesis*

To shed some light on the mode of action underlying brussonol antiplasmodial activity, a structural similarity search in the SciFinder database was performed. The main goal of this approach was to identify whether there were similar compounds with known mechanisms of action. To this end, we set a similarity threshold of >80%. Among the best hits, carnosol (81% similarity), an inhibitor of the squalene synthase (SQS) enzyme, was identified. Carnosol is an essential biomolecule for the biosynthesis of steroids (Figure 7a) [27]. The biosynthesis of steroids is a complex process in which the isoprenoid isopentenyl pyrophosphate (IPP) is one of the precursors [28,29]. In the malaria parasite, the isoprenoid biosynthesis occurs in the apicoplast via an alternate biosynthetic route, the methylerythritol phosphate pathway (MEP), whose components are different from the mevalonate pathway, which is employed by humans to generate isoprenoids [29]. These molecules play central roles in parasite development, including gene expression regulation, and as membrane constituents. Therefore, due to the absence of mammalian homologs and the essentiality of this pathway, the enzymes of the isoprenoid biosynthesis are attractive and validated antimalarial drug targets [30].

To evaluate whether brussonol interfered with the biosynthesis of steroids in malaria parasites, we conducted a chemical rescue assay [31–34]. The assay identifies compounds that interfere with the metabolism of isoprenoids by “rescuing” their growth inhibition through the supplementation of isopentenyl pyrophosphate (IPP), a key precursor of isoprenoid biosynthesis [31]. Therefore, the assay is useful to identify compounds that affect this metabolic pathway and suggest a putative mode of action for compounds under investigation. Thus, the chemical rescue assay compares the IC<sub>50</sub> values of the tested compound in the presence and absence of IPP. We used fosmidomycin (FOS) as a positive control for growth inhibition rescuing upon supplementation of IPP (Figure 7b). In this assay, compounds that interfere in the metabolism of isoprenoids show a significant increment in the IC<sub>50</sub> value in the presence of IPP (Figure 7b). Nevertheless, IPP supplementation did not reverse the growth inhibition by brussonol (Figure 7c). The natural product showed comparable IC<sub>50</sub> values in the presence (IC<sub>50</sub> = 13.9 ± 0.2 μM) and absence (IC<sub>50</sub> = 18 ± 1 μM) of IPP (Figure 7c). These findings indicate that the antiplasmodial activity of brussonol did not rely on the inhibition of the isoprenoid biosynthesis pathway.

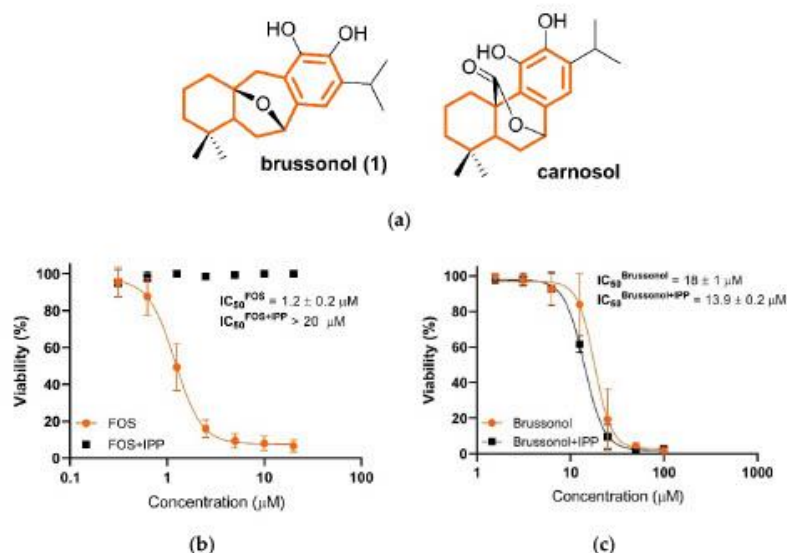


**Figure 7.** Chemical “rescue” assay to evaluate the action of brussonol (1) in the metabolism of isoprenoids (a) Molecular structures of carnosol and brussonol [35]. (b) Concentration–response curves for foemidomycin (FOS, positive control) against *P. falciparum* 3D7 strain with and without the supplementation of IPP. (c) Concentration–response curves for brussonol against *P. falciparum* 3D7 strain with and without supplementation of IPP ( $n \geq 2$ , mean  $\text{IC}_{50} \pm \text{SD}$ ).

### 2.8. Brussonol Induces $[\text{Ca}^{2+}]_{\text{cyt}}$ Rise in *P. falciparum*

One of the compounds identified in the structural similarity search was the cyclopiazonic acid (CPA) (Figure 8a). CPA is a highly selective inhibitor for a *P. falciparum* sarco/endoplasmic reticulum  $\text{Ca}^{2+}$ -ATPase (PfSERCA) pump [36–38]. Because of that, brussonol activity on the modulation of the SERCA pump was investigated. To assess the effect of brussonol on calcium mobilization in *P. falciparum* intraerythrocytic stages, isolated parasites loaded with Fluo-4-AM were exposed to 10  $\mu\text{M}$  brussonol in MOPS  $\text{Ca}^{2+}$  buffer. Brussonol elicited sustained  $[\text{Ca}^{2+}]_{\text{cyt}}$  rise ( $19 \pm 4 \text{ nM}$ ) relative to the basal cytosolic calcium level (Figure 8b,d), which was comparable to the calcium concentration mobilized by CPA ( $23 \pm 2 \text{ nM}$ ) (Figure 8c,d). To verify if the brussonol-elicited  $[\text{Ca}^{2+}]_{\text{cyt}}$  increment originated from the endoplasmic reticulum (ER), targeting the PfSERCA pump, CPA was added before the addition of brussonol. Firstly, as expected, 10  $\mu\text{M}$  CPA significantly led to a transient increment in the cytosolic  $\text{Ca}^{2+}$  concentration ( $23 \pm 2 \text{ nM}$ ) in isolated parasites, consistent with the previous results reported [36–39]. After the CPA addition reached a plateau, we proceeded with the subsequent addition of 10  $\mu\text{M}$  brussonol, which led to an increase in  $[\text{Ca}^{2+}]_{\text{cyt}}$  ( $19 \pm 8 \text{ nM}$ ) comparable to brussonol alone ( $19 \pm 4 \text{ nM}$ ). In the brussonol-pretreated parasites, the addition of CPA still increased the cytosolic  $\text{Ca}^{2+}$  level ( $30 \pm 5 \text{ nM}$ ) (Figure 8d). These results indicated that brussonol induces a  $[\text{Ca}^{2+}]_{\text{cyt}}$  rise in *P. falciparum*; however, the calcium mobilization is carried out by a different mechanism than CPA.

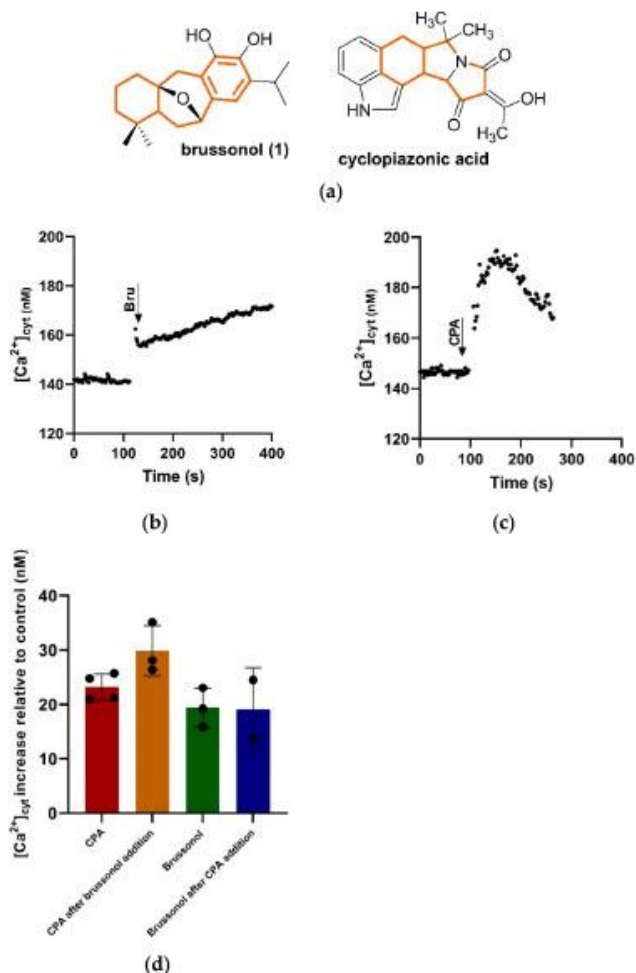


**Figure 8.** Effect of brussonol on the cytosolic  $Ca^{2+}$  mobilization in *P. falciparum* loaded with Fluo-4 AM calcium indicator. (a) Chemical structure of brussonol and CPA. The fused rings are highlighted for comparison purposes. Representative traces of  $[Ca^{2+}]_{cyt}$  rise induced by 10  $\mu$ M brussonol (b) and 10  $\mu$ M CPA (c) in MOPS buffer containing  $Ca^{2+}$ . (d) Histograms of the increase in the cytosolic  $Ca^{2+}$  levels with the addition of CPA (10  $\mu$ M), brussonol (10  $\mu$ M), and brussonol (10  $\mu$ M) after and before treatment with CPA (10  $\mu$ M). The data analyzed were collected from two independent experiments.

### 3. Discussion

The discovery and development of new chemical series to replace the antimalarials with emerging resistance are urgently needed. Brussonol is an attractive natural compound with a new molecular scaffold endowed with promising antiplasmodial activity. The synthetic strategy to obtain brussonol and derivatives required five to seven steps, except for some compounds that required further modification, such as bromination (10 and 14, Table 1). In this sense, we designed and assessed the biological activity against *P. falciparum* of 15 brussonol derivatives (Table 1). Of these, seven compounds showed inhibitory activity in the low micromolar range ( $IC_{50}$ ~5  $\mu$ M), indicating an attractive



potential for further potency improvements. For example, compounds **8**, **10**, and **12** showed promising inhibitory potencies against *P. falciparum* ( $IC_{50}$ s ~5  $\mu$ M), low cytotoxic effects on HepG2 cells ( $IC_{50}$ s > 170  $\mu$ M), and reasonable selectivity indexes (SI > 30). Moreover, brussonol (**1**) showed comparable inhibitory potencies against both *P. falciparum* and *P. knowlesi* ( $IC_{50}$  ~20  $\mu$ M), which indicated that this series has inhibitory activity against different Plasmodium species. The synthesis and assessment of A- and C-ring substitution variants (Figure 1) indicated a clear structure–activity relationship, thereby suggesting that the inhibitory activity of this series can be modulated by suitable chemical groups. For instance, we discovered compounds with 3-fold increased potency compared with brussonol. In this sense, compound **12** stood out as an attractive frontrunner candidate, because it showed inhibitory potency in the low micromolar range ( $IC_{50}$  = 5  $\mu$ M), low cytotoxic effect on liver cells ( $IC_{50}$  > 400  $\mu$ M), and a considerable selectivity index (SI > 62).

A constant challenge for malaria eradication and elimination, as well as for antimalarial drug discovery, relies on the emergence of parasite resistance to available antimalarials [40]. Consequently, it is critical to discover new compounds as drug candidates that overcome the rise of resistance. The Medicines for Malaria Venture (MMV) developed a preclinical resistance assessment strategy to identify active compounds against a collection of resistant strains [41]. In these assays, the  $IC_{50}$ s of selected compounds are determined against genetically defined resistant strains of *P. falciparum* with naturally occurring known resistance mechanisms. In line with this, we assessed the cross-resistance potential of brussonol and verified that the isotexane diterpenoid scaffold was equipotent against a small panel of resistant *P. falciparum* strains (Figure 4). This finding suggested that brussonol is active against resistant strains of the parasite; in addition, the data indicated that antiplasmodial activity relied on a different mode of action than the gold standard antimalarials.

Another important property of new antimalarials is their speed of action. Ideally, new compounds with antimalarial activity should have a fast onset of action, so that the patient's symptoms would be rapidly relieved, and a major parasite population in the human host is killed within the first hours of treatment, minimizing the risk of resistance selection [42,43]. Brussonol showed a speed-of-action profile like artesunate, a known fast-acting antimalarial drug. We observed a pronounced inhibitory activity within the first 24 h in the presence of brussonol (Figure 5). Therefore, these parasites did not recover after washing the drug out, indicating that brussonol was effective in killing the parasites.

The in vitro association assay allowed us to determine if a combination of brussonol with artesunate would be advantageous [25]. Several scientific methods to evaluate this in vitro combination are available [44]. In this study, we applied the isobologram analysis combined with fractional inhibitory concentrations (FICs) so that it allowed the identification of what type of interaction (e.g., additive, synergistic, or antagonistic) there is between brussonol and gold-standard antimalarial [45]. The use of ACTs as the first-line treatment for malaria was crucial to slow down the emergence and the spread of artemisinin resistance [41]. In this context, the combined use of multiple agents to treat malaria is recommended, so that the lifespan of antimalarial agents is likely to improve [45]. The analysis of the isobologram obtained in the combination study indicated that brussonol showed an additive profile with artesunate, thereby suggesting that the combination was favorable for the in vitro inhibitory activity (Figure 6). This finding agrees with other reports that showed that hits and lead compounds can be attractive candidates for ACTs and highlights the importance of the assessment of the combination profile in the early phases of the drug discovery pipeline [46–49].

The identification of the mode of action of new chemical entities (NCE) is a key step in the drug discovery and development paradigm. The definition of how and where a molecule exerts its pharmacological properties significantly helps the lead optimization process of a chemical class and could anticipate the emergence of a resistance mechanism [50]. The study of brussonol's mode of action started by identifying that the compound did not interfere with hemozoin polymerization (Figure S1). Next, a similarity-based search in SciFinder was performed to identify structural-related compounds to brussonol with any

target-associated information. Consequently, this search returned carnosol and cyclopiazonic acid (CPA) as close analogs (Figures 7a and 8a, respectively). Carnosol is a natural product that modulates the biosynthesis of the steroids pathway [27]. Therefore, we tested the ability of brussonol to modulate the isoprenoid biosynthesis pathway. Based on the protocol developed by Yeh and Derisi [31], we verified that brussonol did not interfere in isoprenoid biosynthesis once the parasites treated with this molecule could not be “rescued” by the supplementation with IPP. CPA is a PfSERCA-specific inhibitor that modulates the cytosolic  $\text{Ca}^{2+}$  homeostasis. In Plasmodium species,  $\text{Ca}^{2+}$  signaling plays a central role in the parasite life cycle [38,51], including intraerythrocytic parasite proliferation invasion and egress from the host cell, protein secretion, and cell cycle regulation. The endoplasmic reticulum (ER) is the major intracellular  $\text{Ca}^{2+}$  storage compartment in *P. falciparum* [51] and regulates cytosolic  $\text{Ca}^{2+}$  through the sarco/endoplasmic reticulum  $\text{Ca}^{2+}$ -ATPase (PfSERCA or PfATP6) pump. The addition of 10  $\mu\text{M}$  brussonol in Fluo-4AM-loaded parasites elicited a sustained  $[\text{Ca}^{2+}]_{\text{cyt}}$  rise, which increased steadily even after SERCA was inhibited by CPA. In addition, the calcium mobilization by CPA in the brussonol-pretreated parasites also increased the cytosolic  $\text{Ca}^{2+}$  levels in the same manner (Figure 8). These results suggested that the increase in  $[\text{Ca}^{2+}]_{\text{cyt}}$  by brussonol was not due to the efflux of  $\text{Ca}^{2+}$  from the ER, thereby indicating that brussonol did not target PfSERCA. These findings are in contrast with that observed with artemisinin derivatives, which act on the ER calcium store [52–55]. This  $[\text{Ca}^{2+}]_{\text{cyt}}$  rise elicited by brussonol may originate from the extracellular media via  $\text{Ca}^{2+}$  influx through membrane calcium channels or other intracellular calcium stores in Plasmodium, including mitochondria or acidic organelles [51]. In sum, although the brussonol target remains unknown, it did interfere with the  $\text{Ca}^{2+}$  levels within the parasite, which is an interesting result that could explain the additive effect in the inhibitory activity when brussonol was combined with artesunate. In this case, each drug acts in a different parasite calcium source, thereby impacting on calcium homeostasis and parasite development.

#### 4. Materials and Methods

##### 4.1. Maintenance of In Vitro Culture

The *P. falciparum* strains were cultivated in human blood cells (hRBC)  $\text{O}^+$ , while *P. knowlesi* was cultivated in rhesus red blood cells (rRBC) as described [56]. *P. falciparum* complete RPMI (consisting of RPMI-1640, supplemented with 0.2%  $\text{NaHCO}_3$ , 25 mM HEPES (pH 7.4), 11 mM D-glucose, 10 mg/L hypoxanthine, 25 mg/L gentamicin, and 0.5% (m/v) Albumax II) [57]. The parasitemias of these cultures were maintained below 10% with 2.5% hematocrit. *P. knowlesi* complete RPMI (consisting of RPMI-1640 supplemented with 25 mM HEPES, 50 mg/L mM hypoxanthine, 0.26%  $\text{NaHCO}_3$ , 10 mg/L gentamicin, and 1% Albumax II) [58]. This culture was maintained with RBCs up to 5% hematocrit. The culture medium was changed daily, and all cultures were maintained under a 90%  $\text{N}_2$ /5%  $\text{CO}_2$ /5%  $\text{O}_2$  gas mixture at 37 °C. All compounds were purchased from Sigma-Aldrich (Cotia, Brazil).

##### 4.2. Biological Activity against *P. falciparum* Blood-Stage Parasites In Vitro

The antiplasmodial activity of brussonol and derivatives was evaluated against *P. falciparum* blood parasites 3D7 (chloroquine-sensitive). The parasites were synchronized through sterile 5% (m/v) D-sorbitol treatment over 10 min at 37 °C for the enrichment of ring stages [59]. Centrifugation  $600 \times g$  over 5 min was used to pellet the cultures. The parasitemia was determined by microscope analysis of thin blood smears stained with Giemsa 10% (v/v) after fixation with methanol. The initial parasitemia was calculated for 1000 red blood cells (RBCs), and cultures were diluted to 0.5% parasitemia and 2% hematocrit by the addition of the appropriate volumes of blood and medium. A total of 180  $\mu\text{L}$  aliquots of parasites were distributed into 96-well plates followed by the addition of 20  $\mu\text{L}$  of previously prepared aliquots of ten-fold concentrated compounds, the range of concentrations tested was 10–1.53  $\mu\text{M}$ . Negative and positive control wells, which correspond to non-parasitized erythrocytes and parasite cultures in the absence of compounds,

were set in parallel. The DMSO concentration was maintained below 0.05% (*v/v*) for all compounds except for brussonol, which was 0.5%. The plates were incubated for 72 h at 37 °C in a humidified incubator with a gas mixture of 90% N<sub>2</sub>, 5% O<sub>2</sub>, and 5% CO<sub>2</sub>. Each test was performed in duplicates, and the results were compared with the control cultures. Once completed incubation, the culture medium was removed, and the cells were resuspended in 100 µL PBS (116 mM NaCl, 10 mM NaH<sub>2</sub>PO<sub>4</sub>, 3 mM KH<sub>2</sub>PO<sub>4</sub>) and lysed with 100 µL lysis buffer (20 mM Tris base, 5 mM EDTA, 0.0008% (*v/v*) Triton X-100, 0.008% (*m/v*) saponin, pH 8.0) containing 0.002% (*v/v*) SYBR Green I. Plates were incubated for 30 min at room temperature, and a SpectraMAX Gemini EM plate reader (Molecular Devices Corp., Sunnyvale, CA) was used to determine the fluorescence corresponding to parasitic density (excitation at 485 nm, emission at 535 nm) [60]. The half-maximal inhibitory concentration (IC<sub>50</sub><sup>Pf</sup>) was determined by non-linear regression analysis of the resulting concentration-response curve using the software GraphPad Prism version 8.0.1 for Windows, GraphPad Software, San Diego, California USA, [www.graphpad.com](http://www.graphpad.com), accessed on 3 March 2022".

#### 4.3. Cytotoxic Tests Using Immortalized Cells

The cytotoxic effects of brussonol and derivatives were evaluated against the human hepatocellular carcinoma cell line (HepG2). The cells were cultivated in an RPMI medium supplemented with 10% (*v/v*) fetal bovine serum and 25 µg/mL gentamicin. Conditions for the cultivation of these cells were 37 °C and 5% CO<sub>2</sub>, and every 2 days the supplemented medium was changed.

For experimental procedures, the cells were trypsinized and transferred to a 96-well plate at 30,000 cells per well (180 µL). The plate was incubated at 37 °C and 5% CO<sub>2</sub> to allow cell adhesion. Next, 20 µL of serial dilutions of the compounds tested were added to the plate, with a range of concentrations tested from 400–6.25 µM. Cells without any compounds were used as a positive control for growing and the wells containing only medium were used as negative controls. The plate was incubated for 72 h at 37 °C and 5% CO<sub>2</sub>. After incubation, a microscope was used to determine the highest compound concentration to be used in the experiments (highest concentration without precipitation). A colorimetric assay was used to evaluate cytotoxicity. This assay is based on the metabolic cell activity in the presence of 3-(4,5-dimethylthiazol-2-yl)-2,5-diphenyltetrazolium bromide (MTT) [61]. Shortly after incubation, 20 µL of a solution of MTT at 5 mg/mL (solubilized in phosphate buffer) is added to each well. The plate is incubated for 3 to 4 h at 37 °C to allow MTT cleavage in living cells. Then, the supernatant is removed, and 100 µL of dimethylsulfoxide (DMSO) is added to solubilize the purple formazan crystals. The absorbance, which is proportional to the number of viable cells, was determined using a SpectraMAX Plus 384 plate reader (Molecular Devices Corp., Sunnyvale, CA) ( $\lambda = 570$  nm). All compounds described here were purchased from Sigma-Aldrich (verificar local).

#### 4.4. Calculation of Selectivity Index (SI)

After the IC<sub>50</sub> against the parasite and the human cell line is determined, it is possible to calculate the SI. It is calculated as the formula below:

$$SI = IC_{50}^{HepG2} / IC_{50}^{Pf}.$$

The SI shows the difference between the inhibitory potency against the parasite and the cytotoxic concentration for mammalian cells. For our reference, compounds with SI values higher than 10 are considered well tolerated by the cellular model used, and they are considered for further evaluation.

#### 4.5. In Vitro Evaluation against *P. knowlesi*

Blood-stage *P. knowlesi* cultures were diluted to 0.5% parasitemia and brought to 2% hematocrit for growth in 96-well plates containing the desired drug concentration series (200 µL of culture/well). Plates were incubated for 40 h at 37 °C in a humidified chamber containing a gas mixture of 5% CO<sub>2</sub>, 5% O<sub>2</sub>, and 90% N<sub>2</sub>. Parasite growth in the plates was

measured by luminescence (NanoLuc method) [62]. In this method, plates were removed from the incubator and 100  $\mu$ L of NanoGlo IC50 solution (Promega NanoGlo reaction mixture diluted tenfold in PBS) were added to each well and mixed by pipetting. The plates were then incubated for 3 min at room temperature and the luminescence was assessed using a plate luminometer (Molecular Devices, San Jose, CA, USA) with 1 s integration time. Luminescence readings were normalized to values from control wells containing no drug. IC<sub>50</sub> values were determined from fitted response curves (non-linear regression with variable slope, GraphPad Prism Software), and data from at least two independent assays were used to calculate the average IC<sub>50</sub> value of the *P. knowlesi* pvcen-pvhs70-DNanoLuc transgenic line with each method.

#### 4.6. Resistance Assessment

The antiplasmodial activity of brussonol was assessed against a panel of *P. falciparum* strains: 3D7 (chloroquine-sensitive), K1 (resistant to chloroquine, mefloquine, and sulfadoxine), Dd2 (resistant to chloroquine, mefloquine, and pyrimethamine), TM90C6B (resistant to atovaquone), and 3D7<sup>+</sup>-MMV848 (resistant to MMV692848, a PI4K inhibitor). The assay to determine the IC<sub>50</sub> value of brussonol against the panel of resistant strains was carried out as described above. After the determination of the IC<sub>50</sub> value for each resistant strain, a resistance index (RI) was calculated using the following equation:

$$RI = IC_{50}^{\text{Resistant strain}} / IC_{50}^{3D7}$$

RI values greater than 3 were considered indicative of cross-resistance.

#### 4.7. Speed-of-Action Assay

To determine whether brussonol is a fast- or slow-acting inhibitor, a protocol adapted from Terkuile and collaborators (1993) [63] was used. In this method, three 96-well plates were prepared by adding 180  $\mu$ L of the parasite's inoculum with 0.5% parasitemia and 2% hematocrit. A serial dilution of the compounds was added to each plate; the starting concentration for brussonol was  $6 \times IC_{50}$ , while for artesunate and pyrimethamine (fast- and slow-acting controls, respectively) were  $10 \times IC_{50}$ . In addition, a positive and negative control, which corresponded to parasite cultures with no addition of inhibitor and non-parasitized erythrocytes, respectively, were used for the parasite's control growth. Each plate was treated for a different period (24, 48, or 72 h), and the first two plates were washed twice with fresh medium to remove the inhibitor, followed by incubation of 48 and 24 h, respectively. After 72 h of incubation at 37 °C, all plates were evaluated using SYBR Green I assay to determine the IC<sub>50</sub> for each treatment. A statistical analysis using a one-way ANOVA test was done to compare each time point using GraphPad Prism version 8.0.1 for Windows, GraphPad Software, San Diego, California USA, [www.graphpad.com](http://www.graphpad.com), accessed on 1 February 2022. In parallel, the morphological development of the parasite under the compounds' pressure was assessed by adding the compounds tested at the highest concentration evaluated. Blood smears of each well were made and stained at time points 0, 24, 48, and 72 h.

#### 4.8. In Vitro Combination with Artesunate

This assay was adapted from the work done by Fivelman and collaborators (2004) [64]. Consideration of additivity ranges was included in the analysis, as described by Grabovsky and Tallarida (2004) [26]. Brussonol and artesunate were diluted and combined in a 96-well plate in seven fixed-ratio combinations (1:0, 6:1, 5:2, 4:3, 3:4, 2:5, 1:6, 0:1). Starting concentrations were  $6 \times IC_{50}$  for both compounds. This experiment was performed with 0.5% parasitemia and 2% hematocrit, and controls were drug-free non-parasitized erythrocytes and parasitized erythrocytes. Serial dilutions of these combinations were prepared and incubated with the parasite as described above to determine the antiplasmodial activity against *P. falciparum*. The SYBR Green I test was applied to determine the IC<sub>50</sub> value for each combination, using the software GraphPad Prism version 8.0.1 for Windows,

**Author Contributions:** Conceptualization, C.S.B., A.A., A.C.B.B. and R.V.C.G.; methodology, C.S.B., A.A., S.E.C.M., G.A.H.G. and I.M.R.M.; formal analysis, C.S.B., S.E.C.M., I.M.R.M., R.R.M.B., M.L.G. and G.E.S.; investigation, C.S.B., A.A., S.E.C.M., G.A.H.G. and I.M.R.M.; resources, A.C.B.B. and R.V.C.G.; writing—original draft preparation, C.S.B., A.A., S.E.C.M.; writing—review and editing, C.S.B., A.A., S.E.C.M., I.M.R.M., G.E.S., M.L.G., A.C.C.A., A.C.B.B. and R.V.C.G.; supervision, A.C.C.A., A.C.B.B. and R.V.C.G.; project administration, A.C.C.A., A.C.B.B. and R.V.C.G.; funding acquisition, A.C.B.B. and R.V.C.G. All authors have read and agreed to the published version of the manuscript.

**Funding:** We thank the Sao Paulo Research Foundation—FAPESP for funding the research (CEPID grant 2013/07600-3, 2020/12904-5, 2019/17721-9, 2013/18009-4, 2019/19708-0, 2018/06219-8) and fellowships (2015/20064-0 to A.A., 2018/07287-7 to G.E.S., 2021/14319-5 to G.A.H.G., 2021/03977-1 to I.M.R.M., and 2020/14429-2 to S.E.C.M.). This study was also financed in part by the Coordenação de Aperfeiçoamento de Pessoal de Nível Superior—Brasil (CAPES)—Finance Code 001 and fellowship 88887.369957/2019-00 to CSB.

**Institutional Review Board Statement:** Not applicable.

**Informed Consent Statement:** Not applicable.

**Data Availability Statement:** Data are contained within the article and supplementary materials.

**Acknowledgments:** We are grateful to Flávio Henrique Silva and Alexandrê Budu for their contributions to in vitro studies with calcium measurements.

**Conflicts of Interest:** The authors declare no conflict of interest.

## References

1. World Health Organization *World Malaria Report 2021*; World Health Organization: Geneva, Switzerland, 2021.
2. Yeung, S. Malaria—Update on Antimalarial Resistance and Treatment Approaches. *Pediatr. Infect. Dis. J.* **2018**, *37*, 367–369. [\[CrossRef\]](#)
3. Simmons, E.M.; Sarpong, R. Structure, Biosynthetic Relationships and Chemical Synthesis of the Icetexane Diterpenoids. *Nat. Prod. Rep.* **2009**, *26*, 1195–1217. [\[CrossRef\]](#)
4. Fraga, B.M.; Díaz, C.E.; Guadaño, A.; González-Coloma, A. Diterpenes from *Salvia Broussonetii* Transformed Roots and Their Insecticidal Activity. *J. Agric. Food Chem.* **2005**, *53*, 5200–5206. [\[CrossRef\]](#)
5. Jiang, Z.Y.; Yu, Y.J.; Huang, C.G.; Huang, X.Z.; Hu, Q.F.; Yang, G.Y.; bin Wang, H.; Zhang, X.Y.; Li, G.P. Icetexane Diterpenoids from *Perovskia Atriplicifolia*. *Planta Med.* **2015**, *81*, 241–246. [\[CrossRef\]](#) [\[PubMed\]](#)
6. Uchiyama, N.; Kiuchi, F.; Ito, M.; Honda, G.; Takeda, Y.; Khodzimatov, O.K.; Ashurmetov, O.A. New Icetexane and 20-Norabietane Diterpenes with Trypanocidal Activity from *Dracocephalum Komarovii*. *J. Nat. Prod.* **2003**, *66*, 128–131. [\[CrossRef\]](#) [\[PubMed\]](#)
7. El-Lakary, A.M.; Abdel-Kader, M.S.; Sabri, N.N.; Sternitz, F.R. Lanigerol: A New Antimicrobial Icetexane Diterpene from *Salvia Lanigera*. *Planta Med.* **1995**, *61*, 559–560. [\[CrossRef\]](#) [\[PubMed\]](#)
8. Cezarotto, C.S.; Dorneles, A.; Baldissera, F.G.; da Silva, M.B.; Markoski, M.M.; Júnior, L.C.R.; Peres, A.; Fazolo, T.; Bordignon, S.A.L.; Apel, M.A.; et al. Leishmanicidal and Anticemotactic Activities of Icetexanes from *Salvia Uliginosa* Benth. *Phytomedicine* **2019**, *58*, 152748. [\[CrossRef\]](#) [\[PubMed\]](#)
9. Uchiyama, N.; Kabututu, Z.; Kubata, B.K.; Kiuchi, F.; Ito, M.; Nakajima-Shimada, J.; Aoki, T.; Ohkubo, K.; Fukuzumi, S.; Martin, S.K.; et al. Antichagasic Activity of Komaroviquinone Is Due to Generation of Reactive Oxygen Species Catalyzed by *Trypanosoma Cruzi* Old Yellow Enzyme. *Antimicrob. Agents Chemother.* **2005**, *49*, 5123–5126. [\[CrossRef\]](#)
10. Tabefam, M.; Farimani, M.M.; Danton, O.; Ramseyer, J.; Kaiser, M.; Ebrahimi, S.N.; Salehi, P.; Batooli, H.; Potterat, O.; Hamburger, M. Antiprotozoal Diterpenes from *Perovskia Abrotanoides*. *Planta Med.* **2018**, *84*, 913–919. [\[CrossRef\]](#)
11. Esquivel, B.; Bustos-Brito, C.; Sánchez-Castellanos, M.; Nieto-Camacho, A.; Ramírez-Apar, T.; Joseph-Nathan, P.; Quijano, L. Structure, Absolute Configuration, & Antiproliferative Activity of Abietane & Icetexane Diterpenoids from *Salvia Ballotiflora*. *Molecules* **2017**, *22*, 1690. [\[CrossRef\]](#)
12. Carita, A.; Burtoloso, A.C.B. An Epoxide Ring-Opening Approach for a Short and Stereoselective Synthesis of Icetexane Diterpenoids. *Tetrahedron Lett.* **2010**, *51*, 686–688. [\[CrossRef\]](#)
13. Reddy, K.R.K.K.; Longato, G.B.; de Carvalho, J.E.; Ruiz, A.L.T.G.; Silva, L.F. Populene D Analogs Design, Concise Synthesis and Antiproliferative Activity. *Molecules* **2012**, *17*, 9621–9630. [\[CrossRef\]](#) [\[PubMed\]](#)
14. Tohma, H.; Morioka, H.; Harayama, Y.; Hashizume, M.; Kita, Y. Novel and Efficient Synthesis of P-Quinones in Water via Oxidative Demethylation of Phenol Ethers Using Hypervalent Iodine(III) Reagents. *Tetrahedron Lett.* **2001**, *42*, 6899–6902. [\[CrossRef\]](#)

GraphPad Software, San Diego, CA, USA, [www.graphpad.com](http://www.graphpad.com), accessed on 12 August 2020. The absolute IC<sub>50</sub>s of brussonol and artesunate (proportions 1:0 and 0:1), the partial IC<sub>50</sub>s (IC<sub>50</sub><sup>brussonol</sup> and IC<sub>50</sub><sup>artesunate</sup>) for each combination (6:1, 5:2, 4:3, 3:4, 2:5, 1:6), and the fractional inhibitory concentrations for each combination were determined. FIC pairs were plotted as points in isobolograms, and if the majority of the FIC<sub>50</sub> pairs were above or below the additive range, the combination evaluated showed antagonism or synergic interaction, respectively.

#### 4.9. Chemical Rescue Assay

The chemical rescue assay was carried out as described by Yeh and DeRisi (2011). This assay consists in verifying the IC<sub>50</sub> value of the tested compounds with and without the isopentenyl pyrophosphate (IPP), purchased from Isoprenoids, LC (Florida, USA). Briefly, 3D7 strain ring stages were cultured in 96-well plates, with 0.5% parasitemia and 2% hematocrit. Non-parasitized erythrocytes and parasitized erythrocytes without drugs were used as growth controls, and fosmidomycin (FOS) was used as a positive control for chemical rescue. Serial dilutions of brussonol and FOS were prepared in duplicates. In the same 96-well plate, brussonol and FOS had their antiplasmodial activity evaluated with and without supplementation of 200 µM IPP. Plates were incubated for 72 h and analyzed by the SYBR Green I assay.

#### 4.10. [Ca<sup>2+</sup>]<sub>cyt</sub> Measurements

Isolated parasites were incubated for 1 h at 37 °C with 5 µM of Fluo-4AM in 1 mL MOPS buffer (116 mM NaCl, 5.4 mM KCl, 0.8 mM MgSO<sub>4</sub>, 5.5 mM D-glucose, 50 mM MOPS, and 2 mM CaCl<sub>2</sub>, pH 7.2), with 1 mM probenecid to minimize compartmentalization and extrusion of probe. The parasites were washed three times with the same buffer and transferred to a quartz cuvette. Intracellular calcium was measured continuously using a Hitachi F-7000 spectrofluorimeter (Tokyo, Japan) by measurement of the fluorescence (λ<sub>ex</sub> = 488 nm and λ<sub>em</sub> = 530 nm) at 37 °C, under agitation. When indicated, 10 µM of cyclopiazonic acid (CPA) or 10 µM of brussonol were added to the cuvette. Maximal fluorescence (F<sub>max</sub>) was determined after the lysis of with digitonin 0.15% (m/v), and minimal fluorescence (F<sub>min</sub>) was determined by adding 25 mM EGTA in 3 M Tris, pH 8.8, until no further decrease in fluorescence was observed. The cytosolic calcium concentration ([Ca<sup>2+</sup>]<sub>cyt</sub>) was calculated from the fluorescence data (F) using a K<sub>d</sub> value of 345 nM using the formula:

$$Ca^{2+}_{cyt} = 345 \times [(F - F_{min}) / (F_{max} - F)]$$

The results (n = 2) were analyzed through One-Way ANOVA with Tukey post-test. All compounds described here were purchased from Sigma-Aldrich (verificar local).

## 5. Conclusions

Brussonol and analogs belong to a chemical class of natural product derivatives, which showed promising antiplasmodial profile, including low propensity to cross-resistance, fast-acting inhibition, and an additive profile in combination with artesunate. Mode of action investigation indicates a brussonol-induced [Ca<sup>2+</sup>]<sub>cyt</sub> rise in *P. falciparum*, suggesting that the compound modulates the calcium homeostasis and parasite development. To the best of our knowledge, this is the first report on the antimalarial activity of the icetexane diterpenoid scaffold. Our findings indicated that the brussonol and analogs are new molecular scaffolds endowed with attractive antiplasmodial activities that justify the design of new derivatives with improved properties to deliver new lead candidates for malaria.

**Supplementary Materials:** The following supporting information can be downloaded at: <https://www.mdpi.com/article/10.3390/ph15070814/s1>, Experimental details on the synthesis of compounds 1–15. Figure S1: Hemozoin formation inhibition assay. NMR spectra of compounds 1–15. References [65–69] are cited in the supplementary materials.

15. Ahmad, A.; Burtoloso, A.C.B. Total Synthesis of (±)-Brussonol and (±)-Komaroviquinone via a Regioselective Cross-Electrophile Coupling of Aryl Bromides and Epoxides. *Org. Lett.* **2019**, *21*, 6079–6083. [[CrossRef](#)]
16. Maier, M.E.; Bayer, A. A Formal Total Synthesis of Salvadione. *Eur. J. Org. Chem.* **2006**, *17*, 4034–4043. [[CrossRef](#)]
17. Padwa, A.; Chughtai, M.J.; Boonsombat, J.; Rashatasakhon, P. A Rh(II)-Catalyzed Cycloaddition Approach toward the Synthesis of Komaroviquinone. *Tetrahedron* **2008**, *64*, 4758–4767. [[CrossRef](#)]
18. Stevens, R.V.; Bisacchi, G.S. Benzocyclobutenones as Synthons for the Synthesis of C-11 Oxygenated Diterpenoids. Application to the Total Synthesis of (±)-Taxodione. *J. Org. Chem.* **1982**, *47*, 2396–2399. [[CrossRef](#)]
19. della Ca', N.; Sassi, G.; Catellani, M. A Direct Palladium-Catalyzed Route to Selectively Substituted Carbazoles through Sequential C-C and C-N Bond Formation: Synthesis of Carbazomycin A. *Adv. Synth. Catal.* **2008**, *350*, 2179–2182. [[CrossRef](#)]
20. Zheng, Y.; Liu, Y.; Wang, Q. Collective Asymmetric Synthesis of (-)-Antofine, (-)-Cryptolepine, (-)-Tylophorine, and (-)-Tylocrebrine with Tert-Butanesulfonamide as a Chiral Auxiliary. *J. Org. Chem.* **2014**, *79*, 3348–3357. [[CrossRef](#)]
21. Martínez-Solorio, D.; Jennings, M.P. Convergent Formal Syntheses of (±)-Brussonol and (±)-Abrotanone via an Intramolecular Marsden-Type Cyclization. *Org. Lett.* **2009**, *11*, 189–192. [[CrossRef](#)]
22. Katsuno, K.; Burrows, J.N.; Duncan, K.; van Huijsduijnen, R.H.; Kaneko, T.; Kita, K.; Mowbray, C.E.; Schmatz, D.; Warner, P.; Slingsby, B.T. Hit and Lead Criteria in Drug Discovery for Infectious Diseases of the Developing World. *Nat. Rev. Drug Discov.* **2015**, *14*, 751–758. [[CrossRef](#)] [[PubMed](#)]
23. Chugh, M.; Scheurer, C.; Sax, S.; Bilsland, E.; van Schalkwyk, D.A.; Wicht, K.J.; Hofmann, N.; Sharma, A.; Bhashyam, S.; Singh, S.; et al. Identification and Deconvolution of Cross-Resistance Signals from Antimalarial Compounds Using Multidrug-Resistant Plasmodium Falciparum Strains. *Antimicrob. Agents Chemother.* **2015**, *59*, 1110–1118. [[CrossRef](#)] [[PubMed](#)]
24. Yusof, R.; Lau, Y.L.; Mahmud, R.; Fong, M.Y.; Jelip, J.; Ngian, H.U.; Mustakim, S.; Mat Hussin, H.; Marzuki, N.; Mohd Ali, M. High Proportion of Knowlesi Malaria in Recent Malaria Cases in Malaysia. *Malar. J.* **2014**, *13*, 163. [[CrossRef](#)] [[PubMed](#)]
25. Co, E.M.A.; Denuall, R.A.; Reinbold, D.D.; Waters, N.C.; Johnson, J.D. Assessment of Malaria in Vitro Drug Combination Screening and Mixed-Strain Infections Using the Malaria Sybr Green I-Based Fluorescence Assay. *Antimicrob. Agents Chemother.* **2009**, *53*, 2557–2563. [[CrossRef](#)] [[PubMed](#)]
26. Grabovsky, Y.; Tallarida, R.J. Isobolographic Analysis for Combinations of a Full and Partial Agonist: Curved Isooboles. *J. Pharmacol. Exp. Ther.* **2004**, *310*, 981–986. [[CrossRef](#)]
27. Macías-Alonso, M.; Andrés, L.S.; Córdova-Guerrero, I.; Estolano-Cobián, A.; Díaz-Rubio, L.; Marrero, J.G. Inhibition of Squalene Synthase of Rat Liver by Abietane Diterpenes Derivatives. *Nat. Prod. Res.* **2019**, *35*, 2972–2976. [[CrossRef](#)]
28. Cerqueira, N.M.F.S.A.; Oliveira, E.F.; Gesto, D.S.; Santos-Martins, D.; Moreira, C.; Moorthy, H.N.; Ramos, M.J.; Fernandes, P.A. Cholesterol Biosynthesis: A Mechanistic Overview. *Biochemistry* **2016**, *55*, 5483–5506. [[CrossRef](#)]
29. Guggisberg, A.M.; Anthor, R.E.; Odom, A.R. Isoprenoid Biosynthesis in Plasmodium Falciparum. *Eukaryot. Cell* **2014**, *13*, 1348–1359. [[CrossRef](#)]
30. Edwards, R.L.; Brothers, R.C.; Wang, X.; Maron, M.I.; Ziniel, P.D.; Tsang, P.S.; Kraft, T.E.; Hruz, P.W.; Williamson, K.C.; Dowd, C.S.; et al. MEPicides: Potent Antimalarial Prodrugs Targeting Isoprenoid Biosynthesis. *Sci. Rep.* **2017**, *7*, 8400. [[CrossRef](#)]
31. Yeh, E.; DeRisi, J.L. Chemical Rescue of Malaria Parasites Lacking an Apicoplast Defines Organelle Function in Blood-Stage Plasmodium Falciparum. *PLoS Biol.* **2011**, *9*, e1001138. [[CrossRef](#)]
32. Bowman, J.D.; Merino, E.E.; Brooks, C.F.; Striepen, B.; Carlier, P.R.; Cassera, M.B. Antiapicoplast and Gametocytocidal Screening to Identify the Mechanisms of Action of Compounds within the Malaria Box. *Antimicrob. Agents Chemother.* **2014**, *58*, 811–819. [[CrossRef](#)] [[PubMed](#)]
33. Wu, W.; Herrera, Z.; Ebert, D.; Baska, K.; Cho, S.H.; DeRisi, J.L.; Yeh, E. A Chemical Rescue Screen Identifies a Plasmodium Falciparum Apicoplast Inhibitor Targeting MEP Isoprenoid Precursor Biosynthesis. *Antimicrob. Agents Chemother.* **2015**, *59*, 356–364. [[CrossRef](#)] [[PubMed](#)]
34. Gisselberg, J.E.; Herrera, Z.; Orchard, L.M.; Llinás, M.; Yeh, E. Specific Inhibition of the Bifunctional Farnesyl/Geranylgeranyl Diphosphate Synthase in Malaria Parasites via a New Small-Molecule Binding Site. *Cell Chem. Biol.* **2018**, *25*, 185–193. [[CrossRef](#)] [[PubMed](#)]
35. Backman, T.W.H.; Cao, Y.; Girke, T. ChemMine Tools: An Online Service for Analyzing and Clustering Small Molecules. *Nucleic Acids Res.* **2011**, *39*, W486–W491. [[CrossRef](#)]
36. di Marino, D.; D'Annessa, I.; Coletta, A.; Via, A.; Tramontano, A. Characterization of the Differences in the Cyclopropanoic Acid Binding Mode to Mammalian and P. Falciparum Ca<sup>2+</sup> Pumps: A Computational Study. *Proteins Struct. Funct. Bioinform.* **2015**, *83*, 564–574. [[CrossRef](#)]
37. Arnou, B.; Montigny, C.; Morth, J.P.; Nissen, P.; Jaxel, C.; Møller, J.V.; le Maire, M. The Plasmodium Falciparum Ca<sup>2+</sup>-ATPase PfATP6: Insensitive to Artemisinin, but a Potential Drug Target. *Proc. Biochem. Soc. Trans.* **2011**, *39*, 823–831. [[CrossRef](#)]
38. Pandey, K.; Ferreira, P.E.; Ishikawa, T.; Nagai, T.; Kaneko, O.; Yahata, K. Ca<sup>2+</sup> Monitoring in Plasmodium Falciparum Using the Yellow Cameleon-Nano Biosensor. *Sci. Rep.* **2016**, *6*, 23454. [[CrossRef](#)]
39. Borges-Pereira, L.; Thomas, S.J.; dos Anjos e Silva, A.L.; Bartlett, P.J.; Thomas, A.P.; Garcia, C.R.S. The Genetic Ca<sup>2+</sup> Sensor GCaMP3 Reveals Multiple Ca<sup>2+</sup> Stores Differentially Coupled to Ca<sup>2+</sup> Entry in the Human Malaria Parasite Plasmodium Falciparum. *J. Biol. Chem.* **2020**, *295*, 14998–15012. [[CrossRef](#)]
40. Forte, B.; Otilie, S.; Plater, A.; Campo, B.; Decherer, K.J.; Gamo, F.J.; Goldberg, D.E.; Istvan, E.S.; Lee, M.; Lukens, A.K.; et al. Prioritization of Molecular Targets for Antimalarial Drug Discovery. *ACS Infect. Dis.* **2021**, *7*, 2764–2776. [[CrossRef](#)]

41. Ding, X.C.; Ubben, D.; Wells, T.N. A Framework for Assessing the Risk of Resistance for Anti-Malarials in Development. *Malar. J.* **2012**, *11*, 292. [[CrossRef](#)]
42. Burrows, J.N.; Leroy, D.; Lotharius, J.; Waterson, D. Challenges in Antimalarial Drug Discovery. *Future Med. Chem.* **2011**, *3*, 1401–1412. [[CrossRef](#)] [[PubMed](#)]
43. le Manach, C.; Paquet, T.; González Cabrera, D.; Younis, Y.; Taylor, D.; Wiesner, L.; Lawrence, N.; Schwager, S.; Waterson, D.; Witty, M.J.; et al. Medicinal Chemistry Optimization of Antiplasmodial Imidazopyridazine Hits from High Throughput Screening of a SoftFocus Kinase Library: Part 2. *J. Med. Chem.* **2014**, *57*, 8839–8848. [[CrossRef](#)] [[PubMed](#)]
44. Fouquier, J.; Guedj, M. Analysis of Drug Combinations: Current Methodological Landscape. *Pharmacol. Res. Perspect.* **2015**, *3*, e00149. [[CrossRef](#)] [[PubMed](#)]
45. van der Pluijm, R.W.; Amaratunga, C.; Dhorda, M.; Dondorp, A.M. Triple Artemisinin-Based Combination Therapies for Malaria—A New Paradigm? *Trends Parasitol.* **2021**, *37*, 15–24. [[CrossRef](#)]
46. Aguiar, A.C.C.; Panciera, M.; Simao Dos Santos, E.F.; Singh, M.K.; Garcia, M.L.; de Souza, G.E.; Nakabashi, M.; Costa, J.L.; Garcia, C.R.S.; Oliva, G.; et al. Discovery of Marinoquinolines as Potent and Fast-Acting Plasmodium Falciparum Inhibitors with in Vivo Activity. *J. Med. Chem.* **2018**, *61*, 5547–5568. [[CrossRef](#)] [[PubMed](#)]
47. de Souza, J.O.; Almeida, S.M.; Souza, G.E.; Zanini, C.L.; da Silva, E.M.; Calit, J.; Bargieri, D.Y.; Ampomdanai, K.; Antonyuk, S.; Hasnain, S.S.; et al. Parasitological Profiling Shows 4(1H)-Quinolone Derivatives as New Lead Candidates for Malaria. *Eur. J. Med. Chem. Rep.* **2021**, *3*, 100012. [[CrossRef](#)]
48. Parra, L.L.L.; Bertonha, A.F.; Severo, I.R.M.; Aguiar, A.C.C.; de Souza, G.E.; Oliva, G.; Guido, R.V.C.; Grazia, N.; Costa, T.R.; Miguel, D.C.; et al. Isolation, Derivative Synthesis, and Structure-Activity Relationships of Antiparasitic Bromopyrrole Alkaloids from the Marine Sponge *Tedania Brasiliensis*. *J. Nat. Prod.* **2018**, *81*, 188–202. [[CrossRef](#)]
49. de Souza, G.E.; Bueno, R.V.; de Souza, J.O.; Zanini, C.L.; Cruz, F.C.; Oliva, G.; Guido, R.V.C.; Aguiar, A.C.C. Antiplasmodial Profile of Selected Compounds from Malaria Box: In Vitro Evaluation, Speed of Action and Drug Combination Studies. *Malar. J.* **2019**, *18*, 447. [[CrossRef](#)]
50. Yang, T.; Otilie, S.; Istvan, E.S.; Godinez-Macias, K.P.; Lukens, A.K.; Baragaña, B.; Campo, B.; Walpole, C.; Niles, J.C.; Chibale, K.; et al. MalDA, Accelerating Malaria Drug Discovery. *Trends Parasitol.* **2021**, *37*, 493–507. [[CrossRef](#)]
51. de Oliveira, L.S.; Albohgetti, M.R.; Carneiro, R.G.; Bastos, I.M.D.; Amino, R.; Gréllier, P.; Charneau, S. Calcium in the Backstage of Malaria Parasite Biology. *Front. Cell. Infect. Microbiol.* **2021**, *11*, 708834. [[CrossRef](#)]
52. Moore, C.M.; Wang, J.; Lin, Q.; Ferreira, P.; Avery, M.A.; Elokel, K.; Staines, H.M.; Krishna, S. Selective Inhibition of Plasmodium Falciparum ATPase 6 by Artemisinins and Identification of New Classes of Inhibitors after Expression in Yeast. *Antimicrob. Agents Chemother.* **2022**, *66*, e0207921. [[CrossRef](#)] [[PubMed](#)]
53. Eckstein-Ludwig, U.; Webb, R.J.; van Goethem, I.D.A.; East, J.M.; Lee, A.G.; Kimura, M.; O'Neill, P.M.; Bray, P.G.; Ward, S.A.; Krishna, S. Artemisinins Target the SERCA of Plasmodium Falciparum. *Nature* **2003**, *424*, 957–961. [[CrossRef](#)] [[PubMed](#)]
54. Cardí, D.; Pozza, A.; Arnou, B.; Marchal, E.; Clausen, J.D.; Andersen, J.P.; Krishna, S.; Møller, J.V.; le Maire, M.; Jaxel, C. Purified E255L Mutant SERCA1a and Purified PfATP6 Are Sensitive to SERCA-Type Inhibitors but Insensitive to Artemisinins. *J. Biol. Chem.* **2010**, *285*, 26406–26416. [[CrossRef](#)]
55. Gazarini, M.L.; Sigolo, C.A.; Markus, R.P.; Thomas, A.P.; Garcia, C.R. Antimalarial Drugs Disrupt Ion Homeostasis in Malarial Parasites. *Mem. Inst. Oswaldo Cruz* **2007**, *102*, 329–334. [[CrossRef](#)] [[PubMed](#)]
56. Moraes Barros, R.R.; Gibson, T.J.; Kite, W.A.; Sá, J.M.; Welles, T.E. Comparison of Two Methods for Transformation of Plasmodium Knowlesi: Direct Schizont Electroporation and Spontaneous Plasmid Uptake from Plasmid-Loaded Red Blood Cells. *Mol. Biochem. Parasitol.* **2017**, *218*, 16–22. [[CrossRef](#)] [[PubMed](#)]
57. Trager, W.; Jensen, J.B. Human Malaria Parasites in Continuous Culture. *Science* **1976**, *193*, 673–675. [[CrossRef](#)]
58. Zeeman, A.-M.; Voorberg-van der Wel, A.; Kocken, C.H.M. Ex Vivo Culture of Plasmodium Vivax and Plasmodium Cynomolgi and In Vitro Culture of Plasmodium Knowlesi Blood Stages. *Methods Mol. Biol.* **2013**, *923*, 35–49. [[CrossRef](#)]
59. Lambros, C.; Vanderberg, J.P. Synchronization of Plasmodium Falciparum Erythrocytic Stages in Culture. *J. Parasitol.* **1979**, *65*, 418–420. [[CrossRef](#)]
60. Vossen, M.G.; Pferschy, S.; Chiba, P.; Noeld, H. The SYBR Green I Malaria Drug Sensitivity Assay: Performance in Low Parasitemia Samples. *Am. J. Trop. Med. Hyg.* **2010**, *82*, 398–401. [[CrossRef](#)]
61. Mosmann, T. Rapid Colorimetric Assay for Cellular Growth and Survival: Application to Proliferation and Cytotoxicity Assays. *J. Immunol. Methods* **1983**, *65*, 55–63. [[CrossRef](#)]
62. Moraes Barros, R.R.; Thawnashom, K.; Gibson, T.J.; Armistead, J.S.; Caleon, R.L.; Kaneko, M.; Kite, W.A.; Mershon, J.P.; Brockhurst, J.K.; Engels, T.; et al. Activity of Plasmodium Vivax Promoter Elements in Plasmodium Knowlesi, and a Centromere-Containing Plasmid That Expresses NanoLuc throughout the Parasite Life Cycle. *Malar. J.* **2021**, *20*, 247. [[CrossRef](#)] [[PubMed](#)]
63. ter Kuile, F.; White, N.J.; Holloway, P.; Pasvol, G.; Krishna, S. Plasmodium falciparum: In vitro studies of the pharmacodynamic properties of drugs used for the treatment of severe malaria. *Exp. Parasitol.* **1993**, *76*, 85–95. [[CrossRef](#)] [[PubMed](#)]
64. Fivelman, Q.L.; Adagu, I.S.; Warhurst, D.C. Modified Fixed-Ratio Isobologram Method for Studying in Vitro Interactions between Atovaquone and Proguanil or Dihydroartemisinin against Drug-Resistant Strains of Plasmodium Falciparum. *Antimicrob. Agents Chemother.* **2004**, *48*, 4097–4102. [[CrossRef](#)]
65. Williams, D.B.G.; Lawton, M. Drying of organic solvents: Quantitative evaluation of the efficiency of several desiccants. *J. Org. Chem.* **2010**, *75*, 8351–8354. [[CrossRef](#)]



66. Jiao, Z.W.; Tu, Y.Q.; Zhang, Q.; Liu, W.X.; Zhang, S.Y.; Wang, S.H.; Zhang, F.M.; Jiang, S. Tandem C-H oxidation/cyclization/rearrangement and its application to asymmetric syntheses of (-)-brussonol and (-)-przewalskine E. *Nat. Commun.* **2015**, *6*, 1–7. [[CrossRef](#)] [[PubMed](#)]
67. Majetich, G.; Zhang, Y.; Tian, X.; Britton, J.E.; Li, Y.; Phillips, R. Synthesis of (±)- and (+)-perovskone. *Tetrahedron* **2011**, *67*, 10129–10146. [[CrossRef](#)]
68. Fernandes, R.A.; Mulay, S.V.; Chavan, V.P. A concise total synthesis of arizonins B1 and C1. *Tetrahedron Asymmetry* **2013**, *24*, 1548–1555. [[CrossRef](#)]
69. Huy, N.T.; Uyen, D.T.; Maeda, A.; Trang, D.T.; Oida, T.; Harada, S.; Kamei, K. Simple colorimetric inhibition assay of heme crystallization for high-throughput screening of antimalarial compounds. *Antimicrob. Agents Chemother.* **2007**, *51*, 350–353. [[CrossRef](#)]

## Polyketide- and Terpenoid-Derived Metabolites Produced by a Marine-Derived Fungus, *Peroneutypa* sp.

Marcelo R. de Amorim,\* Camila de S. Barbosa, Tiago A. Paz, Laura P. Ióca, Karen J. Nicácio, Lucianne F. P. de Oliveira, Mirian O. Goulart, Julia M. Paulino, Mateus O. da Cruz, Antonio G. Ferreira, Maysa Furlan, Simone P. de Lira, Raquel A. dos Santos, André Rodrigues, Rafael V. C. Guido,\* and Roberto G. S. Berlinck\*

Cite This: *J. Nat. Prod.* 2023, 86, 1476–1486

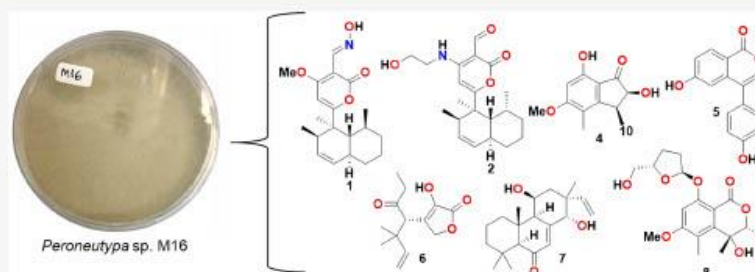
Read Online

ACCESS |

Metrics & More

Article Recommendations

Supporting Information



**ABSTRACT:** Bioassay-guided investigation of the EtOAc-soluble extract of a culture of the marine-derived fungus *Peroneutypa* sp. M16 led to the isolation of seven new polyketide- and terpenoid-derived metabolites (1, 2, 4–8), along with known polyketides (3, 9–13). Structures of compounds 1, 2, and 4–8 were established by analysis of spectroscopic data. Absolute configurations of compounds 1, 2, 4, 6, 7, and 8 were determined by the comparison of experimental ECD spectra with calculated CD data. Compound 5 exhibited moderate antiplasmodial activity against both chloroquine-sensitive and -resistant strains of *Plasmodium falciparum*.

Among fungi under intense chemical and biological scrutiny for the discovery of bioactive secondary metabolites, marine-derived<sup>1,2</sup> and endophytic<sup>3,4</sup> fungal strains stand out as some of the most prolific.<sup>5</sup>

In particular, the discovery of new metabolites with antiplasmodial activity is of much interest, because the available treatment alternatives for malaria are compromised due to the emergence of resistant strains of the *Plasmodium* spp. to clinical drugs, including artemisinin and chloroquine.<sup>6,7</sup> Malaria is now prevalent in 84 countries, with a high rate of mortality and morbidity.<sup>8</sup> In 2021, 247 million new cases and 619,000 deaths caused by malaria have been reported.<sup>8</sup> Four species of *Plasmodium* spp., *P. falciparum*, *P. vivax*, *P. ovale*, and *P. malariae*, are considered true parasites of humans. *P. falciparum* is the etiological agent of the most severe forms of malaria and causes 99% of deaths worldwide.<sup>8</sup> In Brazil, 99.5% of malaria infections are concentrated in the Amazon basin, an economically disfavored region.<sup>9</sup> Between 2019 and 2020, the number of malaria infections had increased 6% worldwide,<sup>9</sup> and there is a need for new antimalarial agents.

Fungi isolated from different environments have yielded metabolites with good antiplasmodial activity. Recent examples include fusaripeptide A,<sup>10</sup> analogues of the compound CJ-15,801,<sup>11</sup> cladospirin derivatives,<sup>12</sup> (–)-luteoskirine,<sup>13</sup> 9-methoxystrobilurine,<sup>14</sup> strasseriolide B,<sup>15</sup> N<sup>14</sup>-palmitolilcoprogen,<sup>16</sup> and diatreto.<sup>17</sup>

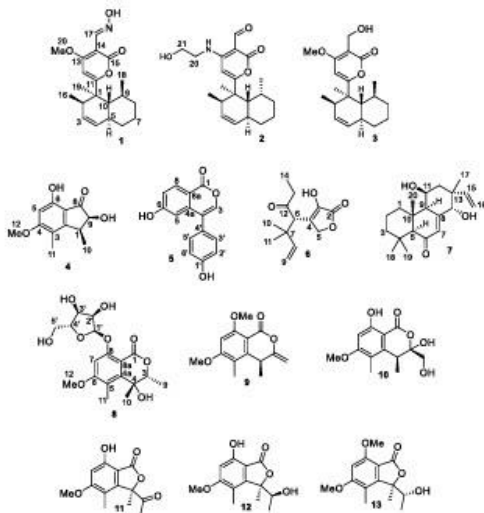
As part of our ongoing program on the discovery of marine-derived and endophytic bioactive metabolites, we isolated 27 fungal strains from the viscera of marine animals. After growth in artificial media, antiplasmodial screening of media organic extracts revealed a *Peroneutypa* sp. M16 strain, isolated from an unidentified sea cucumber, that yielded an EtOAc extract with attractive antiplasmodial activity. There are no reports in the literature on secondary metabolites produced in culture by

Received: March 3, 2023

Published: June 8, 2023



*Peroneutypa* spp. A large-scale cultivation of *Peroneutypa* sp. M16 in potato dextrose broth (PDB) prepared using artificial seawater, followed by bioassay-guided and UV-MS-guided investigation of the EtOAc extract, ultimately resulted in the isolation of seven new compounds (1, 2, 4–8) and six known (3, 9–13) polyketide-derived metabolites. Polyketide-derived 5 showed antiparasmodial activity at a low micromolar level against both sensitive and resistant strains of *P. falciparum*.



## RESULTS AND DISCUSSION

The EtOAc-soluble extract of cultures of *Peroneutypa* sp. M16 was fractionated by size-exclusion chromatography on Sephadex LH-20 (MeOH), to give 11 fractions, which were subjected to antiparasmodial screening. Fractions F2, F3, F4, F5, and F11 showed very good antiparasmodial inhibition (>90% inhibition at 50  $\mu\text{g/mL}$ ). Separation of fractions F4, F5, and F11 by semipreparative HPLC-UV led to the isolation of compounds 1, 2, and 4–8, along with solanapyrone M (3),<sup>18</sup> (+)-(*S*)-6,8-dimethoxy-4,5-dimethyl-3-methyleneisochroman-1-one (9),<sup>19,20</sup> (+)-(*3R,4S*)-3,8-dihydroxy-3-hydroxymethyl-6-methoxy-4,5-dimethylisochroman-1-one (10),<sup>21</sup> (+)-(*R*)-3-acetyl-7-hydroxy-5-methoxy-3,4-dimethyl-3*H*-isobenzofuran-1-one (11),<sup>22</sup> (–)-(*R*)-7-hydroxy-3-(*S*)-1-hydroxyethyl-5-methoxy-3,4-dimethylisobenzofuran-1(*3H*)-one (12),<sup>23</sup> and quadricinctone A (13).<sup>24</sup>

Solanapyrone S (1) was isolated as a white amorphous optically active solid, with  $[\alpha]_D^{25} -173$  (c 0.1, MeOH). Its molecular formula was established as  $\text{C}_{20}\text{H}_{27}\text{NO}_4$  by HRMS, which, along with NMR data (Table 1), indicated eight indexes of hydrogen deficiency. Its UV spectrum exhibited absorption maxima at  $\lambda_{\text{max}}$  215, 245, and 333 nm, while its IR spectrum presented absorptions bands at 3249 ( $\nu_{\text{O-H}}$ ), 2915 ( $\nu_{\text{C-H}}$  aliphatic), 1720 ( $\nu_{\text{C=O}}$  conjugated lactone), and 1600 ( $\nu_{\text{C=C}}$ )  $\text{cm}^{-1}$ , which indicated the presence of hydroxy, carbonyl, and double-bond functional groups. Analysis of 2D NMR data of 1 identified the presence of the decalin and of the  $\alpha$ -pyran moieties, with  $^1\text{H}$  and  $^{13}\text{C}$  chemical shifts very similar to those of solanapyrones J and M (Table S1).<sup>18</sup> The

**Table 1.**  $^1\text{H}$  (600 MHz) and  $^{13}\text{C}$  (150 MHz) Data of Compounds 1 and 2 in  $\text{MeOH-}d_4$

no.	1		2	
	$\delta_{\text{C}}$ , type	$\delta_{\text{H}}$ , mult. ( <i>J</i> in Hz)	$\delta_{\text{C}}$ , type	$\delta_{\text{H}}$ , mult. ( <i>J</i> in Hz)
1	46.2, C		46.2, C	
2	46.7, CH	2.00, m	46.6, CH	1.97, m
3	131.0, CH	5.56, ddd (10.0, 4.7, 2.4)	130.9, CH	5.56, ddd (10.0, 4.7, 2.4)
4	130.5, CH	5.40, dd (10.0, 1.6)	130.5, CH	5.39, dt (10.0, 1.5)
5	41.9, CH	1.88, m	41.8, CH	1.86, m
6	35.6, $\text{CH}_2$	1.27, m; 1.86, m	35.6, $\text{CH}_2$	1.26, m; 1.85, m
7	28.2, $\text{CH}_2$	1.50, m; 1.79, m	28.2, $\text{CH}_2$	1.49, m; 1.79, m
8	39.1, $\text{CH}_2$	1.31, m; 1.69, m	39.1, $\text{CH}_2$	1.32, m; 1.69, m
9	38.0, CH	1.50, m	38.2, CH	1.49, m
10	45.8, CH	1.91, t (9.7)	45.5, CH	1.89, t (9.3)
11	177.3, C		179.0, C	
12	94.9, CH	6.63, s	94.7, CH	6.42, s
13	171.7, C		162.4, C	
14	98.1, C		95.8, C	
15	163.2, C		166.1, C	
16	20.3, $\text{CH}_3$	0.84, d (7.1)	20.3, $\text{CH}_3$	0.90, d (7.1)
17	143.6, CH	8.14, s	191.6, CH	9.91, br s
18	21.2, $\text{CH}_3$	0.65, d (6.9)	21.0, $\text{CH}_3$	0.77, d (6.9)
19	18.9, $\text{CH}_3$	1.38, s	19.0, $\text{CH}_3$	1.35, s
20	58.1, $\text{CH}_3$	4.06, s	46.2, $\text{CH}_2$	3.58, dt (5.2, 1.0)
21			61.4, $\text{CH}_2$	3.76, t (5.2)
OH <sup>a</sup>		11.11, s		

<sup>a</sup>Observed in the spectrum recorded in  $\text{DMSO-}d_6$ .

UV bands were also similar to those of solanapyrone M.<sup>18</sup> The difference is the presence of an oxime group positioned at C-17 in 1, confirmed by HMBC correlations from the methine CH-17 ( $\delta_{\text{H}}$  8.14) to C-13 ( $\delta_{\text{C}}$  171.7), C-14 ( $\delta_{\text{C}}$  98.1), and C-15 ( $\delta_{\text{C}}$  163.2) (Figure 1), indicating a new solanapyrone member. The

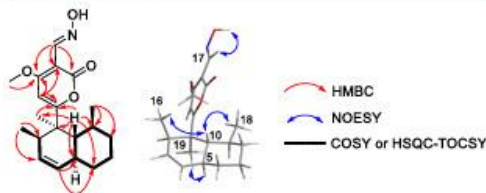


**Figure 1.** Selected HMBC (→), COSY and HSQC-TOCSY (—) correlations, and NOESY (↔) interactions of 1.

oxime functionality was justified by considering the even  $[\text{M} + \text{H}]^+$  ion as the only possible nitrogen-bearing functional group to include a nitrogen atom in 1. Of note, solanapyrones O and P present an ethylenamine moiety attached to the same carbon (C-17) substituted by the enamine group in compound 1.<sup>25</sup>

The relative configuration of 1 was established by analysis of the NOESY spectrum (Figure 1). NOEs observed between H-10 and  $\text{CH}_3$ -16 and  $\text{CH}_3$ -18 indicated pseudoaxial orientations for  $\text{CH}_3$ -16 and H-10 and a pseudoequatorial orientation for  $\text{CH}_3$ -18. The coupling constant of H-10 (t, 9.7 Hz) with both H-5 and H-9 $\alpha$  confirmed that H-5 had a *trans*-diaxial orientation with H-10. The NOE of H-5 with  $\text{CH}_3$ -19 established the orientation of  $\text{CH}_3$ -19 as pseudoaxial on the same side of H-5. In order to establish the oxime geometry, NMR data for 1 were reacquired in  $\text{DMSO-}d_6$ . The oxime

group hydrogen was observed at  $\delta_{\text{H}}$  11.11. A NOE interaction of H-17 ( $\delta_{\text{H}}$  7.95 in DMSO- $d_6$ ) with the oxime hydroxy hydrogen established the geometry of the oxime as *E*. The absolute configuration of **1** was determined by a comparative analysis of experimental and simulated electronic circular dichroism (ECD) spectra. As shown in Figure 2, the

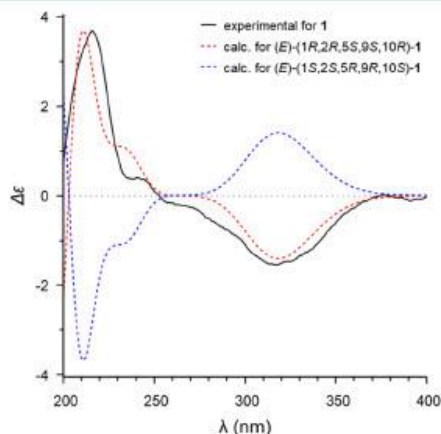


Figure 2. Experimental and calculated ECD curves for compound 1.

Boltzmann-averaged ECD spectrum of (*E*)-(1*R*,2*R*,5*S*,9*S*,10*R*)-**1** matched very well with the experimental spectrum, with a positive Cotton effect at ca. 215 and 250 nm and a negative Cotton effect around 263 and 330 nm. This result unambiguously defined the absolute configuration of **1** as (*E*)-(1*R*,2*R*,5*S*,9*S*,10*R*). Compound **1** was named (–)-(*E*)-(1*R*,2*R*,5*S*,9*S*,10*R*)-solanapyrone **S**.

Solanapyrone **T** (**2**) was isolated as a white amorphous optically active solid, with  $[\alpha]_{\text{D}}^{23}$  –37 (*c* 0.1; MeOH). Its molecular formula was established as  $\text{C}_{21}\text{H}_{29}\text{NO}_4$  by HRMS, which, along with NMR data, indicated eight indexes of hydrogen deficiency. Its UV spectrum exhibited absorption maxima at  $\lambda_{\text{max}}$  237, 283, and 315 nm similar to **1**, while its IR spectrum presented absorptions bands at 3397 ( $\nu_{\text{O-H}}$ ), 3184 ( $\nu_{\text{C-H}}$  vinylic), 2922 ( $\nu_{\text{C-H}}$  aliphatic), 1643 ( $\nu_{\text{C=O}}$  conjugated lactone,  $\beta$ -*N*-substituted and/or conjugated  $\beta$ -*N*-substituted aldehyde carbonyl), 1634 ( $\nu_{\text{C=C}}$  O-substituted), and 1593 ( $\nu_{\text{C=C}}$  conjugated, *N*-substituted)  $\text{cm}^{-1}$ . The  $\text{C}=\text{O}$  band in **1** (1720  $\text{cm}^{-1}$ ) is observed at 1643  $\text{cm}^{-1}$  in **2** probably due to the delocalization of the nitrogen electron pair toward the lactone carbonyl.

Analysis of the NMR data of **2** allowed identifying characteristic  $^1\text{H}$  and  $^{13}\text{C}$  signals very similar to those of **1** and **3** (Table 1 and Table S1), the difference being the replacement of the methoxy at C-13 and the oxime at C-14 in **1** by an ethanolamine group ( $\delta_{\text{H},20}$  3.58,  $\delta_{\text{C},20}$  46.2;  $\delta_{\text{H},21}$  3.76,  $\delta_{\text{C},21}$  61.4) and an aldehyde functionality ( $\delta_{\text{H},17}$  9.91,  $\delta_{\text{C},17}$  191.6), respectively. These assignments were confirmed by observation of HMBC correlations from H<sub>2</sub>-20 to C-13 ( $\delta_{\text{C}}$  162.4) and from H-17 to C-13 and C-14 ( $\delta_{\text{C}}$  95.8) (Figure 3).

NOE interactions between H<sub>3</sub>-16 and H-10 and of H<sub>3</sub>-19 with H-5 and H<sub>3</sub>-18 indicated the orientation of CH<sub>3</sub>-18, H-5, and CH<sub>3</sub>-19 as pseudoaxial on the same side, while pseudoaxial orientations for CH<sub>3</sub>-16 and H-10 were on the opposite side

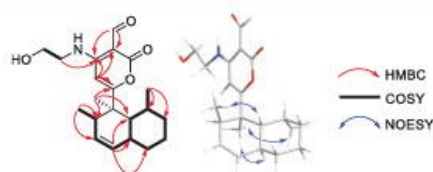


Figure 3. Key HMBC (→) and COSY (—) correlations, and NOESY (↔) interactions of **2**.

(Figure 3). The coupling constant of  $J_{\text{H-5/H-10}}$  (9.7 Hz) confirmed that H-5 had a *trans*-diaxial orientation with H-10. The Boltzmann-averaged ECD spectrum of (1*R*,2*R*,5*S*,9*R*,10*R*)-**2** matched very well with the experimental spectrum, with a positive Cotton effect around 205, 241, and 279 nm and a negative Cotton effect around 313 nm (Figure 4). This result unambiguously defined the absolute configuration of **2** as (1*R*,2*R*,5*S*,9*R*,10*R*), named as (–)-(1*R*,2*R*,5*S*,9*R*,10*R*)-solanapyrone **T**.

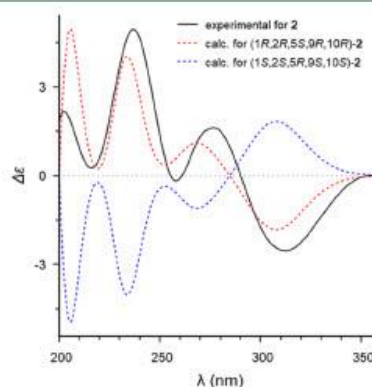


Figure 4. Experimental and calculated ECD curves of compound **2**.

Isolation of solanapyrone **M** (**3**) from the same culture of *Peroneutypa* sp. M16, identified by comparison with literature data,<sup>18</sup> further corroborated the isolation and identification of the new solanapyrones **S** (**1**) and **T** (**2**).

Compound **4** was obtained as an optically active yellowish oil, with  $[\alpha]_{\text{D}}^{23}$  +14 (*c* 0.05; MeOH). Its molecular formula was established as  $\text{C}_{12}\text{H}_{14}\text{O}_4$  by HRMS, corresponding to six indexes of hydrogen deficiency. Its UV spectrum exhibited absorption maxima at  $\lambda_{\text{max}}$  275 and 320 nm, suggesting the presence of an aromatic moiety, while the IR spectrum exhibited bands at 3304 ( $\nu_{\text{O-H}}$ ), 2941 ( $\nu_{\text{C-H}}$  aliphatic), 1686 ( $\nu_{\text{C=O}}$  conjugated), and 1601 ( $\nu_{\text{C=C}}$  aromatic)  $\text{cm}^{-1}$ . Analysis of its  $^1\text{H}$ ,  $^{13}\text{C}$ , and HSQC NMR data, along with the number of hydrogen deficiency, indicated an  $\text{sp}^2$  methine at  $\delta_{\text{H}}$  6.32 ( $\delta_{\text{C}}$  96.8, CH-5) included in a pentasubstituted benzene moiety, in addition to methyl groups at  $\delta_{\text{H}}$  1.16 ( $\delta_{\text{C}}$  15.4, CH<sub>3</sub>-10),  $\delta_{\text{H}}$  2.11 ( $\delta_{\text{C}}$  10.5, CH<sub>3</sub>-11), and  $\delta_{\text{H}}$  3.88 ( $\delta_{\text{C}}$  56.1, CH<sub>3</sub>-12) and a methine group at  $\delta_{\text{H}}$  4.54 ( $\delta_{\text{C}}$  76.2, CH-9) (Table 2). HMBC correlations from the methoxy at  $\delta_{\text{H}}$  3.88 (OCH<sub>3</sub>-12) to C-4 ( $\delta_{\text{C}}$  166.5) and from the methyl group at  $\delta_{\text{H}}$  2.11 (CH<sub>3</sub>-11) to C-4 and C-2 ( $\delta_{\text{C}}$  155.0) allowed connecting both methoxy and

Table 2.  $^1\text{H}$  (600 MHz) and  $^{13}\text{C}$  (150 MHz) NMR Data for 4 in  $\text{CDCl}_3$

no.	$\delta_{\text{C}}$ , type	$\delta_{\text{H}}$ , mult. ( $J$ in Hz)
1	37.8, CH	3.63, qui (7.2)
2	155.0, C	
3	115.3, C	
4	166.5, C	
5	96.8, CH	6.32, s
6	157.4, C	
7	111.2, C	
8	205.3, C	
9	76.2, CH	4.54, d (7.2)
10	15.4, $\text{CH}_3$	1.16, d (7.2)
11	10.5, $\text{CH}_3$	2.11, s
12	56.1, $\text{CH}_3$	3.88, s

methyl groups to the aromatic C-4 and C-3 ( $\delta_{\text{C}}$  115.3), respectively (Figure 5). The COSY spectrum showed the

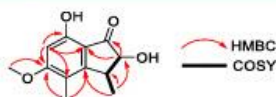


Figure 5. Key HMBC (→) and COSY (—) correlations of 4.

presence of a spin system comprising a  $-(\text{CH}_3-10)-(\text{CH}-1)-(\text{CH}-9)-$  moiety. Methine CH-9 ( $\delta_{\text{H}}$  4.54;  $\delta_{\text{C}}$  76.2) was assigned as oxygenated based on its chemical shift. Key HMBC correlations observed between H-5, H-1 ( $\delta_{\text{H}}$  3.63), and H-9 and the keto carbonyl group (C-8,  $\delta_{\text{C}}$  205.3), as well as HMBC correlations between  $\text{CH}_3-10$  ( $\delta_{\text{H}}$  1.16) and H-1 and C-2, allowed the connection of CH-1 to C-2, while CH-9 was connected to C-8. The connection of the keto carbonyl group at C-8 to C-7 ( $\delta_{\text{C}}$  111.2) was necessary to close the five-membered ring, in agreement with the molecular formula and with the HMBC correlation of H-9 with C-7. The remaining hydroxy group was attached to C-6 ( $\delta_{\text{C}}$  157.4). Positioning of the C-8 carbonyl group was consistent with the IR absorption at  $1686\text{ cm}^{-1}$  for a conjugated  $\text{C}=\text{O}$  group, even though its  $^{13}\text{C}$  NMR chemical shift ( $\delta_{\text{C}}$  205.3) was unusually high, probably due to its position in a strained five-membered ring.

The H-1–H-9 coupling constant ( $J = 7.2\text{ Hz}$ ) suggested an axial–equatorial orientation. The absolute configuration of 4 was determined by a comparative analysis of its experimental and simulated ECD spectra for all its possible stereoisomers. Calculations were performed to obtain the Boltzmann-average ECD spectrum for 4 to compare with the experimental ECD spectrum (Figure 6). Positive Cotton effects around 230 and 265 nm and a negative Cotton effect at around 310 nm allowed the unambiguous assignment of the absolute configuration of 4 as (1*S*,9*S*) (Figure 6), named as (+)-(1*S*,9*S*)-peroneutone.

Compound 5 was isolated as a white amorphous solid. HRMS analysis revealed the molecular formula  $\text{C}_{15}\text{H}_{10}\text{O}_4$ , corresponding to 11 hydrogen deficiency indexes. The UV spectrum exhibited absorption maxima at  $\lambda_{\text{max}}$  249 and 300 nm, typically aromatic, while the IR spectrum exhibited absorption bands at  $3294\text{ cm}^{-1}$  ( $\nu_{\text{O-H}}$ ),  $1674\text{ cm}^{-1}$  ( $\nu_{\text{C=O}}$  conjugated), and  $1585\text{ cm}^{-1}$  ( $\nu_{\text{C=C}}$  conjugated). Its  $^1\text{H}$  NMR spectrum exhibited signals at  $\delta_{\text{H}}$  6.80 (2H, dd 8.6 and 2.5 Hz, H-2' and H-6') and  $\delta_{\text{H}}$  7.37 (2H, dd 8.6 and 2.5 Hz, H-3' and H-5'), characteristic of a *para*-disubstituted benzene moiety (Table

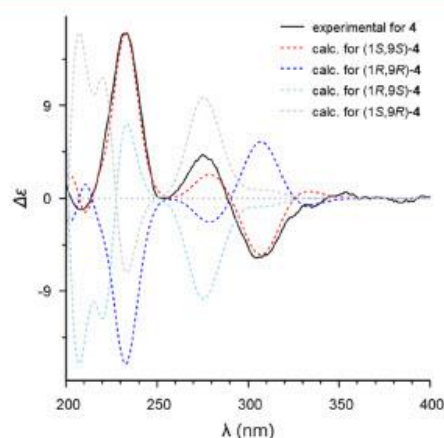


Figure 6. Experimental and calculated ECD curves of compound 4.

3). In addition, the  $^1\text{H}$  NMR spectrum exhibited hydrogens attached to another aromatic portion, with  $^1\text{H}$  signals at  $\delta_{\text{H}}$

Table 3.  $^1\text{H}$  (600 MHz) and  $^{13}\text{C}$  (150 MHz) NMR Data for 5 in  $\text{DMSO}-d_6$ <sup>a</sup>

no.	$\delta_{\text{C}}$ , type	$\delta_{\text{H}}$ , mult. ( $J$ in Hz)
1	174.7, C	
3	152.7, CH	8.27, s
4	123.4, C	
4a	157.4, C	
5	102.0, CH	6.85, d (2.2)
6	162.8, C	
7	115.2, CH	6.92, dd (8.8, 2.2)
8	127.2, CH	7.95, d (8.8)
8a	116.4, C	
1'	157.1, C	
2'	115.0, CH	6.80, dd (8.6, 2.5)
3'	130.0, CH	7.37, dd (8.6, 2.5)
4'	122.5, C	
5'	130.0, CH	7.37, dd (8.6, 2.5)
6'	115.0, CH	6.80, dd (8.6, 2.5)

<sup>a</sup>Signals observed at  $\delta$  165.3 ( $^{13}\text{C}$ ) and  $\delta$  8.34 ( $^1\text{H}$ ) are assigned to formic acid, used in purification of 5.

6.86 (d 2.2 Hz, H-5),  $\delta_{\text{H}}$  6.92 (dd 8.8 and 2.2 Hz, H-7), and  $\delta_{\text{H}}$  7.95 (d 8.8 Hz, H-8) and of an olefinic hydrogen signal at  $\delta_{\text{H}}$  8.27 (s, H-3). Taken together with the analysis of the  $^{13}\text{C}$  NMR information (Table 3), these data indicated a substituted isocoumarin moiety.<sup>26</sup> The vinyl methine CH-3 exhibited HMBC cross peaks to C-4a and C-1, the aromatic methine CH-8 exhibited HMBC correlations to C-1, and the aromatic methine CH-5 exhibited HMBC cross peaks to C-8a and C-4a, corresponding to an isocoumarin substituted at C-4 and a lactone carbonyl attached to C-8a (Figure 7). The connectivity of the *para*-disubstituted benzene portion at C-4 was confirmed by HMBC correlations observed from H-5' and H-3' to C-4, as well as HMBC correlations from H-3 to C-4 and C-4'. Thus, compound 5 was identified as 6-hydroxy-4-(4-hydroxyphenyl)-1*H*-isochromen-1-one.

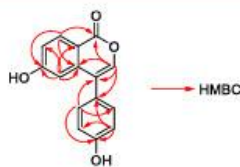


Figure 7. Key HMBC (→) correlations of 5.

Compound 6 was obtained as an optically active colorless oil, with  $[\alpha]_D^{23} +38.6$  ( $c$  0.1, MeOH). HRMS analysis indicated the molecular formula  $C_{13}H_{18}O_4$ , corresponding to five indexes of hydrogen deficiency. The UV spectrum exhibited absorption maxima at  $\lambda_{max}$  247, 279, and 319 nm of a conjugated system. Its IR spectrum exhibited bands at 3333 ( $\nu_{O-H}$ ), 2980 ( $\nu_{C-H}$ ), 1765, and 1699  $cm^{-1}$ , the last two assigned to the enol lactone after structure identification.  $^1H$  and COSY NMR data of 6 showed the presence of two spin systems, an ethyl group ( $CH_3$ -14 and  $CH_2$ -13) and a  $-CH-CH_2-$  moiety (Table 4

Table 4.  $^1H$  (600 MHz) and  $^{13}C$  NMR (150 MHz) Data of 6 in MeOH- $d_4$ 

no.	$\delta_C$ , type	$\delta_H$ , mult. (J in Hz)
2	171.6, C	
3	142.0, C	
4	127.9, C	
5	71.1, $CH_2$	4.58, d (16.8); 4.91, dd (16.8, 0.5)
6	58.9, CH	4.09, s
7	42.8, C	
8	146.6, CH	6.09, dd (17.4, 10.8)
9	113.4, $CH_2$	5.01, dd (17.4, 1.2); 5.03, dd (10.8, 1.2)
10	27.2, $CH_3$	1.12, s
11	24.9, $CH_3$	1.13, s
12	211.6, C	
13	40.1, $CH_2$	2.54, dq (18.5, 7.1); 2.64, dq (18.5, 7.1)
14	7.7, $CH_3$	0.98, t (7.1)

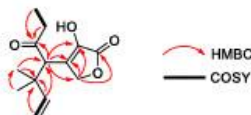


Figure 8. Key HMBC (→) and COSY (—) correlations of 6.

and Figure 8). HMBC correlations for  $CH_6$  ( $\delta_H$  4.09),  $CH_2$ -13 ( $\delta_H$  2.54 and 2.64), and  $CH_3$ -14 ( $\delta_H$  0.98) to C-12 ( $\delta_C$  211.6) indicated a propionyl group substituent at C-6. HMBC correlations of the  $sp^2$  methylene  $CH_2$ -9 to C-7 ( $\delta_C$  42.8), of the methine  $CH$ -8 to C-6 ( $\delta_C$  58.9), C-7, C-10 ( $\delta_C$  27.2), and C-11 ( $\delta_C$  24.9), and from the methyl groups  $CH_3$ -10 and  $CH_3$ -11 to C-7 and C-6 positioned the  $CH_2=CH-C-(CH_3)_2$  moiety. HMBC correlations from H-6 to C-3 and C-4 and from H-5 to C-2, C-3, and C-4 established the presence of a 3-hydroxyfuran-2(*5H*)-one moiety attached at C-6.

The absolute configuration at C-6 was determined by comparison of experimental and simulated ECD spectra. Calculations were performed to obtain the Boltzmann-average ECD spectrum for (*S*)-6 and (*R*)-6 and comparison with the

experimental ECD spectrum (Figure 9). The negative Cotton effect at ca. 240 nm and a positive Cotton effect between 275

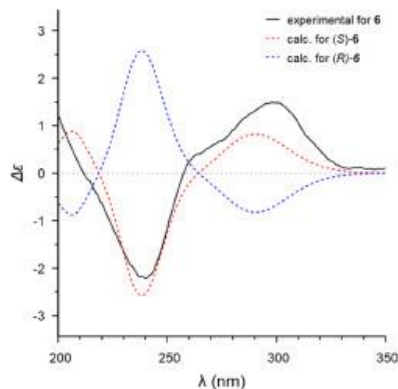


Figure 9. Experimental and calculated ECD curves of compound 6.

and 300 nm defined the absolute configuration of 6 as *S*, named as (+)-(*S*)-perofuranone, a hybrid diisoprenyl-propionate-derived metabolite.

Diterpenoid 7 was obtained as a white optically active compound, with  $[\alpha]_D^{23} +16.5$  ( $c$  0.08; MeOH). It displayed the molecular formula  $C_{20}H_{30}O_3$  by HRMS with six indexes of hydrogen deficiency. The UV spectrum presented absorption maxima at  $\lambda_{max}$  247 and 305 nm of an  $\alpha,\beta$ -conjugated keto carbonyl group. The IR spectrum exhibited bands at 3408 ( $\nu_{O-H}$ ) and 1676 ( $\nu_{C=O}$  conjugated)  $cm^{-1}$ .  $^1H$  and  $^{13}C$  NMR data exhibited signals typically observed for a diterpenoid skeleton (Table 5).<sup>27,28</sup> HMBC correlations of the two methyl groups,  $CH_3$ -18 ( $\delta_H$  1.11) and  $CH_3$ -19 ( $\delta_H$  1.17), to C-3 ( $\delta_C$  44.4), C-4 ( $\delta_C$  33.5), and C-5 ( $\delta_C$  66.7) confirmed their

Table 5.  $^1H$  (600 MHz) and  $^{13}C$  (150 MHz) NMR Data of 7 in MeOH- $d_4$ 

no.	$\delta_C$ , type	$\delta_H$ , mult. (J in Hz)
1	39.9, $CH_2$	1.34, m; 1.94, m
2	19.2, $CH_2$	1.69, m; 1.50, m
3	44.4, $CH_2$	1.38, m; 1.22, m
4	33.5, C	
5	66.7, CH	2.08, s
6	203.7, C	
7	125.8, CH	6.16, t (2.6)
8	165.4, C	
9	57.7, CH	2.47, m
10	45.5, C	
11	64.9, CH	4.31, m
12	46.5, $CH_2$	2.22, dd (15.1, 5.3); 1.75, ddd (15.1, 2.1, 1.0)
13	41.1, C	
14	75.3, CH	4.82, t (2.0)
15	145.1, CH	5.93, dd (17.9, 10.9)
16	113.5, $CH_2$	
17	28.8, $CH_3$	1.24, s
18	34.3, $CH_3$	1.11, s
19	22.2, $CH_3$	1.17, s
20	16.8, $CH_3$	1.14, s

position at C-4. The methyl group CH<sub>3</sub>-20 ( $\delta_{\text{H}}$  1.14) showed HMBC cross peaks to C-1 ( $\delta_{\text{C}}$  39.9), C-9 ( $\delta_{\text{C}}$  57.7), and C-10 ( $\delta_{\text{C}}$  45.5) and was attached to C-10 (Figure 10). The methyl

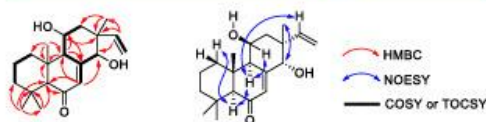


Figure 10. Selected HMBC ( $\rightarrow$ ), COSY or TOCSY ( $\longrightarrow$ ) correlations, and NOESY ( $\leftrightarrow$ ) interactions of 7.

group CH<sub>3</sub>-17 ( $\delta_{\text{H}}$  1.24) was positioned at C-13 ( $\delta_{\text{C}}$  41.1) since it displayed HMBC cross peaks with C-12 ( $\delta_{\text{C}}$  46.5), C-13, C-14 ( $\delta_{\text{C}}$  75.3), and C-15 ( $\delta_{\text{C}}$  145.1). The vinyl group was positioned at C-13 since it showed HMBC correlations from the methine group CH-15 ( $\delta_{\text{H}}$  5.95) to C-17 ( $\delta_{\text{C}}$  28.8), C-12, C-13, and C-14 and between the methylene CH<sub>2</sub>-16 ( $\delta_{\text{H}}$  5.02 and 5.09) and C-13 and C-15. Key HMBC correlations were observed for CH-5 ( $\delta_{\text{H}}$  2.08) with C-6 ( $\delta_{\text{C}}$  203.7) and for the methine CH-7 ( $\delta_{\text{H}}$  6.16) with C-5, C-9, and C-14, which confirmed the ketone carbonyl at C-6 and the unsaturation at C-7/C-8. The sp<sup>2</sup> C-8 ( $\delta_{\text{C}}$  165.4) was positioned by observing HMBC correlations from CH-11 ( $\delta_{\text{H}}$  4.31) and CH-9 ( $\delta_{\text{H}}$  2.47) to C-8. Analysis of COSY and TOCSY data confirmed the spin systems of 7, including allylic couplings of H-7 with H-9 and H-14.

The NOESY spectrum showed cross peaks of H-9 with H-1 $\alpha$ , H-5, H-11, and H-15, between H-14 and H<sub>3</sub>-17, and of H-5 with H-9, H-18, H-1 $\alpha$ , H-2 $\alpha$ , and H-3 $\alpha$ , placing H-5, H-9, H-11, and H-15 on the same side of the molecule, while H-14, H<sub>3</sub>-17, and H<sub>3</sub>-20 were on the opposite face of 7 (Figure 10). The absolute configuration of 7 was determined by a comparative analysis of its experimental and simulated ECD spectra. The Boltzmann-averaged ECD spectrum for (5*S*,9*R*,10*R*,11*S*,13*R*,14*S*)-7 matched very well with the experimental ECD spectrum (Figure 11), with a negative Cotton effect at 215 nm and a positive Cotton effect at 245

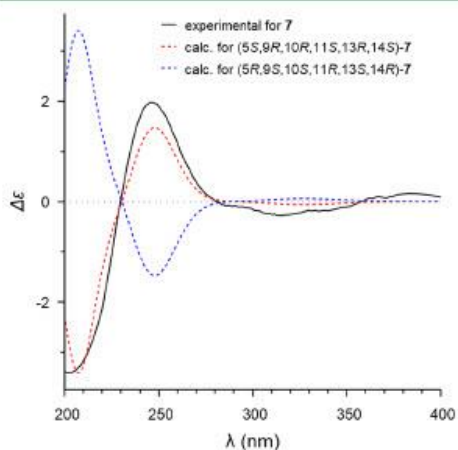


Figure 11. Experimental and calculated ECD curves of compound 7.

nm. The ECD analysis defined the absolute configuration of 7 as (5*S*,9*R*,10*R*,11*S*,13*R*,14*S*), named as (+)-(5*S*,9*R*,10*R*,11*S*,13*R*,14*S*)-peronepene.

Compound 8 was obtained as an optically active colorless oil, with  $[\alpha]_{\text{D}}^{25} +29$  (*c* 0.1; MeOH). Its molecular formula was established as C<sub>18</sub>H<sub>24</sub>O<sub>9</sub> by HRMS and NMR data, corresponding to seven indexes of hydrogen deficiency. Its UV spectrum exhibited absorption maxima at  $\lambda_{\text{max}}$  223, 259, and 291 nm, and the IR spectrum exhibited bands at 3381, 2926, and 1719 cm<sup>-1</sup>. Analysis of its <sup>1</sup>H, <sup>13</sup>C, and HSQC NMR data indicated an sp<sup>2</sup> methine at  $\delta_{\text{H}}$  6.93 ( $\delta_{\text{C}}$  100.8, CH-7) included in a pentasubstituted benzene moiety. Additional <sup>1</sup>H and <sup>13</sup>C signals for methoxy, methyl, methylene, and methine groups were also observed (Table 6). HMBC correlations of

Table 6. <sup>1</sup>H (600 MHz) and <sup>13</sup>C (150 MHz) NMR Data of 8 in MeOH-*d*<sub>4</sub>

no.	$\delta_{\text{C}}$ , type	$\delta_{\text{H}}$ , mult. ( <i>f</i> in Hz)
1	171.2, C	
3	71.2, CH	4.24, q (64)
4	91.4, C	
4a	153.8, C	
5	115.6, C	
6	166.4, C	
7	100.8, CH	6.93, s
8	157.0, C	
8a	108.6, C	
9	17.5, CH <sub>3</sub>	0.85, d (64)
10	21.6, CH <sub>3</sub>	1.75, s
11	11.8, CH <sub>3</sub>	2.19, s
12	57.2, CH <sub>3</sub>	3.95, s
1'	103.6, CH	5.90, d (4.2)
2'	74.1, CH	4.23, dd (6.4, 4.2)
3'	71.8, CH	4.07, dd (6.4, 2.2)
4'	89.3, CH	4.20, ddd (4.1, 3.7, 2.2)
5'	63.3, CH <sub>2</sub>	3.65, dd (12.0, 4.1); 3.68, dd (12.0, 3.7)

the methoxy group at  $\delta_{\text{H}}$  3.95 (OCH<sub>3</sub>-12) with C-6 ( $\delta_{\text{C}}$  166.4) and of the methyl group at  $\delta_{\text{H}}$  2.19 ( $\delta_{\text{C}}$  11.8, CH<sub>3</sub>-11) with C-6, C-5 ( $\delta_{\text{C}}$  115.6), and C-4a ( $\delta_{\text{C}}$  153.8) allowed the placement of both methoxy and methyl groups at C-6 and C-5, respectively (Figure 12). The COSY spectrum showed the

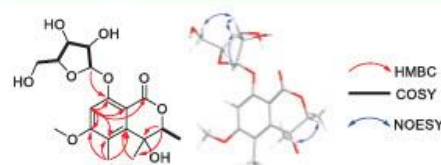


Figure 12. Selected HMBC ( $\rightarrow$ ) and COSY ( $\longrightarrow$ ) correlations and NOESY ( $\leftrightarrow$ ) interactions of 8.

presence of two spin systems present in the structure of 8: -CH<sub>3</sub>-CH- and -CH(O)-CH(O)-CH(O)-CH(O)-CH<sub>2</sub>(O)- moieties. The latter spin system established a ribofuranosyloxy unit that was placed at C-8 by observing an HMBC correlation from H-1' ( $\delta_{\text{H}}$  5.90) to C-8 (Figure 12). Key HMBC correlations between H-7 and the lactone carbonyl group (C-1,  $\delta_{\text{C}}$  171.2), as well as HMBC correlations of H<sub>3</sub>-11 and H<sub>3</sub>-10 ( $\delta_{\text{H}}$  1.75) to C-4a, together with HMBC

correlations from H-3 to C-4 and C-10 ( $\delta_C$  21.6), supported the connection of C-4 and C-4a and from C-1 to C-8 and that C-4 had the methyl CH<sub>3</sub>-10 and a hydroxy group as substituents.

For compound 8, NOEs observed between H-3 and H<sub>3</sub>-10 suggested a pseudo axial–equatorial orientation between them (Figure 12). NOE interactions of H-2' with H-1' and H-3' and interaction of H-5' with H-3', together with the coupling constant of  $J_{H_1} = 4.5$  Hz, defined the configuration as an  $\alpha$ -ribofuranosyl unit.<sup>29</sup> As shown in Figure 13, the Boltzmann-

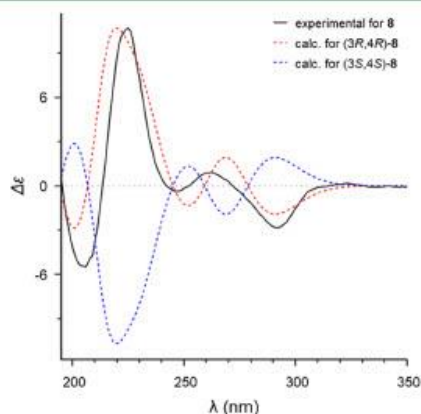


Figure 13. Experimental and calculated ECD curves of compound 8.

averaged ECD spectrum of (3R,4R)-8 matched very well with the experimental spectrum, with a positive Cotton effect around 223 and 263 nm and a negative Cotton effect around 205, 247, and 291 nm. This result unambiguously defined the absolute configuration of 8 at the isochroman-1-one moiety as (3R,4R). No attempt has been made to establish the absolute configuration of the ribosyl moiety due to the small amount (1.0 mg) of 8 obtained. Thus, compound 8 was defined as (+)-(3R,4R)-8-O- $\alpha$ -ribofuranosyl-3,4-dihydro-3-methyl-4-hydroxy-6-methoxy-1H-2-benzopyran-1-one.

Compound 9 was obtained as an optically active white amorphous powder, with  $[\alpha]_D^{25} +188$  ( $c$  0.19; MeOH). It was identified as 6,8-dimethoxy-4,5-dimethyl-3-methyleneisochroman-1-one (9),<sup>19,20</sup> by analysis of spectroscopic data (UV, <sup>1</sup>H, <sup>13</sup>C, and HRMS). However, its configurational assignment has not been previously reported. The absolute configuration of 9 was assigned as S by the match between experimental and simulated ECD data (Figure 14). Thus, the structure of 9 was established as (+)-(S)-6,8-dimethoxy-4,5-dimethyl-3-methyleneisochroman-1-one.

The antiplasmodial activity of compounds 1, 2, and 4–13 was assayed against the *P. falciparum* 3D7 strain (Table S9). Compound 5 showed the most potent antiplasmodial inhibitory activity and showed no cytotoxic effect at a concentration as high as 100  $\mu$ M ( $IC_{50}^{HspG2} > 100 \mu$ M). Solanapyrone S (1) and (+)-(3R, 4S)-3,8-dihydroxy-3-hydroxymethyl-6-methoxy-4,5-dimethyl-isochroman-1-one (12) were also assayed against cancer cells and as antimicrobials against human pathogenic microorganisms,

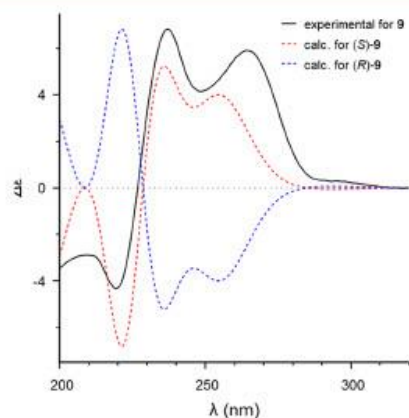


Figure 14. Experimental and calculated ECD curves of compound 9.

including Gram-negative and Gram-positive bacteria and fungi, but were inactive under the assay conditions.

Metabolite 6-hydroxy-4-(4-hydroxyphenyl)-1H-isochroman-1-one (5) showed comparable inhibitory activities against a panel of resistant *P. falciparum* strains, including Dd2 [resistant to chloroquine (CQ), sulfadoxine (SDX), pyrimethamine (PYR), mefloquine (MQ), cycloguanil (CYC)], TM90C6B [resistant to CQ, PYR, atovaquone (ATO)], and 3D7r\_MMV848 (resistant to MMV848)<sup>30</sup> strains, providing resistant index (RI) values lower than 2 (Table 7). These findings indicated that no cross-resistance was observed to the gold-standard antimalarials, thereby suggesting that the antiplasmodial activity of 5 is via a distinct mechanism of action.<sup>31</sup>

Solanapyrones were first isolated from cultures of *Alternaria solani*<sup>32</sup> and subsequently from different strains of fungi,<sup>18,33</sup> including marine.<sup>34</sup> Curiously, the majority of solanapyrones have a *cis*-fused dehydrodecalin moiety, and only solanapyrones D,<sup>32</sup> E,<sup>33c</sup> and M<sup>18</sup> and the solanapyrones S and T herein reported have a *trans*-fused dehydrodecalin portion. Biosynthesis investigations indicated that the enzymatic formation of the *cis*-fused and *trans*-fused dehydrodecalin system in solanapyrones follows the opposite selectivity of the uncatalyzed [4+2] cycloaddition reaction, the exo-selectivity leading to *cis*-fused solanapyrones as the favored catalyzed products.<sup>35</sup> Thus, the isolation of *trans*-fused solanapyrones S (1) and T (2) is further evidence that a different set of cycloaddition enzymes operates via distinct stereoselective pathways among fungal strains. This differentiation is related not only to the formation of the dehydrodecalin moiety but also to the presence of methyl groups at C-1 and C-9, which are likely derived from SAM-catalyzed methylation since propionyl-derived fungal metabolites are rare, possibly because propionate is toxic to fungi.<sup>36</sup>

Polyketide synthases involved in the formation of the rearranged compound 4, the unusually phenol-substituted polyketide 5, and the hybrid terpenoid-polyketide-derived 6 add to the diversity of PKS repertoire of fungal strains. Also, the highly methylated ribosyl-substituted 8 is the first sugar-containing derivative within a series of polyketide-related fungal metabolites.<sup>37</sup>



**Table 7. Antiplasmodial Activity of Compound 5 against a Small Panel of *Plasmodium falciparum* Resistant Strains (Dd2, TM90C6B, and 3D7r\_MMV848)**

metabolite	IC <sub>50</sub> <sup>Dd2</sup> (μM) <sup>a</sup>	IC <sub>50</sub> <sup>Dd2</sup> (μM) <sup>a</sup>	RI	IC <sub>50</sub> <sup>TM90C6B</sup> (μM) <sup>a</sup>	RI	IC <sub>50</sub> <sup>3D7r_MMV848</sup> (μM) <sup>a</sup>	RI
5	19 ± 6	37 ± 12	1.9	19 ± 8	1	23 ± 5	1.2
PYR	0.06 ± 0.01	>10	>166	NT		NT	
ATV	0.0007 ± 0.0003	NT		>1	>1428	NT	
MMV848	0.12 ± 0.02	NT		NT		1.5 ± 0.4	12.5
ART	0.006 ± 0.002	0.011 ± 0.004	2	0.006 ± 0.001	1	0.013 ± 0.004	2

<sup>a</sup>Data represent mean ± standard deviation of two independent experiments conducted in triplicate; RI = IC<sub>50</sub><sup>resistant strain</sup>/IC<sub>50</sub><sup>Dd2</sup>; NT = not tested.

Our results demonstrate the importance of isolating marine microbial strains of limited occurrence not resulting from filter feeding, such as from the gastrointestinal tract of marine animals, that may serve as a source of new bioactive secondary metabolites.

## EXPERIMENTAL SECTION

**General Experimental Procedures.** Optical rotations were measured on a Jasco P-2000 polarimeter. IR spectra were obtained on a Shimadzu IRAffinity-1 FTIR and on a Bomem MB-102 FTIR. UV spectra were recorded on a Jasco V-630 spectrophotometer. NMR experiments were recorded on a Bruker Avance III instrument (14.1 T) with an inverse cryoprobe of 5 mm with z-field gradient. Nondeuterated residual solvent signals were used for referencing the NMR scale. Electronic circular dichroism spectra were measured on a JASCO J-815 spectropolarimeter in the 200–400 nm region using quartz cells (10 mm path length) at 25 °C, bandwidth 1 nm, scanning speed 100 nm/min, 10 accumulations, and samples in MeOH solution.

The analytical HPLC-UV-MS system was a Waters instrument (2695 Alliance separation module, 2696 photodiode array detector) coupled to a Waters Micromass ZQ 2000 mass spectrometer. Analyses were performed using a Waters XTerra RP<sub>18</sub> column (250.0 mm × 4.6 mm, 5 μm) along with the RP<sub>18</sub> protective guard column (4 × 3 mm) and eluting with H<sub>2</sub>O + 0.1% formic acid, MeOH + 0.1% formic acid, and MeCN + 0.1% formic acid using a gradient from 90:5:5 to 0:50:50 of H<sub>2</sub>O/MeOH/MeCN over 22 min, maintaining in 0:50:50 H<sub>2</sub>O/MeOH/MeCN for 8 min, from 0:50:50 to 90:5:5 in 1 min, and maintaining at 90:5:5 for 9 min, using a flow rate of 1.0 mL/min. The PDA detector scanned between λ 200 and 600 nm. The mass spectrometer detector was optimized using the following conditions: capillary voltage 3 kV; temperature of the source 100 °C; desolvation temperature 350 °C; ESI mode, acquisition range 100 to 1200 Da; gas flow without cone 50 L h<sup>-1</sup>; desolvation gas flow 350 L h<sup>-1</sup>. Samples were diluted in MeOH at a concentration of 1 mg mL<sup>-1</sup>. Semipreparative HPLC separations were performed on a Waters system, including a Waters 600 quaternary pump and a Waters 2996 controller coupled to a Waters 2487 dual absorbance detector using a Waters XTerra RP<sub>18</sub> column (150.0 mm × 7.8 mm, 5 μm) along with the RP<sub>18</sub> protective guard column (4 × 3 mm) and a flow rate of 2.5 mL min<sup>-1</sup>.

UPLC-QToF-HRMS analyses were performed on a Waters Acquity H-Class UPLC coupled to a Xevo G2-XS Q-ToF instrument with an electrospray ionization (ESI) interface. The chromatographic separation was performed using a Waters Acquity UPLC BEH column (RP<sub>18</sub>, 2.1 × 100 mm, 1.7 μm), with a mobile phase composed of H<sub>2</sub>O + 0.1% formic acid (A) and MeCN + 0.1% formic acid (B). The following gradient was applied at a flow rate of 0.5 mL min<sup>-1</sup>: 10% to 100% of B in 8 min, maintaining the gradient condition at 100% of B for 0.2 min, then setting it back to 10% of B at t = 8.20 min and keeping it at 10% of B until t = 10 min. The HRESIMS data were acquired in the positive and negative ion mode.

HPLC-grade organic solvents and HPLC-Milli-Q-grade water were filtered prior to use. The size exclusion chromatography was performed on Sephadex LH-20 (200 × 2.0 cm, i.d.). Marine agar (MA) and PDB medium were purchased from Difco and Acumedia,

respectively. Deuterated NMR solvents (MeOH-*d*<sub>4</sub>, DMSO-*d*<sub>6</sub>, and CDCl<sub>3</sub>) were purchased from Cambridge Isotope Laboratories.

**Fungus Strain Isolation and Identification.** The marine fungus *Peroneutypa* sp. M16 strain was isolated from a sea cucumber, collected near Guarapari, Espírito Santo state, Brazil. This fungus was identified by the analysis of ITS and β-tubulin sequences, and its nucleotide sequences were deposited in the GenBank database under the access number OMS838477 and OQ512981, respectively. The axenic strain was preserved in glycerol solutions (25%, v/v) in a freezer at -80 °C and deposited in the Organic Chemistry of Biological Systems (QOSBio) laboratory, Instituto de Química de São Carlos, Universidade de São Paulo, São Carlos, SP, Brazil, under the accession code M16. Detailed methods and results of the morphology investigation of *Peroneutypa* sp. M16 strain can be viewed in the Supporting Information (Figures S85 and S86, procedures S1 and S2). Sampling permit: SisGen code (A840479).

**Fungus Cultivation and Growth Medium Extraction.** The marine-derived fungus *Peroneutypa* sp. M16 strain was inoculated in Petri dishes containing MA in the absence of light and kept in a biochemical oxygen demand (BOD) incubator for 7 days at 28 °C. After precultivation on solid medium, agar disks containing mycelium (5 × 0.5 cm<sup>2</sup>) were used to inoculate into 75 Schott flasks (500 mL) each containing PDB medium (200 mL) prepared with artificial seawater (NaCl 13.6 g L<sup>-1</sup>; CaCl<sub>2</sub>·2H<sub>2</sub>O 1.30 g L<sup>-1</sup>; MgCl<sub>2</sub>·6H<sub>2</sub>O 4.53 g L<sup>-1</sup>; KCl 0.64 g L<sup>-1</sup>; MgSO<sub>4</sub>·7H<sub>2</sub>O 5.94 g L<sup>-1</sup>; Na<sub>2</sub>HPO<sub>4</sub> 10.0 mg L<sup>-1</sup>; NH<sub>4</sub>NO<sub>3</sub> 2.1 mg L<sup>-1</sup>), incubated in BOD in still mode and 28 °C. The liquid medium was autoclaved before inoculation at 121 °C for 20 min. During the fungus growth the glucose level was measured using glucose strips (Uniscan). On day 22 the glucose strip test indicated the absence of glucose in the medium of all cultures. Then, the cultures were filtered, and the filtrate was partitioned with EtOAc (3 × 1.0 L). The EtOAc-soluble fraction was evaporated *in vacuo* to give 1.7 g of the EtOAc extract.

**Isolation of Metabolites 1–13.** The EtOAc extract (1.7 g) was solubilized in MeOH (8.0 mL) in an ultrasound bath and centrifuged for 10 min, and a precipitate (39.0 mg) was filtered off. The supernatant was applied to the Sephadex LH-20 column eluted with MeOH. A total of 167 fractions were collected, analyzed, and combined on the basis of their HPLC-UV-MS patterns. Eleven fractions were obtained [F1 (125.1 mg), F2 (380.2 mg), F3 (147.7 mg), F4 (93.2 mg), F5 (188.0), F6 (80.3 mg), F7 (88.2 mg), F8 (336.1), F9 (50.7 mg), F10 (78.7 mg), and F11 (20.3 mg)]. Fraction F5 was separated by HPLC-UV using a Waters XTerra RP<sub>18</sub> column (150.0 mm × 7.8 mm, 5 μm) and a UV detector at λ<sub>max</sub> 254 and 315 nm, eluting with MeOH + 0.1% formic acid and MeOH + 0.1% formic acid using a gradient from 30:70 to 80:20 of H<sub>2</sub>O/MeOH over 30 min, using a flow rate of 2.5 mL min<sup>-1</sup>, resulting in the isolation of 1 (4.3 mg), 4 (0.5 mg), 9 (4.4 mg), 10 (7.7 mg), and 11 (3.1 mg). Fraction F4 was also separated by HPLC-UV using a Waters XTerra RP<sub>18</sub> column (150.0 mm × 7.8 mm, 5 μm) and monitored by UV at λ<sub>max</sub> 254 nm, eluting with MeOH + 0.1% formic acid and MeOH + 0.1% formic acid using a gradient from 16:84 to 0:100 of H<sub>2</sub>O/MeOH over 30 min, using a flow rate of 2.5 mL min<sup>-1</sup>, to give compounds 6 (0.8 mg), 7 (0.8 mg), and 12 (5.7 mg). Fraction F11 was separated by HPLC-UV using a Waters XTerra RP<sub>18</sub> column (150.0 mm × 7.8 mm, 5 μm) monitored by UV at λ<sub>max</sub> 254 nm, eluting with MeOH + 0.1% formic acid and MeOH + 0.1% formic acid using a gradient from 10:90 to 50:50 of H<sub>2</sub>O/MeOH over 25

min, using a flow rate of 2.5 mL min<sup>-1</sup>, to give 5 (1.0 mg). Fraction F2 (380.2 mg) was solubilized in MeOH/H<sub>2</sub>O (1:1, 5.0 mL) with sonication and applied to a C<sub>18</sub> reversed-phase silica-gel cartridge (5 g) and eluted with a gradient of MeOH in H<sub>2</sub>O. Four fractions were obtained: F2A (54.7 mg), F2B (129.9 mg), F2C (150.3 mg), and F2D (5.7 mg). In the same way, fraction F3 (147.7 mg) was solubilized in MeOH/H<sub>2</sub>O (1:1, 2.0 mL) with sonication, applied to a C<sub>18</sub> reversed-phase silica-gel cartridge (5 g), and eluted with a gradient of MeOH in H<sub>2</sub>O, resulting in the fractions F3A (27.8 mg), F3B (48.5 mg), F3C (59.5 mg), and F3D (7.7 mg). Fraction F3A was also separated by HPLC-UV using a Waters XTerra RP<sub>18</sub> column (150.0 mm × 7.8 mm, 5 μm) and monitored by UV at λ<sub>max</sub> 254 nm, eluting with MeOH and H<sub>2</sub>O using a gradient from 16:84 to 0:100 of H<sub>2</sub>O/MeOH over 30 min, using a flow rate of 2.5 mL min<sup>-1</sup>, to give 2 (0.5 mg) and 3 (0.5 mg). Fraction F2B was separated by HPLC-UV using a Waters XTerra RP<sub>18</sub> column (150.0 mm × 7.8 mm, 5 μm) and a UV detector at λ<sub>max</sub> 237 and 279 nm, eluting with MeOH/MeCN/H<sub>2</sub>O, using a gradient from 5:5:90 to 50:50:0 over 30 min, using a flow rate of 2.5 mL min<sup>-1</sup>, resulting in the isolation of 8 (1.0 mg), 13 (2.2 mg), and 10 (2.3 mg).

(-)-(E)-(1R,2R,5S,9S,10R)-Solanaopyrone 5 (1): white amorphous solid; [α]<sub>D</sub><sup>25</sup> -173 (c 0.1, MeOH); UV λ<sub>max</sub> (MeOH) 215, 245sh, 333 nm; IR (ATR) ν<sub>max</sub> 3249, 2915, 1720, and 1600 cm<sup>-1</sup>; ECD (MeOH) λ<sub>max</sub> (Δε) 212 (+3.7), 240 (+0.4), 320 (-1.4) nm; <sup>1</sup>H and <sup>13</sup>C NMR data presented in Table 1; ESIHRMS m/z 346.2014 [M + H]<sup>+</sup> (calcd for C<sub>20</sub>H<sub>28</sub>NO<sub>4</sub><sup>+</sup>, 346.2013).

(-)-(1R,2R,5S,9R,10R)-Solanaopyrone T (2): white amorphous solid; [α]<sub>D</sub><sup>25</sup> -37 (c 0.1, MeOH); UV λ<sub>max</sub> (MeOH) 237, 283, and 315 nm; IR (Si) ν<sub>max</sub> 3397, 3184, 2922, 2849, 1643, 1634, and 1593 cm<sup>-1</sup>; ECD (MeOH) λ<sub>max</sub> (Δε) 205 (+1.9), 241 (+5.2), 279 (+1.4), 313 (-2.6) nm; <sup>1</sup>H and <sup>13</sup>C NMR data presented in Table 1; ESIHRMS m/z 360.2164 [M + H]<sup>+</sup> (calcd for C<sub>21</sub>H<sub>30</sub>NO<sub>4</sub><sup>+</sup>, 360.2169).

(+)-(1S,9S)-Peroneutone (4): yellowish oil; [α]<sub>D</sub><sup>25</sup> +14 (c 0.05, MeOH); UV λ<sub>max</sub> (MeOH) 275 and 320 nm; IR (Si) ν<sub>max</sub> 3304, 2941, 1686, and 1601 cm<sup>-1</sup>; ECD (MeOH) λ<sub>max</sub> (Δε) 210 (-1.0), 233 (+16.0), 275 (+4.0), 307 (-5.3) nm; <sup>1</sup>H and <sup>13</sup>C NMR data presented in Table 2; ESIHRMS m/z 223.0971 [M + H]<sup>+</sup> (calcd for C<sub>12</sub>H<sub>15</sub>O<sub>4</sub><sup>+</sup>, 223.0965).

6-Hydroxy-4-(4-hydroxyphenyl)-1H-isochromen-1-one (5): white amorphous solid; UV λ<sub>max</sub> (MeOH) 249 and 300 nm; IR (Si) ν<sub>max</sub> 3294, 2918, 1674, and 1585 cm<sup>-1</sup>; <sup>1</sup>H and <sup>13</sup>C NMR data presented in Table 3; ESIHRMS m/z 255.0662 [M + H]<sup>+</sup> (calcd for C<sub>15</sub>H<sub>11</sub>O<sub>4</sub><sup>+</sup>, 255.0652).

(+)-(5)-Perofuranone (6): colorless oil; [α]<sub>D</sub><sup>25</sup> +38.6 (c 0.1, MeOH); UV λ<sub>max</sub> (MeOH) 247, 279sh and 319 nm; IR (Si) ν<sub>max</sub> 3333, 2980, 1765, and 1699 cm<sup>-1</sup>; ECD (MeOH) λ<sub>max</sub> (Δε) 237 (-2.2), 300 (+1.5) nm; <sup>1</sup>H and <sup>13</sup>C NMR data presented in Table 4; ESIHRMS m/z 237.1138 [M - H]<sup>-</sup> (calcd for C<sub>13</sub>H<sub>17</sub>O<sub>4</sub><sup>-</sup>, 237.1132).

(+)-(5S,9R,10R,11S,13R,14S)-Peronepene (7): white amorphous solid; [α]<sub>D</sub><sup>25</sup> +16.5 (c 0.08, MeOH); UV λ<sub>max</sub> (MeOH) 247 and 305 nm; IR (Si) ν<sub>max</sub> 3408, 2924, and 1676 cm<sup>-1</sup>; ECD (MeOH) λ<sub>max</sub> (Δε) 207 (-3.2), 247 (+1.9), 315 (+0.2) nm; <sup>1</sup>H and <sup>13</sup>C NMR data presented in Table 5; ESIHRMS m/z 319.2281 [M + H]<sup>+</sup> (calcd for C<sub>20</sub>H<sub>31</sub>O<sub>3</sub><sup>+</sup>, 319.2268).

(+)-(3R,4R)-8-O-α-Ribofuranosyl-3,4-dihydro-3-methyl-4-hydroxy-6-methoxy-1H-2-benzopyran-1-one (8): colorless oil; [α]<sub>D</sub><sup>25</sup> +29 (c 0.1, MeOH); UV λ<sub>max</sub> (MeOH) 223, 259, and 291 nm; IR (Si) ν<sub>max</sub> 3381, 2926, and 1719 cm<sup>-1</sup>; ECD (MeOH) λ<sub>max</sub> (Δε) 205 (-5.5), 223 (+11), 245 (-0.6), 263 (+1.3), 289 (-2.8) nm; <sup>1</sup>H and <sup>13</sup>C NMR data presented in Table 6; ESIHRMS m/z 407.1314 [M + Na]<sup>+</sup> (calcd for C<sub>19</sub>H<sub>24</sub>O<sub>9</sub>Na<sup>+</sup>, 407.1313).

**Computational Electronic Circular Dichroism.** Conformational searches of all diastereomers were carried out by means of CREST 2.11<sup>38</sup> at the GFN2-xTB<sup>39</sup> tight-binding quantum chemistry level. All other quantum chemical calculations, including density functional theory (DFT) and time-dependent density functional theory (TDDFT), were performed with Gaussian09.<sup>40</sup> Structural optimizations and frequency calculations of all conformers were performed with the B3LYP<sup>41–43</sup> functional and 6-31G(d)<sup>44</sup> as basis

set (gas phase). All conformational geometries, except for compounds 2 and 8, were reoptimized in MeOH (PCM) using the ωB97XD/6-31G+(d,p)<sup>45</sup> level of theory. Compounds 2 and 8 were reoptimized using the levels M06-2X/6-31+G(d,p)<sup>46</sup> and B3LYP/6-31+G(d,p), respectively. TDDFT was used to calculate the excitation energies (in nm) and rotational forces R<sub>i</sub>, in the form of dipole velocity (R<sub>rot</sub> units cgs: 10<sup>-40</sup> erg esu cm Gauss<sup>-1</sup>) using the functionals CAM-B3LYP,<sup>47</sup> B3LYP, ωB97XD, or M06-2X<sup>46</sup> in combination with the TZVP<sup>48</sup> or def2-TZVP<sup>49</sup> as basis sets. The information related to the def2-TZVP basis set was obtained from the Basis Set Exchange Web site.<sup>50</sup> The UV and ECD spectra were obtained using a Boltzmann-weighted average of conformations with relative energies within 3 kcal/mol of the lowest energy conformation and Boltzmann population >1% using the SpecDis 1.71 software.<sup>51</sup>

**In Vitro Antiplasmodial Assay with Plasmodium falciparum.** Compounds 1–13 were assayed against the sensitive *P. falciparum* 3D7 strain. In addition, compound 5 was assayed against resistant strains of the parasite (Dd2, TM90C6B, and 3D7r\_MMV848). *P. falciparum* parasites were cultured in a humidified incubator at 37 °C in RPMI-1640 medium containing 25 mM NaHCO<sub>3</sub>, 25 mM HEPES (pH 7.4), 11 mM D-glucose, 3.67 mM hypoxanthine, and 25 μg mL<sup>-1</sup> gentamicin, supplemented with 0.5% (m/v) AlbuMAX II, and under a gas mixture of 5% CO<sub>2</sub>, 5% O<sub>2</sub>, and 90% N<sub>2</sub>. The culture medium was changed daily, and the parasitemia was maintained below 10% and 2.5% hematocrit.<sup>52</sup> For the biological evaluation, a stock solution of the isolated compounds received was prepared at 20 mM in DMSO. A 96-well culture plate was prepared for IC<sub>50</sub> assays by adding serial dilutions of the isolated compounds (10–0.156 μM), at a final volume of 20 μL. Artesunate was used as a positive control of inhibition. Parasite isolates were prepared as previously described.<sup>53</sup> An aliquot of 180 μL was added at final concentrations of 0.5% parasitemia and 2% hematocrit. The plate was incubated at 37 °C in a humidified incubator with the gas mixture, for 72 h. After incubation, the culture medium was removed, and the cells were resuspended in 100 μL of PBS (116 mM NaCl, 10 mM Na<sub>2</sub>HPO<sub>4</sub>, 3 mM KH<sub>2</sub>PO<sub>4</sub>) followed by lysis with the addition of 100 μL of lysis buffer (20 mM Tris base, 5 mM EDTA, 0.0008% (v/v) Triton X-100, 0.008% (m/v) saponin, pH 8.0) containing 0.002% (v/v) SYBR Green I. The plates were incubated at room temperature for 30 min. The fluorescence corresponding to the parasitic density was measured using a SpectraMAX Gemini EM plate reader (Molecular Devices Corp., Sunnyvale, CA, USA) (excitation at 485 nm, emission at 535 nm).<sup>54</sup> To determine the half-maximal inhibitory concentration (IC<sub>50</sub>)<sup>55</sup>, a nonlinear regression analysis of the resulting concentration–response curve was performed using GraphPad Prism version 9.0.0 for Windows, GraphPad Software, San Diego, CA, USA. The reported data represent mean ± standard deviation of two independent experiments conducted in triplicate.

**The Hepatocarcinoma Cell Culture and Cytotoxic Evaluation.** Compound 5 with IC<sub>50</sub><sup>57</sup> < 10 μM had its cytotoxicity evaluated against a human immortalized cell line of hepatocarcinoma cells (HepG2). These cells were cultured in RPMI medium containing 25 mM NaHCO<sub>3</sub>, 25 mM HEPES (pH 7.4), 11 mM D-glucose, 3.67 mM hypoxanthine, and 25 μg/mL gentamicin supplemented with 10% (v/v) fetal bovine serum. The supplemented medium was changed every 2 days and incubated in a humidified incubator at 37 °C with 5% CO<sub>2</sub>. For biological evaluation, cells were trypsinized and transferred to a 96-well plate (30,000 cells per well in 180 μL of cell suspension). Next, to allow cell adhesion, the plate was incubated for 24 h in the incubator. A 20 μL amount of a serial dilution of the compound was added (concentration range 100–1.56 μM), and the plate was incubated for 72 h. Then, a microscope was used to verify the existence of precipitated compounds to adjust the range of concentration evaluated. A 3-(4,5-dimethylthiazol-2-yl)-2,5-diphenyltetrazolium bromide (MTT) colorimetric assay<sup>55</sup> was performed to evaluate the cytotoxicity of the compounds. After incubation, 20 μL of a solution of MTT at 5 mg/mL (solubilized in phosphate-buffered saline, PBS) was added to each well. The plate was incubated at 37 °C for 3 h to allow MTT cleavage in living cells. The supernatant was removed, followed by addition of 100 μL of DMSO, in each well, to

solubilize the formed purple formazan crystals. A SpectraMAX Plus 384 plate reader (Molecular Devices Corp.) was used to measure the absorbance ( $\lambda = 570$  nm). The half-maximal inhibitory concentration was determined using a nonlinear regression analysis, which was performed using GraphPad Prism version 9.0.0 for Windows.

**Cytotoxicity Assay.** Cancer cell lines MCF-7 (breast adenocarcinoma) and HeLa (cervical carcinoma) were cultured in complete medium containing DMEM/HAM'sF10 medium (1:1, v/v), supplemented with 10% fetal bovine serum and the antibiotic mixture penicillin/streptomycin (10 mL L<sup>-1</sup>) plus kanamycin sulfate (10 mg L<sup>-1</sup>) in 96-well plates (10<sup>4</sup> cell well<sup>-1</sup>) at 37 °C under 5% CO<sub>2</sub>. Cytotoxicity of compounds 1 and 12 was evaluated in different concentrations (0.1, 1, 10, and 100  $\mu$ M) using a cell proliferation kit (Roche) according to the manufacturer's instructions. After 24 h of treatment, the cell plate was washed twice with PBS and the cells were incubated for 4 h with DMEM without phenol red plus XTT/electron solution. Total absorbance was measured at 492 and 690 nm. The number of viable cells was directly proportional to the absorbance, and the percentage was compared with the negative control. The inhibitory concentration (IC<sub>50</sub>) was determined by the nonlinear regression analysis using GraphPad Prism (5.0). All assays were performed in triplicate.

## ■ ASSOCIATED CONTENT

### Supporting Information

The Supporting Information is available free of charge at <https://pubs.acs.org/doi/10.1021/acs.jnatprod.3c00175>.

Spectroscopic and spectrometric analysis of compounds 1, 2, and 4–8; conformers, Gibbs free energies, relative Gibbs free energies, Boltzmann population, imaginary frequencies, and atomic coordinates of the lowest energy conformers of 1, 2, and 4–9; detailed methods and results of the morphology investigation of *Peroneutypa* sp. M16 strain and partial sequence of the ITS and  $\beta$ -tubulin DNA sections (PDF)

## ■ AUTHOR INFORMATION

### Corresponding Authors

Marcelo R. de Amorim – Instituto de Química de São Carlos, Universidade de São Paulo, CEP 13560-970 São Carlos, SP, Brazil; Email: [marceloamorim.unesp@gmail.com](mailto:marceloamorim.unesp@gmail.com)

Rafael V. C. Guido – Instituto de Física de São Carlos, Universidade de São Paulo, CEP 13563-120 São Carlos, SP, Brazil; Email: [rvcguido@ifsc.usp.br](mailto:rvcguido@ifsc.usp.br)

Roberto G. S. Berlinck – Instituto de Química de São Carlos, Universidade de São Paulo, CEP 13560-970 São Carlos, SP, Brazil; [orcid.org/0000-0003-0118-2523](https://orcid.org/0000-0003-0118-2523); Email: [rgsberlinck@iqsc.usp.br](mailto:rgsberlinck@iqsc.usp.br)

### Authors

Camila de S. Barbosa – Instituto de Física de São Carlos, Universidade de São Paulo, CEP 13563-120 São Carlos, SP, Brazil

Tiago A. Paz – Departamento de Análises Clínicas, Toxicológicas e Bromatológicas, Faculdade de Ciências Farmacêuticas de Ribeirão Preto, Universidade de São Paulo, CEP 14040-903 Ribeirão Preto, SP, Brazil

Laura P. Ióca – Instituto de Química de São Carlos, Universidade de São Paulo, CEP 13560-970 São Carlos, SP, Brazil

Karen J. Nicácio – Instituto de Química de São Carlos, Universidade de São Paulo, CEP 13560-970 São Carlos, SP, Brazil; [orcid.org/0000-0001-9790-5786](https://orcid.org/0000-0001-9790-5786)

Lucianne F. P. de Oliveira – Departamento de Ciências Exatas, Escola Superior de Agricultura "Luiz de Queiroz",

Universidade de São Paulo, CEP 13418-900 Piracicaba, SP, Brazil

Mirian O. Goulart – Centro de Pesquisa em Ciência e Tecnologia, Universidade de Franca, CEP 14404-600 Franca, SP, Brazil

Julia M. Paulino – Centro de Pesquisa em Ciência e Tecnologia, Universidade de Franca, CEP 14404-600 Franca, SP, Brazil

Mateus O. da Cruz – Departamento de Biologia Geral e Aplicada, Universidade Estadual Paulista "Júlio de Mesquita Filho", CEP 13506-900 Rio Claro, SP, Brazil

Antonio G. Ferreira – Departamento de Química, Universidade Federal de São Carlos, 13565-905 São Carlos, SP, Brazil

Maysa Furlan – Instituto de Química de Araraquara, Universidade Estadual Paulista "Júlio de Mesquita Filho", CEP 14800-900 Araraquara, SP, Brazil

Simone P. de Lira – Departamento de Ciências Exatas, Escola Superior de Agricultura "Luiz de Queiroz", Universidade de São Paulo, CEP 13418-900 Piracicaba, SP, Brazil; [orcid.org/0000-0003-0692-6237](https://orcid.org/0000-0003-0692-6237)

Raquel A. dos Santos – Centro de Pesquisa em Ciência e Tecnologia, Universidade de Franca, CEP 14404-600 Franca, SP, Brazil

André Rodrigues – Departamento de Biologia Geral e Aplicada, Universidade Estadual Paulista "Júlio de Mesquita Filho", CEP 13506-900 Rio Claro, SP, Brazil

Complete contact information is available at:

<https://pubs.acs.org/doi/10.1021/acs.jnatprod.3c00175>

### Notes

The authors declare no competing financial interest.

## ■ ACKNOWLEDGMENTS

The authors thank the São Paulo State Research Foundation (FAPESP) for financial support (2015/01017-0, 2019/17721-9, and 2020/12904-5), for a postdoctoral scholarship awarded to M.R.A. (2020/01229-5) and a Ph.D. scholarship awarded to L.P.I. (2016/05133-7), as well as the technical support of the Center for Scientific Computing (NCC/GridUNESP) of the São Paulo State University (UNESP). Financial support was also provided by the Coordenação de Aperfeiçoamento de Pessoal de Nível Superior - Brasil (CAPES) - Finance Code 001.

## ■ REFERENCES

- Imhoff, J. F. *Mar. Drugs* 2016, 14, 19.
- Liu, Z.; Frank, M.; Yu, X.; Yu, H.; Tran-Cong, N. M.; Gao, Y.; Proksch, P. *Prog. Chem. Org. Nat. Prod.* 2020, 111, 81–153.
- Adnani, N.; Rajski, S. R.; Bugni, T. S. *Nat. Prod. Rep.* 2017, 34, 784–814.
- Gao, H.; Li, G.; Lou, H.-X. *Molecules* 2018, 23, 646.
- (a) Rustamova, N.; Bozorov, K.; Efferth, T.; Yili, A. *Phytochem. Rev.* 2020, 19, 425–448. (b) Ancheeva, E.; Daletos, G.; Proksch, P. *Curr. Med. Chem.* 2020, 27, 1836–1854. (c) Carroll, A. R.; Copp, B. R.; Davis, R. A.; Keyzers, R. A.; Prinsep, M. R. *Nat. Prod. Rep.* 2021, 38, 362–413.
- Ashley, E. A.; Phyto, A. P. *Drugs* 2018, 78, 861–879.
- Blasco, B.; Leroy, D.; Fidock, D. A. *Nat. Med.* 2017, 23, 917–928.
- World Health Organization. *World Malaria Report 2022*; World Health Organization: Geneva, 2022.
- World Health Organization. *World Malaria Report 2021*; World Health Organization: Geneva, 2021.

- (10) Ibrahim, S. R. M.; Abdallah, H. M.; Elkhayat, E. S.; Al Musayeb, N. M.; Asfour, H. Z.; Zayed, M. F.; Mohamed, G. A. *Nat. Prod. Res.* **2017**, *20*, 1–11.
- (11) Spiry, C.; Sewell, A. L.; Hering, Y.; Villa, M. V. J.; Weber, J.; Hobson, S. J.; Harnor, S. J.; Gul, S.; Marquez, R.; Saliba, K. J. *Eur. J. Med. Chem.* **2018**, *143*, 1139–1147.
- (12) Fredenhagen, A.; Schroer, K.; Schröder, H.; Hoepfner, D.; Ligibel, M.; Zemp, L. P.; Radoch, C.; Freund, E.; Meishammer, A. *ChemBioChem*. **2019**, *20*, 650–654.
- (13) Sadom, K.; Saepua, S.; Boonyuen, N.; Komwijit, S.; Rachtawee, P.; Pittayakhajonwut, P. *Tetrahedron* **2019**, *75*, 3463–3471.
- (14) Kornsakulkarn, J.; Palasarn, S.; Choowong, W.; Thongpanchang, T.; Boonyuen, N.; Choeykin, R.; Boonpratuang, T.; Isaka, M.; Thongpanchang, C. *J. Nat. Prod.* **2020**, *83*, 905–917.
- (15) Annang, F.; Pérez-Moreno, G.; González-Menéndez, V.; Lacret, R.; Pérez-Victoria, I.; Martín, J.; Cantizani, J. de Pedro, N.; Choquesillo-Lazarte, D.; Ruiz-Pérez, L. M.; Gonzalez-Pacanoska, D.; Genilloud, O.; Vicente, F.; Reyes, F. *Org. Lett.* **2020**, *22*, 6709–6713.
- (16) Ouchi, T.; Watanabe, Y.; Nonaka, K.; Muramatsu, R.; Noguchi, C.; Tozawa, M.; Hokari, R.; Ishiyama, A.; Koike, R.; Matsui, H.; Asami, Y.; Inahashi, Y.; Ishii, T.; Teruya, T.; Iwatsuki, M.; Hanada, H.; Omura, S. *J. Antibiot.* **2020**, *73*, 365–371.
- (17) Ishiyama, A.; Hokari, R.; Nonaka, K.; Chiba, T.; Miura, H.; Otoguro, K.; Iwatsuki, M. *J. Antibiot.* **2021**, *74*, 266–268.
- (18) Schmidt, L. E.; Gloer, J. B.; Wicklow, D. T. *J. Nat. Prod.* **2007**, *70*, 1317–1320. In the original report of data for solanapyrone M, the chemical shift assigned to C-9 was misassigned as  $\delta$  47.6, but is likely close to  $\delta$  40 (Professor James B. Gloer, University of Iowa, personal communication).
- (19) Sang, H. S.; Sy, A. A.; Gloer, J. B.; Wicklow, D. T. *Bull. Korean Chem. Soc.* **2008**, *29*, 863–865.
- (20) Hamed, M. M.; Ghareeb, M. A.; Abdel-Aleem, A.-A. H.; Saad, A. M.; Abdel-Aziz, M. S.; Hadad, A. H. *Int. J. Pharm. Sci. Res.* **2017**, *44*, 209–216.
- (21) Tayone, W. C.; Kanamaru, S.; Honma, M.; Tanaka, K.; Nehira, T.; Hashimoto, M. *Biosci. Biotechnol. Biochem.* **2011**, *75*, 2390–2393.
- (22) Chinworrungsee, M.; Kittakoop, P.; Isaka, M.; Chanphen, R.; Tanticharoen, M.; Thebtaranonth, Y. *J. Chem. Soc. Perkin 1* **2002**, *22*, 2473–2476.
- (23) Tayone, W. C.; Honma, M.; Kanamaru, S.; Noguchi, S.; Tanaka, K.; Nehira, T.; Hashimoto, M. *J. Nat. Prod.* **2011**, *74*, 425–429.
- (24) Prompanya, C.; Dethoup, T.; Gales, L.; Lee, M.; Pereira, J. A. C.; Silva, A. M. S.; Pinto, M. M. M.; Kijjoa, A. *Mar. Drugs* **2016**, *14*, 1–26.
- (25) Wu, S.-H.; Chen, Y.-W.; Shao, S.-C.; Wang, L.-D.; Yu, Y.; Li, Z.-Y.; Yang, L.-Y.; Li, S.-L.; Huang, R. *Chem. Biodiv.* **2009**, *6*, 79–85.
- (26) Plunkett, S.; DeRatt, L. G.; Kuduk, S. D.; Balsells, J. *Org. Lett.* **2020**, *22*, 7662–7666.
- (27) Li, X.; Li, X.-D.; Li, X.-M.; Xu, G.-M.; Liu, Y.; Wang, B.-G. *RSC Adv.* **2017**, *7*, 4387–4394.
- (28) Wang, J.-B.; Guo, Y.-W. *Helv. Chim. Acta* **2004**, *87*, 2829–2833.
- (29) Verastegui-Omaña, B.; Rebollar-Ramos, D.; Pérez-Vásquez, A.; Martínez, A. L.; Madariaga-Mazón, A.; Flores-Bocanegra, L.; Mata, R. *J. Nat. Prod.* **2017**, *80*, 190–195.
- (30) Irabuena, C.; Scarone, L.; de Souza, G. E.; Aguiar, A. C. C.; Mendes, G. R.; Guido, R. V. C.; Serra, G. *Med. Chem. Res.* **2022**, *31*, 426–435.
- (31) Chugh, M.; Scheurer, C.; Sax, S.; Bilsland, E.; van Schalkwyk, D. A.; Wicht, K. J.; Hofmann, N.; Sharma, A.; Bashyam, S.; Singh, S.; Oliver, S. G.; Egan, T. J.; Malhotra, P.; Sutherland, C. J.; Beck, H.-P.; Wittlin, S.; Spangenberg, T.; Ding, X. C. *Antimicrob. Agents Chemother.* **2015**, *59*, 1110–1118.
- (32) (a) Ichihara, A.; Tazaki, H.; Sakamura, S. *Tetrahedron Lett.* **1983**, *4*, 5373–5376. (b) Ichihara, A.; Miki, M.; Sakamura, S. *Tetrahedron Lett.* **1985**, *26*, 2453–2454.
- (33) (a) Höhl, B.; Weidemann, C.; Höhl, C.; Barz, C. *J. Phytopathol.* **1991**, *132*, 193–206. (b) Chen, Y. M.; Strange, R. *Plant Pathol.* **1991**, *40*, 401–407. (c) Wu, S.-H.; Chen, Y.-W.; Shao, S.-H.; Wang, L.-D.; Yu, Y.; Li, Z.-Y.; Yang, L.-Y.; Li, S.-L.; Huang, R. *Chem. Biodiv.* **2009**, *6*, 79–85.
- (34) (a) Jenkins, K.; Toske, S. G.; Jensen, P.; Fenical, W. *Phytochem.* **1998**, *49*, 2299–2304. (b) Trisunwan, K.; Rukachaisirikul, V.; Sukpondma, Y.; Preedanon, S.; Phongpaichit, S.; Sakayaroj, J. *Phytochem.* **2009**, *70*, 554–557.
- (35) Campbell, C. D.; Vederas, J. C. *Biopolymers* **2010**, *93*, 755–763.
- (36) (a) Brock, M.; Fischer, R.; Linder, D.; Buckel, W. *Mol. Microbiol.* **2000**, *35*, 961. (b) Zhang, Y.-Q.; Brock, M.; Keller, N. P. *Genetics* **2004**, *168*, 785. (c) Brock, M.; Buckel, W. *Eur. J. Biochem.* **2004**, *271*, 3227.
- (37) (a) Tayone, W. C.; Honma, M.; Kanamaru, S.; Noguchi, S.; Tanaka, K.; Nehira, T.; Hashimoto, M. *J. Nat. Prod.* **2011**, *74*, 425–429. (b) El-Elimat, T.; Raja, H. A.; Figueroa, M.; Falkinham, J. O.; Oberlies, N. H. *Phytochem.* **2014**, *104*, 114–120. (c) Chen, Q.; Yu, J. J.; He, J.; Feng, T.; Liu, J. K. *Phytochem.* **2022**, *195*, 113050.
- (38) Pracht, P.; Bohl, E.; Grimme, S. *Phys. Chem. Chem. Phys.* **2020**, *22*, 7169–7192.
- (39) Bannwarth, C.; Ehlert, S.; Grimme, S. *J. Chem. Theory Comput.* **2019**, *15*, 1652–1671.
- (40) Frisch, M. J.; Trucks, G. W.; Schlegel, H. B.; Scuseria, G. E.; Robb, M. A.; Cheeseman, J. R.; Scalmani, G.; Barone, V.; Mennucci, B.; Petersson, G. A.; Nakatsuji, H.; Caricato, M.; Li, X.; Hratchian, H. P.; Izmaylov, A. F.; Bloino, J.; Zheng, G.; Sonnenberg, J. L.; Hada, M.; Ehara, M.; Toyota, K.; Fukuda, R.; Hasegawa, J.; Ishida, M.; Nakajima, T.; Honda, Y.; Kitao, O.; Nakai, H.; Vreven, T.; Montgomery, J. A.; Peralta, J. E.; Ogliaro, F.; Bearpark, M.; Heyd, J. J.; Brothers, E.; Kudin, K. N.; Staroverov, V. N.; Kobayashi, R.; Normand, J.; Raghavachari, K.; Rendell, A.; Burant, J. C.; Iyengar, S. S.; Tomasi, J.; Cossi, M.; Rega, N.; Millam, J. M.; Klene, M.; Knox, J. E.; Cross, J. B.; Bakken, V.; Adamo, C.; Jaramillo, J.; Gomperts, R.; Stratmann, R. E.; Yazyev, O.; Austin, A. J.; Cammi, R.; Pomelli, C.; Ochterski, J. W.; Martin, R. L.; Morokuma, K.; Zakrzewski, V. G.; Voth, G. A.; Salvador, P.; Dannenberg, J. J.; Dapprich, S.; Daniels, A. D.; Farkas, O.; Foresman, J. B.; Ortiz, J. V.; Cioslowski, J.; Fox, D. J. *Gaussian 09*, Revision A.02; Gaussian, Inc.: Wallingford, CT, 2009.
- (41) Becke, A. D. *J. Chem. Phys.* **1993**, *98*, 5648–5652.
- (42) Lee, C.; Yang, W.; Parr, R. G. *Phys. Rev. B* **1988**, *37*, 785–789.
- (43) Stephens, P. J.; Devlin, F. J.; Chabalowski, C. F.; Frisch, M. J. *J. Phys. Chem.* **1994**, *98*, 11623–11627.
- (44) Ditchfield, R.; Hehre, W. J.; Pople, J. A. *J. Chem. Phys.* **1971**, *54*, 720–723.
- (45) Chai, J.-D.; Head-Gordon, M. *Phys. Chem. Chem. Phys.* **2008**, *10*, 6615–6620.
- (46) Yanai, T.; Tew, D. P.; Handy, N. C. *Chem. Phys. Lett.* **2004**, *393*, 51–57.
- (47) Zhao, Y.; Truhlar, D. G. *Theor. Chem. Acc.* **2008**, *120*, 215–241.
- (48) Schäfer, A.; Huber, C.; Ahlrichs, R. *J. Chem. Phys.* **1994**, *100*, 5829–5835.
- (49) Weigend, F.; Ahlrichs, R. *Phys. Chem. Chem. Phys.* **2005**, *7*, 3297–3305.
- (50) Pritchard, B. P.; Altarawy, D.; Didier, B.; Gibson, T. D.; Windus, T. L. *J. Chem. Inf. Model.* **2019**, *59*, 4814–4820.
- (51) Bruhn, T.; Schaumlöffel, A.; Hemberger, Y.; Bringmann, G. *Chirality* **2013**, *25*, 243–249.
- (52) Trager, W.; Jensen, J. B. *Science* **1976**, *193*, 673–675.
- (53) De Souza, G. E.; Bueno, R. V.; De Souza, J. O.; Zanini, C. L.; Cruz, F. C.; Oliva, G.; Guido, R. V. C.; Aguiar, A. C. C. *Malar. J.* **2019**, *18*, 447.
- (54) Vossen, M. G.; Pferschy, S.; Chiba, P.; Noedl, H. *Am. J. Trop. Med. Hyg.* **2010**, *82*, 398–401.
- (55) Mosmann, T. *J. Immunol. Meth.* **1983**, *65*, 55–63.

**Parasitological profiling of the marine guanidine alkaloids batzelladines F and L  
as inhibitors of *Plasmodium falciparum* with *in vivo* antimalarial activity**

Giovana Rossi Mendes<sup>1#</sup>, Anderson R. Noronha<sup>2#</sup>, Igor M. R. de Moura<sup>1</sup>, Natália M. Moreira<sup>1</sup>,  
Camila S. Barbosa<sup>1</sup>, Sarah El Chamy Maluf<sup>1</sup>, Guilherme Eduardo de Souza<sup>1</sup>, Marcelo Rodrigues de  
Amorim,<sup>2</sup> Anna Caroline C Aguiar<sup>3</sup>, Fabio C. Cruz<sup>4</sup>, Amália dos Santos Ferreira<sup>5</sup>, Carolina Bioni  
Garcia Teles<sup>5</sup>, Dhelio B. Pereira<sup>6</sup>, Eduardo Hajdu,<sup>7</sup> Antonio G. Ferreira,<sup>8</sup> Roberto G. S. Berlinck<sup>2\*</sup>,  
Rafael V. C. Guido<sup>1\*</sup>

**Susceptibility of Brazilian *Plasmodium vivax* and *Plasmodium falciparum* Isolates to current  
antimalarials**

Guilherme Eduardo de Souza<sup>1</sup>, Amália Ferreira dos Santos Trajano<sup>2</sup>, Yasmin Annunziato<sup>3</sup>, Camila Lima  
Zanini<sup>1</sup>, Juliana Oliveira de Souza<sup>1</sup> (*in memoriam*), Camila de Souza Barbosa<sup>1</sup>, Giovana Rossi Mendes<sup>1</sup>, Igor  
Mota Rodrigues de Moura<sup>1</sup>, Gabriela Silva de Oliveira<sup>1</sup>, Carolina Bioni Garcia Telles<sup>2</sup>, Brice Campo<sup>4</sup>,  
Mélanie Rouillier<sup>4</sup>, Dhelio Batista Pereira<sup>5</sup>, Rafael Victorio Carvalho Guido<sup>1\*</sup>, Anna Caroline Campos  
Aguiar<sup>3\*</sup>